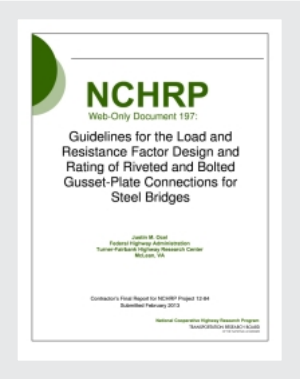

Guidelines for the Load and Resistance Factor Design and Rating of Riveted and Bolted Gusset-Plate Connections for Steel Bridges

DETAILS

163 pages | 8.5 x 11 | PAPERBACK

ISBN 978-0-309-43437-9 | DOI 10.17226/22584

AUTHORS

Ocel, Justin M.

ACKNOWLEDGMENT

This work was sponsored by the American Association of State Highway and Transportation Officials (AASHTO), in cooperation with the Federal Highway Administration, and was conducted in the National Cooperative Highway Research Program (NCHRP), which is administered by the Transportation Research Board (TRB) of the National Academies.

THE NATIONAL ACADEMIES

Advisers to the Nation on Science, Engineering, and Medicine

The **National Academy of Sciences** is a private, nonprofit, self-perpetuating society of distinguished scholars engaged in scientific and engineering research, dedicated to the furtherance of science and technology and to their use for the general welfare. On the authority of the charter granted to it by the Congress in 1863, the Academy has a mandate that requires it to advise the federal government on scientific and technical matters. Dr. Ralph J. Cicerone is president of the National Academy of Sciences.

The **National Academy of Engineering** was established in 1964, under the charter of the National Academy of Sciences, as a parallel organization of outstanding engineers. It is autonomous in its administration and in the selection of its members, sharing with the National Academy of Sciences the responsibility for advising the federal government. The National Academy of Engineering also sponsors engineering programs aimed at meeting national needs, encourages education and research, and recognizes the superior achievements of engineers. Dr. Charles M. Vest is president of the National Academy of Engineering.

The **Institute of Medicine** was established in 1970 by the National Academy of Sciences to secure the services of eminent members of appropriate professions in the examination of policy matters pertaining to the health of the public. The Institute acts under the responsibility given to the National Academy of Sciences by its congressional charter to be an adviser to the federal government and, on its own initiative, to identify issues of medical care, research, and education. Dr. Harvey V. Fineberg is president of the Institute of Medicine.

The **National Research Council** was organized by the National Academy of Sciences in 1916 to associate the broad community of science and technology with the Academy's purposes of furthering knowledge and advising the federal government. Functioning in accordance with general policies determined by the Academy, the Council has become the principal operating agency of both the National Academy of Sciences and the National Academy of Engineering in providing services to the government, the public, and the scientific and engineering communities. The Council is administered jointly by both Academies and the Institute of Medicine. Dr. Ralph J. Cicerone and Dr. Charles M. Vest are chair and vice chair, respectively, of the National Research Council.

The **Transportation Research Board** is one of six major divisions of the National Research Council. The mission of the Transportation Research Board is to provide leadership in transportation innovation and progress through research and information exchange, conducted within a setting that is objective, interdisciplinary, and multimodal. The Board's varied activities annually engage about 7,000 engineers, scientists, and other transportation researchers and practitioners from the public and private sectors and academia, all of whom contribute their expertise in the public interest. The program is supported by state transportation departments, federal agencies including the component administrations of the U.S. Department of Transportation, and other organizations and individuals interested in the development of transportation. **www.TRB.org**

www.national-academies.org

CONTENTS

ACKNOWLEDGMENTS

The research reported in this report was performed under direction of the Federal Highway Administration in collaboration with the National Cooperative Highway Research Program for NCHRP Project 12-84, "Guidelines for the Load and Resistance Factor Design and Rating of Riveted and Bolted Gusset-Plate Connections for Steel Bridges."

The author of this report would to thank the following for their contributions in conducting this research; it could not have been a success without their diligent efforts. First and foremost, I'd like to thank Dr. William Wright and Dr. Joseph Hartmann who were the first and second principle investigators on this project; they set the path of the project and I merely completed it. The following Turner-Fairbank Highway Research Center staff from the Structures Laboratory were integral in conducting the experimental testing: Fassil Beshah, Linfeng Chen, Kevin Deasy, Gary Greene, Paul Ryberg, Brian Story, Tim Tuggle, Robert Zobel, and interns Zachary May and Colby Nurse. Collaboration in developing the experimental program and the laborious task of conducting all the finite element simulations was completed by the Georgia Institute of Technology under the direction of Professors Roberto Leon and Donald White, Dr. Yoon Duk Kim, Yavuz Mentes, Mohammad Towhid Bhuiyan, and Jong Wan Hu.

Final thanks should be given to those who helped with internal Federal Highway Administration (FHWA) reviews of the work, namely Thomas Everett, Dr. Joseph Hartmann, Dr. Firas Ibrahim, Dr. Brian Kozy, and Lou Triandafilou.

ABSTRACT

This report presents the findings of an experimental and analytical investigation exploring the failure modes of steel truss bridge gusset plated connections. This research was conducted based on a recommendation provided by the National Transportation Safety Board at the conclusion of the I-35W Bridge collapse investigation. In particular, they recommended that gusset plates be included in the load rating process and the data produced in this project provides the justification to support the resistance equations for the various failure modes. Primarily the research focused on buckling and shear failure modes of gusset plates, including the effects of section loss, multi-layered plates, and edge stiffening. The project also presented a comprehensive review of past literature on the strength of hot-driven rivets. Resistance equations were defined and calibrated ϕ-factors are provided for each equation according to a load and resistance factor philosophy. Two-column draft specification language is provided for ready adoption into the American Association of State Highway Transportation Officials (AASHTO) LRFD Bridge Design Specifications and the AASHTO Manual for Bridge Evaluation.

EXECUTIVE SUMMARY

The collapse of the I-35W Bridge in Minneapolis, MN, on August 1, 2007, was attributed to a design error that underspecified the thickness of steel gusset plates connecting the truss members at a particular joint. Certainly the heightened awareness of an Interstate bridge collapse prompted national attention to the design and load rating of gusset plates. Up until that point, the AASHTO documents were unspecific regarding the design and rating of gusset plates leaving considerable discretion to engineers. After the collapse, bridge owners were highly encouraged to include gusset plates as part of the normal bridge rating, something not done routinely prior to the collapse unless there was a change in condition (i.e., corrosion, impact, cracking, etc.). To unify the load rating of gusset plates, the Federal Highway Administration (FHWA) published a guidance document outlining the minimum number of resistance equations that must be checked to adequately load rate a gusset plate. There were certain criticisms of the document and AASHTO (through the National Academies) along with the FHWA sponsored an experimental program to further enhance the understanding of gusset plate failure mechanisms and create proper resistance equations that could predict the various failure modes of gusset plates. These equations were to be consistent with a load and resistance factor philosophy.

The research conducted included both experimental and analytical modeling. Primarily the physical limitations and expense of experimental testing dictated that a small population of specimens would be tested to provide an adequate number of finite element model calibration points. Once a robust modeling philosophy could be established, then a much broader study of different connection geometries could be conducted analytically to encompass the types of gusset plates that are in the nation's inventory of truss bridges.

The experimental program specifically tested 13 full-scale gusset plate connections (though one was accidently destroyed). The members were reusable and each new specimen was only defined to be two new gusset plates and a set of chord splice plates. The configuration of the experimental connections used five separate members; two were collinear chords, one compression diagonal framing in at 45 degrees to the chord, one tension diagonal framing in at 45 degrees to the chord, and a vertical member that could be in either tension or compression framing in perpendicular to the chords. Six geometries of plates were tested that differed on how closely the compression diagonal was to the chords, how long the free edge was, and what type of fastener was used. In addition, four specimens were tested with simulated section loss and one specimen had edge stiffeners. One-half of the specimens failed by buckling of the gusset plate causing the compression diagonal to sway out-of-plane as a rigid body. The other half of the specimens failed by full width shear yielding along the horizontal plane just above the chord.

Analytical models of the specimens were used to define the level of detail needed to predict the experimental failure with certainty. It was found that a three-dimensional shell model of the gusset plates and members was necessary to properly predict the failure of the connection. For the purposes of shear yielding and buckling, fastener holes did not need to be modeled. However,

nonlinear material and geometric properties of the gusset plate were necessary along with initial geometric imperfections.

The robust finite element modeling technique was applied to a parametric study that increased the breadth and depth of studied connection geometries over the experimental study. In particular this included connections with diagonal framing angles other than 45 degrees, chords that were not collinear, corner joints, Warren and Pratt configurations, loading scenarios representing joints over a pier, at midspan, and near inflection points of trusses, gusset plates with edge stiffening, gusset plates with section loss, and multi-layered gusset plates. Due to the fidelity of the models, only buckling, shear yielding, and chord splice failure modes could be identified. The models did not have the fidelity to capture net section type failures.

Data from both the experimental specimens and analytical models were used to determine the best resistance equations to predict a particular failure mode. Since many bridge owners had begun to load rate gussets according to the initial FHWA guidance while this research was being conducted, it was decided to largely validate that guidance and change as little as possible unless warranted. For shear yielding, it was found that a plastic shear stress distribution could be used to predict shear yielding. For buckling, it was found that the Whitmore buckling model was appropriate, but recognizing it uses a column analogy to predict plate behavior, required an equivalent length factor of 0.5 for all gusset plates. In addition, the length of the Whitmore column should only use the length from the middle of the Whitmore section to the nearest adjacent fastener line. However, it was found that many compact connections still failed in buckling that was unconservatively predicted using the new Whitmore buckling model. In these compact geometries where the members are spaced very close together, buckling only occurred after a significant amount of yielding that was dominated by shear. In these situations, the buckling was better predicted by determining the load in a member that would cause a partial plane to yield in shear. The variability of the resistance equations was used in Monte Carlo simulations to define resistance factors according to a load and resistance factor philosophy. The ϕ-factors were provided at a variety of dead-to-live load ratios and two different reliability indices.

The resistance equations were found to be valid even for connections that had simulated corrosion. In this case, the average plate thicknesses remaining in a failure plane could be used reliably in the resistance equations. No correlation between edge slenderness and buckling resistance could be identified. However, stiffening a free edge was found to be an effective retrofit for connections that have low buckling resistance according to the Whitmore buckling theory. For connections where the buckling resistance is controlled by partial plane shear yielding, edge stiffening could not provide any enhancement in buckling resistance.

CHAPTER 1. BACKGROUND

The collapse of the I-35W Bridge has focused significant attention on the reliability and safety of truss bridges in the U.S. The National Transportation Safety Board (NTSB) concluded the collapse was attributed to under-designed gusset plates at the U10 nodes. [(1)] Roughly the plates were about half as thick as they should have been. The under-sized plates resulted in a large portion of the plate yielded in shear, which in turn lead to a reduced capacity against out-of-plane sway. Ultimately, failure of the U10 connection occurred when the compression diagonal swayed out of the main truss plane and the connection destroyed itself as it then fell through the compression diagonal. A forensic design review of all gusset plates in the bridge indicated that the gusset plates at the U10 and L11 nodes were all under-sized, clearly as the result of an error in the design process. [(2)] The intended margin of safety against connection failure was far below that of a typical truss design.

In its final report, the NTSB issued five recommendations to the FHWA and the American Association of State Highway Transportation Officials (AASHTO) to prevent such future catastrophes. These were:

1) Develop and implement a strategy to increase quality control measures for reviewing and approving bridge plans.

2) Develop guidance for owners regarding the placement of construction loads on bridges during construction and maintenance.

3) Require owners to assess regions where gusset plates cannot be inspected visually and recommend nondestructive techniques to assess hidden corrosion.

4) Revise inspection manuals and training materials to include guidance for gusset plates.

5) Require owners to include gusset plates as part of the load rating process.

To address the fifth recommendation, FHWA issued Technical Advisory 5140.29 in January 2008 stressing the need to check connection capacity along with member capacity in the load rating process. [(3)] Based on feedback from many sources, it became apparent that there was no clear consensus on the specific procedures to follow for design or rating of gusset plates. The AASHTO code is vague on the subject, leaving room for considerable engineering discretion and judgment in the process.

Load rating describes calculating how much live load an element can carry considering its current condition. To provide a uniform standard for load rating gusset plates, FHWA issued a guidance document in February 2009 based on the best available information on gusset plate design. [(4)] This document will herein be referred to as the "FHWA Guide" or "Guidance". Early experience showed that some of the truss bridges in service will fail certain limit-state checks

when analyzed with respect to the FHWA Guide. This is not surprising considering that the original bridge designers had considerable discretion and probably did not follow or know of the exact procedures outlined in the FHWA Guide. These inconsistencies generate a fundamental question: Is the FHWA Guide overly conservative or are many of the existing truss bridges inadequately designed?

Unfortunately, there is only limited research to support some of the provisions in the FHWA Guide. There has been limited experimental research on the ultimate strength of gusset plates, much of it directed to performance of tension members and their connections. There has been little experimental work on the compression capacity and stability of gusset plates and most of what exists focuses on bracing connections common in building structures. Only two references were found that report experimental results of ultimate capacity of large scale gusset-plated bridge connections. [5, 6] A meeting was held in April 2008 in Nashville, TN, to discuss gusset plate design provisions and to help refine the FHWA Guide provisions. This meeting was led by the Chairman (at the time) of the AASHTO T-14 Committee on Structural Steel Design, Ed Wasserman of Tennessee Department of Transportation (DOT), and included the following experts:

• Robert Connor	Purdue University
• Rick Crawford	Tennessee DOT
• John Fisher	Lehigh University
• Theodore Galambos	University of Minnesota
• Joseph Hartmann	FHWA
• Firas Ibrahim	FHWA
• John Kulicki	Modjeski & Masters
• William Wright	FHWA
• Joseph Yura	University of Texas/Austin

It became apparent following the meeting that there was insufficient research to fully support refinement of many of the limit-state checks in the FHWA Guide. There was no clear consensus among the experts on what procedures were best to perform stress and stability checks for gusset plates in compression, and no clear consensus on which checks might typically govern design. While it was generally acknowledged that the current draft of the FHWA Guide represents the best available knowledge on gusset plate design, it was also acknowledged that it may be overly conservative for some limit-state checks.

DISCUSSION ON GUSSET PLATE DESIGN

The following discussion examines the individual design checks in the FHWA Guide and sets the framework for the issues addressed by this research. Although no formal minutes were generated at the Nashville meeting, opinions from this group will be discussed where appropriate. In addition, some results from FHWA work on the I-35W Bridge failure

investigation will be discussed as they pertain to the limit-states examined. The discussion will also reflect results from a literature review of gusset plate research.

Throughout this document references will be made to the AASHTO LRFD Bridge Design Specifications herein referred to as the "BDS".[7] The AASHTO Manual for Bridge Evaluation will herein be referred to as the "MBE".[8]

Resistance of Fasteners

Numerous researchers have studied the performance of tension member connections for both bolted and riveted structures. The research has shown that connections are capable of redistributing load between fasteners as the connection nears ultimate capacity. Therefore, it is generally assumed that each fastener carries an equal share of the load (for non-eccentric connections less than 50 inches in length).

Trusses built prior to 1965 typically have riveted gusset plates but more modern bridges typically use high-strength bolts. Rivet capacity is an area of concern, particularly for rating older bridges built prior to the ASTM A502 Specifications for rivet strength. This project will review all available literature involving rivet tests to determine what capacities are supported by research. Beyond that, no experimental work to determine bolt or rivet capacity will be included in the present study.

It is possible, however, that the capacity of gusset plates will be somewhat different depending on whether rivets or bolts are used to assemble the connection. Bolted connections, particularly friction connections can be expected to be stiffer compared to riveted connections. This can possibly alter the way stress flows from the connected member into the gusset plate which can have an effect on the peak stress magnitude and location within the gusset plate. It can also alter the boundary conditions for stability analysis. This project will attempt to determine if this effect is significant and if different gusset plate design provisions are required for bolted versus riveted connections.

Gusset Plates in Tension

The basic capacity of gusset plates in tension is evaluated using the AASHTO provisions for the tension capacity of members (Section 6.8.2). The specific limit-state checks are for yielding on the gross section and fracture on the net section. It has become common practice to use the "Whitmore" method for determining both the gross and net section areas used for these two checks at member ends. Whitmore showed that this method provided a reasonable estimate of the elastic stress state observed in a series of scale model experiments.[9] Kulak and others have confirmed Whitmore's conclusions by analyzing gusset plates using the finite element method.[10]

There are several potential problems encountered in applying the Whitmore method to "tight" gusset connections where there is little space between members. It is common for the Whitmore

section from one member to overlap another, raising the question of how to handle interaction effects between members. There is no evidence to suggest a problem exists due to the Whitmore method providing unconservative results, but additional verification of results from a wide range of geometries would be valuable.

The AASHTO code also requires a check of block shear rupture resistance (Section 6.13.4). This failure mode has been studied by various researchers and various methodologies. Richard has proposed this type of check as a suitable approach for gusset plate design, but more study is needed to determine if it can be utilized to the exclusion of checking the Whitmore section.(11) Cai and Driver have recently provided recommendations that unify the block shear resistance calculation with other local limit-state yielding and rupture checks.(12) It is recommended in the "Design Guide for Bolted and Riveted Connections" that both the Whitmore and block shear checks should be performed with the lowest capacity controlling the gusset plate design.(10)

The typical method of checking the general capacity of gusset plates is to section the plate along various planes and calculate the resulting moment and shear on the free body diagram. Finite element results performed at FHWA for the I-35W Bridge suggest that this may not accurately capture the magnitude and location of maximum tension stress in the plate. Figure 1 shows the U10 gusset plate layout from the I-35W Bridge and defines section A-A along the bottom of the top chord. The member forces are calculated by a finite element model considering the dead load and all live load on the bridge at the time of failure.

Figure 2 shows the normal stress occurring across the horizontal plane below the chords for the U10 gusset plate assuming it was properly detailed with a 1.0 inch thick gusset plate (tension is positive). For reference the dashed line shows the theoretical stress state calculated by summing the moment and axial force from the free body diagram. The peak stress magnitude correlates fairly well between the theoretical prediction and the finite element results. However, there is a large discrepancy in the location of the peak stress.

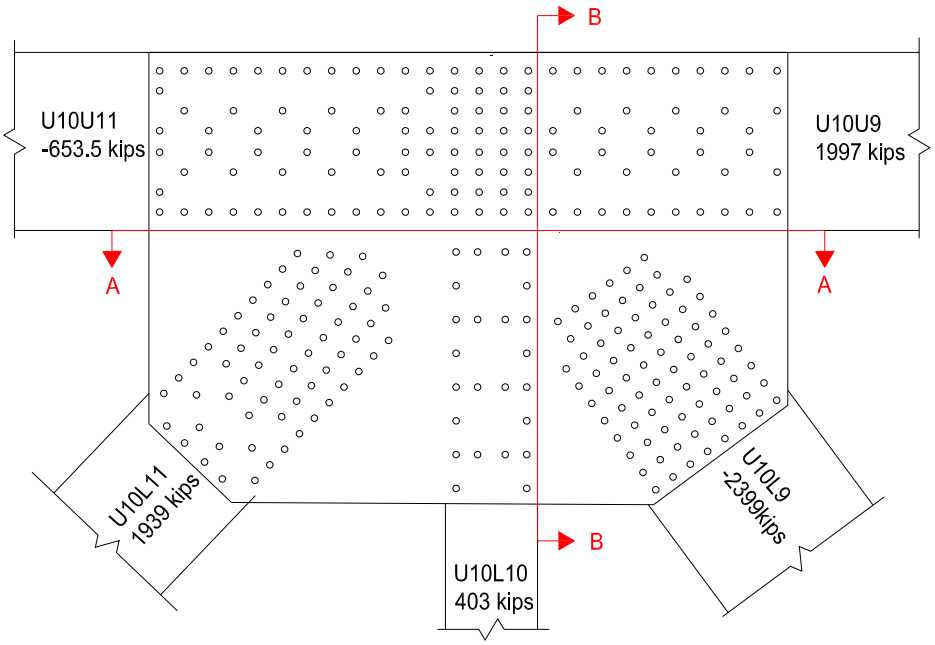

Figure 1. U10 gusset plate from the I-35W Bridge showing the plane for plotting stress distribution (A-A) from the finite element model results at FHWA.

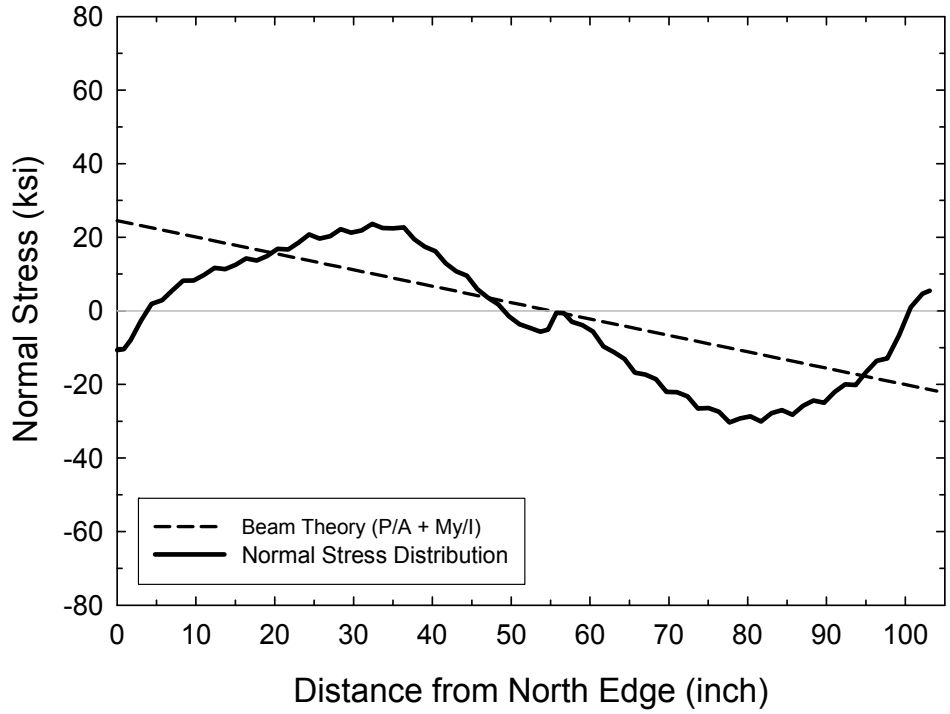

Figure 2. Elastic normal stress distribution along section A-A showing a comparison between the finite element model results and beam theory of a 1 inch thick gusset.

Gusset Plates in Shear

The fundamental shear resistance of gusset plates is (BDS Section 6.13.5.3):

$$\phi R_n = \phi_{vy}(0.58 A_g F_y \Omega) \quad \text{(Eq.1)}$$

The reduction factor Ω comes from BDS Section 6.14.2.8 and is taken as 1.0 if the shear stress distribution along the plane being checked is uniform. If the plate is not thought to be dominated by flexural shear then Ω is taken as 0.74. The theoretical parabolic shear distribution would result in Ω = 0.66 but this was considered to be an overly conservative reduction in shear resistance by the code authors. The factor of 0.74 represents a 10% relaxation of the theoretical parabolic shear distribution and is considered to be a more accurate basis to predict flexural shear resistance. LRFD defines the shear resistance factor as ϕ_v=1.00 but the FHWA Guide recommends using ϕ_{vy}=0.95 to be consistent with the resistance factor for tension yielding. It is not clear if this change is warranted, since the shear failure mode is not necessarily equivalent to the tension failure mode.

The FHWA Guide also recommends checking the ultimate shear capacity along the net section:

$$\phi R_n = \phi_{vu}(0.58 A_n F_u) \quad \text{(Eq. 2)}$$

The resistance factor for this check is recommended as to be consistent with the block shear provisions. Checking for shear rupture on the net section seems to be a logical extension of the block shear provisions, but this needs to be studied further. Many possible shear planes through gusset plates involve a significant net section. However, the AASHTO specification does not specifically require this check for shear in gusset plates. The need for this check will be explored further in the present study. If this check is needed, the appropriate reduction factor Ω needs to be determined. Since ϕ_{vu}=0.80 already provides an added factor of safety against this mode of failure, adding an additional reduction factor may be overly conservative.

One problem that arises when checking gusset plate shear is that neither the uniform nor parabolic shear assumptions apply in many cases. On most shear planes in properly designed gusset plates the amount of bending is minimal. This would suggest that the direct shear distribution should govern the design. However, the complicated load paths through the typical truss gusset plate result in a non-uniform stress distribution in which the peak shear stress substantially exceeds the uniform stress model. This peak shear is primarily caused by interaction between the direct stress paths for tension and compression through the plate and the average shear required for connection equilibrium. That is, there are local effects on the maximum stress that cannot be predicted well using beam theory.

Figure 3 shows the finite element results for a shear check along the A-A plane through the gusset plate at location U10 in the I-35W Bridge. Again, the plate thickness was increased from 0.5 inch to 1.0 inch to represent a properly designed gusset plate. For reference, the dashed lines represent the theoretical uniform shear and parabolic shear distributions. It can be seen that the

peak shear stress exceeds that predicted by the uniform shear distribution and is slightly less than that predicted by the parabolic shear model. It may be fortuitous, but the AASHTO flexural shear provisions ($\Omega = 0.74$) give a reasonable estimate of peak shear along the section for this example. However, it should be noted that the peak shear in the I-35W Bridge gusset plate is caused by stress concentrations at the ends of the diagonal members and not by bending along the horizontal plane.

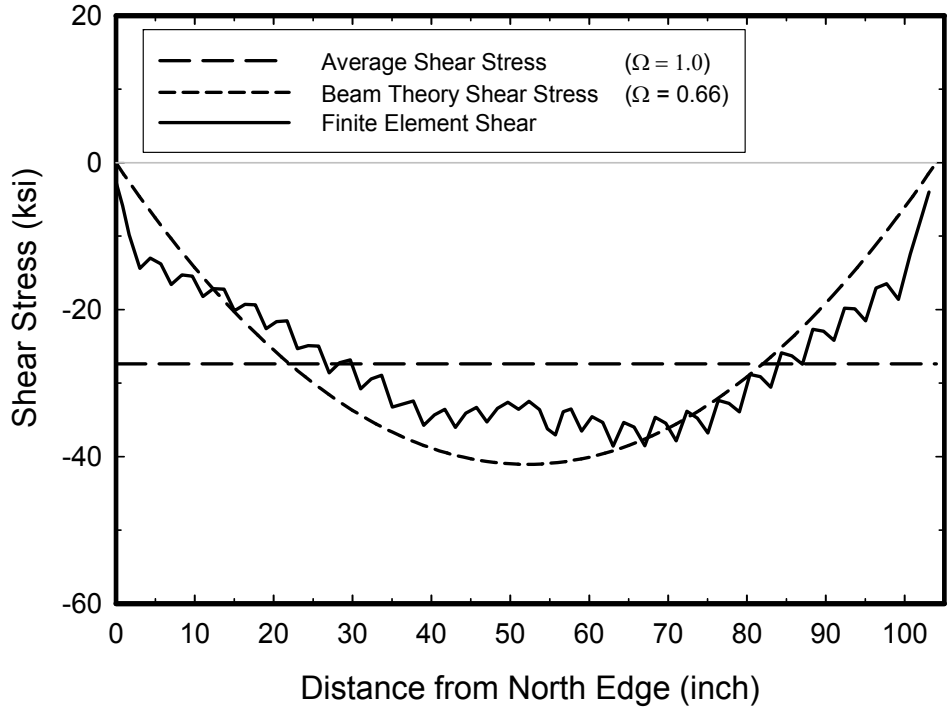

Figure 3. Elastic shear stress distribution along section A-A showing a comparison between the finite element model results and two different theoretical shear stress distributions (based on a correctly designed U10 gusset plate).

Although $\Omega = 0.74$ seems to work reasonably well for the I-35W Bridge example in predicting peak shear stress, more study is needed to determine if this is the correct factor to apply for shear resistance. Since the peak shear stress is not induced by flexure, it might be expected that different geometries and loading conditions will result in different reduction factors. More importantly, it needs to be determined if the peak shear is the most suitable basis for determining shear resistance. Setting the resistance level based on a localized stress concentration ignores the ability of the gusset plate to redistribute stress prior to reaching ultimate capacity. The present study will consider the inelastic redistribution of shear and determine if inelastic effects should be considered when predicting shear resistance. Inelastic action is already recognized in many parts of the AASHTO specifications when checking the capacity of members and connections.

Preliminary feedback from state DOTs involved in checking truss gusset plates indicates that many connections will have a rating factor in excess of 1.0 when shear calculations are based on

$\Omega = 1.0$, but will be less than 1.0 when $\Omega = 0.74$. Therefore, the method used to calculate shear resistance can have a substantial impact on evaluating bridge safety and determining the need for strengthening retrofits. This project will attempt to determine if the current AASHTO shear strength model applies to gusset plates and what reduction factor, if any, is needed to ensure safety. The project will also investigate alternate methods of checking shear resistance. One method that was discussed at the Nashville meeting was to calculate uniform shear on an effective area. In this case, areas of the shear plane where the capacity is compromised due to interaction effects or stability would be subtracted from the gross area for shear checks. Such a method will be explored in the current research. Overall, the goal is to determine a straightforward method of checking shear resistance that will define the minimum resistance required to ensure bridge safety.

Gusset Plates in Compression

There are a number of questions concerning the methodology used to evaluate the strength of gusset plates in compression. The AASHTO specifications provide little guidance in this area and it is essentially left to the designer to develop some sort of reasonable column or plate analogy to evaluate buckling capacity. Given the wide range of geometries encountered in gusset plates, it is unlikely that a single analogy will work for all cases. The current AASHTO specifications do, however, provide an edge slenderness limit for unstiffened edges that presumably ensure that the gusset plates perform as compact elements (i.e., this limit presumably ensures that resistance is not degraded by local plate buckling failure modes when the gusset plate is modeled to fail in a column buckling fashion).

Crush Capacity

The crushing capacity of the gusset plate in compression is usually assessed by evaluating the compressive stress at the base of the compression member using the Whitmore method. Reaching this limit-state obviously assumes that stability failure does not occur first. Experiments performed by Brown on gusset plates typical to building construction in compression showed that buckling of the free edge of the gusset always preceded crushing failure for the geometries tested.[13] If this conclusion can be verified for a comprehensive range of bridge truss gusset plates, then checking the crush resistance may not be required.

Stability

The methodology used to determine the critical buckling load for gusset plates is inexact at best. Given the complexity of the gusset geometry and loading, no exact solutions exist for this limit-state. Considerable engineering judgment is required to apply existing column or plate buckling solutions to the problem. The Nashville meeting showed that there is no clear consensus among experts about the best way to address this issue. A review of literature shows few studies of gusset plates in compression have been performed and those that exist were conducted on building connections. Modern finite element methods are capable of providing accurate estimates of buckling capacity but this requires considerable effort to develop connection-specific models.

Clearly an uncomplicated and consistent method of checking stability, even if the results are conservative, is a needed addition to the specifications.

Initially, to address stability, the model that best predicts buckling in gusset plates needs to be determined. Brown investigated both plate and column buckling analogies and concluded that the column analogy seemed to work best based on the experimental data. Lacking specific guidance, the FHWA Guide advises using the procedures in BDS Sections 6.9.2.1 and 6.9.4.1 for axial resistance of compression members. It is left up to the engineer, however, to determine the effective slenderness ratio, *KL/r* , to apply the equations to gusset plates. All three terms in this ratio can vary widely depending on assumptions made by the engineer.

Calculation of the terms "*L*" and "*r*" involves determining the shape of an equivalent rectangular column in the triangular area of the gusset plate. The FHWA Guide recommends using the Whitmore section to set the column width. The unbraced length is determined as the distance from the Whitmore plane to the closest adjacent member parallel to the axis of the compression member. This approach seems reasonable, but there is little research evidence to support the accuracy. The problem of applying the Whitmore section to tight connections still exists since it will typically overlap adjacent members or adjacent equivalent struts in the gusset plate. Brown observed that edge buckling always preceded buckling or crushing of the triangular area at the base of the compression member. If this can be verified for a wide range of gusset geometries, a stability check of the gusset at the base of the compression member might not be required.

The other inherent problem is determination of the K-factor for the gusset plate geometry. The FHWA Guide indicates that K ranges from 1.2 to 2.1 for gusset plates subject to sidesway, depending on the anticipated buckled shape. This topic was discussed at the Nashville meeting and it became clear that this is a judgment issue. The I-35W Bridge gusset plate at U10 appears to have failed in a sidesway buckling mode which suggests $1.2 < K < 2.1$ bounds the correct value. Finite element modeling performed by the FHWA suggests $K = 1.3$ when the FHWA Guide model is applied, assuming a gusset plate with adequate thickness. The FHWA Guide model is also suggesting that K varies between 0.2 and 0.5 when the model is braced to prevent sidesway buckling. The FHWA Guide recommends using $0.65 < K < 1.0$ for braced gusset plates, again depending on the mode shape assumed by the designer. Given that both the unbraced length and the K-factor have equal influence on buckling capacity and given that both terms are subject to engineering judgment, it is difficult to refine the value of either term to the exclusion of the other.

Possibly the most important provisions in the AASHTO specifications for the stability of gusset plates are the edge slenderness limits. As previously mentioned, Brown found that the buckling limit-state was associated predominantly with out-of-plane bending along the free edge of the gusset with relatively little change in axial load. This plate edge buckling was identified as the most important parameter affecting connection capacity. The FHWA modeling of the I-35W Bridge gusset plate failure shows that once the critical buckling load is reached there is a large change in lateral displacement at approximately constant load. This is consistent with the

behavior observed by Brown.[13] The FHWA model also shows that adding initial geometric imperfections along the gusset plate edge produces a significant reduction in the critical buckling load. Results show about a 40% capacity reduction when imperfections are added to the U10 node model within expected tolerances. This suggests that edge stiffening may be a very effective means to increase or ensure gusset plate capacity.

The AASHTO specifications provide the following edge slenderness limit for unstiffened gusset plates in compression (Section 6.14.2.8):

$$\frac{l}{t} \leq 2.06\left(\frac{E}{F_y}\right)^{1/2} \qquad \text{(Eq. 3)}$$

The exact origin of this limit has not yet been determined. However, this limit was present in the 1963 AASHO Specifications and the 1985 AASHTO Guide Specifications for Strength Design of Truss Bridges (Load Factor Design), and it has been carried forward into the current LRFD Specifications. Brown speculates that this limit was derived based on a plate buckling model for gusset plates.

The origin and applicability of this limit needs to be thoroughly investigated in the proposed research. Presumably the intent of this limit is to ensure that gusset plates behave as compact sections (i.e., no degradation of the equivalent column flexural buckling resistance) prior to developing their intended strength. The finite element modeling performed at FHWA indicates that meeting this limit alone would not have prevented buckling as the mode of failure when the U10 gusset plates reached their ultimate capacity. The FHWA model investigated the effect of gusset plate thickness on the behavior of the U10 connection in I-35W, varying the thickness from 3/8 inch to 1.5 inches. The failure mode, sidesway buckling, remained essentially the same even down to a plate edge slenderness of $^{l}/_{t}$=20 . It is possible that the current requirement was derived assuming sidesway was prevented in the connection.

An edge slenderness requirement, if one can be determined, that prevents gusset "local" buckling would be a very straightforward check in the evaluation of gusset plates. In design, the most cost effective solution for plates failing this requirement is probably to increase plate thickness. For existing bridges, addition of edge stiffening provides a relatively cost effective retrofit. For these reasons, the research project will thoroughly investigate the edge slenderness limit and the effect of this limit on different potential gusset plate failure modes. The FHWA Guide currently states that the AASHTO edge slenderness limit should not be checked as part of the rating process. This needs to be examined closely in this study. Some sort of compactness criteria will be needed to enable consideration of inelastic capacity for other strength checks of gusset plates.

Inspection and Retrofit

The primary purpose of inspection is to look for changes and deterioration in a bridge's condition that would affect its ability to perform in service. For gusset plates, the two applicable

deterioration mechanisms are corrosion and fatigue. Of the two, corrosion is clearly more important from a strength perspective. General experience has shown that fatigue cracking has not been a significant problem in truss bridge gusset plates. Normally the live load stress range is below the fatigue threshold so infinite life is expected. This conclusion may change if significant pitting or pack-out corrosion exists as these forms of deterioration can amplify stresses significantly. Since corrosion will probably always precede the onset of fatigue, evaluating the impact of corrosion is the primary need for the present study.

Corrosion can have a significant effect on the compression and tension capacity of gusset plates. This was clearly demonstrated by the failure of the gusset plate in the I-90 Bridge over Grand River in Ohio.[14] Significant corrosion loss reduced the capacity of the gusset plate at a lower truss connection adjacent to one of the main piers, allowing the plate to buckle. In this case, the compression diagonal went into bearing and prevented collapse even though the critical buckling load for the gusset plate was exceeded. The U10 gusset plate in the I-35W Bridge also failed by buckling although inadequate design, not corrosion, was the primary cause.

Assessment of the capacity of gusset plates with corrosion damage is not always a simple procedure. Prucz and Kulicki indicate that when the corrosion is moderate and uniformly distributed it is appropriate to analyze the gusset plate as a member with reduced thickness.[15] This approach probably works well for checking stress in the gusset, particularly for tension members, as long as there is no severe pitting or other localized section loss. Severe pitting will induce local stress concentration effects that will create a more severe condition than that predicted by average section loss calculations.

The effect of section loss on compression stability is more difficult to analyze. Corrosion in gusset plates is typically more severe in the localized areas along the edge of members where debris accumulates. This localized weakening of the plate can significantly change the boundary conditions assumed in buckling models. Since the buckling models used for gusset plates already involve many assumptions, it is difficult to assess this boundary effect without further research. It is also common to have conditions where crevice corrosion and pack rust induce out-of-plane deformation in the gusset plate. This again will alter the fundamental assumptions of the buckling model.

The presence of corrosion in gusset plates further complicates the already complicated models used to evaluate stability. However, this is a very real concern for engineers faced with rating existing truss bridges. The second experimental phase of this study will try to address this issue by performing tests on gusset plates with simulated corrosion damage. Better guidance will be developed for assessing the effect of corrosion on the compression capacity of gussets.

It is probably too ambitious to develop comprehensive gusset retrofit guidelines under this project. The primary focus will concentrate on methods to determine gusset plate capacity. If the capacity is determined to be inadequate, the option always exists to replace or add doubler plates

to the gusset. While effective, this is typically a very costly and time consuming operation and is best avoided unless absolutely necessary.

The FHWA modeling of the U10 gusset plates on the I-35W Bridge showed that edge stiffening will provide a significant strength increase to gusset plates in compression. Compared to the alternatives, edge stiffening is a relatively simple and inexpensive retrofit to perform. Therefore, this research will include experiments to determine the effect of edge stiffening. An attempt will be made to develop guidelines for evaluation of edge stiffened gussets under this project.

There are very few cases where in-service truss bridges have failed. The I-35W Bridge failed in a catastrophic manner, but a severe design error made this structure artificially weak. There are several examples of partial bridge failures where gusset plates were considerably weakened by section loss due to corrosion. For example, four deteriorating corroded steel plates supporting the eastbound I-90 Grand River Bridge in Perry Township, Ohio, buckled in 1996 while work crews were preparing them for painting. The partial collapse dropped part of the span 3 inches. No one was hurt, but the bridge was closed nearly six months for repairs that cost $1.6 million.[1, 14] However, while deterioration always needs to be considered with regard to the performance of existing structures, these failures are primarily a maintenance issue and not a gusset plate design issue. In addition, very few new truss bridges are currently being built around the country since other design types are generally more cost effective. Therefore, the dominant issue with truss bridges is rating of the existing inventory, including bridges that have some degree of corrosion damage.

SELECTION OF REPRESENTATIVE JOINTS

Before the larger experimental and analytical studies were undertaken, the NCHRP panel requested the research team to model typical gusset-plated connections to help guide the research project, and to possibly offer immediate relief to the provisions of the FHWA Guide. This section will briefly describe those modeling efforts and some of the results derived from them. It must be pointed out that this was the project's first attempt at modeling joints and as the project evolved, so did the finite element modeling methodology. The modeling methodology is described more in Chapter 2 and Appendix I, but exact details for these joints can be found in the work performed by Mentez.[16] This portion of the work is only meant to convey a broad overview of this early modeling effort and not necessarily convey more detailed aspects of how the models were created.

Five joints were selected by the research team for further study. One joint was the I-35W U10 joint because FHWA had performed the forensic analysis and it was an obvious joint to include. The other four joints are all based on the original design drawings without considering any changes that occurred during the life of the bridge. The forces on some members are changed from the original design, which give only envelope values, to obtain equilibrium in the FEA truss model. In addition, assumptions for the material and fastener models had to be made. Specific attributes of each selected connection are explained in detail below:

a) Original I-35W Bridge over Mississippi River (MN)

This joint (shown in Figure 4) was pinpointed as the failure trigger to the collapse of this bridge and actually represents a true failure point. The joint was located two panel points off the pier and was approximately located at the theoretical inflection point of the continuous structure. As such, the joint was subjected to a large horizontal shear force. At failure, much of the horizontal plane was yielded and ultimately the gusset plate buckled and the compression diagonal swayed out-of-plane leading to an overall rupture of the connection. Some of the modeling details were first reported in Ocel and Wright [17], those not covered in that report were completed as part of this project.

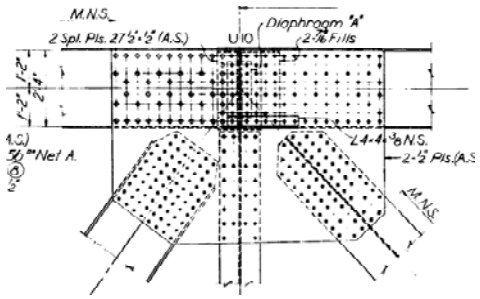

Figure 4. I-35W U10 joint geometry.

b) I-94 Bridge over the Little Calumet River (IL)

The L2 joint (shown in Figure 5) from the I-94 Bridge over the Little Calumet River Bridge in Cook County, IL, is selected. This bridge is a deep truss with a substantially steep (60° from horizontal) angle for the diagonal members. The diagonals have a relatively large distance from the work point of the joint resulting in a relatively long gusset plate free edge between the compression diagonal and the chord member. This joint is a relatively modern bridge design using high-strength bolts (1990).

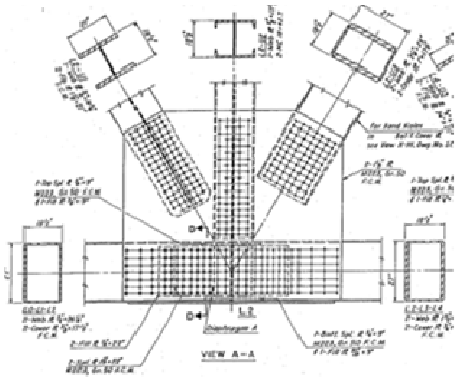

Figure 5. I-94 joint geometry.

c) HW-23 Bridge over the Mississippi River (MN)

The U2 joint (shown in Figure 6) from the Highway 23 Bridge over the Mississippi River in St. Cloud, MN, is selected since it has relatively flat angles for the diagonal members (37° from horizontal), resulting in a relatively long gusset plate free edge between the diagonal members and the vertical member. The Minnesota Department of Transportation found "buckled" gusset plates in this bridge and it was decommissioned after rating calculations indicated a possible unsafe condition. This bridge is a representative design from the 1950s utilizing welded members and riveted gusset plate connections.

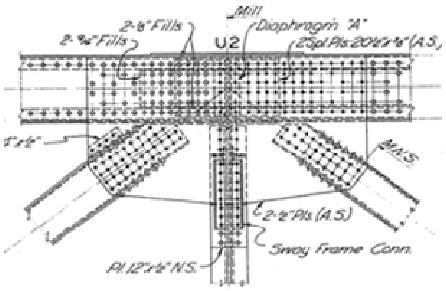

Figure 6. HW-23 joint geometry.

d) I-40 Bridge over the French Broad River (TN)

The U8 joint (shown in Figure 7) from the I-40 Bridge over the French Broad River in Jefferson County, TN, is selected since it provides an example with shingle (double) gusset plates. Similar to the HW-23 Bridge, this bridge also represents a 1950s design with welded members and riveted gusset plate connections.

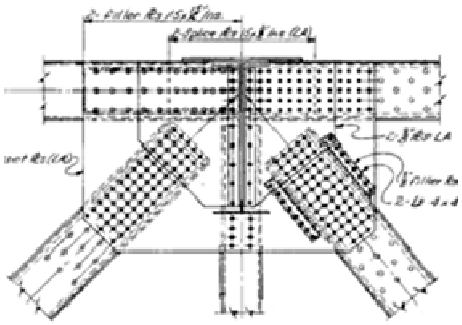

Figure 7. I-40 joint geometry.

e) I-80 Bridge over the Clarion River (PA)

The last connection selected for the preliminary studies is the hypothetical joint used in the FHWA Guide as an example. The connection is a modification of the L3 joint (shown

in Figure 8) in the I-80 Bridge over the Clarion River in Pennsylvania. FHWA made changes to the joint to facilitate the illustration of the guidance provisions. These changes include the angle of chord members, the reduction in gusset plate strength from 50 to 36 ksi, and an increase in member forces as compared to the original design.

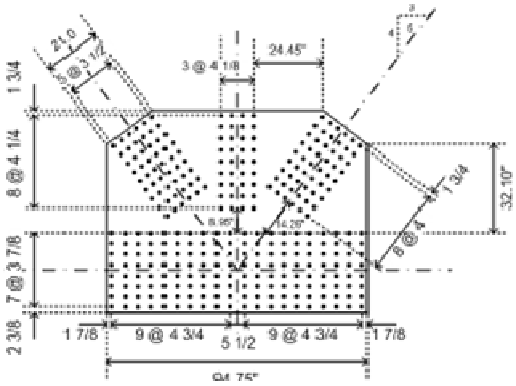

Figure 8. I-80 joint geometry.

Analysis Procedure

Nonlinear finite element analysis of the four joints was performed using the Abaqus analysis engine and the nodal loads calculated from the original design drawings.[18] Both dead load (DC) and live load plus dynamic load allowance or impact (LL+I) are imposed on the truss members using the appropriate load factors for LRFD Strength I load combination. The member forces in the model are set so that the forces exactly match the envelope values for the compression diagonal and the chord member nearest to it. Adjustments are required for the forces in the remaining three members relative to the values on the engineering drawings to satisfy the joint equilibrium (the forces on the engineering drawings are envelope values). The main reason for the equilibrium mismatch is the force in the vertical member of the truss. For trusses with parallel top and bottom chords, this is ideally a zero force member or it is subjected to relatively small loads directly applied from the deck system of the bridge.

The analysis is implemented in two steps. First, the factored dead load is applied to the truss nodes. Second, the factored live load plus impact load is incrementally applied. From the analysis, the total factored load at any stage of the loading for the first five joint analyses can be calculated using Equation 4. A wearing surface component is included in the equation because that information was available for the I-80 joint. For the other joints, all dead load was assumed to be from components (i.e., DC).

$$P_{FEA} = \gamma_D(DC) + \gamma_{DW}(DW) + ALF\left[\gamma_{LL+I}(LL+IM)\right] \quad \text{(Eq. 4)}$$

The term "ALF" used in the equation represents the Applied Load Fraction (i.e., the multiple) of the factored LL+IM loads applied at a given stage of the finite element analysis. The load factors are taken as $\gamma_D = 1.25$, $\gamma_{DW} = 1.50$ and $\gamma_{LL+IM} = 1.75$ corresponding to the Strength I limit-state.

Failure Determination

With the exception of the I-35W joint, members had to be modeled with elastic properties to identify the failure mode of the gusset. Had they been modeled with inelastic properties the members would fail before the gusset plate. This means four of the joints represented properly designed connections that were stronger than the members they connected.

The primary mode of failure in the finite element model is difficult to define in most cases since multiple failure modes are often occurring simultaneously. However, the analyses show that a significant amount of the gusset plate material reaches the yield strength limit based on the Von Mises yield criterion prior to the ultimate load. It is important to decide the load level at which the gusset plate reaches its analytical resistance. However, the gusset plate may reach a "limit of maximum useful resistance" prior to achieving a limit load in the analysis due to other factors such as significant plasticity or excessive fastener displacement. Therefore, the following three load levels are considered in assessing the joint response; the first one reached determines the resistance of the joint.

1) 4% equivalent plastic strain (PEEQ) at mid-thickness

   In the finite element models, the actual bolt holes are not modeled and fracture of the steel is not incorporated into the nonlinear material model. Hence, the models cannot capture net section limit-states. Typically the gusset plates undergo a significant amount of plasticity beyond the Strength I limit. This criterion is indicative of when ductile fracture may start to be of concern. This value is arbitrarily set at 4%, but the experience of the research team has found this to be an indicative strain level where faith in the model may begin to become unreliable (i.e., when net section failures may occur considering net sections are not modeled.

2) 0.2 inch fastener shear displacement

   The fastener models used in the analyses are also nonlinear. The ALF value at a fastener shear displacement of 0.2 inches is decided to be a practical limit of fastener useful resistance. Fastener shear fracture may start to be of concern for shear displacements beyond this limit.

3) Peak of the load versus displacement curve

In general, the load versus displacement curve from the analysis has a loading and a post-peak unloading path. The peak ALF value from this plot is another important limit for the joint response.

RESULTS OF TYPICAL JOINTS

This section discusses the observations from the nonlinear finite element analysis performed on each of the joints. A brief summary on the initial imperfection sensitivity and stress and strain distributions within the gusset plates at the Strength I and ultimate resistance levels are provided respectively. As the FEA model does not always create output exactly at ALF = 1.0 , the load step closest to 1.0 is chosen as the Strength I load level for output of the stresses and strains. All stress contours in this section are presented as the Von Mises stress to show the combined effect of all the stress components toward yielding. In addition, the equivalent plastic strain contours (PEEQ contours) are presented to show the plasticity patterns and degree of yielding in the gusset plates.

I-35W U10 Joint Analysis

The U10 connection utilized 0.5 inch thick gusset plates fabricated from grade 50 material connected together with 1 inch A502 Grade II rivets. The NTSB concluded this connection failed due to a design error leading to gusset plate thickness roughly half as thick as necessary to carry the design loads. [(1)] The ultimate failure of the connection was inelastic sidesway buckling of the gusset plate after a significant portion of the plates reached yield along the horizontal plane and at the base of the compression diagonal.

The finite element load-displacement plot shown in Figure 9 indicates the connection failed at *95% of the 1.25DL portion of the Strength I* load combination. This is not surprising given the under-designed condition of the gusset plates. The primary failure mode of the model was sidesway buckling of the gusset plate that displaces the compression diagonal out-of-plane. Simultaneous gross yielding occurred along the A-A plane. Figure 10 shows the normalized Von Mises stress contours at the point when the model became unstable. The red contour indicates areas very close or just exceeding the yield strength. The equivalent plastic strain contour shown in Figure 11 more clearly shows the areas where plastic deformation is occurring (any contour other than dark blue is actively yielding). This is most pronounced around the base of the compression diagonal and along the horizontal plane along the chords.

Figure 12 shows the normal and shear stress distributions along the horizontal plane at peak load. Each of the stress plots has been normalized by the factored design stress for shear and bending, respectively. Both distributions are disturbed in the area around the compression diagonal (70-104 inches on the x-axis). This is caused by out-of-plane bending and the resulting P-Δ effects on gusset plate stress. The plot clearly shows that the shear capacity has been reached along much of the horizontal plane. This effectively softens the plate and reduces the out-of-plane stiffness resisting sidesway.

Figure 13 shows the shear and normal stresses occurring along the B-B plane. The B-B plane stresses are harder to interpret because of the out-of plane bending effects around the compression diagonal. The normal stress certainly does not follow a linear bending stress distribution as it decreases toward the bottom edge of the plate and it is very uniform along the top 30 inches. The chord members are roughly 29 inches deep and the uniform normal stress distribution shows that the gusset plate is primarily acting as a chord splice in this region. Superposition of bending and axial stress distributions cannot be assumed valid across the entire plane due to yielding.

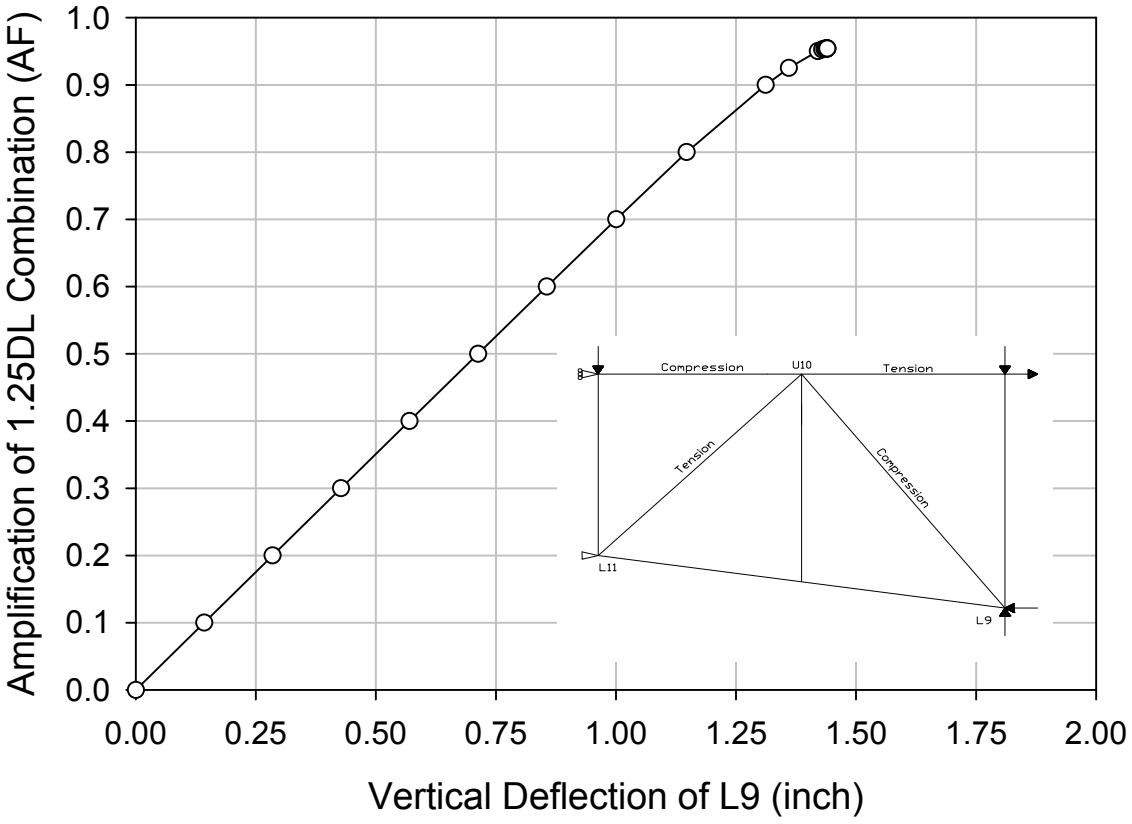

Figure 9. Load-Displacement plot for 0.5 inch gusset plates.

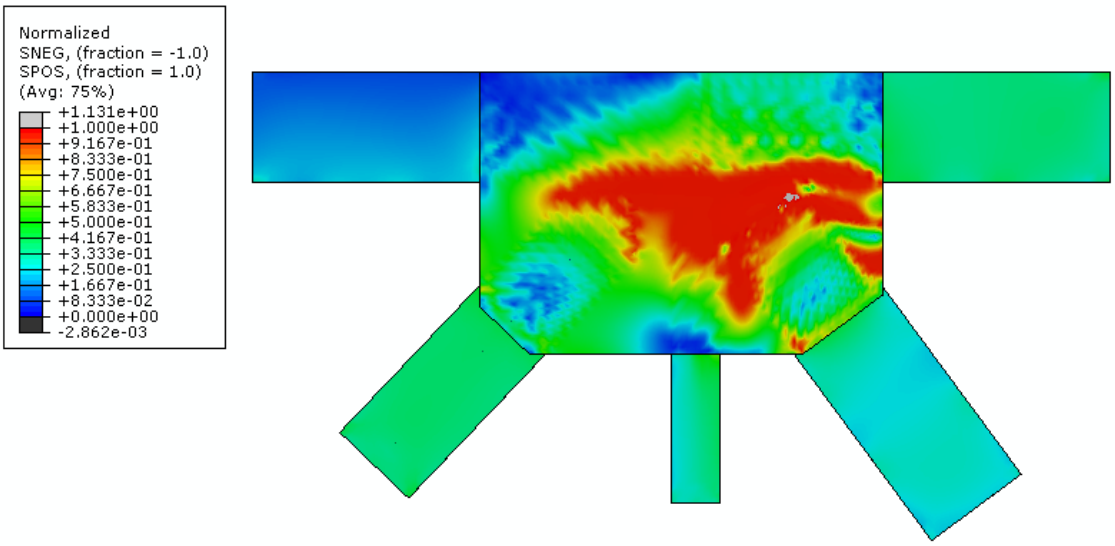

Figure 10. Von Mises stress contour normalized to the yield stress at the peak load for I-35W U10 connection.

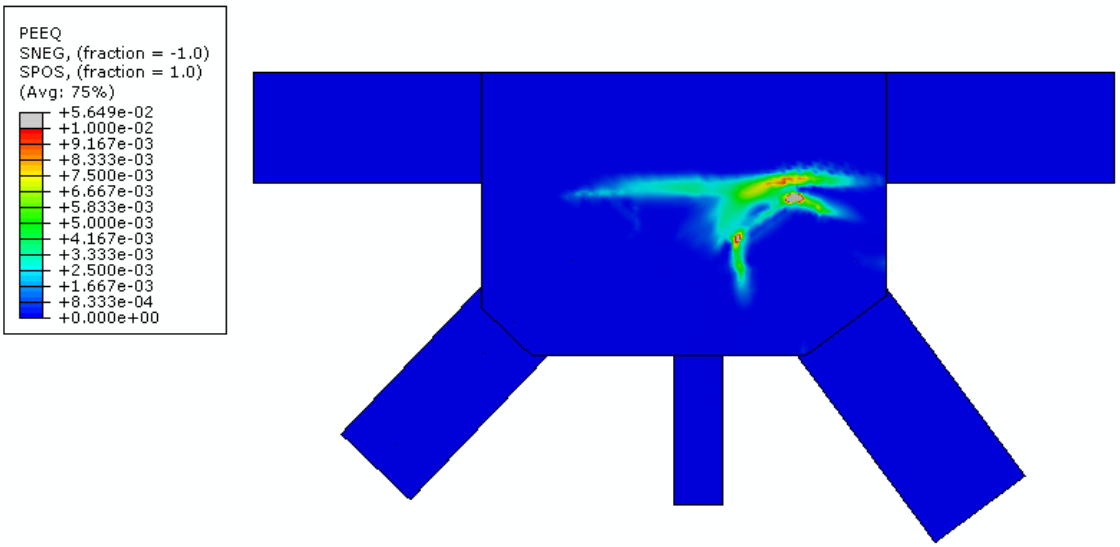

Figure 11. Equivalent plastic strain plot at failure for I-35W U10 connection.

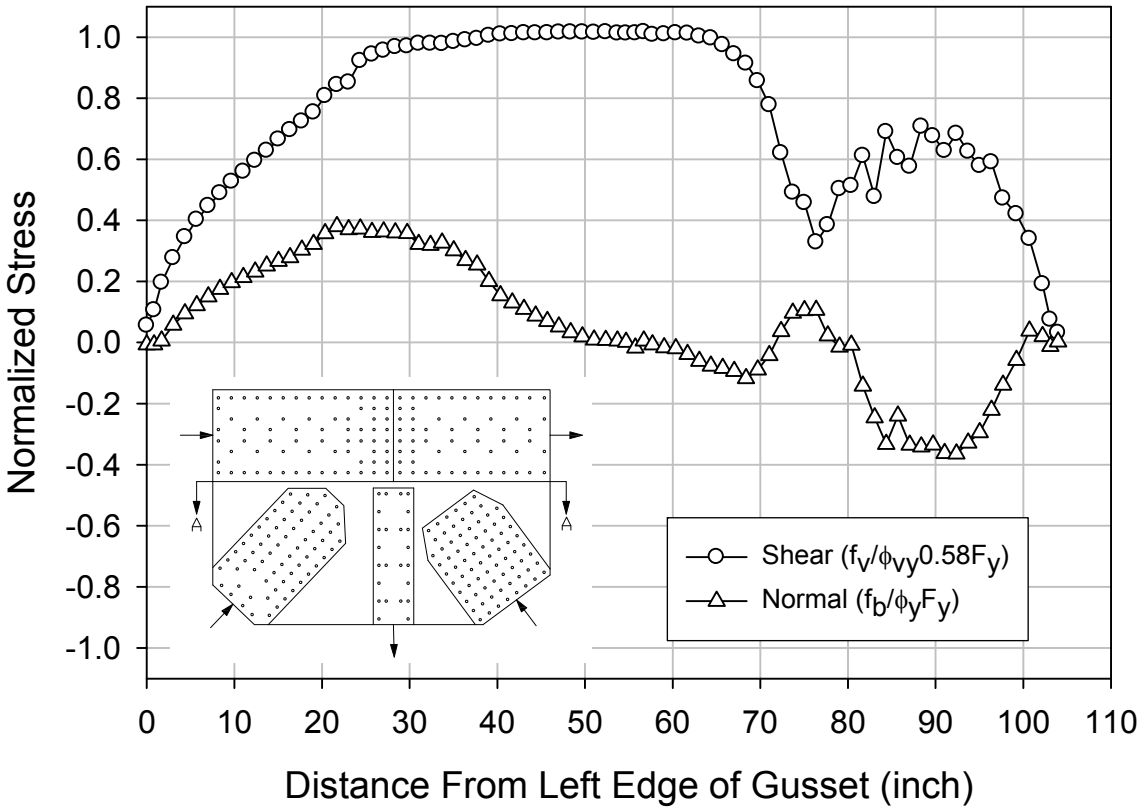

Figure 12. Section A-A mid-thickness shear and normal stresses at connection failure.

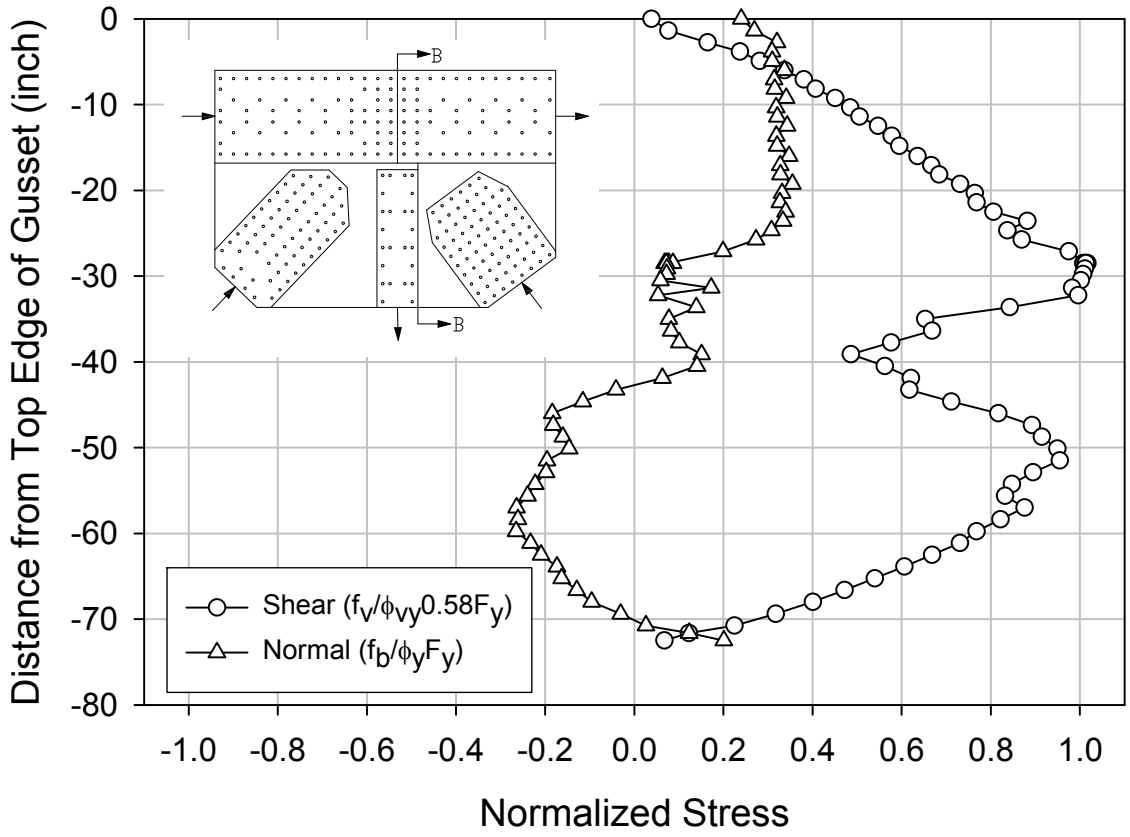

Figure 13. Section B-B mid-thickness shear and normal stresses at failure.

I-94 Bridge (Joint L2)

Based on the criteria defined at the beginning of this chapter, important load levels are identified on the ALF vs. out-of-plane displacement plot as shown in Figure 14. The Strength I load level occurs at an ALF=1.05. The 4% PEEQ limit is reached just after the peak load. Without showing a figure, the maximum stress in the gusset plate at the Strength I limit is approximately 25 ksi, or about half of its yield strength. Therefore, this connection has a considerable amount of reserve capacity beyond the Strength I load level.

The Von Mises stress state in the gusset plate corresponding to the limit load at ALF = 9.72 is shown in Figure 15. The plate has reached its yield strength at its mid-thickness at areas shown with the grey contours. Figure 16 shows the corresponding equivalent plastic strain contours. The material that is still elastic is shown as dark blue, while the light blue and green areas indicate the variation of higher magnitudes of plastic deformation. The largest amount of plastic deformation occurs in the region between the compression diagonal and the chord member. The displaced shape, shown in both figures with a deformation scale factor of 5.0, confirms that the final joint mode of failure is out-of-plane compression buckling of the gusset plate.

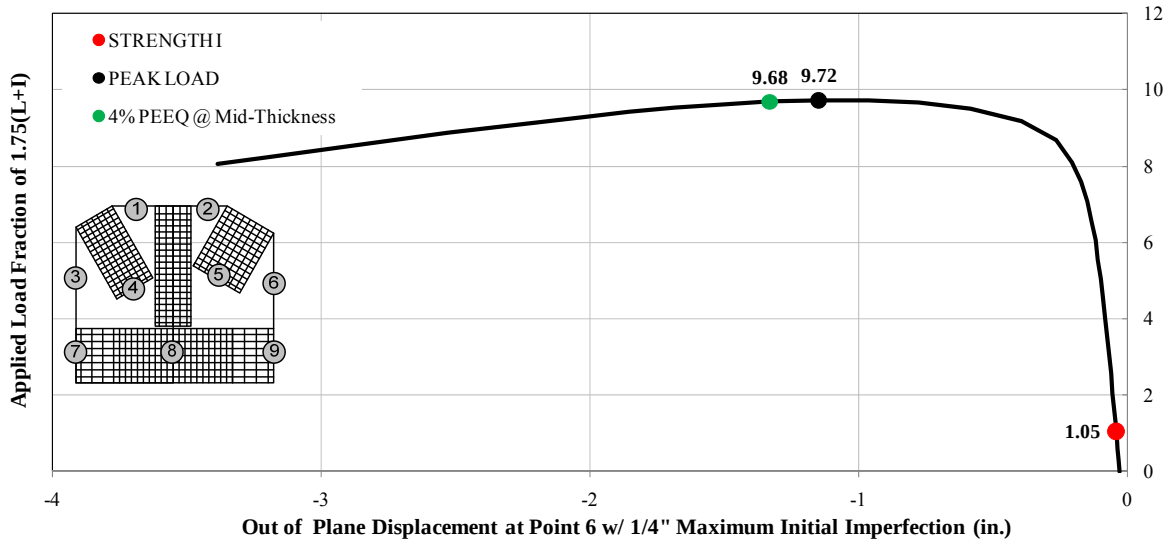

Figure 14. Plot of out-of-plane displacement motion of Point 6 versus the ALF.

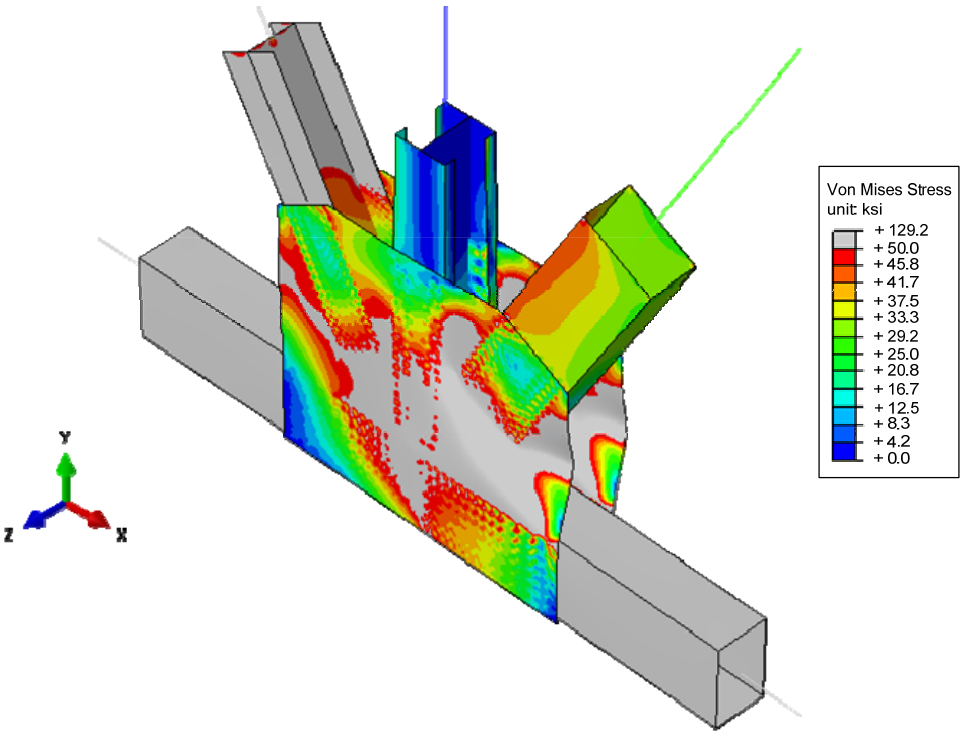

Figure 15. Von Mises stress response contours at the limit load (ALF=9.72).

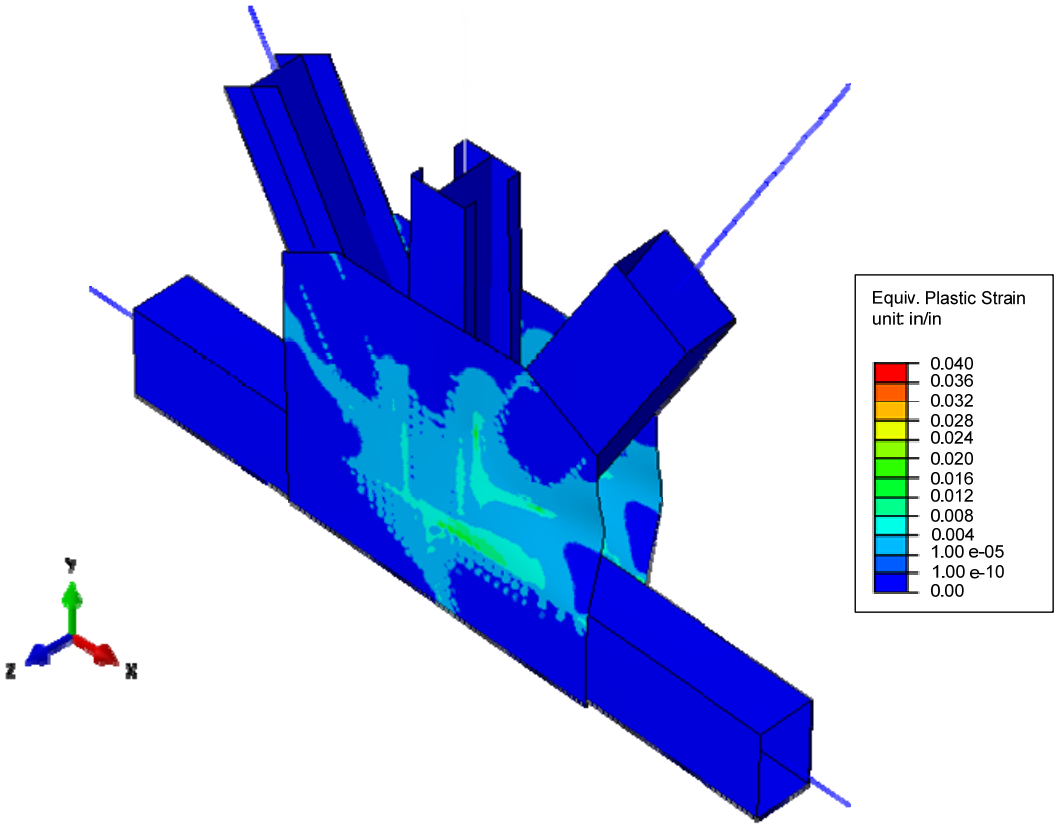

Figure 16. Equivalent plastic strain response contours at the limit load (ALF=9.72).

HW-23 Bridge (Joint U2)

Figure 17 shows the important load levels on the ALF versus out-of-plane displacement plot. At the Strength I load the ALF=0.97 at which point the gusset plate was entirely elastic. Similar to the previous case the usefulness of the connection is determined by the peak load at an ALF=2.70 and the 4% PEEQ occur well beyond the peak load. This also demonstrates that the connection has reserve capacity to extend almost three times beyond the Strength I load level.

The Von Mises stresses in the gusset plate corresponding to the peak load at an ALF = 2.70 is shown in Figure 18. The plate reaches its yield strength at areas shown with grey contours. Figure 19 shows the corresponding equivalent plastic strain contours. The largest amount of plastic deformation is occurring in the splice region and the horizontal plane just below the chord members. The displaced shape observed in both contour plots with a deformation scale factor of 5.0 also confirms that out-of-plane compression buckling of the gusset plate does occur. However, these two plots show the difficulty in interpreting the results as likely this connection would first suffer failure of the chord splice (though it is a compression chord splice that could go into a bearing condition and suppress that failure mode), followed by horizontal shear and/or buckling around the compression diagonal.

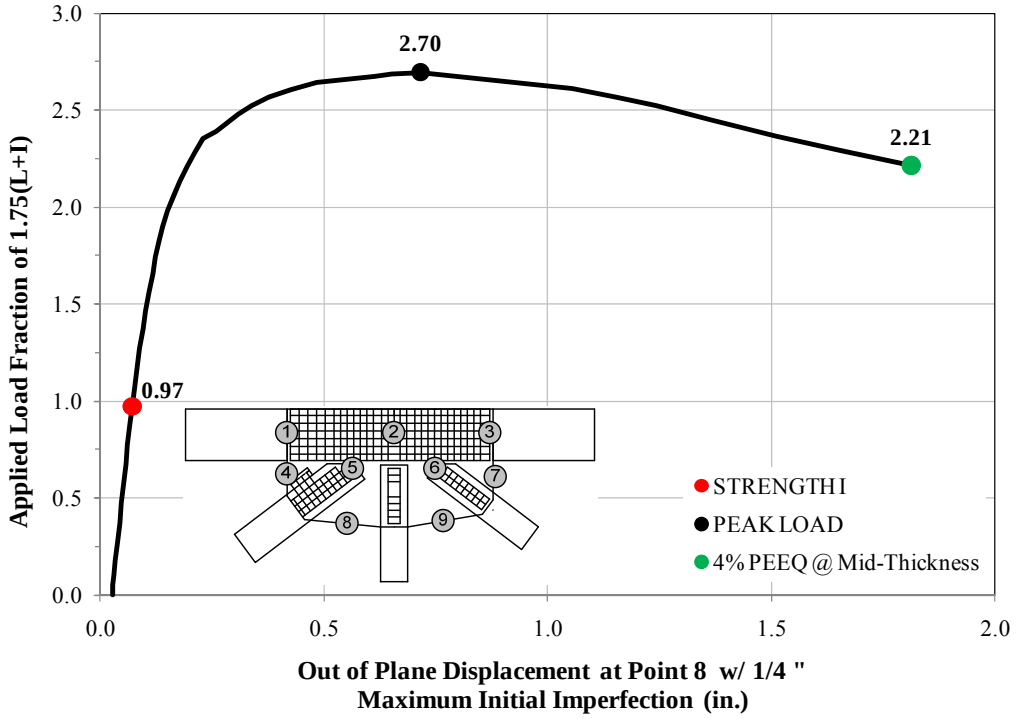

Figure 17. Plot of out-of-plane displacement motion of Point 8 versus the ALF.

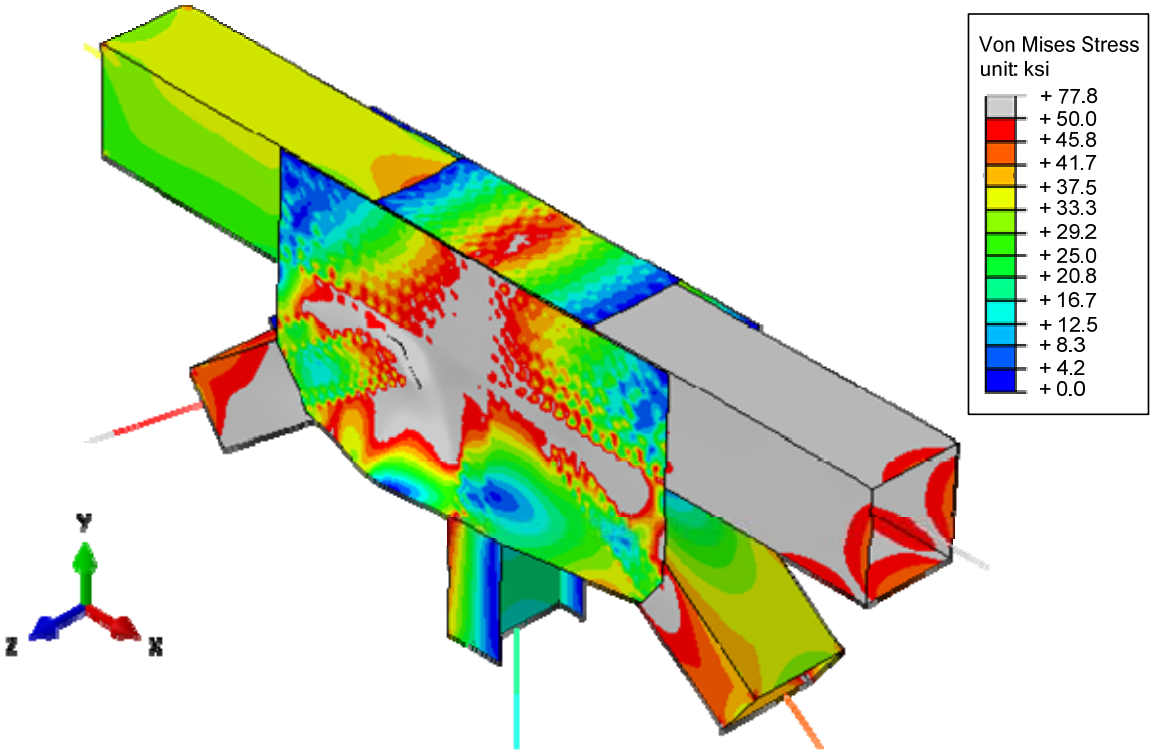

Figure 18. Von Mises stress response contours at the limit load (ALF=2.70).

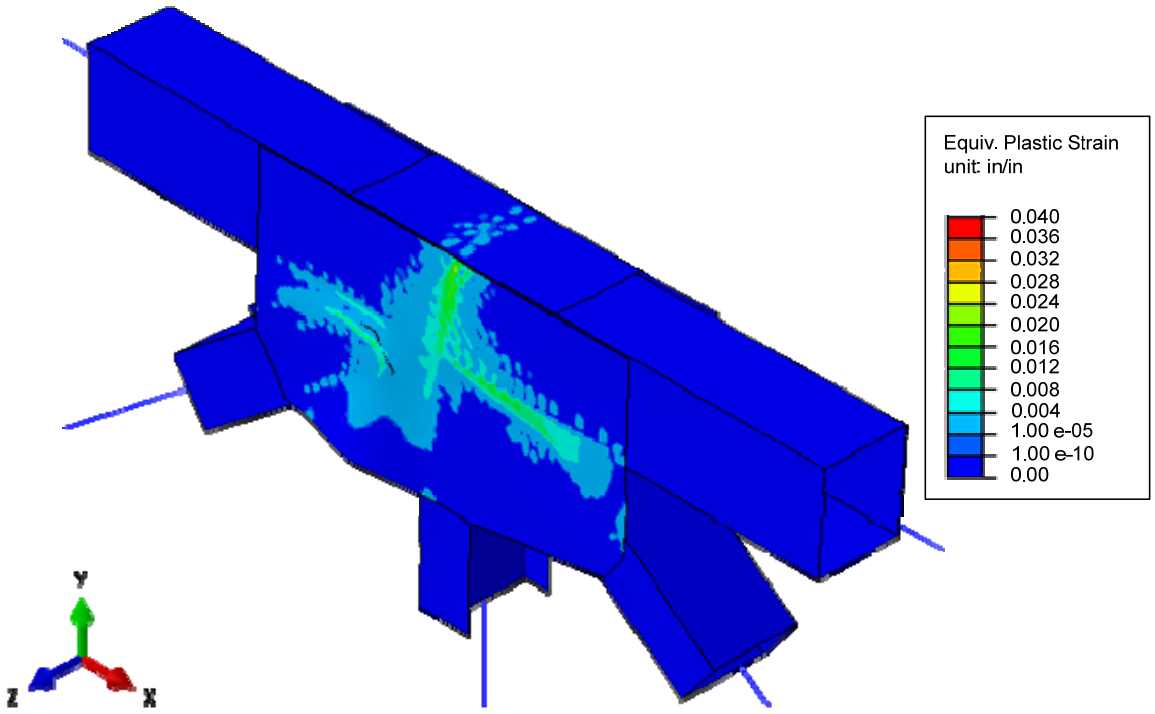

Figure 19. Equivalent plastic strain response contours at the limit load (ALF=2.70).

I-40 Bridge (Joint U8)

Important load levels on the ALF versus the out-of-plane displacement plot are shown in Figure 20. The Strength I load occurs at an ALF = 1.04 where the entire connection was elastic. For this connection, the maximum usefulness of the connection is dictated by the strength of the fasteners in the chords as the 0.2 inch fastener deformation limit first occurs at an ALF=2.16, which still shows this connection has considerable capacity beyond the Strength I limit. The shear rupture of the critical fastener is precipitated by extensive tension yielding of an inside web splice plate in the chord, resulting in redistribution of shear forces to the plane between the chord and the gusset.

The Von Mises stresses at an ALF = 2.16 is shown in Figure 21 where grey contours show areas exceeding yield which are limited to the primary gusset plate. Figure 22 shows the corresponding equivalent plastic strain contours at the same load level. The shingle plate does not have plastic strains although the plasticity is significant in the gusset plate at this load level. The displaced shape observed in the contour plots with a deformation scale factor of 5.0 also confirms that buckling of the gusset plate does not occur for this joint.

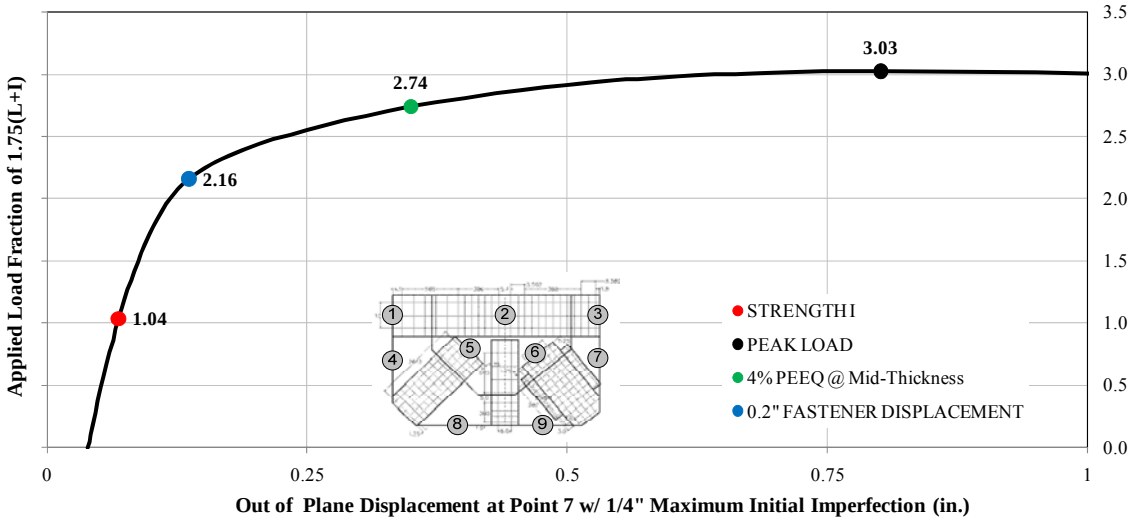

Figure 20. Plot of out-of-plane displacement motion of Point 7 versus the ALF.

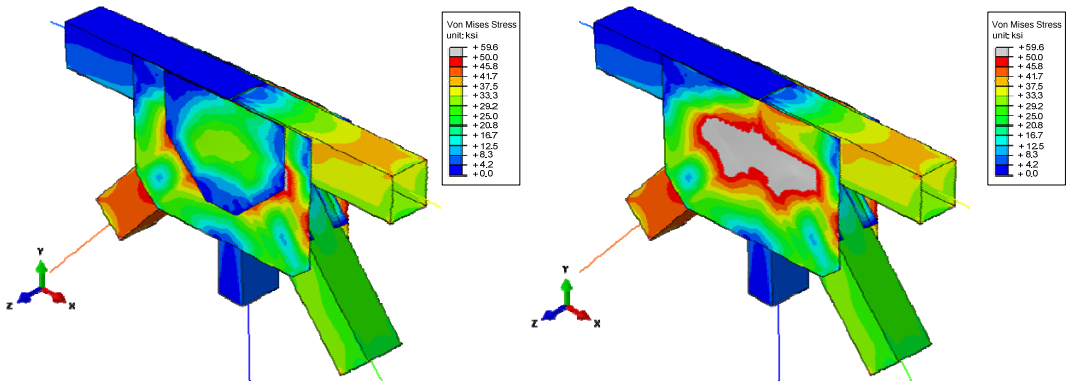

Figure 21. Von Mises stress response contours at limit load (ALF=2.16). (Left) Showing with the shingle plate in place. (Right) Showing with the shingle plate removed.

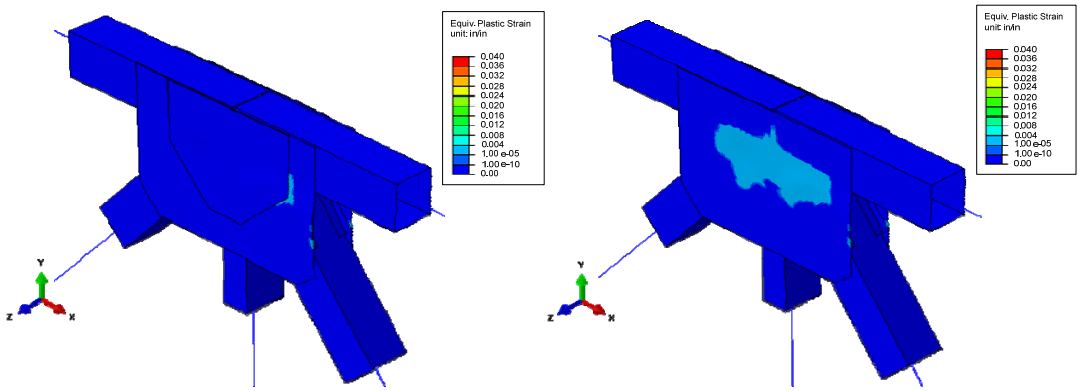

Figure 22. Equivalent plastic strain response contours at limit load (ALF=2.16). (Left) Showing with the shingle plate in place. (Right) Showing with the shingle plate removed.

I-80 Bridge (Joint L3)

Important load levels on the ALF versus out-of-plane displacement plot are shown in Figure 23. The Strength I load is attained at an ALF=1.03. Shown in Figure 24 the connection is not elastic at the Strength I load level, though it must be restated that this connection was originally designed using 50 ksi yield properties, though 36 ksi yield strengths were used in the FHWA Guide. The maximum usefulness of the connection is determined using the 4% PEEQ criterion at an ALF=1.76.

The Von Mises stress and equivalent plastic strain contours at an ALF=1.76 are shown in Figure 25. Much of the gusset plate has yielded, though the likely failure mode of the connection would be failure of the tension chord splice. There is also evidence that block shear of the right-hand chord could also occur.

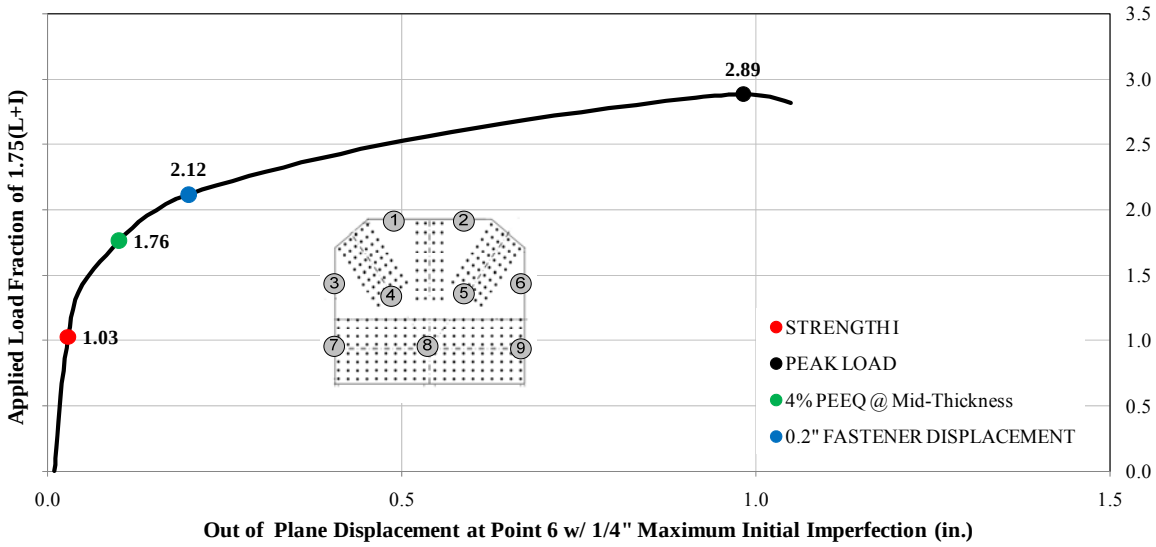

Figure 23. Plot of out-of-plane displacement motion of Point 6 versus the ALF.

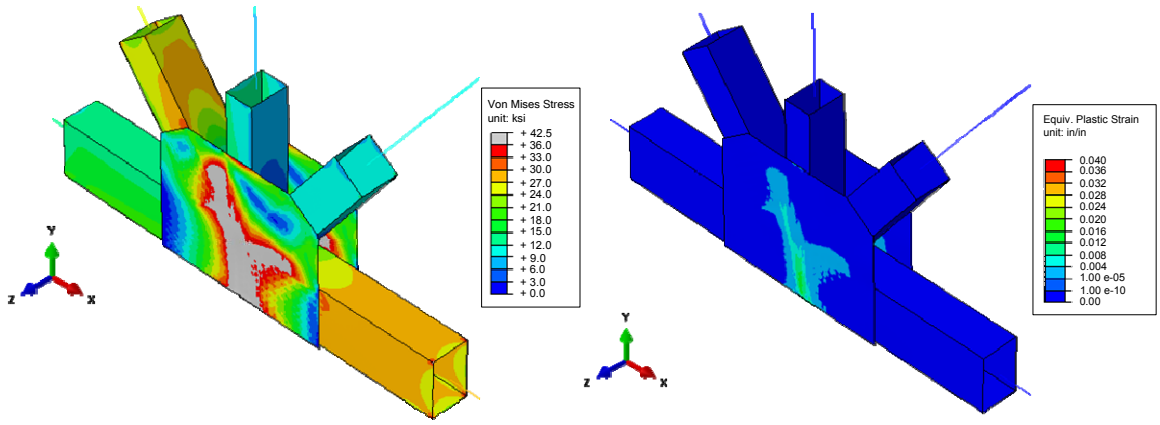

Figure 24. Response contours at Strength-1 level (ALF=1.03). (Left) Von Mises stress contours. (Right) Equivalent plastic strain contours.

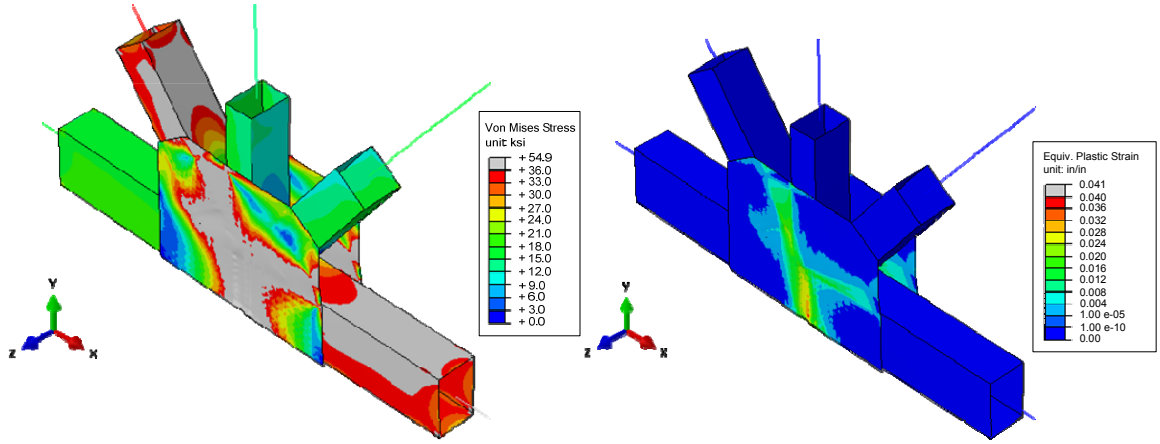

Figure 25. Response contours at limit load (ALF=1.76). (Left) Von Mises stress contours. (Right) Equivalent plastic strain contours.

SUMMARY OF THE RESULTS

For each of the five connections, the FHWA Guide was used to calculate the LRFR Inventory Rating Factor (RF) for each member. The RF is calculated using Equation 2, where ϕR_n is the factored nominal resistance, *DL* is the dead load resisted by the element, and *LL+IM* is the live load amplified by the dynamic load allowance (impact) resisted by the element. The load modifier, η, was assumed to be 1.0 and the condition and systems factors specified in LRFR are also assumed to be 1.0.

$$RF = \frac{\phi R_n - 1.25(DL)}{1.75(LL + IM)} \qquad \text{(Eq. 5)}$$

Table 1 shows the resulting LRFR rating factors for each of the five connections. The I-94 connections used high-strength A325 bolts and therefore the slip capacity of the fasteners was checked, but not on the other joints which used rivets. The Whitmore buckling checks for compression diagonals all assumed the equivalent column length factor (i.e., K-factor) was equal to 1.2. For the Whitmore buckling checks of compression chords a K-factor of 0.65 was used and it was assumed the force was proportioned between the gusset plate and additional chord splice plates by their area.

The shaded cells in the table indicate the most likely failure modes observed from the analysis. In all the joints, except for I-35W, the smallest rating factor was 1.87 with the majority of them greater than 2.00. Note these favorable rating factors are attained using LRFR despite none of the connections being designed to an LRFD philosophy. The I-35W joint is recognized to be an under-designed gusset plate and as expected it has either negative or rating factor less than 0.50.

The data shown in Table 2 is in a different form as a professional factor, which is the unfactored failure load from the model divided by the unfactored nominal resistance check (i.e., $R_{FEA}/R_{nominal}$). Professional factors greater than 1.0 represent conservative predictions and are favorable over ratios less than 1.0 that are unconservative. As will be further described in Chapters 3 and 4, it assesses the accuracy of the nominal strength check and plays a role in the LRFD calibration. As done in Table 1, the failure modes identified to be likely are shaded in Table 2. It is important that the professional factors presented in unshaded cells are studied carefully as more often than not they are less than 1.0. This is not to mean that the resistance equation is unconservative because it must be tempered that the connection did not fail in this limit-state and it would be an unfair judgment. Only professional factors in shaded cells should be used to judge the conservatism of a particular resistance equation.

After performing the detailed analysis of the five joints, the following anomalies were noted by the research team in comparing the results of the finite element simulation versus the predictions of the FHWA Guide. These items were given full consideration when developing the experimental and paramedic finite element studies.

1) The application of the Whitmore section approach for both tension and compression chords is questionable. Since all five of the gusseted connections also performed as chord splices, a distribution of force between the gusset plate and the additional chord splice plates had to be assumed. Since the I-80 and HW-23 joints likely failed in the chord splice, the professional factors for the Whitmore checks for these two connections were an unconservative 0.91 and 0.37. This shows that chord splice failure is not well predicted by the Whitmore section checks. This likely has to do with the assumptions of how stress is distributed between the gusset plate and alternate chord splice plates.

2) No glaring issues could be identified with tension member checks. However, it was noted that Whitmore tension and block shear checks did produce about the same resistance and

there may be the possibility that the two checks are redundant. The sensitivity of the Whitmore section crossing over multiple members should also be evaluated.

3) There is a great amount of uncertainty with the buckling checks of compression members. In the three connections that may have buckled, the Whitmore buckling professional factors varied greatly. There are four unknowns that exist with the resistance check. First, what K-factor should be used because considering boundary conditions, K=1.2 appears to be most appropriate, though it produced very conservative professional factors for some connections. Second, what equivalent column length should be used, because in many cases the Whitmore width overlaps adjoining fastener lines and a zero length is attained of which the sensitivity needs to be addressed. Third, what is the sensitivity of the Whitmore section overlapping neighboring members and should it be truncated. Fourth, does the free edge slenderness have a role in the buckling resistance as the current limit does not appear to be a good predictor of buckling.

4) In the evaluation of shear, it is critical that the Ω-factor is explored because as shown for the two connections that possibly failed in shear, the professional factors using Ω=1.00 produce the best results. Based on these five analyzes, the Ω-factor is somewhere in-between the current limits, likely closer to 0.90.

5) The load sharing of multi-layered (i.e., shingled) gusset plates needs to be verified. The model of the I-40 connection had multi-layered gusset plates, but it is important to evaluate the validity of the fastener models to ensure that the results of load sharing are true.

6) The role of section loss within all the limit-states needs to be addressed. Frequently, field inspections show that gusset plates often suffer from section loss due to corrosion and it is not well understood how it should be integrated into the various resistance checks.

Table 1 Rating Factors for Five Representative Joints

Type of Check	I-80	I-40	I-94	HW-23	I-35W
TENSION CHORD					
Whitmore Section	2.60	3.71	9.75	N/A	5.62
Block Shear	2.30	2.96	9.92	N/A	5.63
Fastener Shear Capacity	2.75	4.73	9.67	N/A	3.38
Fastener Slip Capacity	N/A	N/A	4.28	N/A	N/A
COMPRESSION CHORD					
Whitmore Buckling	N/A	N/A	N/A	3.27	9.43
Fastener Shear Capacity	N/A	N/A	N/A	4.38	7.58
TENSION DIAGONAL					
Whitmore Section	2.86	6.93	14.87	4.41	2.25
Block Shear	2.66	3.82	6.17	3.58	1.38
Fastener Shear Capacity	2.31	2.32	9.42	2.66	2.54
Fastener Slip Capacity	N/A	N/A	4.30	N/A	N/A
COMPRESSION DIAGONAL					
Whitmore Buckling	3.88	5.83	8.84	2.98	0.29
Edge Slenderness[(a)]	37.3 (58.5)	54.7 (49.6)	45.3 (49.6)	77.1 (49.6)	60.4 (49.6)
Fastener Shear Capacity	3.55	3.52[(b)]	7.24	2.32	1.62
Fastener Slip Capacity	N/A	N/A	3.05	N/A	N/A
A-A SECTION SHEAR					
Gross Yield (Ω = 0.74)	1.87	2.28	8.27	2.15	-0.33
Gross Yield (Ω = 1.0)	2.91	3.80	12.24	3.14	0.45
Net Section Fracture	3.05	2.96	10.40	2.50	-0.15
B-B SECTION SHEAR					
Gross Yield (Ω = 0.74)	1.87	3.21	8.62	2.92	-0.19
Gross Yield (Ω = 1.0)	2.99	5.05	12.72	4.26	0.44
Net Section Fracture	3.03	4.41	11.45	3.63	0.10

N/A = Not Applicable
[a] - Edge slenderness (Slenderness limit)
[b] - Includes angles along top and bottom of compression diagonal

Table 2 Professional Factors for Five Connections, ($R_{FEA}/R_{nominal}$)

Type of Check	I-80	I-40	I-94	HW-23	I-35W
TENSION CHORD					
Whitmore Section	0.91	0.95	0.91	N/A	0.26
Block Shear	0.82	1.01	0.88	N/A	0.26
Fastener Shear Capacity	0.77	0.91	1.34	N/A	0.46
Fastener Slip Capacity	N/A	N/A	3.10	N/A	N/A
COMPRESSION CHORD					
Whitmore Buckling	N/A	N/A	N/A	0.37	0.06
Fastener Shear Capacity	N/A	N/A	N/A	0.63	0.09
TENSION DIAGONAL					
Whitmore Section	0.94	0.69	2.09	0.73	0.66
Block Shear	0.83	0.90	3.42	0.74	0.66
Fastener Shear Capacity	1.14	1.51	1.10	1.21	0.67
Fastener Slip Capacity	N/A	N/A	4.11	N/A	N/A
COMPRESSION DIAGONAL					
Whitmore Buckling	0.63	0.85	3.63	1.29	1.00
Edge Slenderness	Pass	Pass	Pass	Fail	Fail
Fastener Shear Capacity	0.74	1.18[(a)]	1.32	1.60	0.71
Fastener Slip Capacity	N/A	N/A	4.91	N/A	N/A
A-A SECTION SHEAR					
Gross Yield (Ω = 0.74)	1.19	1.44	3.29	1.52	1.325
Gross Yield (Ω = 1.0)	0.88	1.07	2.43	1.12	0.98
Net Section Fracture	0.72	1.05	2.33	1.14	1.03
B-B SECTION SHEAR					
Gross Yield (Ω = 0.74)	1.23	1.19	3.21	0.69	0.96
Gross Yield (Ω = 1.0)	1.10	1.14	2.38	0.51	0.71
Net Section Fracture	0.76	0.82	2.18	0.49	0.72

N/A = Not Applicable
[a] - Includes angles along top and bottom of compression diagonal

CHAPTER 2. RESEARCH APPROACH

REVIEW OF BRIDGE PLANS

The plans for 20 different truss bridges were reviewed to help the research team understand the range of designs that might be encountered in the rating process to help guide the research. The findings from this process can be found in greater detail in Appendix A.

As a summary, the plans were from eight different states were designed between the years 1929 and 1990, and encompassed a variety of span arrangements and lengths. Some important points that helped to guide the research project were that the overwhelming majority of gusset plates were between 0.500 and 0.938 inches thick while none were observed to be thinner than 0.375 inches. Finally, all connections used either $^{7}/_{8}$ or 1 inch diameter fasteners that were either rivets or high-strength bolts.

It also became clear that there is no such gusset plate that can be termed as "typical." There are numerous variations of geometry, material properties, and force combinations evident in the large gusset plates on the bridges described in Appendix A. Such variations make it impossible to arrive at reasonable conclusions on gusset plate resistance based purely on physical tests. The numbers of tests needed to accomplish this task would be prohibitively expensive. The only viable alternative is to develop robust analytical models that can be used both to explore many more configurations than is possible to test in the laboratory and to assess how independent checks for failure modes can be developed.

EXPERIMENTAL PROGRAM

Load Frame

For successful completion of the project, a unique load frame had to be designed that could load a gusset plate connection to failure. A detailed description of the load frame and its capabilities are further described in Appendix B.

Data Systems

To capture the variety and magnitude of data required to meet the project's objectives, innovative measurement systems that transcend conventional practices were employed during the gusset plate testing. Typically, experiments of this type utilize a combination of LVDTs and strain gauges (single axis or rosettes) to measure displacements and strains. This combination works well when the directions of principal strains and locations of maximum deformations can be reliably anticipated. However, the strain fields within a gusset plate are so complex that an impractical number of strain gauges would be needed to characterize that strain distribution. In addition, the displacement patterns of the gusset plates in three dimensions (i.e., buckled shapes) are difficult to anticipate and thus would also require a large number of deformation sensors to

be properly characterized. For this experiment, optical techniques capable of full-field rather than discrete measurements were used to monitor each of the gusset plates.

Photostress Camera

Each test will consider a pair of gusset plates. During testing, one gusset of the pair will be monitored with a GFP1400 photostress camera furnished by Stress Photonics capable of capturing the full strain field of the gusset plate. The system involves coating the gusset with a tinted epoxy that has certain birefringent characteristics. In this case, stress applied to the epoxy causes a phase shift of the light components transmitted through the epoxy. The phase shift is a circular function expressed in terms of fringes. To maintain elastic superposition principles, this camera and its associated post-processing software recommends keeping the epoxy strains within 1/3 of the first fringe where the circular function is approximately linear. If a certain strain capacity is needed, only the thickness of the coating can be altered to meet this requirement. For the gusset plate experiments, the optimal coating thickness is between 10 and 15 mils yielding a maximum shear strain capacity of ~2000με (this correlates to a uniaxial strain of approximately 1500με). The trade-off with reducing the coating thickness is a decrease in the strain resolution, but this coating thickness should provide approximately a 30με resolution.

The photostress camera by itself is only able to resolve 2/3 of the entire strain tensor. It is able to determine the diameter of the Mohr's Circle and direction to the first principal strain, but cannot distinguish the center location of the Circle. The most useful data output by the camera system software is the Maximum Shear Strain contours which is the difference between the two principal strains (i.e., the diameter of Mohr's Circle).

Data collected from the photostress camera for each specimen is presented in Appendix E.

Digital Image Correlation (DIC)

The National Institute of Standards and Technology (NIST) performed digital image correlation (DIC) monitoring of the second gusset plate. This system uses two digital cameras in a stereoscopic arrangement. The two cameras take pictures of a randomized pattern applied to the gusset and post-processing software tracks points in the pattern. The system can then provide in-plane strain fields, as well as the full three-dimensional displacement fields of the gusset plate. However, the system is most reliable post-elastic when displacements become large. The data in the elastic regime can be used for qualitative results, but once the plate has yielded extensively, the results become very reliable. Further description of the DIC system can be found in Appendix F.

FARO ION Laser Tracker

In lieu of conventional LVDTs, a FARO ION laser tracking system was used to measure displacements of discrete points on the specimen. Similar to a total station used for surveying, the system uses a centralized head unit housing the absolute distance measurement (ADM)

system, guidance system, and encoders (for zenith and azimuth). It does not have the same distance measurement capacity as a total station (only ~130 feet), but the trade-off is better precision than a total station at about 0.0005 inches. The other difference is the system automatically tracks a spherically mounted reflector (SMR) rather than the user manually adjusting the horizontal and vertical angles to focus on a prism. The primary purpose of these systems is for reverse engineering or quality control purposes, but it provides definite advantages in an experimental environment where one laser measurement is equal to having three LVDTs orthogonally mounted at the same point.

The standard SMR is a 1.5 inch diameter steel ball with a prism precisely mounted at the center of the sphere. The SMR can either be touched to a surface of an object or a standard tool set accompanies it that can measure holes, edges, or machine targets. The tracking system automatically follows the motion of the SMR and with a remote control, the user can record the position of the SMR on demand. The system software automatically compensates the measurement accounting for the diameter of the SMR so the measurement correlates to the surface being measured. The software also has the capability of continuous recording such that the SMR can be swept across a surface to attain a true surface profile.

The laser tracker had three main uses during the full-scale gusset plate tests. First, it was able to provide accurate initial position/shape of the members and gusset plate before the test began. This data was used to introduce real initial imperfections into the finite element models that predicted specimen behavior. Second, it tracked the motions of targets placed on the specimen (members and gusset) during a test. Finally, post-failure the SMR was swept across the surface of the gussets to determine the final deformed shape.

FARO data for each specimen are presented in Appendix H.

Strain Gauges

Conventional strain gauges were still used to augment the data from the imaging systems. Rosettes and single-axis gauges where applied on the back sides of the gusset plates to provide correlation to the results of the various imaging systems. Strain gauges were also applied at select cross-sections of the five members to determine the axial and bending forces within the members to ensure the loading system is acting as expected. Within the connection region, single-axis gauges were used to help determine how the load is shed from the chords into the gussets, as well as how load is shared between the gussets and the splice plates. Locations of these gauges can be found in Appendix G for each specimen.

Data Acquisition

All sensor data was collected via a Hewlett-Packard (HP) VXI CT100B mainframe. This included all strain gauges and conditioned voltages from the MTS FlexTest GT controller (i.e., the load and stroke of each jack). The system operated by custom written software that queries

the system for data and writes it to a text file and collected data continuously at a rate of 1Hz throughout the duration of testing.

The collection software had no capabilities to visualize the data in real time, beyond just showing the current sensor value. To enhance the visualization and post-processing of the data, a detailed Excel spreadsheet was written that queried the data file and performed post-processing to help visualize the raw data easier.

The photostress system used its own laptop computer to collect and store images. The data were represented in the form of an image stored in a proprietary format. It had no ability to be synced with an external signal, such as an actuator load signal. Therefore, hand notes were used to identify which strain gauge data should be used for each image collected.

The FARO ION system also had its own stand-alone laptop to collect the coordinate data. The data were stored in a proprietary format but the 3-dimensional coordinate data was easily exported to Excel for plotting purposes. This system also did not have the ability to be synced with an external signal and hand written notes were used to sync its data with that from other systems.

The DIC system collected camera images via a stand-alone computer system. The system could accept up to four external voltage signals so it could be synced to strain gauge data. In this case, the DIC system collected the conditioned voltages from two actuator loads and strokes so that at any point in time, the images could be synced to the strain gauge data sets via loads being applied to the specimen.

Specimen Design

The primary intent of the experimental design was to produce physical results of the different failure modes of concern in gusset plate connections and provide data to calibrate finite element modeling techniques. Among these are shear failure of the bolts or rivets, net section fractures in the members, buckling of the plates (either along the free edges or at the end of the compression members), and shear along a plane parallel and perpendicular to the chord. From the preliminary finite element studies it is clear that many of these failure modes interact with one another and that it would be difficult to isolate them in a physical test, particularly as the gussets begin to move out-of-plane. Thus the design of the specimens was broken into two phases, each with six full-scale specimens. The Phase I specimens were intended to assess primarily shear in the A-A plane and buckling at the end of the compression flange. The Phase 2 specimens were meant to investigate the effects of corrosion, stiffening, and other aspects the oversight panel felt appropriate that were not addressed in Phase 1.

In Phase 1, four main variables were explored: the type of fastener, the distances within the gusset plate between the ends of the compression diagonal and the other truss members, the length (or slenderness) of the plate edge, and the thickness of the gusset plate.

The first test variable considered was the type of fasteners. Two types of fasteners are typical in gusset plates: A502 rivets and A325 structural bolts. For this research, the A490 bolts were chosen in lieu of A325 to make the fastener patterns as small as possible. After considerable research, it was decided for practical reasons that A502 rivets would be very difficult and expensive to install properly. Based on the work of Roeder et al., it was decided to use A307 bolts initially in bearing in lieu of rivets.[20] In addition, further fastener characterization was performed as part of this research described in Appendix C that further validated this claim. Therefore, the unfactored design values for ultimate shear strength for the A307 bolts and the design slip values for the A490 bolts were used to design the fastener patterns for the Phase 1 specimens. The fastener patterns were designed to resist 1200 kips for the chords and diagonals and 440 kips for the vertical member. At times, more fasteners were used than required for strength; this was controlled by other geometric parameters of the overall connection and the fastener patterns were staggered if possible to reduce the amount of overdesign for fastener shear.

The standoff distance and free edge length were controlled through the positioning of the compression diagonal and the fastener pattern. The standoff distance is defined as the length of free plate between the compression diagonal and the chord. It is measured via the gap between the lower corner of the compression diagonal and chord which was either 1.0 or 4.5 inches. The 1.0 inch gap was referred to as "short" distance and the 4.5 inch gap was called the "long" distance.

The free edge length was varied by adding additional fastener rows over what was determined via fastener shear design criteria. The standoff distance coupled with the fastener pattern fixed the free edge lengths, which were referred to as the "short" free-edge length. However, in two of the specimens, additional rows of fasteners were provided (i.e., over-designed for shear), which increased the free edge length (also referred to as the "long" free edge length) without changing the standoff length.

The tests are labeled as GPwwwxyz-a, where "www" is the bolt type (either 307 or 490 for the grade of fastener), "x" refers to the standoff distance (S for short, L for long), "y" refers to the free edge length (S for short, L for long), "z" is the plate thickness in eighths of an inch (either 3 or 4 for ⅜ inch and ½ inch plate), and "a" is a sequential number as some of the geometries were replicated. Thus, the test with A307 bolts, ⅜ inch plate, long end distance and short edges will be GP307LS3. For brevity this would often be referred to as the 307LS3 or sometimes just the LS3 geometry.

Phase 1

The two most compact SS3 geometries are shown in Figure 26. These are considered the baseline specimens where the fastener patterns for the diagonals were as small as possible to transfer the design force of the members as well as using the "short" standoff distance. The LS3 geometries shown in Figure 27 maintain the same fastener patterns, but back the compression

diagonal out of the connection thus increasing the standoff distance to the "long" condition. The free edge length also increases with the LS3 geometries over the baseline SS3 geometries. The philosophy behind the SL3 and SL4 geometries shown in Figure 28 was to maintain the "short" standoff distance, but engage more rows of fasteners such that the free edge length is nearly the same as the LS3 geometries. The SL geometry was tested using both ⅜ and ½ inch thick plates because each of those thicknesses should result in edge slenderness less than and greater than the existing free edge slenderness criterion in the FHWA Guide.

Notice that at times the fastener patterns in the chords and diagonals have fasteners missing from the full pattern. As mentioned before, this was to keep the fastener shear limit-state in balance with the design force as much as possible. At the same time symmetry was maintained about the member force line of action while maintaining a constant pitch and gage around the perimeter of the patterns. For the chord splice, a full pattern of fasteners was used for the first four columns of fasteners in each chord to facilitate bolting of internal web splice plates.

There was always a 0.5 inch gap between the two chords at the chord splice. This was done for two reasons: (1) it represented the worst possible situation as most of the reviewed bridge plans called for a "milled to bear" condition at compression chord splices and (2) the overall fabrication cost of the two chords was reduced without the ends having to be "mill-to-bear." To further enhance the strength of the chord splice, additional web, top, and bottom splice plates were added in parallel to the main gusset plate. The schematic shown in Figure 29 shows the placement of these four additional splice plates. The top and bottom splice plates were bolted to the outside of the chord members through the coverplates of the chord cross-section (shown as a green fill in Figure 29). The web splice plates were bolted to the sideplates of the chord cross-section and were inside the chord member (shown with a light blue fill in Figure 29). In all connections, the four splice plates were the same thickness as the gusset plate, and were also cut from the same parent plate as the gusset plate (i.e., the material properties should be uniform for the two gusset and four splice plates.)

In all of the Phase 1 specimens, there was a full fastener pattern along the perimeter of the chord members. This was done to balance the likelihood of shear yield on the gross area versus fracture on the net area of the holes in the horizontal plane of the gusset along the top of the chord. Using design yield and tensile properties, the ratio between the shear yield force to the shear fracture force for all six Phase 1 specimens was 0.98 with a full fastener pattern and 1.16 with a staggered fastener pattern.

In the Phase 1 testing, there was a hydraulic malfunction that accidently crushed the GP490LS3 geometry before it had failed under controlled conditions. Therefore, in the purchase of some Phase 2 gusset plates, replacement 490LS3 plates were attained and it was called GP490LS3-1.

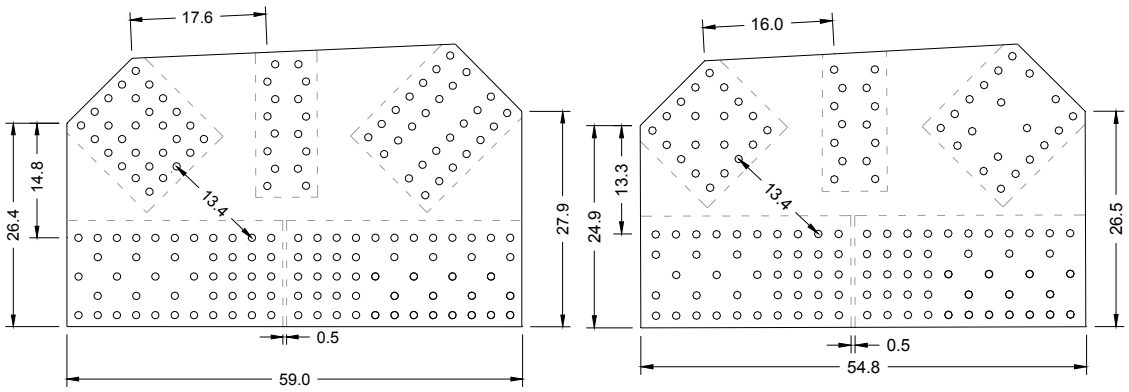

Figure 26. Dimensions in inches for SS3 specimens. (left) GP307SS3. (right) GP490SS3.

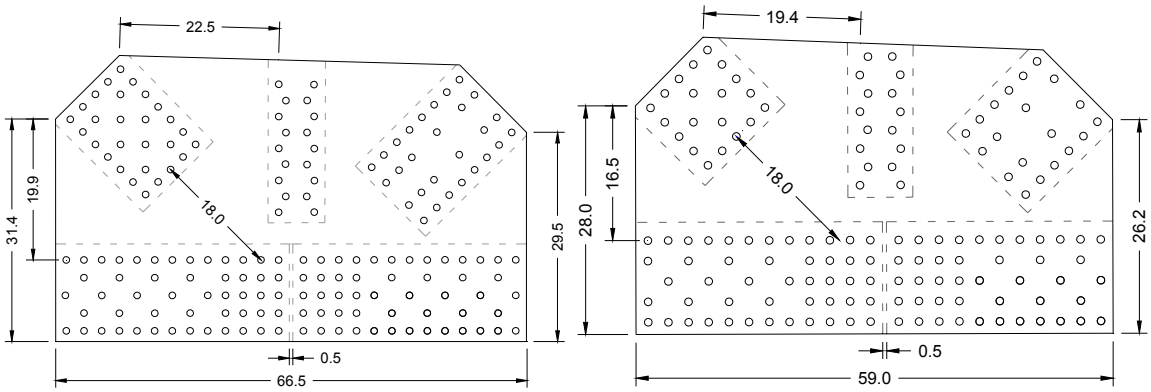

Figure 27. Dimensions in inches for LS3 specimens. (left) GP307LS3. (right) GP490LS3.

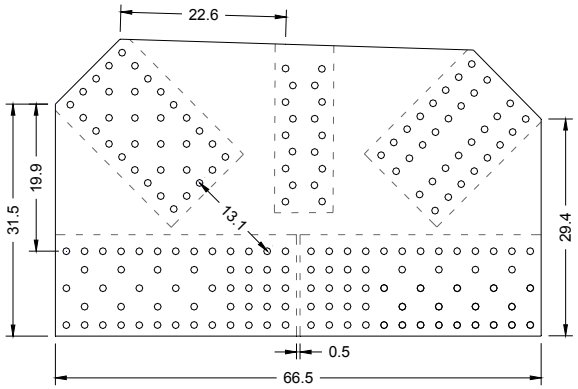

Figure 28. Dimensions in inches for SL3 and SL4 specimens.

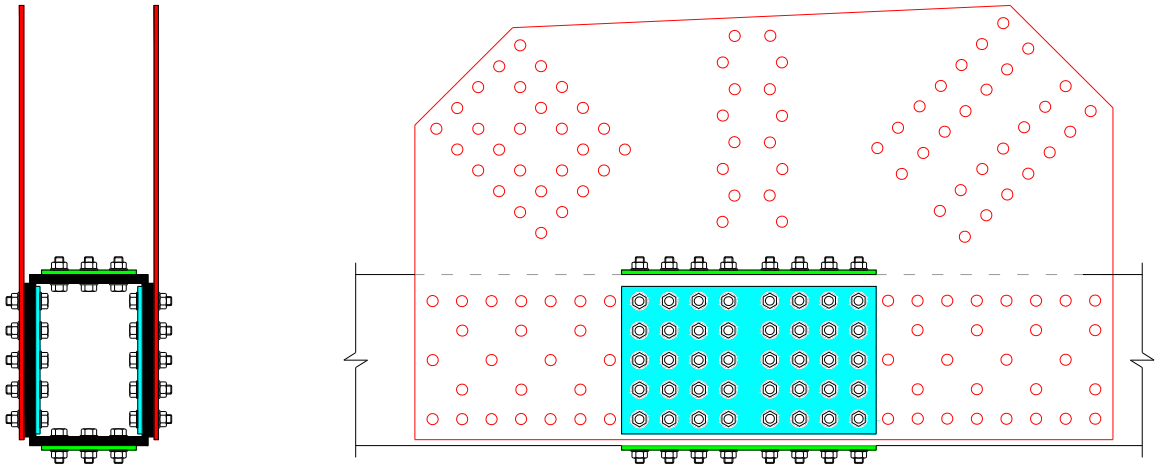

Figure 29. General detailing of chord splice plates. End view (left). Elevation view (right)

Phase 2

The Phase 2 specimens did not introduce any new connection geometries over the five used in Phase 1. Rather, Phase 2 investigated variations of some Phase 1 geometries that investigated the effects of corrosion, retrofit strategies with shingle plates and stiffening angles, and for one connection a defined shear resistance failure. The Phase 2 specimens were selected at three distinct points in time after the Phase 1 testing began, primarily to react to outcomes during Phase 1 and from panel input through quarterly progress reports.

Unlike the Phase 1 specimen, all Phase 2 specimens were tested with the addition of a work point brace that provided out-of-plane restraint to the work point. This is described in Appendix B.

Specimens with Simulated Corrosion

Early in Phase 1 it was noted that specimens replicating corrosion would have to be tested as part of the overall research program and it was decided to limit this to just corrosion within the gusset plates, not the fasteners. There were many questions as how to integrate non-uniform remaining sections into load rating calculations and how the section loss would affect various limit-states. To make the corrosion as realistic as possible the intent was to corrode the gusset plate specimens by cathodic means. The obstacle to this approach is it would be a timely process which was calculated to take approximately 6 months. Therefore, when the Phase 1 gusset plates were purchased, so were two additional 307SS3 geometries that could be cathodically corroded while the Phase 1 testing was occurring. Unfortunately, the cathodic corrosion approach did not work and in the end the corrosion was simulated by milling away sections from the plate in a predetermined pattern.

Shown in Figure 30 is the shape of the simulated corrosion pattern for each of these two connections. These two specimens were named GP307SS3-1 and GP307SS3-2. As can be seen,

the simulated corrosion shape was the same for all four plates and was symmetric for each connection. What cannot be pictorially shown in the figure is the pattern that was milled into the surface of the plate that would be interior to the connection. The shape was derived from looking at pictures of corroded gusset plates in inspection reports submitted to the research team by the state of Illinois and the city of Chicago. What was evident in those reports was that corrosion was often non-uniform and in many cases vast areas of the plate between members suffered from section loss. The depth of the corrosion was purposely different for the tension and compression diagonal side of the plate in order to assess non-uniform corrosion across a plate. Each of the plates were 0.375 inches thick and the figure outlines a percentage of the plate thickness that was removed by milling. The only difference between the two separate connections was that the 50% and 30% thickness reduction was flip-flopped for each connection.

The panel had concerns that the simulated corrosion patterns in 307SS3-1 and 307SS3-2 did not cover enough situations, and asked that two additional Phase 2 specimens investigate other corrosion patterns. Primarily some panel members preferred to see the simulated corrosion only on one plate (so the connection stiffness would be unbalanced) and that the shape should be more narrow-banded above the chord. Like the other simulated corrosion specimens, these two additional specimens also used the Phase 1 307SS3 geometry. In each case, only the plate on the north side of the connection had simulated corrosion milled into it; the south plate was undamaged.

The third and fourth simulated corrosion specimens were called GP307SS3-3 and GP307SS3-4 respectively. Each of these specimens used the same corrosion pattern on just their north plate as shown in Figure 31. The simulated corrosion pattern is 1.5 inches tall and 48 inches long, and was milled 0.188 inches deep into the plate for a nominal 50% section loss. The bottom of the simulated corrosion pattern was in-line with the top edge of the chord side plate where corrosion would develop if this were a real lower chord truss connection. The intent of the GP307SS3-3 specimen was to investigate the role of corrosion on just one plate of the connection.

The GP307SS3-4 connection then investigated how to retrofit this simulated corrosion pattern through the use of a shingle plate added to the exterior of the connection. The schematic shown in Figure 32 shows the corrosion pattern on the inside of the plate, but also the outline of the shingle plate that was also bolted to the outside of the plate. Again, the south gusset plate did not have simulated corrosion, nor a shingle plate. The shingle plate was installed with the primary gusset plate and therefore did not represent the stress conditions that would be present in a gusset plate if the shingle were to be added as a retrofit. This was deemed too unsafe to perform in the lab while under hydraulic control.

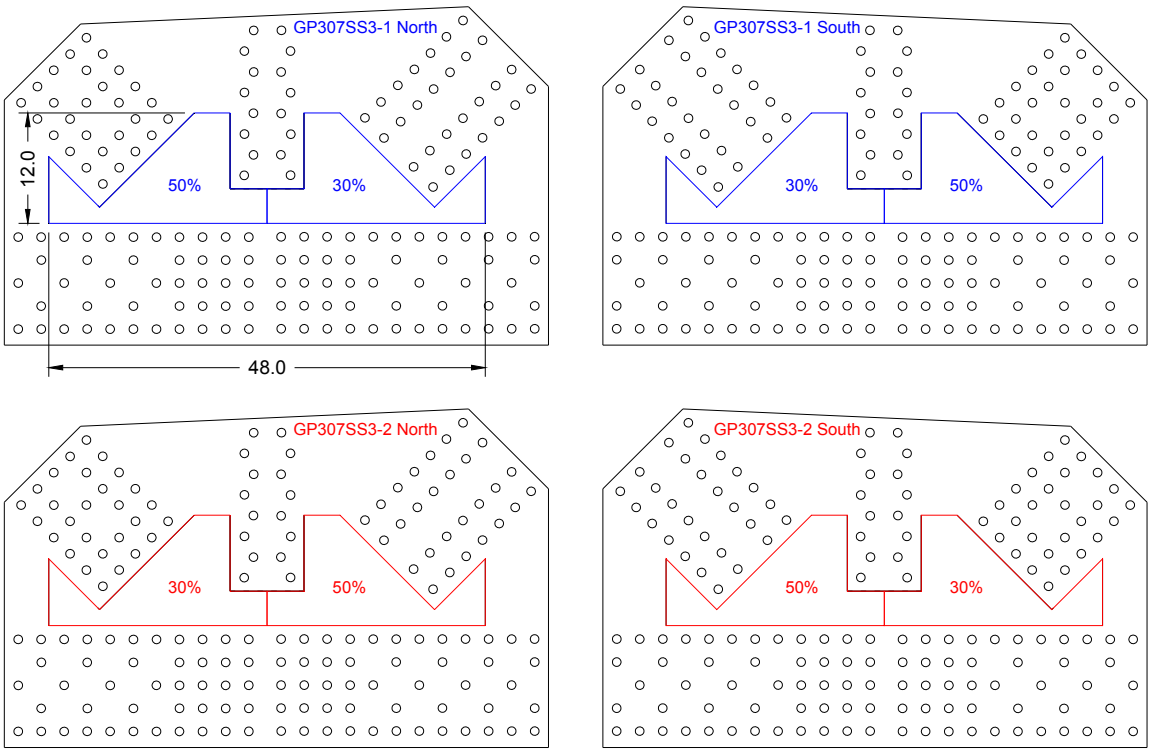

Figure 30. Pattern of corrosion milled into interior surface of 307SS3-1 plates (top) and 307SS3-2 plates (bottom).

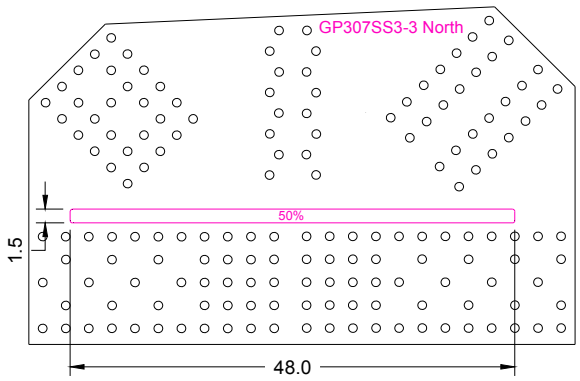

Figure 31. Corrosion pattern of GP307SS3-3 and GP307SS3-4 north plate.

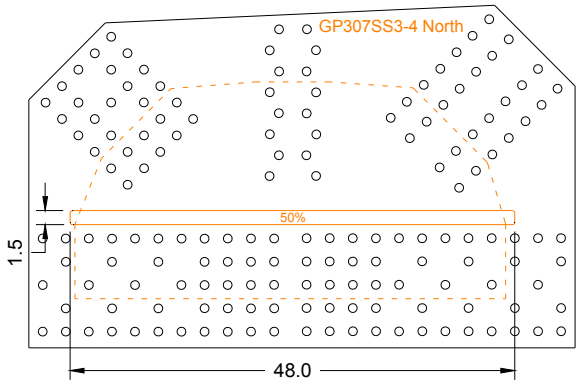

Figure 32. Corrosion pattern of GP307SS3-4 north plate.

GP490SS3-1 and GP490LS3-2

An interim meeting with the panel was held after the fourth Phase 1 specimen was tested to give the panel an opportunity to personally see the experimental testing. At that point the first four Phase 1 specimens had failed via buckling and it appeared a shear failure would not occur throughout the experimental testing. In that meeting, the panel requested a retest of one Phase 1 geometry; however, they requested that the researchers fully restrain it out-of-plane to force the shear failure. In addition to the work point brace already being used in Phase 2, this specimen also braced the compression diagonal against the shearwalls so it could not move out-of-plane. The research team opted to retest the 490SS3 geometry as it was the most compact plate that would have the greatest success of shearing within the load capacity of the frame and it was called GP490SS3-1. A schematic of the plate geometry can be seen in Figure 33. The only difference made with this geometry was 12 bolts were removed from the chord fastener pattern. This increased the net section area so as to have a greater success of causing a gross shear yield failure.

At the same meeting, the panel also requested testing an edge stiffened connection. The research team opted to retest the 490LS3 geometry as it had the lowest buckling resistance and thus would benefit the most if it could be stiffened. The intent of this specimen was to investigate the edge stiffening as a retrofit to enhance buckling resistance, not to assess the role of free edge slenderness criteria. Prior to finalization of the tested geometry, preliminary finite element analysis was performed to understand how much strength increase the retrofit could provide.

Three scenarios were investigated: placing stiffening angles on the interior free edges around the compression diagonal, adding a plate diaphragm between the same interior angles, and placing the angles external to the connection. These three options are shown in Figure 34. These three retrofit strategies were analyzed with two different Phase 1 specimen geometries, the 490SS3 and 490LS3. Even though this Phase 2 specimen was to use the 490LS3 geometry, analyzing with two different geometries was done for analysis redundancy. The results of the analysis are

shown in Table 3 and presented in terms of the maximum load proportioning factor (LPF). The LPF is a multiple of the reference load state by which the analysis can no longer converge to a solution and is really a non-dimensional form of peak load at failure. Typically, a state of non-convergence was due to nonlinear geometric effects, in this case buckling. The table presents a percentage increase in LPF for each of the three retrofits over the connection with no stiffening. For each of the two connections, the interior angles were inadequate to increase the buckling resistance of the connection, at best only able to provide 3% extra strength. Adding a diaphragm plate between angles increased the buckling strength by 11.5% and 30.1%; however, the drawback with this retrofit is it reduces the ability to inspect inside the connection. Therefore, the best retrofit was to externally stiffen the entire plate edges on each side of the compression diagonal which had even more strength than the internal angles with a plate diaphragm (25.3% and 44.9% increase of the unstiffened case). The disparity of the three retrofit strategies arises because in all situations, when gusset plates buckle, they always buckle in a sidesway mode. In this case, interior angles do not contribute much stiffness against this mode. The key was to add stiffness across the planes that would bend in sidesway; therefore, for the external angle retrofit to be most effective, it must be carried into the chord and vertical fastener patterns.

Shown in Figure 35 is the final geometry of the GP490LS3-2 specimen. The edges were stiffened with 3x3x½ inch angles that were bolted to the outside of the gusset plates. Finally, in accordance with the pretest analysis results, the stiffening angle was placed along the entire length of the gusset plate edge, thus bridging across the planes that would bend in sidesway.

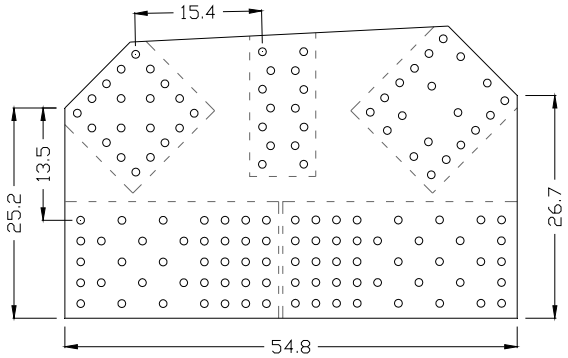

Figure 33. Dimensions in inches of GP490SS3-1.

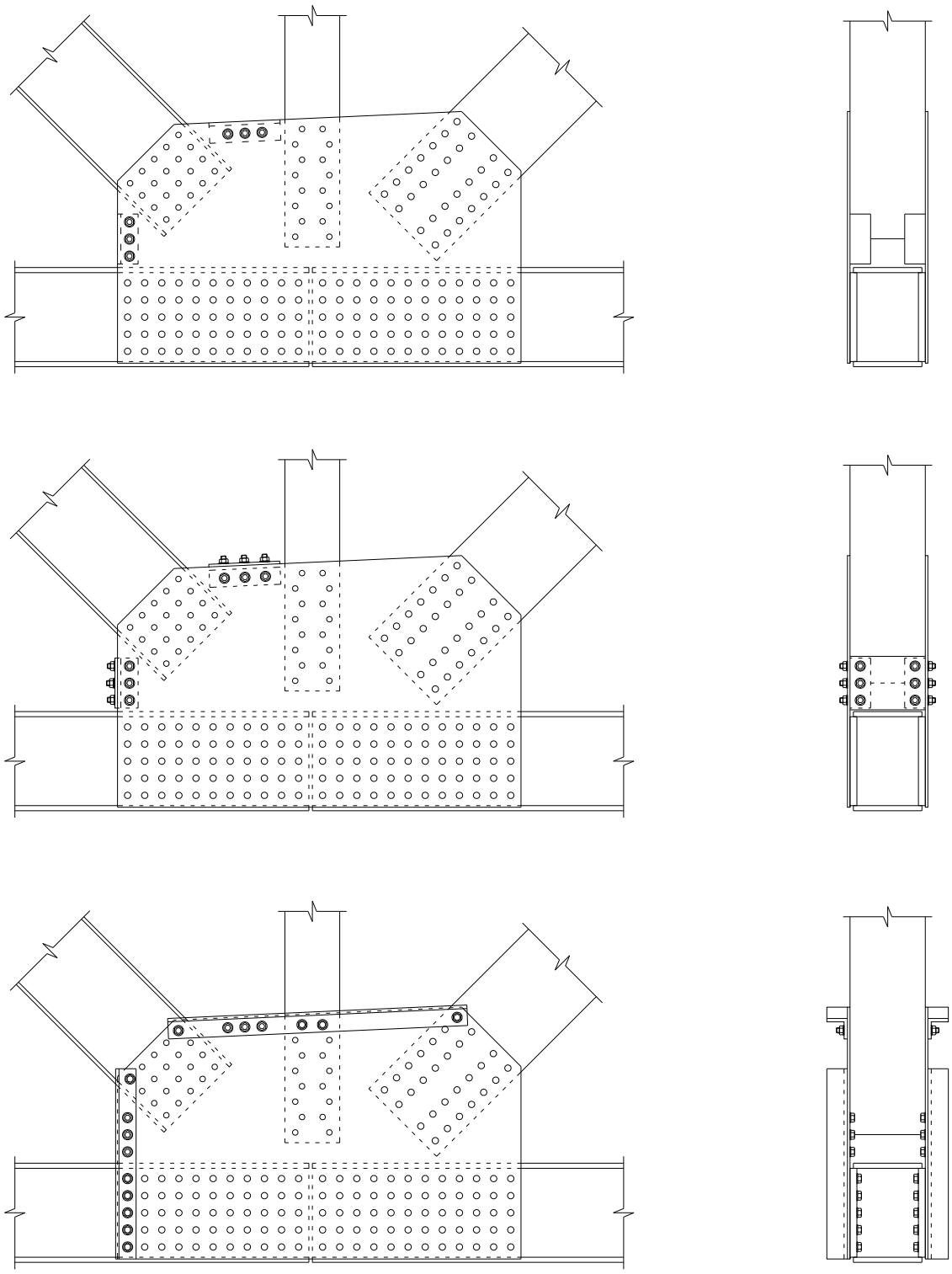

Figure 34. Angle stiffening options. Internal angle (top). Internal angles with plate diaphragm (middle). Exterior angles (bottom).

Table 3 Results of Preliminary Edge Stiffening Strategies

	GP490SS3		GP490LS3	
	Max. LPF	% Increase	Max. LPF	% Increase
No Stiffeners	0.712	-	0.579	-
Interior Angles	0.715	0.4	0.598	3.3
Interior Angles with Plate Diaphragm	0.794	11.5	0.753	30.1
Exterior Angles	0.892	25.3	0.839	44.9
Stiffening angles were L3x3x½ inch and plate diaphragm was the same thickness as the gusset plate "LPF" stands for Load Proportioning Factor				

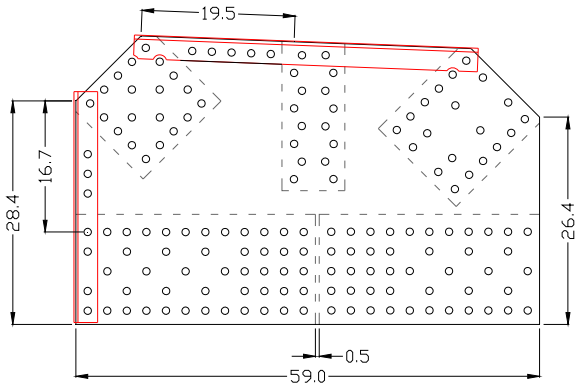

Figure 35. Dimensions in inches of GP490LS3-2. Stiffening angles shown in red.

Applied Loads During Testing

Before each connection was tested to failure a series of elastic tests were performed primarily to understand how load flowed through the gusset plates, primarily based on data from the photostress system. In these tests, the loads were proportioned until the maximum stress in the plate was about 70% of nominal yield according to a finite element simulation. Table 4 outlines the variety of normalized load combinations used for the elastic loading scenarios. For all but one specimen, 307LS3, only load combinations 1-11 and 13-15 were used. Specimen 307LS3 was tested with both chords in tension and load combinations 12a-12h were used exclusively for that specimen. The elastic load scenarios were repeated with and without horizontal continuity plates in the chords.

After the two elastic tests series (with and without continuity plates) were complete, a load combination was selected and the connection was proportionally loaded until failure. Generally, to loading was stepwise, monotonic, with between 10 and 20 load steps until the specimen failed. At load holds, FARO and DIC data were collected, while strain data was continuously monitored through the loading. The load combination used in the failure test is shown in Table 5 for each of the 13 specimens.

Table 4 Reference Load Combinations

Load Combination	F1	F2	F3	F4	F5	Shear on A-A plane
1	-1	0.707	0	-0.707	0	1
2	0	0.707	0	-0.707	1	1
3	-0.707	1	0	-1	0.707	1.414
4	-0.5	1	-0.207	-0.707	0.707	1.207
5	-0.5	0.707	0.207	-1	0.707	1.207
6	-0.707	1	-0.207	-0.707	0.5	1.207
7	-0.707	0.707	0.207	-1	0.5	1.207
8	-1	0.707	0.207	-1	0	1
9	-0.207	0.707	0.207	-1	1	1.207
10	-1	1	-0.207	-0.707	0.207	1.207
11	-0.207	1	-0.207	-0.707	1	1.207
12a	-1	0.330	0.117	-0.496	-0.416	0.584
12b	-1	0.650	0	-0.650	-0.081	0.919
12c	-1	0.375	0	-0.375	-0.469	0.531
12d	-1	0.088	0	-0.088	-0.876	0.124
12e	-1	0.672	-0.119	-0.504	-0.168	0.832
12f	-1	0.504	0.119	-0.672	-0.168	0.832
12g	-1	0.697	-0.246	-0.348	-0.261	0.739
12h	-1	0.348	0.246	-0.697	-0.261	0.739
13	0.431	0.322	0.117	-0.483	1	0.569
14	-0.597	1	-0.090	-0.874	0.728	1.325
15	-0.446	0.482	0.365	-1	0.602	1.048
15m	-0.531	0.600	0.282	-1	0.600	1.131
16	-0.531	1	-0.282	-0.600	0.600	1.131

Sign convention of above load ratios

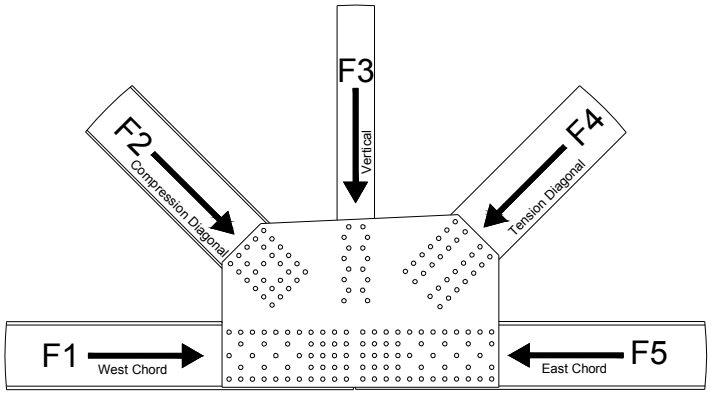

Table 5 Failure Load Combination for Each Specimen

Phase	Specimen	Load Combination
1	307SS3	4
	490SS3	3
	307LS3	12g
	490LS3	15m
	307SL3	3
	307SL4	3
2	490LS3-1	15m
	490LS3-2	16
	490SS3-1	15m
	307SS3-1	4
	307SS3-2	5
	307SS3-3	5
	307SS3-4	5

ANALYTICAL

Finite element studies were run from the beginning of the project all the way through completion. Within that time period, there was an evolution of how the modeling was conducted, along with the focus of its outcome. At first, the NCHRP panel requested immediate in-depth analysis of four representative joints taken from real bridges; this was described in Chapter 1. While it did not lead to revision of the FHWA Guide, the task did highlight issues that were unknown to the research team such as the role of chord splice plates, and the intricacies associated with multi-layered gusset plates. In this phase a finite element modeling philosophy for gusset plates was first established, loading the connections in a two-panel truss system, and representing the joint with nonlinear shell elements connected with fastener elements representing the bolts or rivets.

The second phase of the finite element modeling effort refined the initial modeling philosophy by benchmarking against the experimental specimen results. The first five tested connections were modeled pre- and post-test to establish what had to be done to produce accurate results. In this stage, the fastener elements were refined based on single shear lap splice tests conducted as part of the experimental program (described in Appendix C). It was also found that the initial shape of the gusset plates was very important for attaining highly correlated results between the model and the experiment. All 13 of the experimental specimens were modeled pre-test to attain predictions of the behavior, necessary for setting up the data collection and hydraulic interface computers.

The final, and largest, part of the finite element modeling effort was conducted in parallel with the testing of the Phase 2 experimental specimens. This was the parametric study that analyzed a wide variety of gusset plate geometries and evaluated their failure modes. The data from the parametric finite element study and the results from the experimental testing were used in the calibration of resistance equations. The remainder of this section will describe the specific details of how the simulations were performed.

Modeling Philosophy

In this research, finite element simulations were performed using Abaqus.[18] In all models, gusset plates, splice plates, and parts of members that are in the vicinity of the given gusset plate joint are modeled using four-node, reduced integration, linear formulation shell elements referred to as S4R elements within Abaqus. It was targeted to model truss members using shell elements within a minimum of three times the connection length of a given truss member (i.e., the shell representation of the member extended two connection lengths beyond the edge of the gusset). However, to increase efficiency of the finite element modeling procedures, members are modeled with shell elements for the first 200 inches unless otherwise noted. A typical connection model is shown in Figure 36. All the parts not shown as lines were modeled using S4R elements. The remaining lengths of the truss members outside of the 200 inch limit, as well as the truss members that are not connected to the gusset plate joints, were modeled using 2-node linear beam elements (the B31 element in Abaqus). Multi-point constraints were used to connect a cross-section modeled with shell elements to an end node of a beam element.

The basic concept of the model was to isolate the connection of interest into a two-panel truss system. In all subsequent discussions, points in two-panel systems are always referred to as U1 through U3 for points on the upper chords and L1 through L3 for points on the lower chords. For all cases, the gusset plate joints under consideration are located either at U2 or at L2 locations. For example, for the connection shown in Figure 36, the gusset plate joint is located at U2. Also represented in this figure are the boundary conditions imposed upon the model. All the end nodes of truss members that are on the outside perimeter of the two-panel system are restrained in the out-of-plane direction. For in-plane movements, a simply supported condition is modeled. In addition, an out-of-plane restraint is applied at one node at the center of the top or bottom splice plates, to represent the out-of-plane restraint typically provided by floor systems. However, the out-of-plane reaction due to floor system restraint was found to be negligible in all the study joints.

As shown in Figure 36, all the loads representing dead and live loads are applied in the plane of the truss to nodes that do not have restraint in the direction of the load. The only exception was that of the vertical member. For vertical members, the panel point load was applied at the intersection of the beam and shell element transition. This decision was based on the fact that in most bridges, this load is transferred from a floor beam which is attached below the joint. By applying this load at the end node of a beam element, the issues associated with the stress concentrations at the location where the load is applied to the shell element can be avoided.

In the analysis of the experimental specimens, the joints were modeled as they were tested, and did not require the two-panel truss to apply the loads. Rather, loads and boundary conditions were modeled as they were applied in the laboratory. The meshing of the gusset plates and members used the same philosophy as those in the two-panel truss configurations.

Geometric Imperfections

For all connection models, excluding the laboratory specimens, Figure 37 shows typical geometric imperfection shapes used in the simulations. It can be seen that geometric imperfections are incorporated not only on the gusset plates but also on the compression member itself. These imperfections are generated by a separate linear elastic analysis of the given test joint model. In this separate analysis, pressure loads are applied on the gusset plates so that out-of-straightness of gusset plates on the compression diagonal side is generated and out-of-plane displacements are applied at the end of the compression diagonal so that initial out-of-plane plumbness of the member is also generated. These imperfections generally look like the first mode buckling behavior of the gusset plate which is an out-of-plane sway mode. While real imperfections may not follow this shape, in a buckling analysis it would represent the lower bound of the buckling resistance produced by the analysis.

After the deformed shape is obtained from the pressure load analysis, the deformations are scaled such that the maximum magnitude of the out-of-straightness of gusset plates and the out-of-plumbness of a diagonal member match selected maximum imperfection limits. The selected limits are: (1) $L_{max}/150$ for the maximum out-of-straightness of gusset plates, where L_{max} is the maximum length of free edges adjacent to the compression diagonal and (2) $0.1L_{gap}$ for the maximum out-of- plumbness of the compression diagonal, where L_{gap} is the smallest length of the gap between the compression diagonal and the adjacent members. For the connection shown in Figure 37, the vertical free edge between the left chord and the compression diagonal gives L_{max} of 35.17 inches. Therefore, the maximum out-of-straightness of the gusset plate was scaled to be 0.235 inches. In addition, L_{gap} is 1.0 inch between the compression diagonal and the vertical member. Therefore, a maximum out-of-plumbness of the compression diagonal of 0.1 inch was used.

While the limits may seem arbitrary, the research team tried to use relevant codes and standards to determine what kind of fabrication or erection standards may be applicable to truss connections that may influence the alignment of truss members and hence cause gusset plate imperfections. However, no specific language could be identified that spoke to allowable tolerances of as-built gusset plates as most tolerances have to do with allowable sweep of compression members. For instance, the American Welding Society D1.5 “Bridge Welding Code” contains a section on dimensional tolerances which limits the out-of-straightness of welded members (i.e., built-up truss members) to 0.125 inches per 10 feet of length which translates to L/960 or an end slope of 0.00419 (based on circular curvature).[19] If the gusset plate is assumed to be drawn to the framed member by bolting it will assume the same slope as the member since it is much more flexible out-of-plane. Thus a 48 inch wide plate could be pulled

out-of-straight by 0.20 inches at maximum tolerance. Again, since this is not exclusively meant for gusset plates, a sensitivity study on the magnitude of the imperfections was performed early in the project. What was found is once the imperfections exceeded approximately 0.06 inches, the change in the buckling resistance was relatively small. Therefore, imperfection limits used in the research were a middle ground between what could be found in a relevant specification versus pure analysis.

In the analysis of the experimental specimens, the real shape of the gusset plates and orientation of the members extracted from the FARO data was entered directly into the analysis and an assumed shape was not used.

Material Properties

Figure 16 shows the true stress-strain curves for Grade 50 and Grade 100 steel used in the parametric study simulations. The yield strength of the material was determined based on a bias of 1.10 of true yield strength from the nominal specified and a reduction of 2 ksi to account for the difference between the 0.2 % offset and static yield strengths. The 2 ksi reduction was based on observations collecting coupon data in support of the experimental testing. Therefore, for Grade 50 steel, the static yield strength, F_{ys}, is 50 ksi × 1.10 – 2 ksi = 53 ksi. After this decision had been made, it was found that static yield strength typically has a bias of 1.05, or 52.5 ksi for a Grade 50 material which reinforced the chosen value.[21]

The true stress-strain curve shown in Figure 38 is based on curve-fitting data from some of the coupon tests performed as part of the experimental program. The curve-fit defined the shape of the curve post-yield and it was adjusted to have a yield strength of 53 ksi. In the simulations, all the data points shown in Figure 38 are input explicitly from the point where the plastic strain is 0.0 to 0.2. Abaqus assumes a flat plateau after the last data point.

As mentioned above, the Grade 100 steel was also used in the simulations of selected cases. The static yield strength of Grade 100 steel is also obtained as described above and as a result, F_{ys} = 100 ksi × 1.10 – 2 ksi = 108 ksi. The true stress-strain curve shown in Figure 38 is based on curve-fitting data of coupon tests performed for the experimental member plate which was ASTM A514. The stress-strain curve data of Grade 100 steel for test simulations is input in Abaqus as described above.

When modeling the experimental specimens, the real plate properties were used. As described further in Appendix D, 14 coupons were tested from each parent plate that the gusset and splice plate for each specimen were fabricated from. A single material model was then defined for each specimen by averaging the results from all 14 coupons.

Fastener Strengths

For all the test simulations, the fasteners are modeled with nonlinear strength properties. In Abaqus, fasteners can be modeled using connector elements with nonlinear properties. Figure 39

shows the nonlinear shear-force and shear-displacement curves for A307 and A490 bolts and hot-driven rivets. There are stark contrasts between the three models because they are in terms of the shear force, not stress. For instance, there is a marked difference in cross-sectional areas between the 7/8 inch diameter A307-N bolt and nominal 7/8 inch rivet driven into a standard oversized hole. In addition, these fastener models also considered the deformation of the bolt holes as holes were not considered in the finite element simulation. For this reason, the curve for a 7/8 inch A490-X bolt did not result in the shear failure of the bolt, rather all the deformation was ovalization of the bolt hole leading to the apparent ductility of the fastener model. The fastener properties are modeled such that the strength curves are applied to the square root of the sum of squares of all the shear loads within the fastener element. For the places where fasteners connect three or more plates, these fasteners have two or more layers of connector elements. For the out-of-plane component, elastic behavior is assumed with a stiffness of EA/L, where E is Young's modulus, A is the cross-section area of a fastener, and L is the total length of a fastener. Relative movements at the ends of connector elements are modeled such that relative rotations are restrained but the independent displacements are allowed.

Failure Criteria

Determining the point of failure for each analytical model was controlled by three criteria; the first one reached determined the failure point. These were:

1) Peak of the load versus displacement curve

   In general, the load versus displacement curve from the analysis has a loading and a post-peak unloading path.

2) 4% equivalent plastic strain (PEEQ) at mid-thickness

   In the finite element models, the actual bolt holes are not modeled and fracture of the steel is not incorporated into the nonlinear material model. Hence, the models cannot capture net section limit-states. This value is arbitrarily set at 4%, but the experience of the research team has found this to be an indicative strain level where faith in the model may begin to become unreliable (i.e., when net section failures may occur considering net sections are not modeled.

3) 0.2 inch fastener shear displacement

   In the component tests performed and reported upon in Appendix C, it was noted that generally rivets and bolts failed in shear after approximately 0.2 inches of shear displacement. Since the fastener models used in the analyses are also nonlinear, this limit represents when fasteners may begin to fail and control the strength of the connection. Overall, this limit is rarely controlled.

.

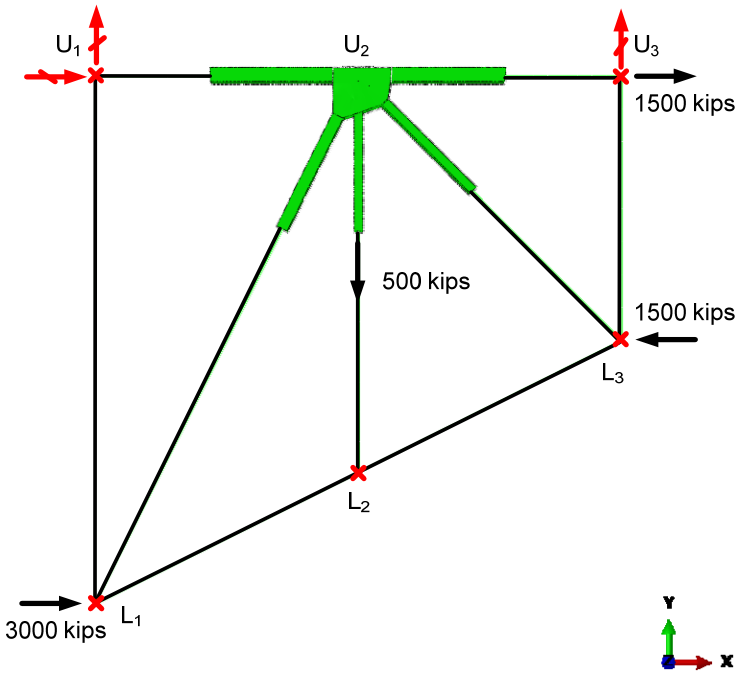

Figure 36. Typical loading and boundary conditions.

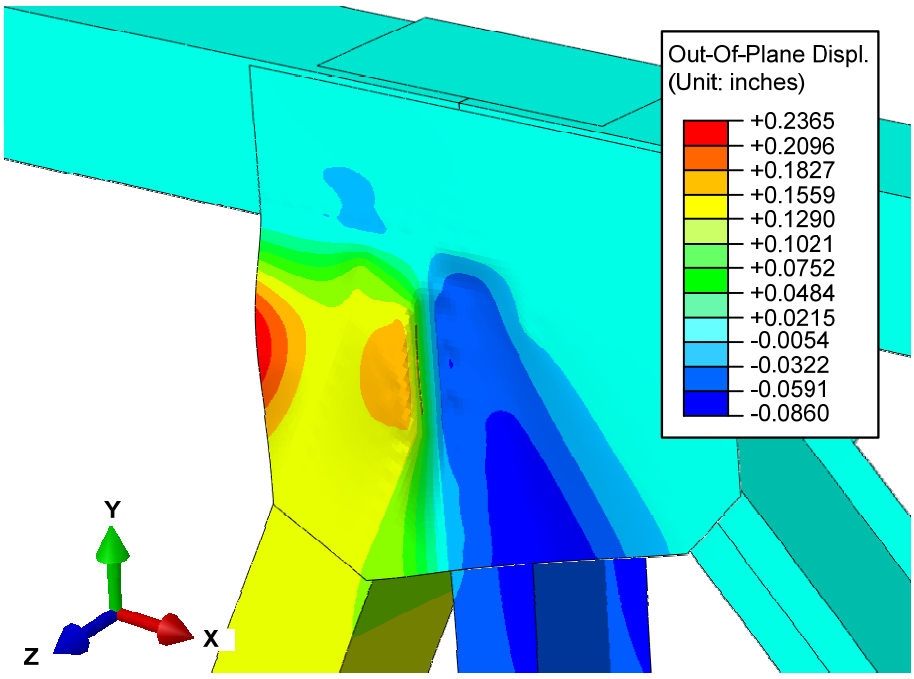

Figure 37. Typical geometric imperfection shapes on gusset plate joints.

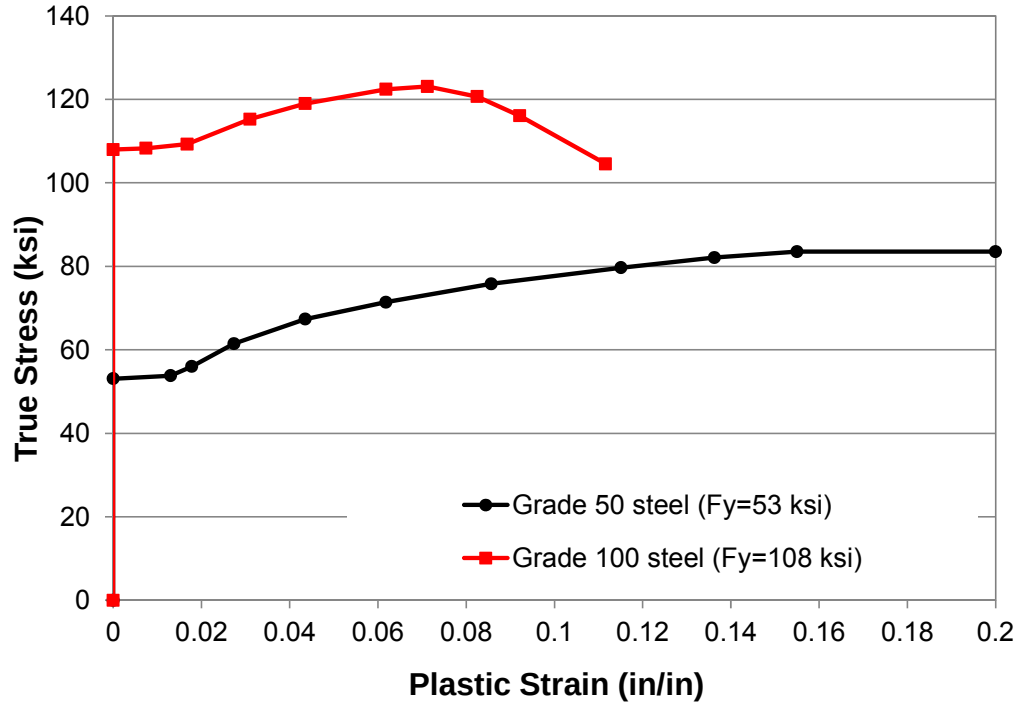

Figure 38. True stress-strain curves for Grade 50 and Grade 100 steel.

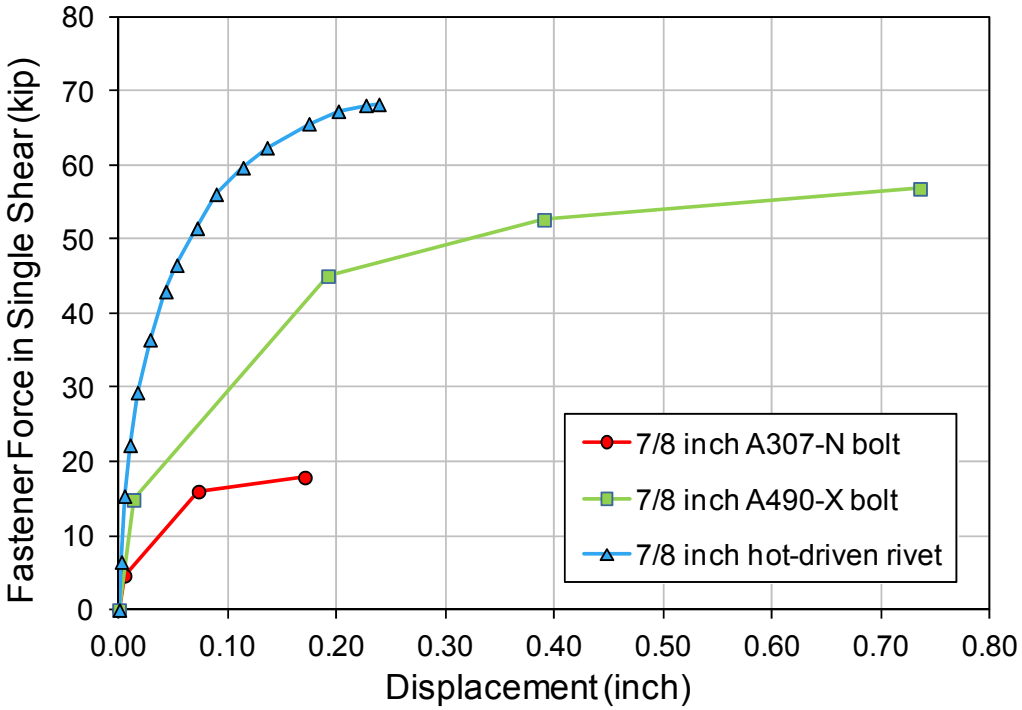

Figure 39. Nonlinear shear-force shear-displacement curves 7/8 inch A307, A490 bolts and hot-driven rivets.

Analysis Matrix

In total there were 201 different models analyzed as part of the parametric finite element study. This section will briefly describe the matrix, but more detailed information can be found in Appendix I.

Three main truss bridge configurations were used in the parametric study. These are (1) Warren trusses with vertical members, (2) Pratt trusses, and (3) Warren trusses without vertical members. Examination of the available bridge plans indicated that longer bridges with continuous spans generally have Warren configurations with or without vertical members (see Appendix A). In addition, the NCHRP 12-84 project panel indicated that Warren trusses without verticals are common in more recent construction, and that Pratt truss configurations are used mostly for shorter single span bridges.

For the selected parametric bridge configurations, a number of typical joints were extracted and designed for different locations within the hypothetical bridge spans. The selection of locations and the corresponding loading scenarios for these joints are discussed below. In addition to the test joints for the above three bridge configurations (Warren with verticals, Pratt, and Warren without verticals) six additional test joints were designed to incorporate other specific cases. These include corner joints, joints that have a positive angle between the chord members on each side of the joint, and joints that have a negative angle between the chord members on each side of the joint.

With the exception of corner joints, all the test configurations are two-panel subassemblies with the test joint in the middle. By using two-panel systems, the loads from the bridge can be applied at the ends of the subassembly and the two-panel system in essence imposes realistic equilibrium and kinematic conditions at the test joint.

Figures 40 through 43 summarize the 20 base geometries investigated in the parametric study. Within the four figures, the joints are titled based on location within a truss either being at midspan, near a pier, at a pier, and inflection point. The location within the truss gives a broad description of the type of loading imposed upon the gusset plate. For instance, midspan joints have light loading on the diagonals, but very large chord loads. Joints at a pier generally have very large loads where all members are either compressive or tensile depending if it is an upper or lower joint. Joints at an inflection point generally have high diagonal member loads with chord loads in a coincident direction leading to large shear forces through the gusset. In addition, different truss depths were used to attain different framing angles between diagonals and chords.

The 20 base geometries were designed to meet the five resistance checks of the FHWA Guide. The members had their ends chamfered to create the most compact joints possible. The 20 connections were first analyzed according to the FHWA Guide design then additional variations on these 20 base geometries were developed to construct the matrix of 201 models. These additional model parameters are described herein.

Plate Thickness

The advantage to using shell element formulations in a parametric study is that the plate thickness can easily be changed to create a new model. Many of the base geometries were quickly reanalyzed by varying the gusset plate thickness from 0.25 to 0.625 inches in 0.125 inch increments. In doing this, there was a pronounced transition from buckling to shear failures as the plate thickness increased.

Mill-to-Bear versus Non-Mill-to-Bear Compression Splices

Four connections were selected to study the effects of mill-to-bear conditions at compression chord splices. Since the original series of study joints had a gap between adjoining chord members, the joint failed via crushing of the gusset in the chord splice. Adding the mill-to-bear condition in select joints allows for the next failure mode to be identified. The selected connections are P1, P11, P19, and P20. In finite element models, the continuity between chord members is modeled by *tie* constraints between all the nodes of the cross-section at the end of chord members. That is, all the displacements and rotations of the cross-section at the end of one of the chord members are completely *tied* to the cross-section of the other chord member; these are kinematic couplings that actually reduce the overall degrees of freedom of the model.

Material Strength

All the initial joints were analyzed using Grade 50 materials for their gusset plates and splice plates. To study the effect of high-strength materials on the behavior of gusset plate connections, three test joints were selected to be analyzed using Grade 100 materials for gusset and splice plates. For the first set of analyses, the gusset plates have the same thickness as the initial designs but have Grade 100 material. Then for the second set of analyses, the gusset plate thicknesses are reduced so that the plates have the same strength based on their area and the material strengths.

Member Chamfer versus No Member Chamfer

As mentioned above, the initial set of joints was designed using chamfered members. In other words, all these joints have diagonals that are chamfered as much as possible until only two fasteners can be attached at the end of members. When members are chamfered, the areas between chamfered edges and the adjacent members are extremely small and as a result, the gusset plate area is relatively small. After the initial set of joints was analyzed, a number of test joints were selected and redesigned with *unchamfered* members. In general, when the members are unchamfered, the areas between diagonals and chords and/or diagonals and vertical members are larger than the ones in joints with chamfered members. As a result, the lengths of free edges are longer (relative to the overall area of the plate). Therefore, by varying member chamfers, the effect of larger distances between members and longer free edges on the failure modes and maximum capacities was studied.

Shingle Plates

All the gusset plate joints were initially designed without shingle plates. However, joints at piers generally have shingle plates because otherwise the main gusset plates need to be significantly thicker in order to transfer large member forces into the pier. Therefore, several cases were selected to study the behavior of shingle plates. The goal of this study was to develop design methods for shingle plates, which can be one retrofit option.

Edge Stiffening

One of the common practices to retrofit gusset plate joints is to add edge stiffeners on the free edges. Engineers commonly add short angles on the inside of gusset plates between members, e.g., between a chord and a diagonal. In this study, the effect of stiffeners on the maximum capacities of gusset plate joints was studied.

Corrosion

The effect of corrosion on the behavior of gusset plate joints was also studied in this research. A number of joints were selected to be modeled including holes and corroded regions. These corroded test cases were then analyzed with shingle plates to investigate the benefits from adding shingle plates as a retrofit method for corroded gusset plate joints.

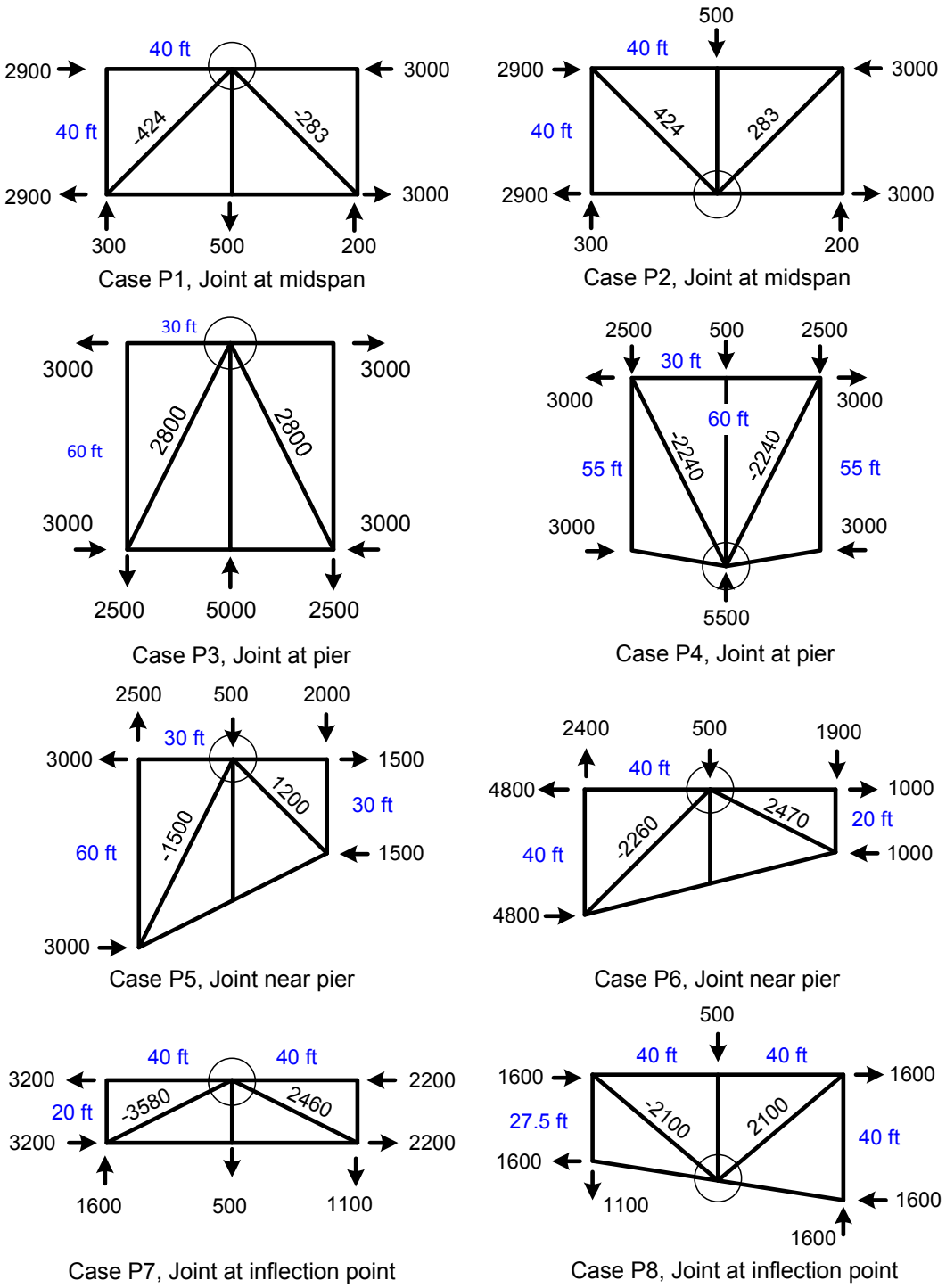

Figure 40. Warren with vertical configurations.

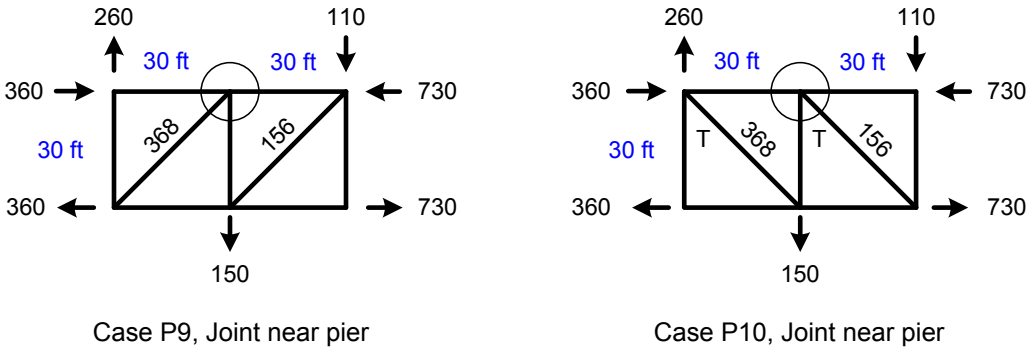

Case P9, Joint near pier

Case P10, Joint near pier

Figure 41. Pratt configurations.

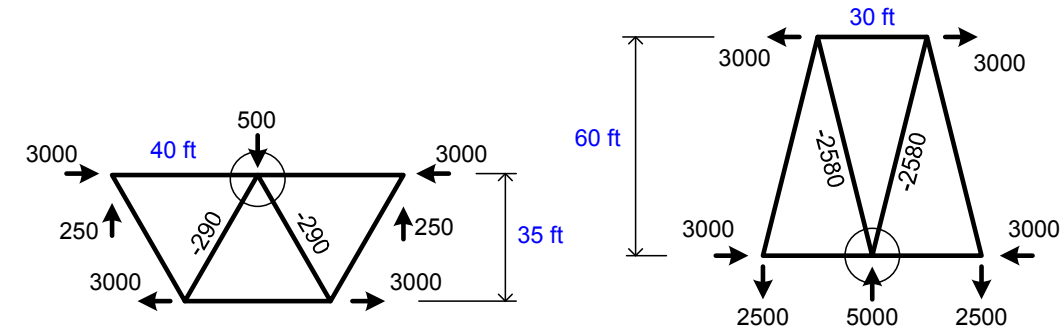

Case P11, Joint at midspan

Case P12, Joint at pier

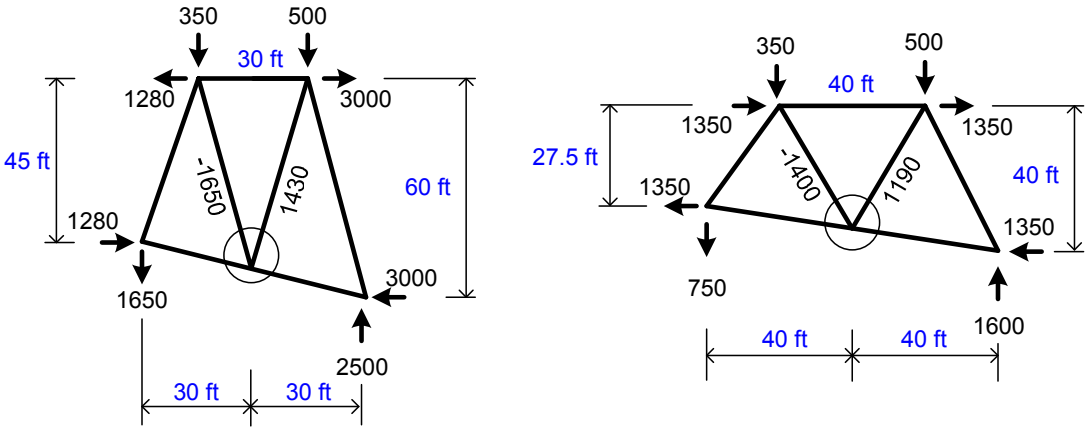

Case P13, Joint near pier

Case P14, Joint at inflection point

Figure 42. Warren without vertical configurations.

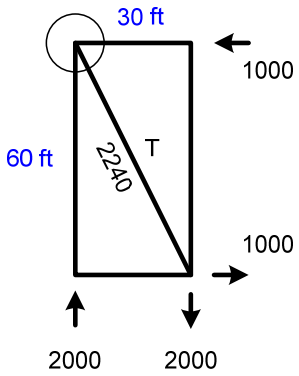

Case P15, Corner Joint

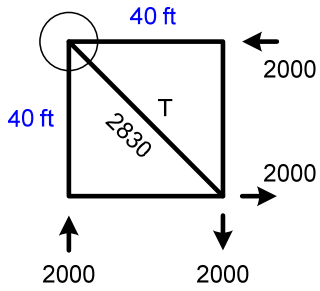

Case P16, Corner Joint

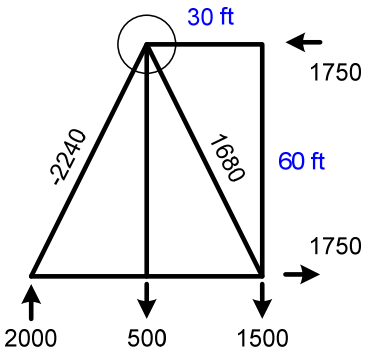

Case P17, Joint with positive angle between chords

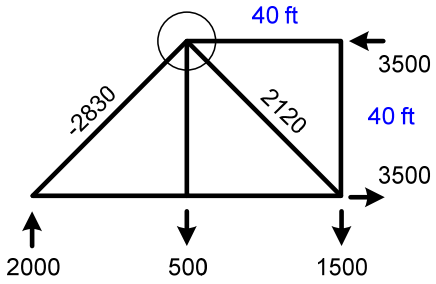

Case P18, Joint with positive angle between chords

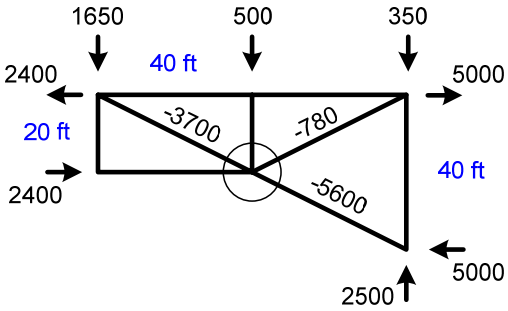

Case P19, Joint with negative angle between chords

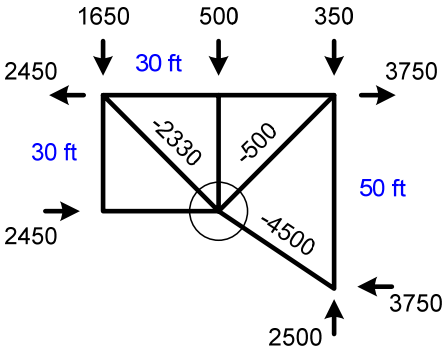

Case P20, Joint with negative angle between chords

Figure 43. Other configurations.

CHAPTER 3. FINDINGS AND APPLICATIONS

This chapter will focus on the results of both the experimental load testing performed at Turner-Fairbank Highway Research Center and the analytical work performed at Georgia Tech. Although elastic load scenarios were investigated both analytically and experimentally for many, but not all specimens, the data gathered during these elastic loading scenarios will not be presented herein, but rather will be provided in the report appendices. This chapter is intended to convey only the results from the final failure load tests that were performed on each specimen in the testing matrix and the analytical work performed at Georgia Tech. A discussion of the specimen-specific loading protocols, the predicted and actual loads at failure, the failure mode, and accompanying pertinent data will be presented herein.

EXPERIMENTAL SPECIMENS

In total there were 13 connections tested; however, one of the tests, 490LS3, was an accidental failure where operator error uncontrollably crushed the specimen. The specimen geometry was retested and called 490LS3-1. All 12 specimens either failed via buckling of the gusset plate whereby the end of the compression diagonal moved out-of-plane, or by shear along the horizontal plane along the chord. All the raw data from the various instrumentation systems is graphically shown in Appendices E, F, G, and H, only data relevant to the discussion will be presented in this part of the report.

Buckling failures were easy to distinguish because failure was visually apparent and in all specimens, buckling resulted in out-of-plane movement of the compression diagonal. A typical buckle is shown in Figure 44 where it can be seen that when the gusset plate buckles, the compression diagonal moves out-of-plane essentially as a rigid body. Unfortunately, post-test visual observations of all the specimens seem to indicate failure due to buckling. Even though shear may have been the failure mode, after so much shear deformation, the compression diagonal still moved out-of-plane. To isolate out the shear failures, both the FARO and DIC data had to be queried to determine whether or not shear had occurred. For instance, shown in Figure 45 are two plots created from FARO data. The vectors show the displacement of select bolt targets on the gusset plate, with the tail representing the pretest locations, and the head as the post-test locations amplified 25 times. In both plots, the six vectors in the upper left are for targets over the compression diagonal. In buckling failures, the large vector motions are isolated around the compression diagonal, whereas for shear failures, large vector motions are similar for both diagonals and vertical members and generally pointing to the right indicating the upper half of the plate sheared relative to the lower half. The DIC data was looked at to verify that there was a large amount of straining along this plane (generally in excess of 1.5% Tresca strain).

Table 6 contains a summary of the member loads entering each experimental connection at failure (which was either buckling or shear). Also shown in Table 6 are shaded cells highlighting the failure mode and either the load in the compression diagonal or internal shear depending if it

was a buckling or shear failure. Only the static yield strength of the plate material is also shown. For further information on the testing of the plate material, see Appendix D.

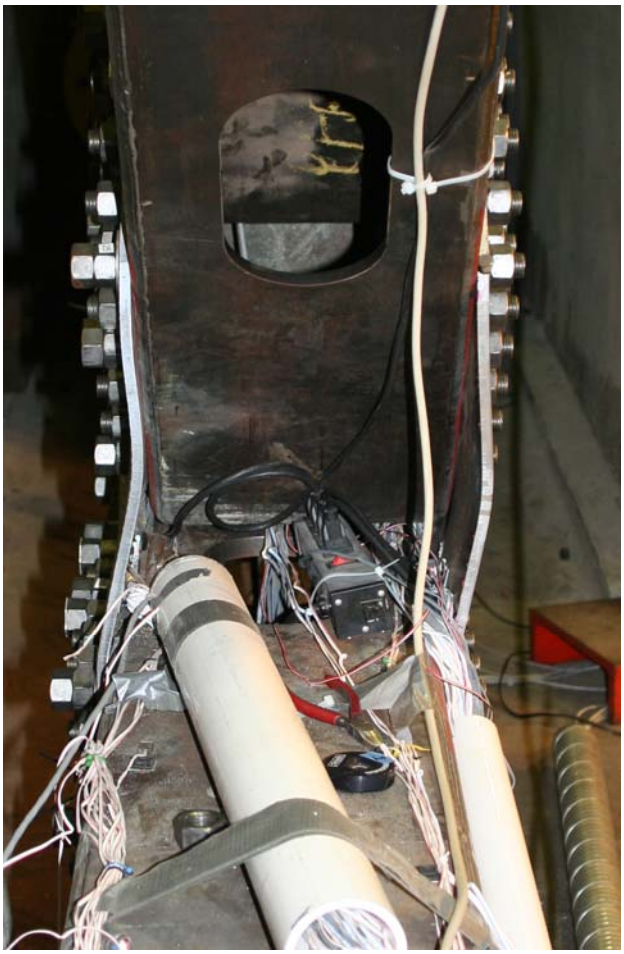

Figure 44. View looking down chord at out-of-plane sway buckle of gusset plate, specimen GP307SS3.

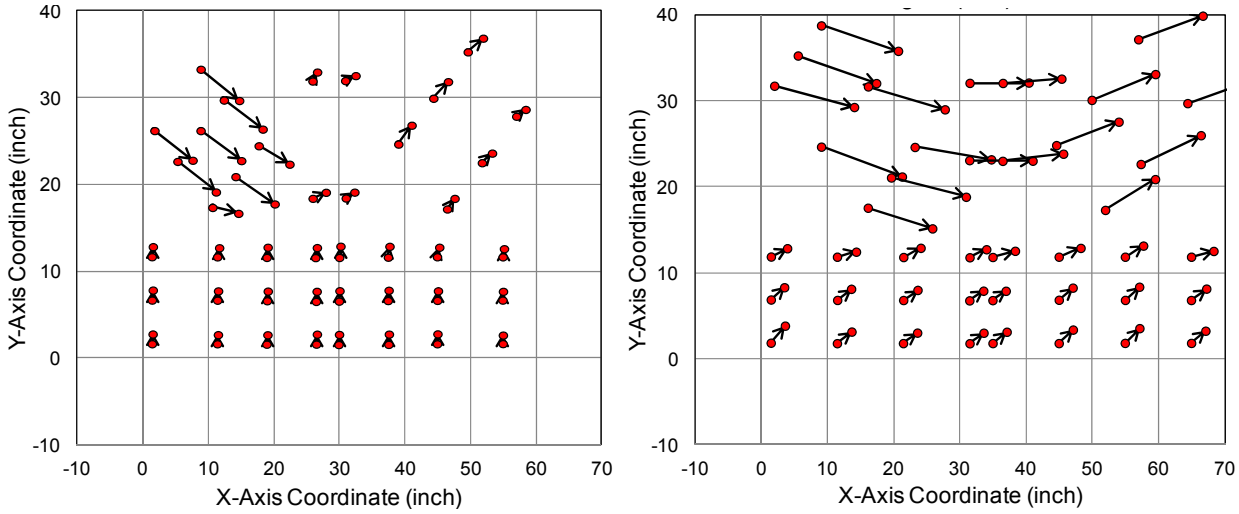

Figure 45. Vector motions of gusset plate targets amplified 25 times. Specimen 307SS3 (left). Specimen 307LS3 (right).

Table 6 Summary of Failure Loads and Modes of Experimental Specimens

Specimen	Phase 1							Phase 2					
	307SS3	490SS3	490LS3 [a]	490LS3-1	307LS3	307SL3	307SL4	490LS3-2	490SS3-1	307SS3-1	307SS3-2	307SS3-3	307SS3-4
Static Yield Strength (ksi)	36.4	46.4	45.6	48.5	48.2	46.6	33.0	45.5	45.7	47.2	47.8	37.9	38.0
Comp. Diag. Load [b] (kips)	-716	-728	-498	-527	-796	-946	-1070	-865	-633	-446	-482	-519	-712
Tens. Diag. Load [b] (kips)	507	728	830	881	405	929	1066	483	915	285	696	735	1003
Vertical Load [b] (kips)	141	0	-234	-248	280	0	0	245	-195	90	-148	-154	-215
East Chord Load [b] (kips)	-520	-528	-498	-529	290	-706	-770	-526	-659	-321	-512	-533	-680
West Chord Load [b] (kips)	345	501	441	446	994	620	740	427	435	196	321	354	533
Horizontal Shear Force (kips)	865	1029	939	995	849	1326	1510	953	1094	517	833	887	1213
Failure Mode	Buckling	Shear & Buckling	Note a	Buckling	Buckling	Shear	Shear	Buckling	Shear	Buckling	Shear	Shear	Shear

NOTES
[a] – Specimen accidently crushed after failure of vertical actuator bracing
[b] – Negative loads represent internal axial loads that are compressive

ANALYTICAL

The parametric analytical study was performed by Georgia Tech and is reported in full detail in Appendix I. This included the detailed analysis of 201 finite element models that considered a wide variety of gusset plate geometries, under different loading configurations, different plate thicknesses, with and without multi-layered gussets, and also included the effects of corrosion. This section will only present the results of that study in terms of the various limit-states that were observed and how they relate to simple prediction equations. The goal of these analyses is to verify the predictive equations and to understand the statistical variation in the analytical models of each failure mode that can be used in the LRFD calibration task. As such, the analytical data is also complemented with the experimental results where appropriate. *This report was written after the submission of Appendix I and there are some differences of interpretation of model results between the PI and the authors of Appendix I. These differences are mainly attributed to mixed-mode failure models where shear yielding and buckling appear to be occurring simultaneously, making it somewhat subjective. This is not to detract from the accuracy of what is reported in Appendix I, although keen readers may note differences between data reported in the main report and Appendix I.*

SYNTHESIS OF RESULTS

It is important to make a distinction between design and rating in the results from this research, since the greater challenge pertains to rating of the existing inventory. It is more expensive to retrofit an existing gusset plate with inadequate rating than to increase the plate thickness in design. The sections to follow outline the results attained in both the experimental and analytical work in term of the individual failure modes that were observed. The statistical variation of this data is integral to the ϕ-factor calibrations that will be discussed in Chapter 4. Two of the limit-states will present different statistics, one using all the data, and the other using data from gusset plates 0.375 inches thick or greater. The reasoning behind this is that different calibrations were performed for the BDS and the MBE. The scatter associated with plates thinner than 0.375 inches was greater, leading to less favorable ϕ-factors. Therefore, for design it was assumed that a thickness limit could be imposed for the gusset plates and the data for "thin" gussets could be ignored. However, in rating, the plate thickness is a given and since the existing inventory of gusset plates has "thin" plates in it, the statistics used in determining MBE ϕ-factors must include all the data.

Shear Failures

Tables 7 and 8 summarize the associated relevant data for analytical and experimental connections that failed in shear. Within each table, the shear load at which the connection failed ($V_{failure}$) and the nominal calculated resistance for shear yielding (V_{ny}) and shear fracture (V_{nu}) are tabulated. While the parametric study did not use models with the fidelity required to capture shear fracture, nor was it observed in the seven experimental shear failures, the shear fracture calculations are shown for completeness. The nominal shear yield resistance does not consider

the Ω reduction factor used in the FHWA Guide (i.e., $V_n=0.58F_yA_g$) and this will be derived from the LRFD calibration in the next chapter.

The ratios between the failure load and the associated resistance calculations are also tabulated in the tables which represent the professional factor to use in calibration. However, the shear fracture state will not be calibrated. The cells in the table shaded grey represent the controlling nominal resistance equation. In many cases it can be seen that the nominal shear fracture limit-state would control the design/rating, despite it not being an observed failure in the experimental connections, nor could that mode even be captured in the finite element models. This shows that there is probably some excess conservatism in the shear fracture equation, though this project does not have the required data to support or refute that claim.

In total there were 44 observed shear yielding failures. The professional factor data is graphically shown in Figure 46. While they were not included in the statistical calculations of the professional factor, the data from the three experimental shear failures with simulated section loss and the I-35W U10 joint are shown in the plot. The data from the 41 failures (excluding those with section loss) are plotted on normal probability paper in Figure 47. The best-fit line on the probability paper was used to determine the professional factor statistics for the shear yielding limit-state; the average and coefficient of variation (COV) of the data is 1.017 and 0.069 respectively. Only one failure had a plate thinner than 0.375 inches. Its professional factor was near the mean; therefore, the statistics would not change when ignoring plates thinner than 0.375 inches.

Table 7 Shear Data of Analytical Connections that Failed in Shear

	Specimen	Plate Thickness (inch)	Length of Shear Plane (inches)	$V_{failure}$ (kips)	Full Plane Yield $[0.58F_yA_g]$ (kips)	$V_{failure}/V_{ny}$	Full Plane Fracture $[0.58F_uA_n]$ (kips)	$V_{failure}/V_{nu}$
UNCHAMFERED	E1WV-307SS	0.6250	59	1653	1557	1.06	1634	1.01
	E3WV-307SL	0.4375	66.5	1604	1573	1.02	1336	1.20
		0.5000	66.5	1856	1797	1.03	1527	1.22
		0.6250	66.5	2333	2247	1.04	1909	1.22
	E4WV-490SS	0.4375	54.8	1318	1290	1.02	1118	1.18
		0.5000	54.8	1513	1475	1.03	1278	1.18
		0.6250	54.8	1894	1843	1.03	1598	1.19
	E1W-307SS	0.4375 [a]	59	1023	1090	0.94	1144	0.89
		0.5000 [a]	59	1246	1246	1.00	1307	0.95
		0.6250	59	1742	1557	1.12	1634	1.07
	E3W-307SL	0.3750 [a]	66.5	1326	1348	0.98	1145	1.16
		0.4375 [a]	66.5	1604	1573	1.02	1336	1.20
		0.5000	66.5	1830	1797	1.02	1527	1.20
		0.6250	66.5	2294	2247	1.02	1909	1.20
	E4W-490SS	0.4375 [a]	54.8	1235	1290	0.96	1118	1.10
		0.5000	54.8	1483	1475	1.01	1278	1.16
		0.6250	54.8	1884	1843	1.02	1598	1.18
	P8U-WV-INF-02	0.5000 [a]	105.6	2923	3246	0.90	3276	0.89
	P14U-W-INF-01	0.6250 [a]	57.1	2052	2194	0.94	2210	0.93
CHAMFERED	P5C-WV-NP-01	0.5000 [a]	69.5	1914	2136	0.90	2158	0.89
		0.6250	69.5	2507	2671	0.94	2697	0.93
	P6C-WV-NP-02	0.5000	128.1	3731	3938	0.95	3995	0.93
		0.6250	128.1	4911	4922	1.00	4994	0.98
	P7C-WV-INF-01	0.4375	142.2	3944	3825	1.03	3865	1.02
		0.5000	142.2	4754	4371	1.09	4417	1.08
		0.6250	142.2	6051	5464	1.11	5522	1.10
		0.7000	142.2	6915	6120	1.13	6184	1.12
	P8C-WV-INF-02	0.3125	94.1	1884	1808	1.04	1830	1.03
		0.3750	94.1	2339	2169	1.08	2196	1.07
		0.4375	94.1	2729	2531	1.08	2562	1.07
		0.5000	94.1	3151	2893	1.09	2928	1.08
		0.6250	94.1	3898	3616	1.08	3660	1.07
	P14C-W-INF-01	0.5000 [a]	57.1	1626	1755	0.93	1768	0.92
		0.6250	57.1	2132	2194	0.97	2210	0.96
	P15C-CJ-01	0.5000	69.7	2304	2143	1.08	2167	1.06
	P7C-HS1	0.7000	142.2	12317	12470	0.99	9276	1.33
	P8C-HS1	0.5000	94.1	5815	5894	0.99	4392	1.32
	I-35W U10 [b]	0.5000	104.0	2753.869	3076	0.90	3468	0.79

[a] – These specimens had mixed shear and buckling failure response and were included in both limit-states.
[b] – This connection likely failed by buckling, though a significant portion of its horizontal plane was yielded at failure and it is shown for reference. The connection is not included in any statistical calculations.

Table 8 Shear Data of Experimental Connections that Failed in Shear

	Specimen	Plate Thickness (inch)	Length of Shear Plane (inches)	$V_{failure}$ (kips)	Full Plane Yield $[0.58F_yA_g]$ (kips)	$V_{failure}/V_{ny}$	Full Plane Fracture $[0.58F_uA_n]$ (kips)	$V_{failure}/V_{nu}$
UNCHAMFERED	GP307SL3	0.3750	66.5	1326	1348	0.98	1145	1.16
	GP307SL4	0.5000	66.5	1510	1273	1.19	1452	1.04
	GP490SS	0.3750	54.8	1030	1106	0.93	959	1.07
	GP490SS-1	0.3750	54.8	1095	1089	1.00	1150	0.95
	GP307SS3-2 [a]	0.3750	59	833	779	1.07	1041	0.80[b]
	GP307SS3-3 [a]	0.3750	59	887	787	1.13	987	0.90[b]
	GP307SS3-4 [a]	0.3750	59	1213	1242	0.98	1274	0.95[b]

[a] – These connections had simulated corrosion and were not considered in the statistical analysis of shear failures.
[b] – The net section calculation only subtracted the area of the holes in the shear plane; it neglected the effects of the simulated section loss as they were not coincident with each other.

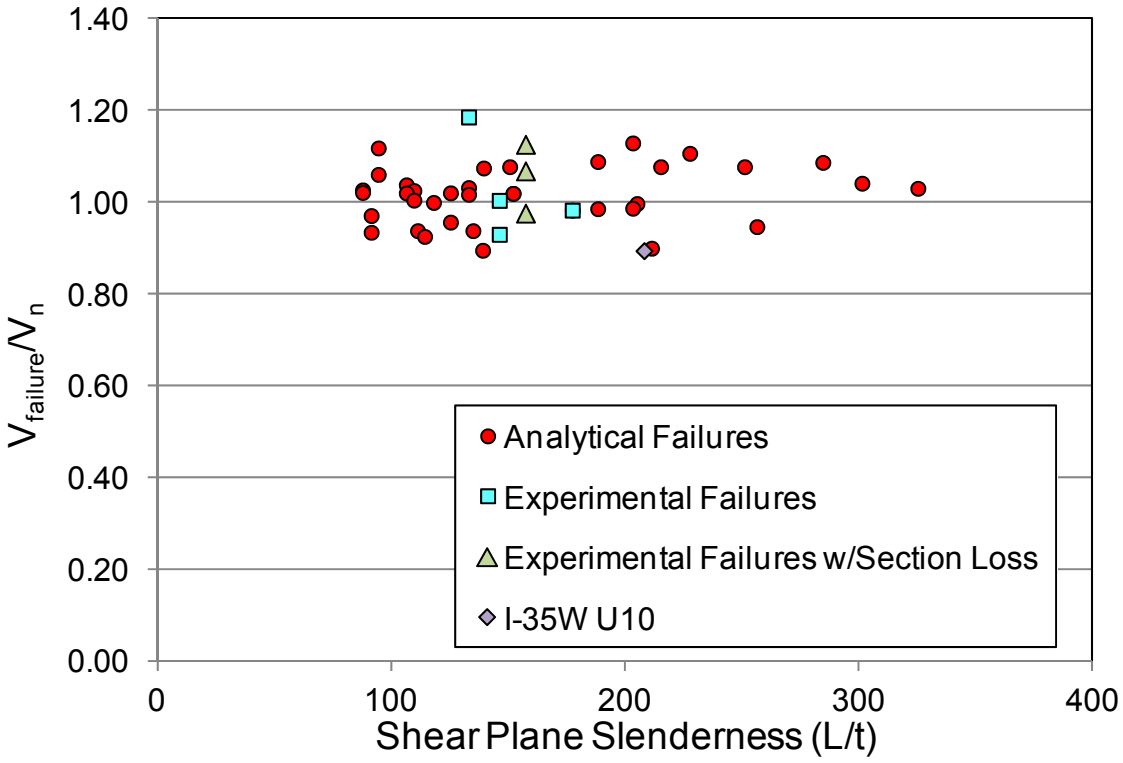

Figure 46. Shear yielding professional factor data.

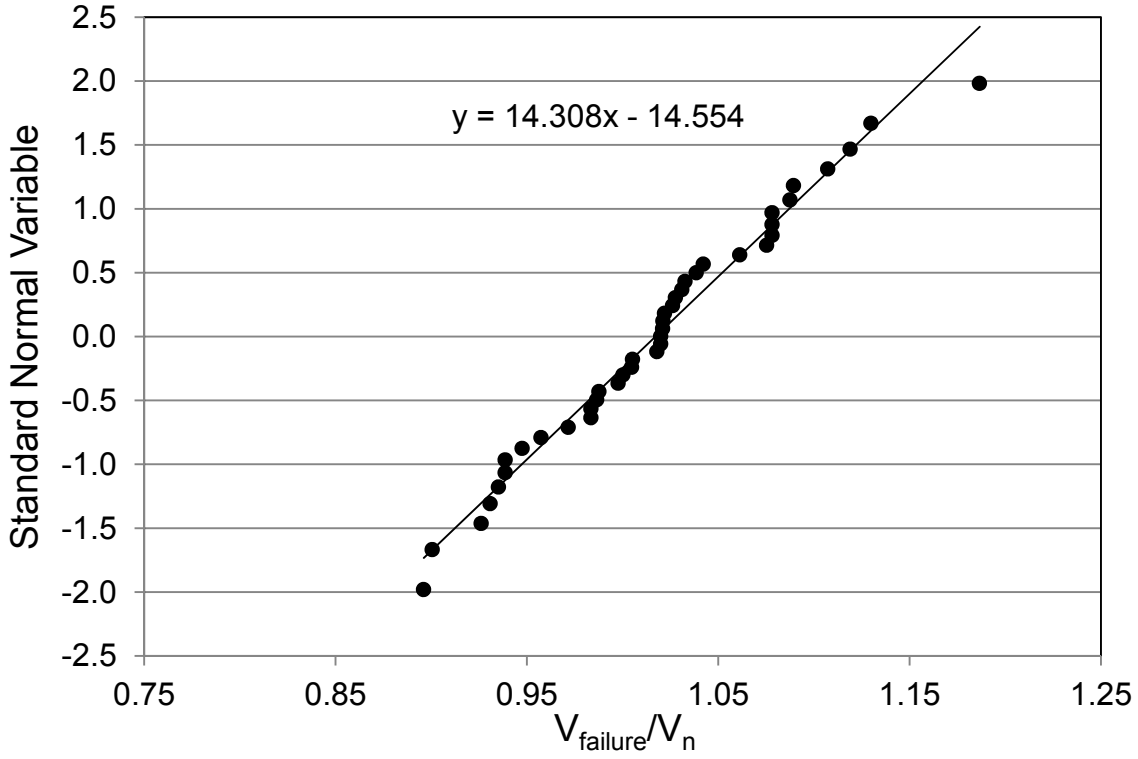

Figure 47. Shear yielding professional factor plotted on normal probability paper.

Buckling Failures

The reporting of buckling failures ignored connections that had edge stiffening, multi-layered gusset plates, or simulated section loss. The effects of these parameters were investigated independently and were purposely excluded to avoid influencing the statistics on buckling.

The data were analyzed according to a buckling calculation method similar to that in the FHWA Guide. The FHWA Guide recommends an equivalent column approach using a Whitmore section. For this work, the Whitmore section is determined using the 30 dispersion angle. Other angles were explored, though they did not change the results and it was deemed better to retain the 30 degree dispersion angle since it is so widely used in the literature. However, this work will explore the influence of the column length in terms of both the physical length calculation and the K-factor. The physical column length is schematically shown in Figure 48. The current FHWA Guide recommends averaging the three lengths from the Whitmore section to the nearest adjacent fastener line, taken at the two ends and middle of the Whitmore section (i.e., average of L_1, L_{mid}, L_3 as shown in Figure 48). If the Whitmore section intersects a fastener line, that length is considered zero. This is considered the average length, or L_{avg}. The other length explored was just the length taken at the middle of the Whitmore section, or L_{mid}.

Tables 9 through 13 outline the data for all the specimens that failed by buckling. In total, there were 124 data points including four experimental connections from this study, five experimental

connections from the Oregon State University testing [23], and one data point representing the I-35W U10 connection. The data summarize the length of the equivalent column in terms of L_{avg} and L_{mid}. The buckling parameter, λ, is calculated at each of these lengths using equivalent column length factors of 1.2 and 0.5, using the equations below.

$$\lambda_{avg} = \left(\frac{KL_{avg}}{r\pi}\right)^2 \frac{F_y}{E} = 12\left(\frac{KL_{avg}}{t\pi}\right)^2 \frac{F_y}{E} \quad \text{(Eq. 6)}$$

$$\lambda_{mid} = \left(\frac{KL_{mid}}{r\pi}\right)^2 \frac{F_y}{E} = 12\left(\frac{KL_{mid}}{t\pi}\right)^2 \frac{F_y}{E} \quad \text{(Eq. 7)}$$

where K is the equivalent column length factor, t is the plate thickness, F_y is the plate's yield strength, and E is the plate's modulus of elasticity.

The five columns to the extreme right of the tables represent the ratio between the actual buckling load of the plate to the unfactored, calculated resistance using the associated λ-value. The calculated resistance just uses the noncomposite column buckling equations in Section 6.9.4 in the LRFD Bridge Design Specification. This ratio will be referred to as the professional factor. Ideally the professional factor should be 1.0 and values less than 1.0 represent unconservative predictions while those greater than 1.0 represent conservative values.

The plots shown in Figure 49 show the variation of professional factor against the associated λ-values. For both equivalent column length formulations (L_{avg} and L_{mid}), the higher K-factors produce very conservative professional factors as the plates become more slender. K-factors less than 1.0 produce much better professional factors, yet in all cases there are still many unconservative professional factors for connections with very compact plates. These plots seem to indicate that having a K-factor of 0.5 and using the L_{mid} column length produces the most favorable professional factors (i.e., closest values to 1.0 with the least scatter). However, even using K=0.5 and L_{mid}, there are still a large number of connections with professional factors much less than 1.0. To understand where this comes from, the same plot in Figure 49(d) is reproduced in Figure 50 with a different y-axis scale and with the analytical connections being segregated into those with and without chamfered members. This clearly shows that the connections with the poor professional factors are mostly those with chamfered members.

The poor buckling prediction for chamfered members is better illustrated in Figure 51. In this figure, essentially the same connection geometry is being compared except for the notion that one uses chamfered members and the other uses unchamfered members. For each case a Von Mises stress contour is shown at failure of each connection where the grey-pink color represents areas that have exceeded yield. The connection with the unchamfered member buckles in a sidesway mode with relatively little yielding and in this case, the Whitmore buckling prediction is accurate. When the members are chamfered, the gusset still buckles, though after a significant amount of yielding around the horizontal and vertical planes of the compression diagonal of which the Whitmore buckling model tends to over predict the available strength. Therefore a two-folded check is recommended that determines the buckling resistance from the minimum of

the Whitmore buckling check using K=0.5 and L_{mid}, or the load in the compression member that would cause a partial plane around that member to yield.

The length of the partial plane is schematically shown in Figure 52. In most cases of subdivided Warren joints, there will be two partial shear planes around a compression member. It is the length along the nearest adjoining fastener pattern between the gusset edge and the intersection with the other fastener pattern. Three simple rules are used to determine which partial plane is critical:

1. The one that parallels the chamfer in the member,
2. The one nearest the smaller framing angle between the compression member and other adjoining members,
3. The one with the minimum shear area if the first two criteria are equal.

In general, the partial plane shear yielding is not intended to be checked for chord or vertical members because there is not an admissible shear plane that would cause out-of-plane instability of the gusset plate.

Using this two-folded approach to predict buckling does provide an overall better approximation of buckling resistance. The data for the 124 models and specimens evaluated with the combined Whitmore buckling and partial plane shear yield model is presented in Tables 14 through 18, using both L_{avg} and L_{mid} and K=0.5. The two columns to the extreme right show the professional factors of the controlling resistance from either Whitmore buckling (using L_{avg} and L_{mid}) or partial plane shear yield. Predictions controlled by Whitmore buckling are shaded yellow whereas those controlled by partial plane shear yielding are shaded green. Graphically, this data is represented in Figures 53 and 54 in terms of the professional factor and λ-value. In both cases, the partial shear plane yield check reduces the propensity of professional factors less than 1.0, and using L_{mid} produces the least number of professional factors less than 1.0.

All the data from Tables 14 through 18 are plotted on normal probability paper in Figure 55. The plots are broken down by those data calculated with L_{mid} and L_{avg}, and further separated considering all the data, and neglecting the data from plates thinner than 3/8 of an inch thick. The data from plates thinner than 3/8 of an inch produced the most scattered professional factors. Therefore calibrations for rating would have to consider all the data since the current inventory has plates thinner than 3/8 of an inch. However, for design calibration, the data can be parsed assuming new gusset plate designs mandate a minimum of 3/8 inch gusset thickness. Most of the data sets plot linearly on the normal probability paper indicating that the normal probability distribution fits them well. The one exception is Whitmore buckling calculated with L_{mid} for all the data, because the upper tail data deviates quite a bit from the best-fit line. However, in resistance factor calibration, the lower tail data controls and a best-fit line can neglect the upper tail data points.[22] The best-fit lines from the data represented on normal probability paper can be

used to calculate the calibration statistics. The means and coefficients of variation are shown in Table 19.

While not presented in this report, the scatter in the Whitmore predictions minimized when K was approximately 0.3. However, this K-value does not have a physical meaning and K is recommended to be 0.5 for all gusset plates. The data presented also show that the best predictions of buckling strength come from using L_{mid} versus the current use of L_{avg} by the FHWA Guide. Overlap of the Whitmore section into other adjoining members was included in the analysis and there appears to be no reason to truncate it, thus making evaluations simpler. Finally, it was shown that for very compact plates, the Whitmore buckling model overpredicts the buckling resistance and a partial shear plane yielding concept has to be used in conjunction with it to accurately predict buckling resistance.

Free Edge Slenderness

There is a common perception that the buckling strength of a gusset-plated connection may be correlated to the slenderness of the free edge. Figure 56 shows the failure load normalized to the yield load on the Whitmore section versus the non-dimensional buckling parameter, λ. Two data series are shown for λ calculated with L_{mid} and L_{free_edge}. The data based on L_{mid} was not plotted if the partial plane shear yield criteria was controlled, hence why there appear to be more data points for the free edge. There appears to be no correlation to the buckling resistance using the free edge slenderness since the data is spread through a variety of λ values, and nowhere near the column buckling curves. The data based on L_{mid} is highly correlated and tracks the AASHTO column buckling curve quite well.

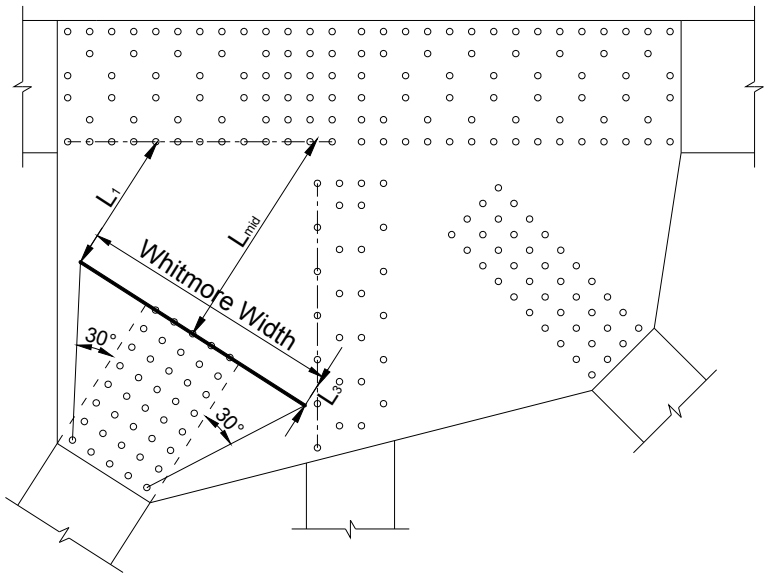

Figure 48. Calculation of equivalent column length.

Table 9 Summary of Models with Buckling Failures

Specimen	Thick. (inch)	F_y (ksi)	$W_{whitmore}$ (inch)	L_{mid} (inch)	L_{avg} (inch)	$P_{failure}$ (kips)	λ_{avg}		λ_{mid}		$P_{failure}/P_n$			
							K=1.2	K=0.5	K=1.2	K=0.5	L_{avg} K=1.2	L_{avg} K=0.50	L_{mid} K=1.2	L_{mid} K=0.5
E1WV-307SS	0.2500	36.4	24.43	13.16	6.20	380	1.35	0.23	6.09	1.06	1.50	0.94	5.91	1.32
	0.3125					530	0.87	0.15	3.90	0.68	1.37	1.01	4.22	1.26
	0.4375					817	0.44	0.08	1.99	0.35	1.26	1.08	2.40	1.21
	0.5000					974	0.34	0.06	1.52	0.26	1.26	1.12	2.06	1.22
E2WV-307LS	0.2500	48.2	27.32	18.11	10.20	398	4.84	0.84	15.27	2.65	3.33	0.86	10.49	1.82
	0.3125					653	3.10	0.54	9.77	1.70	2.79	0.99	8.81	1.61
	0.4375					1091	1.58	0.27	4.99	0.87	1.83	1.06	5.36	1.36
	0.5000					1305	1.21	0.21	3.82	0.66	1.64	1.08	4.30	1.31
	0.6250					1703	0.78	0.13	2.44	0.42	1.43	1.09	2.87	1.23
E3WV-307SL	0.2500	46.6	33.09	13.16	4.40	568	0.87	0.15	7.80	1.35	1.06	0.78	6.52	1.29
	0.3125					738	0.56	0.10	4.99	0.87	0.97	0.80	4.34	1.10
	0.3750					946	0.39	0.07	3.46	0.60	0.96	0.84	3.22	1.05
	0.4375					1145	0.28	0.05	2.55	0.44	0.95	0.87	2.45	1.02
E4WV-490SS	0.2500	46.4	21.55	13.16	7.20	444	2.32	0.40	7.76	1.35	2.35	1.05	7.84	1.56
	0.3125					597	1.49	0.26	4.97	0.86	1.77	1.06	5.39	1.37
	0.4375					874	0.76	0.13	2.53	0.44	1.37	1.05	2.88	1.20
E5WV-490LS	0.2500	45.6	21.55	18.11	12.10	296	6.45	1.12	14.45	2.51	4.42	0.96	9.90	1.72
	0.3125					459	4.13	0.72	9.25	1.61	3.50	1.01	7.85	1.46
	0.4375					803	2.11	0.37	4.72	0.82	2.24	1.09	5.01	1.31
	0.5000					975	1.61	0.28	3.61	0.63	1.94	1.11	4.07	1.29
	0.6250					1276	1.03	0.18	2.31	0.40	1.60	1.12	2.73	1.23
E1W-307SS	0.2500	36.4	24.43	13.16	13.20	322	6.13	1.06	6.09	1.06	5.05	1.13	5.02	1.12
	0.3125					466	3.92	0.68	3.90	0.68	3.73	1.11	3.71	1.11
	0.3750					595	2.72	0.47	2.71	0.47	2.76	1.08	2.74	1.08
	0.4375					723	2.00	0.35	1.99	0.35	2.13	1.07	2.12	1.07
	0.5000					881	1.53	0.27	1.52	0.26	1.87	1.11	1.86	1.11

Table 10 Summary of Models with Buckling Failures –Continued

Specimen	Thick. (inch)	F_y (ksi)	$W_{whitmore}$ (inch)	L_{mid} (inch)	L_{avg} (inch)	$P_{failure}$ (kips)	λ_{avg}		λ_{mid}		$P_{failure}/P_n$			
							K=1.2	K=0.5	K=1.2	K=0.5	L_{avg} K=1.2	L_{avg} K=0.50	L_{mid} K=1.2	L_{mid} K=0.5
E2W-307LS	0.2500	48.2	27.32	18.11	18.10	326	15.25	2.65	15.27	2.65	8.59	1.49	8.60	1.49
	0.3125					541	9.76	1.69	9.77	1.70	7.30	1.33	7.30	1.33
	0.3750					756	6.78	1.18	6.79	1.18	5.90	1.25	5.91	1.25
	0.4375					963	4.98	0.86	4.99	0.87	4.73	1.20	4.74	1.20
	0.5000					1146	3.81	0.66	3.82	0.66	3.77	1.15	3.78	1.15
	0.625					1504	2.44	0.42	2.44	0.42	2.53	1.09	2.54	1.09
E3W-307SL	0.2500	46.6	33.09	13.16	14.30	501	9.21	1.60	7.80	1.35	6.80	1.26	5.76	1.14
	0.3125					728	5.89	1.02	4.99	0.87	5.06	1.16	4.28	1.08
	0.3750					946	4.09	0.71	3.46	0.60	3.80	1.10	3.22	1.05
	0.4375					1145	3.01	0.52	2.55	0.44	2.90	1.05	2.45	1.02
E4W-490SS	0.2500	46.4	21.55	13.16	13.20	400	7.81	1.36	7.76	1.35	7.11	1.41	7.07	1.40
	0.3125					568	5.00	0.87	4.97	0.86	5.16	1.30	5.13	1.30
	0.3750					713	3.47	0.60	3.45	0.60	3.75	1.22	3.73	1.22
	0.4375					874	2.55	0.44	2.53	0.44	2.89	1.20	2.88	1.20
E5W-490LS	0.2500	45.6	21.55	18.11	16.50	253	11.99	2.08	14.45	2.51	7.03	1.22	8.47	1.47
	0.3125					406	7.68	1.33	9.25	1.61	5.77	1.15	6.95	1.29
	0.3750					588	5.33	0.93	6.42	1.11	4.83	1.17	5.82	1.27
	0.4375					760	3.92	0.68	4.72	0.82	3.93	1.17	4.74	1.24
	0.5000					937	3.00	0.52	3.61	0.63	3.25	1.18	3.91	1.24
	0.6250					1248	1.92	0.33	2.31	0.40	2.25	1.17	2.67	1.20
P5U-WV-NP-01	0.2500	53	43.18	23.83	12.83	525	8.43	1.46	29.07	5.05	4.39	0.84	15.16	2.63
	0.3125					780	5.39	0.94	18.61	3.23	3.34	0.80	11.53	2.00
	0.3750					1050	3.75	0.65	12.92	2.24	2.60	0.80	8.98	1.55
	0.4000					1170	3.29	0.57	11.36	1.97	2.39	0.81	8.25	1.45
	0.4375					1350	2.75	0.48	9.49	1.65	2.11	0.82	7.27	1.34
	0.5000					1635	2.11	0.37	7.27	1.26	1.71	0.83	5.90	1.21
	0.6250					2145	1.35	0.23	4.65	0.81	1.31	0.83	3.96	1.05

Table 11 Summary of Models with Buckling Failures –Continued

Specimen	Thick. (inch)	F_y (ksi)	$W_{whitmore}$ (inch)	L_{mid} (inch)	L_{avg} (inch)	$P_{failure}$ (kips)	λ_{avg}		λ_{mid}		$P_{failure}/P_n$			
							K=1.2	K=0.5	K=1.2	K=0.5	L_{avg} K=1.2	L_{avg} K=0.50	L_{mid} K=1.2	L_{mid} K=0.5
P6U-WV-NP-02	0.2500	53	46.18	18.54	7.50	520	2.88	0.50	17.60	3.06	1.39	0.52	8.49	1.47
	0.3125					791	1.84	0.32	11.26	1.96	1.11	0.59	6.62	1.17
	0.3750					1107	1.28	0.22	7.82	1.36	1.03	0.66	5.36	1.06
	0.4375					1446	0.94	0.16	5.75	1.00	1.00	0.72	4.41	1.02
	0.5000					1808	0.72	0.12	4.40	0.76	1.00	0.78	3.69	1.01
	0.6000					2396	0.50	0.09	3.06	0.53	1.00	0.85	2.83	1.02
	0.6250					2531	0.46	0.08	2.82	0.49	1.00	0.86	2.65	1.01
P8U-WV-INF-02	0.5000	53	49.64	25.27	11.80	1974	1.78	0.31	8.17	1.42	1.57	0.85	6.97	1.35
P13U-W-NP-01	0.2500	53	46.64	19.56	8.60	644	3.79	0.66	19.59	3.40	2.24	0.68	11.59	2.01
	0.3125					957	2.42	0.42	12.54	2.18	1.71	0.74	8.82	1.53
	0.3750					1271	1.68	0.29	8.71	1.51	1.38	0.77	6.78	1.28
	0.4000					1403	1.48	0.26	7.65	1.33	1.31	0.79	6.17	1.23
	0.4375					1584	1.24	0.21	6.40	1.11	1.22	0.80	5.32	1.16
	0.5000					1914	0.95	0.16	4.90	0.85	1.15	0.83	4.31	1.10
	0.6250					2525	0.61	0.11	3.13	0.54	1.05	0.85	2.91	1.02
P14U-W-INF-01	0.2500	53	43.64	11.82	4.10	546	0.86	0.15	7.15	1.24	0.68	0.50	3.84	0.79
	0.3125					812	0.55	0.10	4.58	0.79	0.71	0.58	2.92	0.78
	0.3750					1106	0.38	0.07	3.18	0.55	0.75	0.66	2.30	0.80
	0.4375					1386	0.28	0.05	2.34	0.41	0.77	0.70	1.82	0.81
	0.5000					1652	0.22	0.04	1.79	0.31	0.78	0.73	1.50	0.81
	0.6250					2156	0.14	0.02	1.14	0.20	0.79	0.75	1.20	0.81
P5C-WV-NP-01	0.2500	53	49.70	8.57	2.86	780	0.42	0.07	3.76	0.65	0.70	0.61	2.53	0.78
	0.3125					1050	0.27	0.05	2.41	0.42	0.71	0.65	1.74	0.76
	0.3750					1305	0.19	0.03	1.67	0.29	0.71	0.67	1.32	0.75
	0.4000					1410	0.16	0.03	1.47	0.26	0.72	0.68	1.23	0.74
	0.4375					1590	0.14	0.02	1.23	0.21	0.73	0.70	1.15	0.75
	0.5000					1890	0.10	0.02	0.94	0.16	0.75	0.72	1.06	0.77

Table 12 Summary of Models with Buckling Failures –Continued

Specimen	Thick. (inch)	F_y (ksi)	$W_{whitmore}$ (inch)	L_{mid} (inch)	L_{avg} (inch)	$P_{failure}$ (kips)	λ_{avg}		λ_{mid}		$P_{failure}/P_n$			
							K=1.2	K=0.5	K=1.2	K=0.5	L_{avg} K=1.2	L_{avg} K=0.50	L_{mid} K=1.2	L_{mid} K=0.5
P6C-WV-NP-02	0.2500	53	60.03	7.82	2.60	814	0.35	0.06	3.13	0.54	0.59	0.52	1.82	0.64
	0.3125					1153	0.22	0.04	2.00	0.35	0.64	0.59	1.33	0.67
	0.3750					1514	0.15	0.03	1.39	0.24	0.68	0.64	1.13	0.70
	0.4375					1853	0.11	0.02	1.02	0.18	0.70	0.67	1.02	0.72
P7C-WV-INF-01	0.2500	53	57.00	13.7	4.60	1217	1.08	0.19	9.61	1.67	1.26	0.87	8.80	1.61
	0.3125					1647	0.69	0.12	6.15	1.07	1.16	0.92	6.10	1.36
	0.3750					2112	0.48	0.08	4.27	0.74	1.14	0.97	4.52	1.27
P8C-WV-INF-02	0.2500	53	50.60	8.5	2.80	882	0.40	0.07	3.70	0.64	0.78	0.68	2.76	0.86
P9C-P-NP-01	0.2000	53	26.32	8.86	3.00	353	0.72	0.12	6.28	1.09	0.85	0.67	4.52	1.00
P13C-W-NP-01	0.2500	53	46.64	11.13	3.70	858	0.70	0.12	6.34	1.10	0.93	0.73	5.00	1.10
	0.3125					1172	0.45	0.08	4.06	0.70	0.91	0.78	3.50	1.02
	0.3750					1502	0.31	0.05	2.82	0.49	0.92	0.83	2.59	0.99
	0.4000					1634	0.27	0.05	2.48	0.43	0.93	0.84	2.33	0.99
	0.4375					1832	0.23	0.04	2.07	0.36	0.93	0.86	2.00	0.98
	0.5000					2112	0.18	0.03	1.59	0.28	0.92	0.87	1.65	0.96
	0.6250					2640	0.11	0.02	1.01	0.18	0.90	0.86	1.30	0.92
P14C-W-INF-01	0.2500	53	47.11	8.14	2.70	644	0.37	0.06	3.39	0.59	0.60	0.53	1.99	0.66
	0.3125					910	0.24	0.04	2.17	0.38	0.64	0.59	1.44	0.68
	0.3750					1190	0.17	0.03	1.51	0.26	0.68	0.64	1.19	0.71
	0.4375					1442	0.12	0.02	1.11	0.19	0.69	0.67	1.05	0.72
	0.5000					1708	0.09	0.02	0.85	0.15	0.71	0.69	0.97	0.73
P19C-MTB	0.6000	53	64.50	3.91	1.30	3737	0.02	0.00	0.14	0.02	0.92	0.91	0.96	0.92
P20C-MTB	0.6000	53	60.03	7.58	2.50	2843	0.06	0.01	0.51	0.09	0.76	0.75	0.92	0.77
P1C-MTB	0.3500	53	26.32	9.01	3.00	831	0.24	0.04	2.12	0.37	0.94	0.87	2.05	0.99
P5C-HS1	0.4000	108	49.70	8.57	2.86	2535	0.33	0.06	2.99	0.52	0.68	0.60	2.01	0.73
P5C-HS2	0.2000	108	49.70	8.57	2.86	960	1.33	0.23	11.97	2.08	0.78	0.49	6.08	1.06
P7C-HS2	0.3500	108	59.20	0.87	4.60	3544	1.13	0.20	0.04	0.01	1.26	0.86	0.81	0.79
P8C-HS2	0.2500	108	49.28	8.5	2.80	1617	0.82	0.14	7.54	1.31	0.85	0.64	5.20	1.05

Table 13 Summary of Models and Specimens with Buckling Failures

Specimen	Thick. (inch)	F_y (ksi)	$W_{whitmore}$ (inch)	L_{mid} (inch)	L_{avg} (inch)	$P_{failure}$ (kips)	λ_{avg}		λ_{mid}		$P_{failure}/P_n$			
							K=1.2	K=0.5	K=1.2	K=0.5	L_{avg} K=1.2	L_{avg} K=0.65	L_{mid} K=1.2	L_{mid} K=0.5
P3C-WV-P01	0.2500	53	87.08	7.57	7.57	2250	2.93	0.51	2.93	0.51	3.25	1.20	3.25	1.20
	0.3125	53	87.08	7.57	7.57	2900	1.88	0.33	1.88	0.33	2.19	1.15	2.19	1.15
	0.3750	53	87.08	7.57	7.57	3550	1.30	0.23	1.30	0.23	1.76	1.13	1.76	1.13
	0.4375	53	87.08	7.57	7.57	4250	0.96	0.17	0.96	0.17	1.57	1.13	1.57	1.13
	0.5000	53	87.08	7.57	7.57	4900	0.73	0.13	0.73	0.13	1.44	1.12	1.44	1.12
	0.6250	53	87.08	7.57	7.57	6350	0.47	0.08	0.47	0.08	1.34	1.14	1.34	1.14
GP307SS3	0.3750	36.4	24.43	13.16	6.20	716	0.60	0.10	2.71	0.47	1.38	1.12	3.30	1.31
GP490SS3	0.3750	46.4	21.55	13.16	7.20	728	1.03	0.18	3.45	0.60	1.49	1.05	3.81	1.25
GP490LS3	0.3750	45.6	21.55	18.11	12.10	527	2.87	0.50	6.42	1.11	2.33	0.88	5.22	1.14
GP307LS3	0.3750	48.2	27.32	18.11	10.20	796	2.15	0.37	6.79	1.18	1.97	0.94	6.22	1.32
OSU 1	0.2500	47.0	34.78	26.7	15.53	290	10.95	1.90	32.38	5.62	4.41	0.78	13.05	2.27
OSU 2	0.2500	45.1	34.78	26.7	15.53	325	10.51	1.82	31.07	5.39	4.95	0.88	14.62	2.54
OSU 3	0.3750	45.9	34.78	26.7	15.53	545	4.76	0.83	14.06	2.44	2.46	0.64	7.27	1.26
OSU 4	0.2500	45.1	34.78	26.7	15.53	261	10.51	1.82	31.06	5.39	3.97	0.71	11.74	2.04
OSU 5	0.3750	46.1	34.78	26.7	15.53	579	4.78	0.83	14.12	2.45	2.61	0.68	7.72	1.34
I35W U10	0.5000	51.0	60.87	15.7	5.23	2388	0.34	0.06	3.04	0.53	0.88	0.79	2.65	0.96

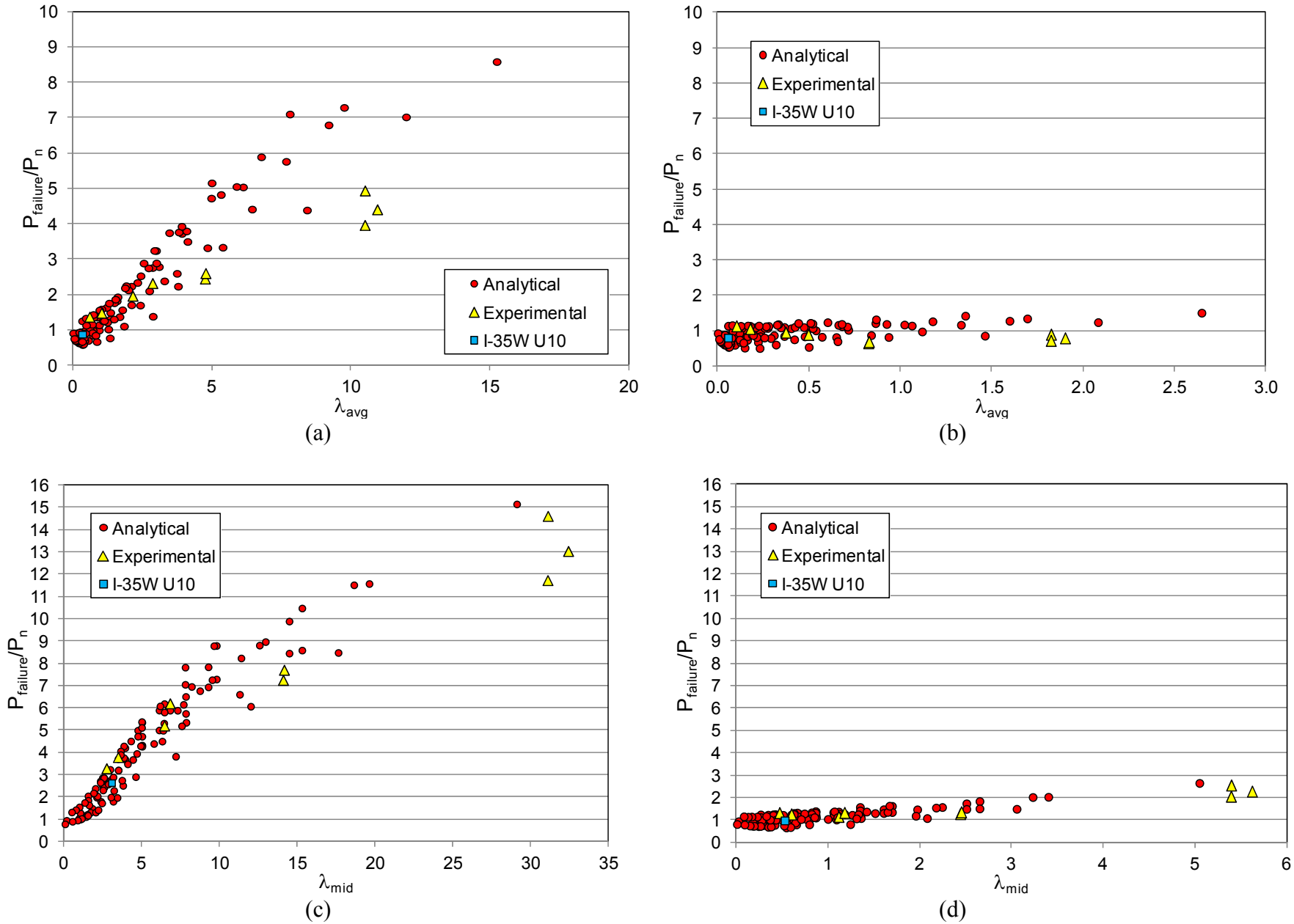

Figure 49. Professional factor data of buckling failures evaluated with: (a) K=1.2 and L_{avg}. (b) K=0.50 and L_{avg}. (c) K=1.2 and L_{mid}. (d) K=0.50 and L_{mid}.

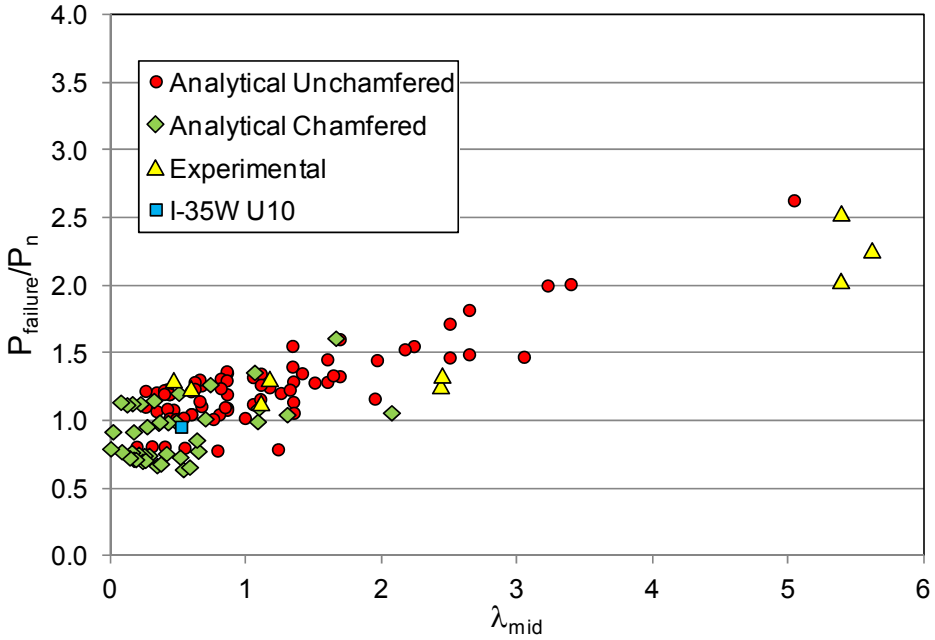

Figure 50. Professional factor breakdown between chamfered and unchamfered models using K=0.5 and L_{mid}.

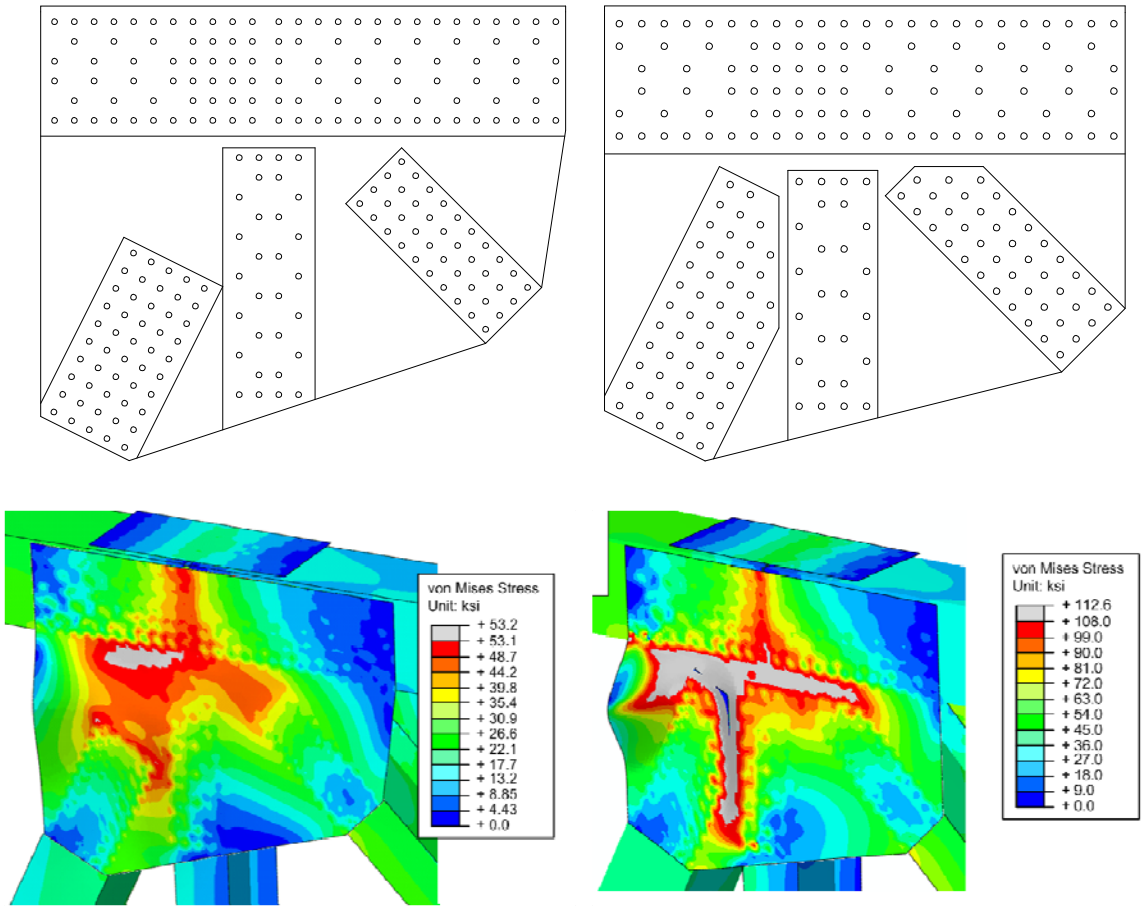

Figure 51. Difference in buckling with chamfered and unchamfered member. (Top) Schematics of each connection. (Bottom) Von Mises stresses at failure (stresses exceeding yield are shown in grey/pink).

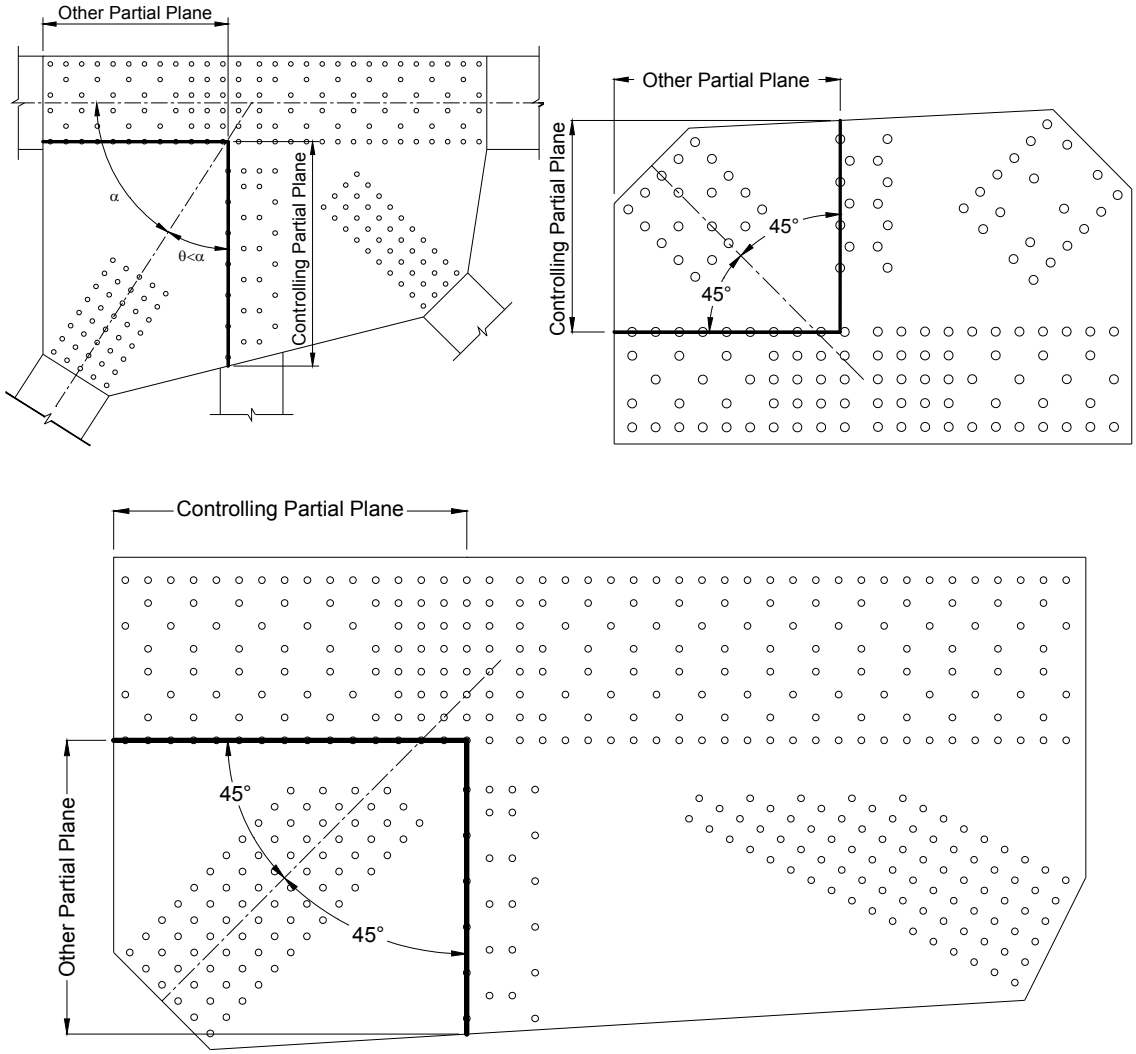

Figure 52. Schematic of various partial shear plane. (Top-Left) Controlling plane dictated by framing θ being less than α. (Top-Right) Controlling plane is dictated by one with shorter length because first two criteria are equal. (Bottom) Controlling plane is that paralleling the member chamfer.

Table 14 Summary of Two-Folded Buckling Evaluation Criteria

Specimen	Plate Thickness (inch)	Yield Strength (ksi)	Whitmore Width (inch)	Length of Partial Shear Plane (inch)	L_{mid} (inch)	L_{avg} (inch)	λ_{mid} (K=0.5)	λ_{avg} (K=0.5)	$P_{Failure}$ (kips)	$P_{whitmore}$ using L_{avg} (kips)	$P_{whitmore}$ using L_{mid} (kips)	$P_{partial\_shear}$ (kips)	Controlling Ratio using L_{avg} [a,b]	Controlling Ratio using L_{mid} [a,b]
E1WV-307SS	0.250	36.4	24.43	23.97	13.16	6.20	1.06	0.23	380	403	287	358	1.06	1.32
	0.313						0.68	0.15	530	522	420	447	1.19	1.26
	0.438						0.35	0.08	817	754	674	626	1.30	1.30
	0.500						0.26	0.06	974	868	797	716	1.36	1.36
E2WV-307LS	0.250	48.2	27.32	27.68	18.11	10.20	2.65	0.84	398	464	219	547	0.86	1.82
	0.313						1.70	0.54	653	658	407	684	0.99	1.61
	0.438						0.87	0.27	1091	1028	804	958	1.14	1.36
	0.500						0.66	0.21	1305	1207	1000	1094	1.19	1.31
	0.625						0.42	0.13	1703	1557	1380	1368	1.25	1.25
E3WV-307SL	0.250	46.6	33.09	27.68	13.16	4.40	1.35	0.15	568	724	439	529	1.07	1.29
	0.313						0.87	0.10	738	926	673	661	1.12	1.12
	0.375						0.60	0.07	946	1125	901	794	1.19	1.19
	0.438						0.44	0.05	1145	1322	1123	926	1.24	1.24
E4WV-490SS	0.250	46.4	21.55	22.18	13.16	7.20	1.35	0.40	444	423	286	422	1.05	1.56
	0.313						0.86	0.26	597	561	437	528	1.13	1.37
	0.438						0.44	0.13	874	828	729	739	1.18	1.20
E5WV-490LS	0.250	45.6	21.55	24.18	18.11	12.10	2.51	1.12	296	309	172	452	0.96	1.72
	0.313						1.61	0.72	459	456	315	565	1.01	1.46
	0.438						0.82	0.37	803	739	612	791	1.09	1.31
	0.500						0.63	0.28	975	875	757	904	1.11	1.29
	0.625						0.40	0.18	1276	1140	1040	1131	1.13	1.23
E1W-307SS	0.250	36.4	24.43	26.15	13.16	13.20	1.06	1.06	322	286	287	390	1.13	1.12
	0.313						0.68	0.68	466	419	420	488	1.11	1.11
	0.375						0.47	0.47	595	548	549	586	1.08	1.08
	0.438						0.35	0.35	723	674	674	683	1.07	1.07
	0.500						0.26	0.27	881	796	797	781	1.13	1.13

[a] - Green shading represents cases controlled by Partial Shear Plane Yielding.
[b] - Yellow shading represents cases controlled by Whitmore Buckling.

Table 15 Summary of Two-Folded Buckling Evaluation Criteria (Continued)

Specimen	Plate Thickness (inch)	Yield Strength (ksi)	Whitmore Width (inch)	Length of Partial Shear Plane (inch)	L_{mid} (inch)	L_{avg} (inch)	λ_{mid}	λ_{avg}	$P_{Failure}$ (kips)	$P_{whitmore}$ using L_{avg} (kips)	$P_{whitmore}$ using L_{mid} (kips)	$P_{partial\_shear}$ (kips)	Controlling Ratio using L_{avg} [a,b]	Controlling Ratio using L_{mid} [a,b]
E2W-307LS	0.250	48.2	27.32	31.5	18.11	18.10	2.65	2.65	326	219	219	623	1.49	1.49
	0.313						1.70	1.69	541	407	407	778	1.33	1.33
	0.375						1.18	1.18	756	606	605	934	1.25	1.25
	0.438						0.87	0.86	963	804	804	1090	1.20	1.20
	0.500						0.66	0.66	1146	1000	1000	1245	1.15	1.15
	0.625						0.42	0.42	1504	1380	1380	1557	1.09	1.09
E3W-307SL	0.250	46.6	33.09	31.5	13.16	14.30	1.35	1.60	501	397	439	602	1.26	1.14
	0.313						0.87	1.02	728	630	673	753	1.16	1.08
	0.375						0.60	0.71	946	861	901	903	1.10	1.05
	0.438						0.44	0.52	1145	1086	1123	1054	1.09	1.09
E4W-490SS	0.250	46.4	21.55	23.98	13.16	13.20	1.35	1.36	400	285	286	456	1.41	1.40
	0.313						0.86	0.87	568	436	437	570	1.30	1.30
	0.375						0.60	0.60	713	584	585	684	1.22	1.22
	0.438						0.44	0.44	874	728	729	799	1.20	1.20
E5W-490LS	0.250	45.6	21.55	27.8	18.11	16.50	2.51	2.08	253	207	172	520	1.22	1.47
	0.313						1.61	1.33	406	353	315	650	1.15	1.29
	0.375						1.11	0.93	588	502	464	780	1.17	1.27
	0.438						0.82	0.68	760	648	612	910	1.17	1.24
	0.500						0.63	0.52	937	791	757	1040	1.18	1.24
	0.625						0.40	0.33	1248	1069	1040	1300	1.17	1.20
P5U-WV-NP-01	0.250	53	43.18	46.17	23.83	12.83	5.05	1.46	525	623	199	793	0.84	2.63
	0.313						3.23	0.94	780	969	390	992	0.80	2.00
	0.375						2.24	0.65	1050	1310	676	1190	0.88	1.55
	0.400						1.97	0.57	1170	1444	807	1269	0.92	1.45
	0.438						1.65	0.48	1350	1642	1010	1388	0.97	1.34
	0.500						1.26	0.37	1635	1966	1355	1587	1.03	1.21
	0.625						0.81	0.23	2145	2595	2045	1984	1.08	1.08

[a] - Green shading represents cases controlled by Partial Shear Plane Yielding.
[b] - Yellow shading represents cases controlled by Whitmore Buckling.

Table 16 Summary of Two-Folded Buckling Evaluation Criteria (Continued)

Specimen	Plate Thickness (inch)	Yield Strength (ksi)	Whitmore Width (inch)	Length of Partial Shear Plane (inch)	L_{mid} (inch)	L_{avg} (inch)	λ_{mid}	λ_{avg}	$P_{Failure}$ (kips)	$P_{whitmore}$ using L_{avg} (kips)	$P_{whitmore}$ using L_{mid} (kips)	$P_{partial\_shear}$ (kips)	Controlling Ratio using L_{avg} [a,b]	Controlling Ratio using L_{mid} [a,b]
P6U-WV-NP-02	0.250	53	46.18	41.07	18.54	7.50	3.06	0.50	520	994	352	893	0.58	1.47
	0.313						1.96	0.32	791	1339	679	1116	0.71	1.17
	0.375						1.36	0.22	1107	1674	1044	1339	0.83	1.06
	0.438						1.00	0.16	1446	2001	1415	1562	0.93	1.02
	0.500						0.76	0.12	1808	2324	1782	1785	1.01	1.01
	0.600						0.53	0.09	2396	2833	2356	2143	1.12	1.12
	0.625						0.49	0.08	2531	2959	2497	2232	1.13	1.13
P8U-WV-INF-02	0.500	53	49.64	57.26	25.27	11.80	1.42	0.31	1974	2314	1459	2059	0.96	1.35
P13U-W-NP-01	0.250	53	46.64	44.67	19.56	8.60	3.40	0.66	644	941	320	809	0.80	2.01
	0.313						2.18	0.42	957	1297	625	1011	0.95	1.53
	0.375						1.51	0.29	1271	1642	989	1213	1.05	1.28
	0.400						1.33	0.26	1403	1777	1139	1294	1.08	1.23
	0.438						1.11	0.21	1584	1978	1364	1415	1.12	1.16
	0.500						0.85	0.16	1914	2309	1736	1617	1.18	1.18
	0.625						0.54	0.11	2525	2958	2465	2022	1.25	1.25
P14U-W-INF-01	0.250	53	43.64	33.10	11.82	4.10	1.24	0.15	546	1087	690	799	0.68	0.79
	0.313						0.79	0.10	812	1389	1039	999	0.81	0.81
	0.375						0.55	0.07	1106	1688	1379	1199	0.92	0.92
	0.438						0.41	0.05	1386	1983	1710	1399	0.99	0.99
	0.500						0.31	0.04	1652	2277	2033	1599	1.03	1.03
	0.625						0.20	0.02	2156	2863	2662	1998	1.08	1.08
P5C-WV-NP-01	0.250	53	49.70	40.24	8.57	2.86	0.65	0.07	780	1278	1004	692	1.13	1.13
	0.313						0.42	0.05	1050	1615	1384	864	1.21	1.21
	0.375						0.29	0.03	1305	1949	1751	1037	1.26	1.26
	0.400						0.26	0.03	1410	2083	1895	1106	1.27	1.27
	0.438						0.21	0.02	1590	2282	2109	1210	1.31	1.31
	0.500						0.16	0.02	1890	2614	2461	1383	1.37	1.37

[a] - Green shading represents cases controlled by Partial Shear Plane Yielding.
[b] - Yellow shading represents cases controlled by Whitmore Buckling.

Table 17 Summary of Two-Folded Buckling Evaluation Criteria (Continued)

Specimen	Plate Thickness (inch)	Yield Strength (ksi)	Whitmore Width (inch)	Length of Partial Shear Plane (inch)	L_{mid} (inch)	L_{avg} (inch)	λ_{mid}	λ_{avg}	$P_{Failure}$ (kips)	$P_{whitmore}$ using L_{avg} (kips)	$P_{whitmore}$ using L_{mid} (kips)	$P_{partial\_shear}$ (kips)	Controlling Ratio using L_{avg} [a,b]	Controlling Ratio using L_{mid} [a,b]
P6C-WV-NP-02	0.250	53	60.03	46.53	7.82	2.60	0.54	0.06	814	1552	1269	1011	0.80	0.80
	0.313						0.35	0.04	1153	1957	1721	1264	0.91	0.91
	0.375						0.24	0.03	1514	2360	2158	1517	1.00	1.00
	0.438						0.18	0.02	1853	2761	2586	1770	1.05	1.05
P7C-WV-INF-01	0.250	53	57.00	70.98	13.70	4.60	1.67	0.19	1217	1397	755	1220	1.00	1.61
	0.313						1.07	0.12	1647	1796	1212	1525	1.08	1.36
	0.375						0.74	0.08	2112	2188	1665	1830	1.15	1.27
P8C-WV-INF-02	0.250	53	50.60	48.53	8.50	2.80	0.64	0.07	882	1303	1027	873	1.01	1.01
P9C-P-NP-01	0.200	53	26.32	25.00	8.86	3.00	1.09	0.12	353	530	355	435	0.81	1.00
P13C-W-NP-01	0.250	53	46.64	43.33	11.13	3.70	1.10	0.12	858	1175	782	784	1.09	1.10
	0.313						0.70	0.08	1172	1496	1153	980	1.19	1.19
	0.375						0.49	0.05	1502	1813	1513	1177	1.28	1.28
	0.400						0.43	0.05	1634	1939	1654	1255	1.30	1.30
	0.438						0.36	0.04	1832	2128	1863	1373	1.33	1.33
	0.500						0.28	0.03	2112	2441	2205	1569	1.35	1.35
	0.625						0.18	0.02	2640	3065	2872	1961	1.35	1.35
P14C-W-INF-01	0.250	53	47.11	33.06	8.14	2.70	0.59	0.06	644	1215	977	798	0.81	0.81
	0.313						0.38	0.04	910	1534	1334	998	0.91	0.91
	0.375						0.26	0.03	1190	1850	1679	1197	0.99	0.99
	0.438						0.19	0.02	1442	2165	2017	1397	1.03	1.03
	0.500						0.15	0.02	1708	2480	2348	1597	1.07	1.07
P19C-MTB	0.600	53	64.50	77.8	3.91	1.30	0.02	0.00	3737	4098	4062	3209	1.16	1.16
P20C-MTB	0.600	53	60.03	47.13	7.58	2.50	0.09	0.01	2843	3803	3680	2459	1.16	1.16
P1C-MTB	0.350	53	26.32	25.5	9.01	3.00	0.37	0.04	831	960	838	776	1.07	1.07
P5C-HS1	0.400	108	49.70	40.24	8.57	2.86	0.52	0.06	2535	4192	3460	2255	1.12	1.12
P5C-HS2	0.200						2.08	0.23	960	1950	905	1127	0.85	1.06
P7C-HS2	0.350	108	59.20	70.98	0.87	4.60	0.01	0.20	3544	4126	4463	3480	1.02	1.02
P8C-HS2	0.250	108	49.28	48.53	8.50	2.80	1.31	0.14	1617	2509	1545	1778	0.91	1.05

[a] - Green shading represents cases controlled by Partial Shear Plane Yielding.
[b] - Yellow shading represents cases controlled by Whitmore Buckling.

Table 18 Summary of Two-Folded Buckling Evaluation Criteria (Continued)

Specimen	Plate Thickness (inch)	Yield Strength (ksi)	Whitmore Width (inch)	Length of Partial Shear Plane (inch)	L_{mid} (inch)	L_{avg} (inch)	λ_{mid}	λ_{avg}	$P_{Failure}$ (kips)	$P_{whitmore}$ using L_{avg} (kips)	$P_{whitmore}$ using L_{mid} (kips)	$P_{partial\_shear}$ (kips)	Controlling Ratio using L_{avg} [a,b]	Controlling Ratio using L_{mid} [a,b]
P3C-WV-P01	0.2500	53	87.08	69.08	7.57	7.57	0.51	0.51	2250	1867	1867	2124	1.20	1.20
	0.3125						0.33	0.33	2900	2519	2519	2654	1.15	1.15
	0.3750						0.23	0.23	3550	3151	3151	3185	1.13	1.13
	0.4375						0.17	0.17	4250	3769	3769	3716	1.14	1.14
	0.5000						0.13	0.13	4900	4377	4377	4247	1.15	1.15
	0.6250						0.08	0.08	6350	5577	5577	5309	1.20	1.20
E1WV-307SS [c]	0.375	36.4	24.43	23.97	13.16	6.20	0.47	0.10	716	639	549	537	1.33	1.33
E4WV-490SS [c]	0.375	46.4	21.55	22.18	13.16	7.20	0.60	0.18	728	696	585	633	1.15	1.25
E5WV-490LS [c]	0.375	45.6	21.55	24.18	18.11	12.10	1.11	0.50	527	599	464	678	0.88	1.14
E2WV-307LS [c]	0.375	48.2	27.32	27.68	18.11	10.20	1.18	0.37	796	846	605	821	0.97	1.32
OSU 1 [d]	0.250	47.0	34.78	41.62	26.70	15.53	5.62	1.90	290	371	128	706	0.78	2.27
OSU 2 [d]	0.250	45.1					5.39	1.82	325	368	128	677	0.88	2.54
OSU 3 [d]	0.375	45.9					2.44	0.83	545	850	432	1034	0.64	1.26
OSU 4 [d]	0.250	45.1					5.39	1.82	261	368	128	677	0.71	2.04
OSU 5 [d]	0.375	46.1					2.45	0.83	579	853	432	1039	0.68	1.34
I35W U10	0.500	51.0	60.87	46.75	15.70	5.23	0.53	0.06	2388	3030	2494	1720	1.39	1.39

[a] - Green shading represents cases controlled by Partial Shear Plane Yielding.
[b] - Yellow shading represents cases controlled by Whitmore Buckling.
[c] – Denotes an experimental specimen.
[d] – Oregon State University specimen reported in Reference 23.

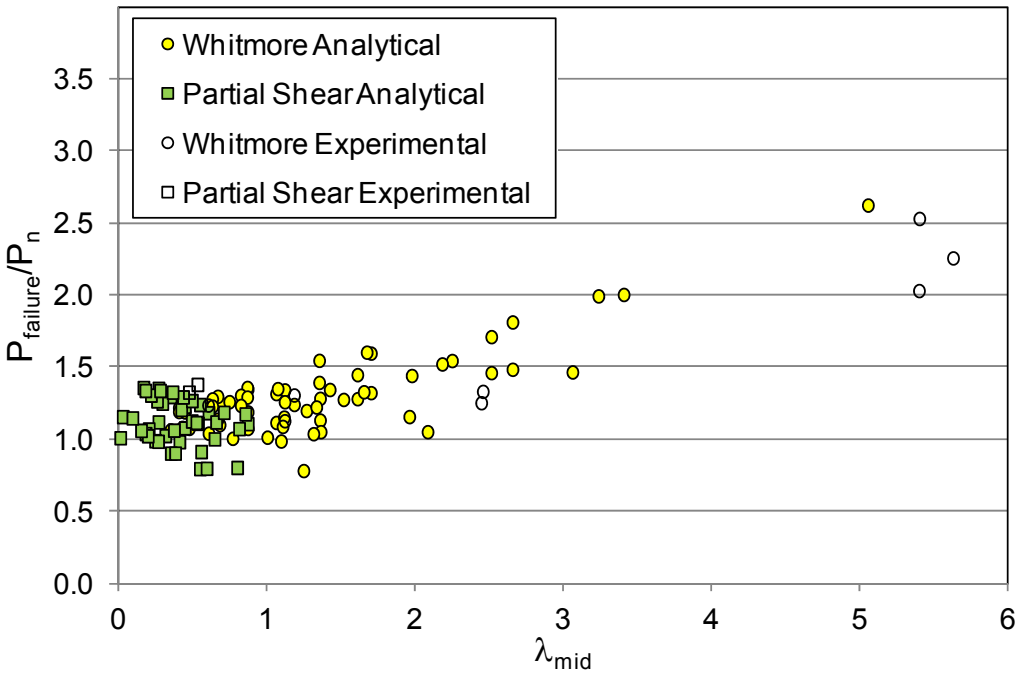

Figure 53. Plot of professional factors using two-folded Whitmore and partial plane shear approach to predict buckling with L_{mid}.

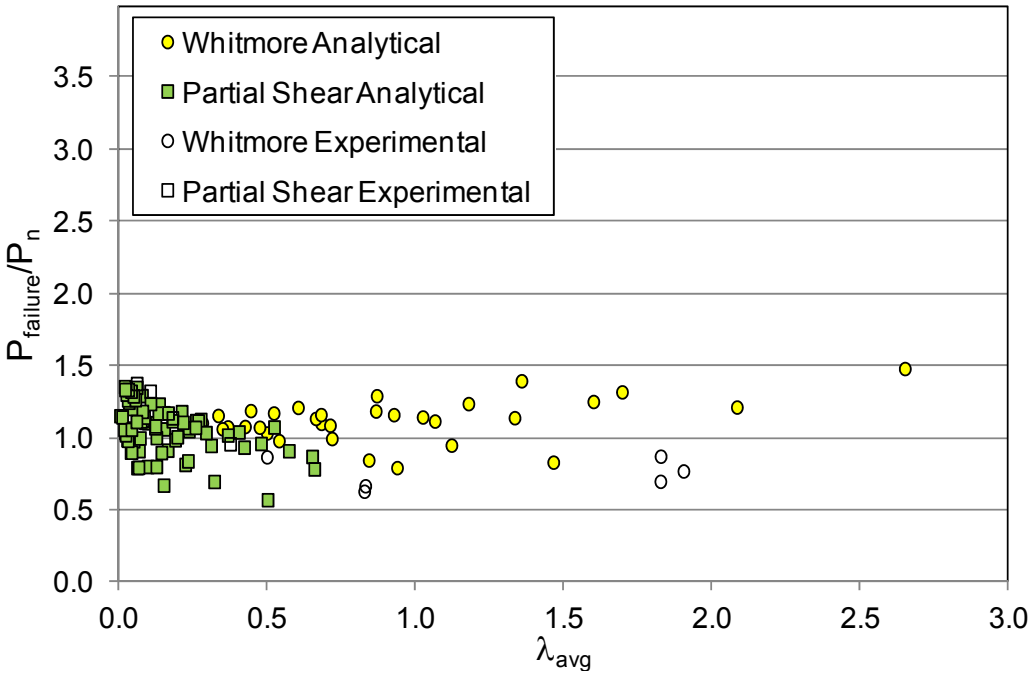

Figure 54. Plot of professional factors using two-folded Whitmore and partial plane shear approach to predict buckling with L_{avg}.

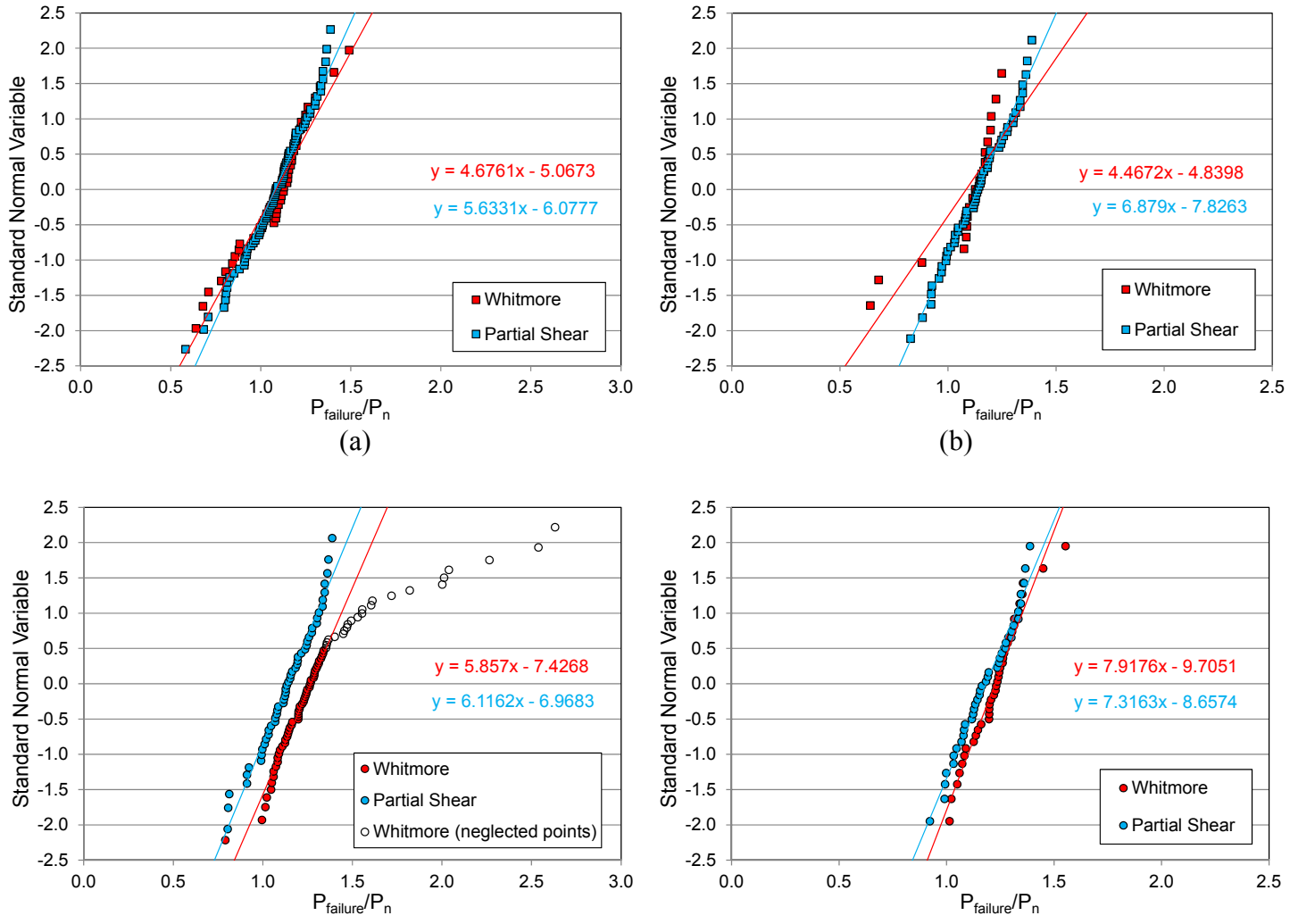

Figure 55. Failures using two-folded approach plotted on normal probability paper. (a) Using L_{avg} and all data points. (b) Using L_{avg} and neglecting plates thinner than 3/8 inches. (c) Using L_{mid} and all data points. (d) Using L_{mid} and neglecting plates thinner than 3/8 inches.

Table 19 Calibration Statistics for Gusset Plate Buckling

		Using All Data		Neglecting Plates <3/8" Thick	
		Whitmore	Partial Shear	Whitmore	Partial Shear
L_{avg}	Average	1.084	1.079	1.083	1.138
	COV	0.197	0.165	0.207	0.128
L_{mid}	Average	1.268	1.139	1.226	1.183
	COV	0.135	0.144	0.103	0.116

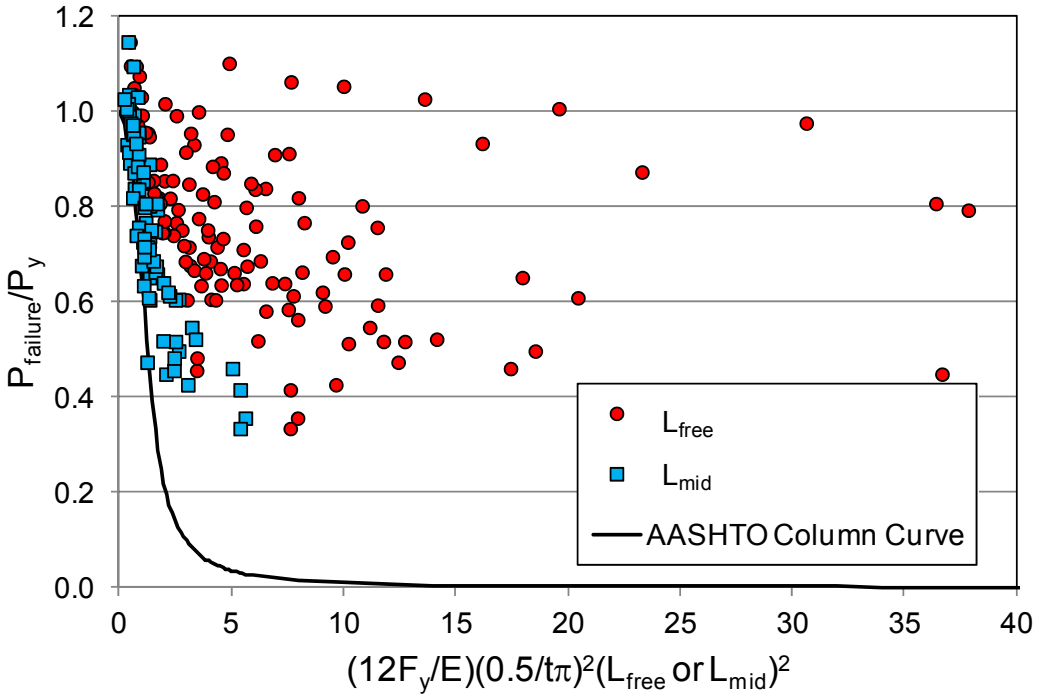

Figure 56. Buckling resistance comparison between L_{mid} and L_{free}.

Chord Splice

In Chapter 1 it was noted that there were anomalies that arose due to checking compression or tension chord splices with the Whitmore approach as demonstrated in the FHWA Guide. In particular, an assumption of the load sharing between the gusset plate and alternate chord splice plates had to be made, and dividing the load based on cross-sectional area was deemed appropriate. However, the area of the gusset plate was based on the Whitmore section, which is questionable.

In this project, only analytical models were observed to fail in the chord splice. The resistance of the chord splice was treated as if it were a composite beam in bending. That is, the gusset plate and associated splice plates were assumed composite with each other to resist the axial chord

splice load, along with the bending due to the eccentricity of the loads from the centroid of the section. Failure was assumed as the first yield in the composite section for gross sections and first reaching the tensile strength for net sections.

For tension chord splices both gross and net sections should be considered with stresses of F_y and F_u applied to the appropriate gross and net sections. For compression chord splices, a critical buckling stress should be used; however, if *KL/r* of the gusset plate is less than 25 (which is usually the case), the full yield stress can be assumed. In this case K=0.5 and *L* would be the center-to-center distance between fastener lines at the ends of the adjoining chords. Therefore, three resistance equations exist, one for compression chord splices, and two for tension chord splices.

$$P = F_{cr}\left(\frac{S_g A_g}{S_g + e_p A_g}\right) \quad \text{(Eq. 8)}$$

$$P = F_y\left(\frac{S_g A_g}{S_g + e_p A_g}\right) \quad \text{(Eq. 9)}$$

$$P = F_u\left(\frac{S_n A_n}{S_n + e_p A_n}\right) \quad \text{(Eq. 10)}$$

where A_g is the gross area of all the plates, A_n is the net area of all the plates, S_g is the gross area section modulus of all the plates, S_n is the net area section modulus of all the plates, and e_p is the eccentricity from the resultant load in the splice and the centroid of A_n or A_g.

In total there were 33 analytical models that were identified to fail in the chord splice. The resistance of each was calculated according to either Eq. 8 or 9 depending on the loading within the chord splice. The net section resistance was not checked for tension chord splices because the analytical models did not have the fidelity to capture net section failure. The failure load from the model is divided by the calculated resistance and reported in Table 20 as the professional factor for each of the failures.

The same data is plotted on normal probability paper and shown in Figure 57. Both data sets plot linearly indicating that the normal probability distribution is appropriate. The best-fit line through each data set can be used to calculate the statistics for use in the resistance factor calibration. Considering all plate thicknesses, the mean would be 1.224 and the COV is 0.164. Neglecting the failures of plates thinner than 3/8 of an inch, the mean is 1.284 and the COV is 0.163.

The approach of calculating resistance via a composite section analysis differs from the way shown in Appendix I. In Appendix I, a different approach published by Kulicki and Reiner was

assessed.[24] The professional factors do not vary too much between the methods; however the composite section method presented herein was primarily chosen because it was easier to describe and codify.

Table 20 Chord Splice Professional Factor Data

Model	Plate Thickness (inch)	R_{FEA}/R_n
P1-C-CCS-WV-M	0.2500	1.01
	0.3125	1.08
	0.3750	1.34
	0.4000	1.32
	0.4375	1.39
	0.5000	1.43
	0.6250	1.44
P2-C-TCS-WV-M	0.2500	1.18
	0.3125	1.24
	0.3750	1.30
	0.4000	1.28
	0.4375	1.26
	0.5000	1.31
	0.6250	1.39
P4-C-WV-P	0.8000	1.58
P10-C-P-NP	0.2000	0.95
	0.2500	1.07
	0.3125	1.18
	0.3750	1.26
	0.4375	1.30
	0.5000	1.35
P11-C-W-M	0.2500	0.90
	0.3125	1.26
	0.3750	1.35
	0.4500	1.40
	0.5000	1.45
P13-C-W-NP	0.4000 [a]	0.84
	0.4375 [a]	0.91
	0.5000 [a]	1.01
	0.6250 [a]	1.16
P19-C-CCS-NEG	0.6000	1.18
P20-C-CCS-NEG	0.6000	1.06

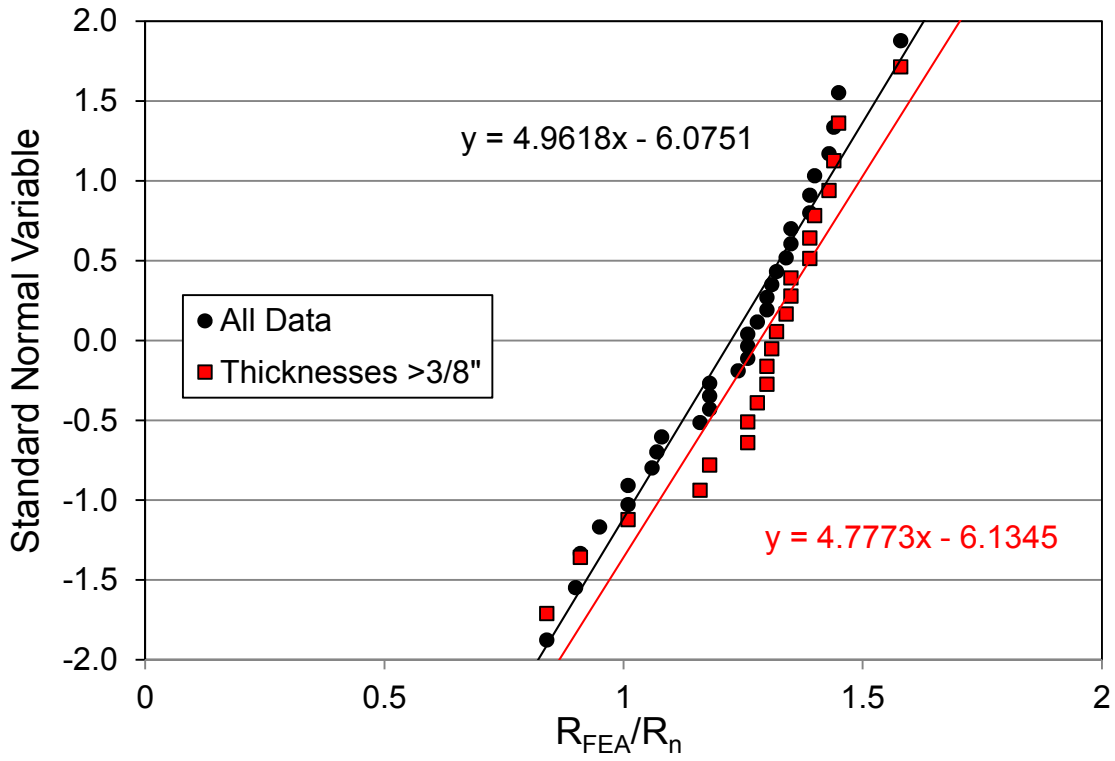

Figure 57. Chord splice professional factors plotted on normal probability paper.

Tension Members

One of the shortfalls of both the experimental and parametric studies was the lack of tension failures. Perhaps this shows that gusset plates are primarily susceptible to shear and buckling but this cannot be definitively proven through the results attained in this project. The overarching reason this occurred is that the finite element modeling methodology made the models computationally efficient by not explicitly modeling fastener holes. This means net section failure modes could not be captured in the modeling.

The current FHWA Guide recommends three checks for tension members: Whitmore yield and fracture checks, plus a block shear check.

Block Shear

This research specifically did not address the block shear limit-state because there is an abundant amount of experimental data available in the available literature. The best summary of the available block shear data can be found in Huns, Grondin, and Driver.[25] This paper summarizes 133 experiments reported from eight different sources. The paper also provides the professional factor and COV for the test data using the existing AASHTO block shear equation (Eqn. 6.13.4-1) to be 1.18 and 0.060 respectively. This data can directly be used to calibrate a block shear ϕ-factor in Chapter 4.

Whitmore Yield and Fracture

Only three parametric models (P16C, P17C. and P18C) had just tension diagonal and/or vertical members that demonstrated pure tensile failure modes. All other models or specimens had tension members in conjunction with compression members that failed in buckling or shear. Therefore, no data are available to provide a statistically significant sample to derive professional factors for tensile failure modes.

Coupling of Tension Modes with Other Limit-States

To assess the relevance of these failure models, they were checked against all the tension members in connections that were identified to have failed in other modes (shear yielding, buckling, chord splice, etc.). This did not include the checks for parametric models P16C, P17C, and P18C. Out of 155 connections that were identified to fail in shear, buckling, or in the chord splice (not including models with corrosion or edge stiffening), only 15 would have been controlled by Whitmore yield or block shear. This is demonstrated in Table 21, which outlines the specific models and specimens that had professional factors in excess of 1.00 for Whitmore yield, Whitmore fracture, and block shear indicating that the limit-state had been exceeded. The right-handed column of this table shows the professional factors for the observed failure mode without considering tensile failure modes. Cells that are highlighted grey represent the most conservative professional factor that would control the design of the joints. In only three connection geometries would the Whitmore yield or block shear criterion control. While this does not provide statistical data to calibrate the limit-states, it does show that an extra level of conservatism is added into the calibrated limit-states of buckling and shear yielding considering that tensile modes must be checked also.

Other Tensile Failure Modes

The three tension checks on parametric models P16C, P17C, and P18C are shown in Table 22, which are the only connections that have pure tension failure. Unfortunately, the professional factor data shown in Table 22 do not support the three tension failure models well. Only the block shear check on the tension diagonal of P18C has a conservative professional factor. The other two connections failed from excessive yielding but all three tension limit-state models produce unconservative professional factors. The yielding patterns of each of these connections can be found in Appendix I and each show that failure planes may go beyond the three traditional tension limit-state checks. Specifically, it appears that there is a coupling of closely spaced tension diagonals wherein a block shear type failure mechanism can develop on a plane bounded by multiple members. These alternate failure patterns are shown in Figure 58, some of which have been suggested by Astaneh-Asl.[26] Since this research did not include the effects of net sections, it is beyond the scope of this research to draw any conclusions regarding these coupled mechanism failures. This is a needed area of research.

Table 21 Tension Failure Predictions of Connections Identified to Fail in Alternative Mode

Model or Specimen	Plate Thickness (inch)	Member Type	Professional Factors ($T_{failure}/T_n$)			
			Whitmore Yield	Whitmore Fracture	Block Shear	Other Failure Modes
E2W-307LS3	0.5000	Chord	[a]	[a]	1.01	1.306 (WB)
	0.6250	Chord			1.06	1.245 (PPSY)
E5WV-490LS	0.3750	Diagonal	0.97	0.87	1.03	1.136 (WB)
P2C	0.2500	Chord	[a]	[a]	1.52	1.229 (CS)
	0.3125	Chord			1.43	1.295 (CS)
	0.3750	Chord			1.60	1.356 (CS)
	0.4000	Chord			1.52	1.339 (CS)
	0.4375	Chord			1.52	1.324 (CS)
	0.5000	Chord			1.45	1.371 (CS)
	0.6250	Chord			1.29	1.458 (CS)
P5C-WV-NP-01	0.5000	Chord	[a]	[a]	1.00	1.367 (PPSY)
	0.6250	Chord			1.15	0.94 (FPSY)
P8C-WV-INF-02	0.3125	Diagonal	0.69	0.48	1.05	1.04 (FPSY)
	0.3750	Diagonal	0.72	0.49	1.09	1.08 (FPSY)
	0.4375	Diagonal	0.72	0.49	1.09	1.08 (FPSY)
	0.5000	Diagonal	0.72	0.50	1.10	1.09 (FPSY)
	0.6250	Diagonal	0.72	0.49	1.09	1.08 (FPSY)
P8C-HS1	0.5000	Diagonal	0.70	0.71	1.30	0.85 (FPSY)
	0.2500	Diagonal	0.60	0.61	1.12	1.047 (WB)
307SL4 [b]	0.5000	Diagonal	1.05	0.64	0.89	1.19 (FPSY)
490SS3-1 [b]	0.3750	Diagonal	1.07	0.86	1.02	1.00 (FPSY)

[a] – Calculation is for a chord member which Whitmore analysis will no longer apply to based on chord splice check.
[b] – Denotes an experimental specimen.

FPSY=Full Plane Shear Yield
WB=Whitmore Buckling
PPSY=Partial Plane Shear Yield
CS=Chord Splice

Table 22 Tension Checks for P16C, P17C, and P18C

Model or Specimen	Plate Thickness (inch)	Member Type	Professional Factors ($T_{failure}/T_n$)		
			Whitmore Yield	Whitmore Fracture	Block Shear
P16C-CJ-02	0.85	Diagonal	0.57	0.39	0.78
P17C-POS	0.60	Diagonal	0.84	0.61	0.98
		Vertical	0.44	0.31	0.54
P18C-POS	0.60	Diagonal	0.77	0.53	1.31
		Vertical	0.39	0.28	0.55

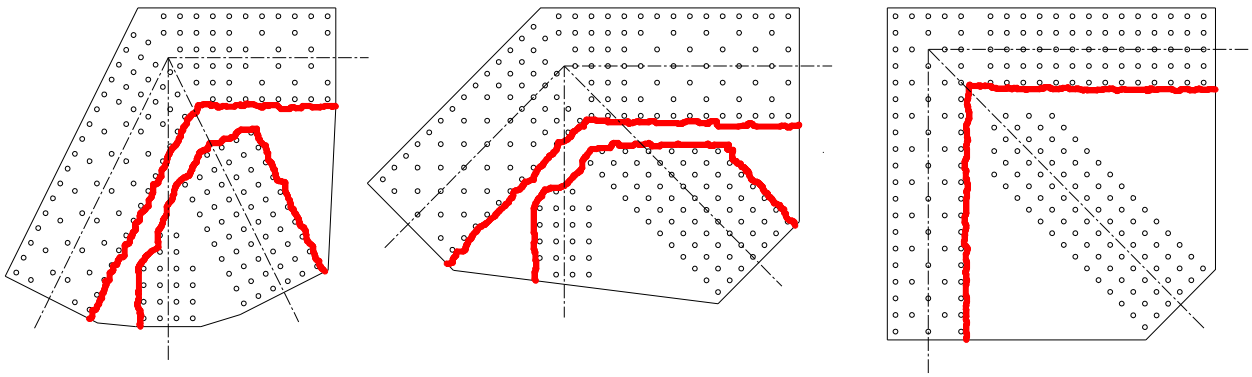

Figure 58. Alternate fracture patterns for connections P16C, P17C, and P18C.

Multi-Layered Plates

Only two analytical geometries and one experimental geometry were tested with multi-layered, or shingle plates. This does not provide enough data to make any firm conclusions regarding how multi-layered plates fail; however, their treatment in the previously described resistance equations will be assessed.

The only experimental connection tested with a shingle plate was GP307SS3-4. This connection tested a shingle plate combined with simulated section loss and was described in Chapter 2. The connection failed in shear at an internal shear load of 1213 kips. The relevant connection properties for shear calculations are presented in Table 23. The individual shear resistances for each plate are calculated individually (using Ω=1.00) and added together to determine the total nominal resistance. This assumption neglects any composite behavior between the plate layers and should be a conservative assumption. In fact, the professional factor for shear in the connection is 0.98 indicating that the calculation procedure fits within the scatter band of all the other full plane shear yield data, and it is appropriate to consider the total shear resistance to be the total of the individual shear resistances.

The analytical base geometries of P3C and P5C were each analyzed with three different combinations of gusset and shingle plate thicknesses. A summary of these six connections is presented in Table 24, all of which failed in buckling. The compression resistance is calculated using the two-folded approach described in the prior section. The extreme right-hand column presents the professional factor of these six shingle plated connections using the two-folded compression resistance approach. In the calculations, the gusset and shingle plates are considered to be uncoupled and the strength of each is added together for the total resistance. In all six cases the professional factors conservatively vary between 1.09 and 1.26 indicating that the methodology is conservative.

Table 23 Shear Calculations of Specimen GP307SS3-4

Specimen	Plate Thickness (inch)		Yield Strength (ksi)	Width of Plate (inch)	A_g (inch^2)	$V_{Failure}$ (kips)	$V_{nominal}$ [d] (kips)	$V_{failure}/V_{nominal}$
GP307SS3-4	South Gusset	0.375	38.0	59.0	22.13	1213	488	0.98
	North Gusset	0.367 [a]	38.0	59.0	12.97 [c]		286	
	North Shingle	0.375	46.3	46.0 [b]	17.25		463	

[a] – The real thickness of the plate was reported because an ultrasonic thickness meter had to be used to determine the remaining section thickness. This was not done for plates with no simulated section loss.
[b] – Width of shingle plate was taken at middle of simulate corrosion section.
[c] – The gross area was reduced by the simulated section loss of (48 inch)*(0.185 inch)=8.880 inch^2.
[d] – Ω=1.00 was used in the shear resistance calculation.

Table 24 Buckling Calculations of Models with Multi-Layered Gusset Plates

Specimen	Plate Thickness (inch)		Yield Strength (ksi)	Whitmore Width (inch)	Length of Partial Shear Plane (inch)	L_{mid} (inch)	λ_{mid}	$P_{Failure}$ (kips)	$P_{whitmore}$ using L_{mid} (kips)	$P_{partial\_shear}$ (kips)	Controlling Ratio using L_{mid} [a, b]
P5C-SP1-1.5:1	Gusset	0.300	53	49.70	40.24	8.57	0.45	1425	1309	830	1.16
	Shingle	0.200		29.32	28.78	8.57	1.02		407	396	
P5C-SP2-1:1	Gusset	0.300	53	49.70	40.24	8.57	0.45	1710	1309	830	1.20
	Shingle	0.300		29.32	28.78	8.57	0.45		772	593	
P5C-SPR-1.6:1	Gusset	0.400	53	49.70	40.24	8.57	0.26	2010	1895	1106	1.26
	Shingle	0.250		29.32	28.78	8.57	0.65		592	495	
P3-C-SP(2:1)-WV-P	Gusset	0.500	53	87.08	69.08	7.57	0.13	5850	4377	4247	1.10
	Shingle	0.250		48.71	34.21	7.57	0.51		1045	1052	
P3-C-SP(2:1)-WV-P	Gusset	0.400	53	87.08	69.08	7.57	0.20	4500	3399	3398	1.09
	Shingle	0.200		48.71	34.21	7.57	0.80		742	841	
P3-C-SP(1:1)-WV-P	Gusset	0.300	53	87.08	69.08	7.57	0.35	3950	2391	2548	1.26
	Shingle	0.200		48.71	34.21	7.57	0.80		742	841	

[a] - Green shading represents cases controlled by Partial Shear Plane Yielding.
[b] - Yellow shading represents cases controlled by Whitmore Buckling.

Edge Stiffening

In the previous section it was shown that the free edge slenderness could not be correlated to the buckling strength of the connection. However, if properly implemented, supplemental stiffening could be used to enhance the buckling resistance of some gusset plates.

Experimentally this was investigated with the GP490LS3-2 geometry that had exterior 3x3x1/2 inch angles applied to the free edges. Though not a direct comparison, the results of this test could be compared to the GP490LS3-1 geometry, which was the unstiffened version of the geometry. However, the yield strength and load proportioning between the connections was slightly different. Schematics of the two connections are shown in Figure 35 and Figure 27. The data from the two connections is summarized in Table 25. Because these two specimens were tested under different load proportioning, two columns are provided in Table 25 that report the load in both the compression and tension diagonals at failure of the connection. For the experimental 490LS3 geometry, the externally applied stiffeners result in a 64% increase in buckling resistance over the unstiffened geometry.

Since the two experimental connections were tested under different load proportioning, a more direct comparison was made analytically with the E5-490LS geometry, which did use the same loading scenario for each geometry. Data are also shown in Table 25 for the unstiffened, stiffened with internal angles, and stiffened with external angles (refer to Figure 34 for description of interior and exterior angles). The data show the internal angle stiffening option only results in a 3% increase in buckling capacity, though the external angle option results in a 45% increase in buckling resistance. The reason for the large increase in compressive strength is due to this geometry. Using the new two-folded compression resistance check, this geometry has a Whitmore buckling resistance of 464 kips versus 678 for the partial plane shear yield. In this case, the angles are able to suppress the Whitmore buckling until the partial plane shear yield controls the failure.

The E4-490SS geometry was also analytically investigated to show the relative increase in compressive strength between internally and externally applied 3x3x1/2 inch angles. The internal angles had no gain in compression resistance while the external angles produced a 17% gain. The unstiffened version of E4-490SS had a mixed failure mode between buckling and full plane horizontal shear yield. For this connection, the Whitmore buckling criteria predicts failure at 585 kips while the partial plane shear yielding occurs at 633 kips, which are only different by 8%. This shows that as the connection gets closer to being controlled by the partial plane shear yield criteria, the less effective the edge stiffening strategy will become.

Table 25 also shows the results between the stiffened and unstiffened version of the analytical P5U and P14C geometries. Both these stiffened connections resulted in 24% and 8% increases in buckling strength, respectively. The P5U connection was predicted to fail at a compression diagonal load of 807 kips and 1269 kips using the respective Whitmore and partial plane shear yield resistance equations. With this large disparity, it is expected that the edge stiffening

approach would be fruitful, and the results prove this with a 45% gain in compressive strength. With the P14C connection, the calculated resistances are 2348 and 1597 kips for the respective Whitmore and partial plane shear yield resistance equations respectively. In this case, since the partial shear equation already controls the compressive strength, the edge stiffening approach would not be considered effective, and in the end it only results in an 8% gain in compressive resistance.

Further analytical work was performed on P5U and P14C connections to understand how the stiffness of the stiffening element influences the buckling resistance. This was done by varying the size of the angle and, for just the P5U connection, the plate thickness too. Figure 59 demonstrates the relationship between a percent increase in the compression resistance and a relative ratio of the moment of inertia of the angles to the stiffness of the gusset plates, $I_{stiffener}/I_{gp}$. The calculation of the angle's moment of inertia must be taken about the surface of the plate as depicted in Figure 60. As shown in the figure, there is a variation in the increase in compression strength versus the angle stiffness and gusset plate thickness.

A couple of observations can be made from Figure 59. First, there appears to be a limiting stiffness by which no additional gain in compression resistance can be achieved, and this limit appears to be approximately at an $I_{stiffener}/I_{gp}$ ratio of 500. The gain in compressive resistance is also proportional to the geometry of the connection according to the assertions above. From the data, it appears that adding stiffness to the free edge suppresses buckling until the next limit-state begins to control. That is, if the connection was relatively compact and would have failed either the partial or full plane shear checks, then the extra stiffness will not provide much benefit; this was the case with the E4-490SS and P14C geometries. However, in the case of the GP490LS3 and P5U geometries which are more slender connections, the added stiffness to the free edge can suppress the buckling until the partial shear or full plane shear yield limits govern. For simplicity, the added cross-section from the stiffening technique should not be considered in the resistance equation.

Table 25 Increase in Compression Resistance with Edge Stiffening

Specimen or Model		Stiffening type	Plate Thickness (inch)	Yield Strength (ksi)	$C_{failure}$ [a] (kip)	$T_{failure}$ [b] (kip)	Increase over Unstiffened Geometry
GP490LS3-1	Experimental	None	0.375	48.5	527	881	[c]
GP490LS3-2	Experimental	External 3x3x1/2 angles	0.375	45.5	865	483	1.64
E5-490LS	Analytical	None	0.375	45.6	579	579	[c]
E5-490LS-SES	Analytical	Internal 3x3x1/2 angles	0.375	45.6	598	598	1.03
E5-490LS-EES	Analytical	External 3x3x1/2 angles	0.375	45.6	839	839	1.45
E4-490SS	Analytical	None	0.375	46.4	712	712	[c]
E4-490SS-SES	Analytical	Internal 3x3x1/2 angles	0.375	46.4	715	715	1.00
E4-490SS-EES	Analytical	External 3x3x1/2 angles	0.375	46.4	835	835	1.17
P5U-WV-NP	Analytical	None	0.400	53	1170	936	[c]
P5U-EES-WV-NP	Analytical	External 3x3x1/2 angles	0.400	53	1455	1164	1.24
P14C-W-INF	Analytical	None	0.500	53	1708	1452	[c]
P14C-EES-W-INF	Analytical	External 3.5x3.5x1/2 angles	0.500	53	1845	1568	1.08

[a] – Load in tension diagonal at failure.
[b] – Load in the compression diagonal at failure.
[c] – This is the unstiffened geometry that represents the baseline for comparison.

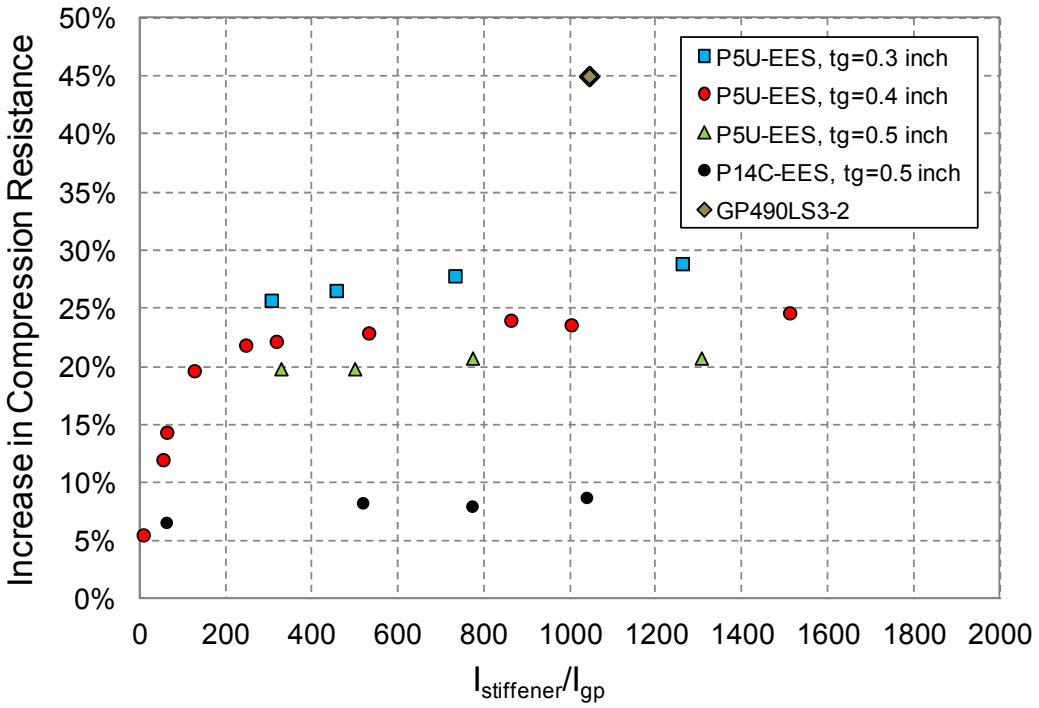

Figure 59. Increase in compression resistance for externally applied stiffening angles.

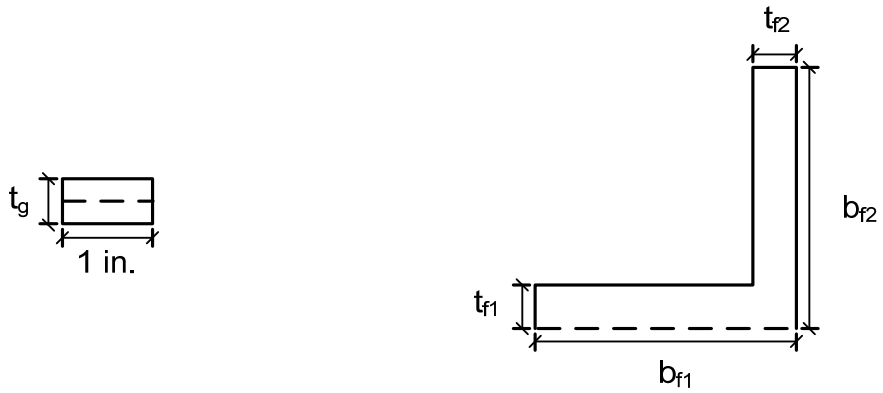

$$I_{gp} = \frac{(t_g)^3}{12} \qquad I_{stiffener} = \frac{b_{f1}{t_{f1}}^3}{3} + \frac{t_{f2}(b_{f2}-t_{f1})^3}{12} + t_{f2}(b_{f2}-t_{f1})\left(\frac{b_{f2}-t_{f1}}{2}+t_{f1}\right)^2$$

Figure 60. Calculation of external angle properties.

Corrosion

Four experimental connections and 10 analytical connections had simulated section loss (i.e., corrosion), all either failed in buckling or full plane shear yielding. A description of the experimental connections was provided in Chapter 2, and the analytical connections are described in Appendix I. This section will describe how the new resistance equations for shear

and buckling can be used to evaluate the reduction in resistance due to section loss. Since the consideration of section loss due to corrosion is a challenge when developing a rating on existing bridges, plates thinner than 0.375 inch were included in the analysis.

The methodology used in the resistance equations is to average out any section loss over the entire area being evaluated into an equivalent thickness to use in the compression and shear resistance equations. As an example, Figure 61 shows one of the investigated corrosion patterns in the P8C connection (see Appendix I for more details). There are two thicknesses of remaining section and three distinct holes along the horizontal plane above the chords. It is not obvious via inspection what the minimum shear plan area will be so both possible shear planes should be investigated. To calculate the equivalent thickness ($t_{average}$), calculate the real area in the shear plane and divide by the total width of the plane. Using Figure 61 as an example, the minimum shear area on the full shear plane is 29.075 inch^2, divided by the 94.1 inch wide plane yields $t_{average}$=0.309 inch. When calculating the nominal shear resistance of the full plane, $t_{average}$=0.309 inch would be used rather than the nominal thickness of 0.500 inch. The same notion would extend to partial shear planes.

For compression checks, the equivalent thickness on a Whitmore section must be calculated. The philosophy used projects any corrosion onto the Whitmore plane in the direction of the member. This is better illustrated in Figure 62, which uses three different colors to represent the different remaining plate thicknesses. Lines paralleling the framing angle of the section loss project from the middle of the section loss onto the Whitmore plane. For easier visualization, the Whitmore plane is colored depicting the areas where the various remaining section is being projected onto the Whitmore plane. The total cross-sectional area considering the remaining section thicknesses is calculated over the entire width of the Whitmore plane, then divided by the total width of the Whitmore plane to determine the equivalent thickness.

A summary of the experimental connection results and associated resistance equation predictions is provided in Table 26. Of the four connections, only one failed in buckling and the buckling professional factor is a conservative 1.30. The remaining three experimental connections failed in full plane shear yielding and their associated professional factors vary from 0.98 to 1.13, which fits within the scatter band of normal full plane shear failures shown in Figure 46. Of the four experimental connections, the resistance equations correctly identified the failure mode in three of them, lending further credence to the approach. Therefore, the equivalent thickness approach used for both buckling and shear is considered a valid approach because it is either conservative, or fits within the associated statistics that ϕ-factors will be calibrated with.

Table 27 shows the same type of results associated with the 10 analytical connections with simulated section loss. Some of these connections had multi-layered plates and are described in this section. Out of the 10 simulations, the correct failure mode was only identified half the time, though in each situation (buckling and shear), the professional factors were within the scatter bands used in the ϕ-factor calibrations.

The data presented in this section show that for the evaluation of gusset plates with section loss, the resistance prediction equations for shear yielding and buckling can provide conservative resistance predictions. This approach relies on using an equivalent thickness approach where the section loss is "smeared" over the entire plane of failure. In these cases, the resistance equations produced conservative predictions, even if the section loss was unbalanced across the plate, if only one of two plates in the connection had section loss, or if multi-layered plates were used.

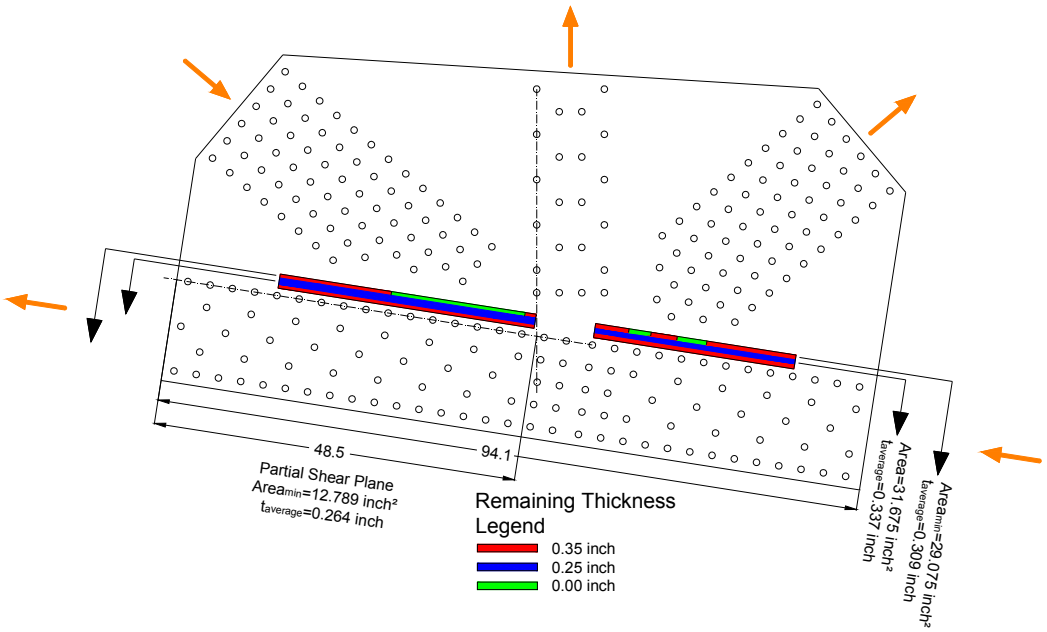

Figure 61. Evaluation of equivalent shear area through section loss for P8C.

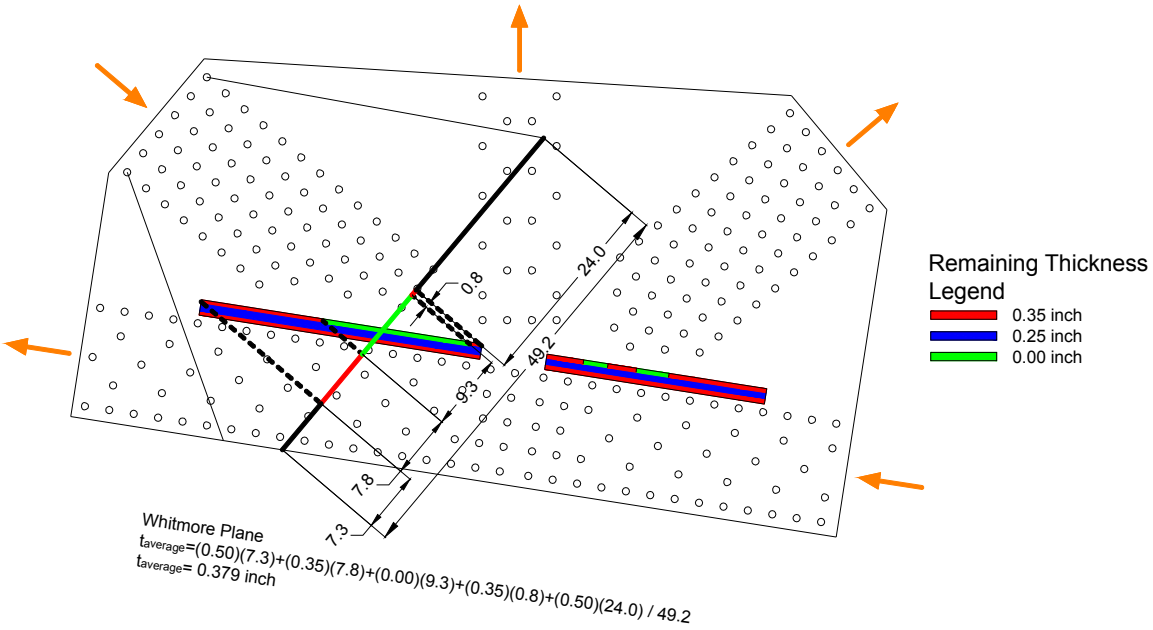

Figure 62. Evaluation of equivalent Whitmore plane thickness for section loss in P8C.

Table 26 Resistance Predictions of Experimental Connection with Section Loss

Specimen	Plate Thickness (inch) [a]	Yield Strength (ksi)	Whitmore Width (inch)	Length of Partial Shear Plane (inch)	Whitmore Buckling $t_{average}$ (inch) [b]	Full Plane Shear $t_{average}$ (inch) [c]	Partial Plane Shear $t_{average}$ (inch) [d]	$P_{failure}$ (kips) [e]	$V_{failure}$ (kips) [e]	V_{ny} (kips)	P_{n_whit} (kips)	P_{n_ps} (kips)	$P_{failure}/P_n$ [f]	$V_{failure}/V_n$ [f]
GP307SS3-1	0.3710	47.2	24.43	26	0.191	0.241	0.211	446	517	390	170	212	1.30	0.67
	0.3660	47.2	24.43	26	0.194	0.238	0.213			384	172	214		
GP307SS3-2	0.3650	47.8	24.43	26	0.248	0.239	0.261	482	833	391	221	266	0.94	1.07
	0.3670	47.8	24.43	26	0.250	0.238	0.263			389	292	268		
GP307SS3-3	0.3710	37.9	24.43	26	0.268	0.232	0.229	519	887	301	202	185	1.07	1.13
	0.3750	37.9	24.43	26	0.375	0.375	0.375			486	283	303		
GP307SS3-4	0.3670	38	24.43	26	0.258	0.220	0.217	712	1213	286	194	176	1.09	0.98
	0.3750	38	24.43	26	0.375	0.375	0.375			488	284	304		
	0.3750	46.3	12.87	20.73	0.375	0.375	0.375			468	174	295		

[a] – For some plates, the measured thickness using an ultrasonic thickness gauge was used for the plate thickness and remaining section. This was done because the thickness milled away was variable depending on how the plate was clamped to the mill, and this eliminated any variability in the remaining section calculation.
[b] – The average thickness of the Whitmore section by projecting all section loss between the Whitmore section and the adjoining member fastener lines onto the Whitmore section.
[c] – The average thickness of the full width shear plane considering the minimum shear section along that plane.
[d] – The average thickness of the partial shear plane considering the minimum section along that plane.
[e] – Cells shaded grey represent the failure mode of the connection.
[f] – Cells shaded green mean the calculated resistance is controlled by full plane shear yielding; yellow shading represents cases controlled by calculated compression resistance.

Table 27 Resistance Predictions of Analytical Connection with Section Loss

Specimen	Plate Thickness (inch)	Yield Strength (ksi)	Whitmore Width (inch)	Length of Partial Shear Plane (inch)	Whitmore Buckling $t_{average}$ (inch) [a]	Full Plane Shear $t_{average}$ (inch) [b]	Partial Plane Shear $t_{average}$ (inch) [c]	$P_{failure}$ (kips) [d]	$V_{failure}$ (kips) [d]	V_{ny} (kips)	P_{n_whit} (kips)	P_{n_ps} (kips)	$P_{failure}/P_n$ [e]	$V_{failure}/V_n$ [e]
P8C-C1	0.5000	53	49.28	48.53	0.379	0.309	0.264	1281	1982	1788	1848	920	1.39	1.11
P8C-C2	0.5000	53	49.28	48.53	0.405	0.367	0.315	1596	2469	2124	1977	1098	1.45	1.16
P8C-COS	0.5000	53	49.28	48.53	0.378	0.309	0.264	1743	2696	894	1848	920	0.65	1.15
	0.5000	53	49.28	48.53	0.500	0.500	0.500			1446	2443	1746		
P14U-C1	0.5000	53	43.64	33.1	0.328	0.349	0.262	1316	1253	1225	1334	838	1.57	1.02
P14U-C2	0.5000	53	43.64	33.1	0.348	0.349	0.262	1330	1266	1225	1413	840	1.58	1.03
P14U-COS	0.5000	53	43.64	33.1	0.328	0.349	0.262	1498	1426	612	1334	838	0.61	0.96
	0.5000	53	43.64	33.1	0.500	0.500	0.500			878	2033	1600		
P8C-C1-SP	0.5000	53	49.28	48.53	0.378	0.309	0.264	1953	3021	1788	1848	920	1.33	1.09
	0.2500	53	32.32	30.5	0.250	0.250	0.250			988	656	549		
P8C-COS-SP	0.5000	53	49.28	48.53	0.378	0.309	0.264	1995	3086	894	1848	920	0.62	1.09
	0.5000	53	49.28	48.53	0.500	0.500	0.500			1446	2443	1746		
	0.2500	53	32.32	30.5	0.250	0.250	0.250			494	656	549		
P14U-C1-SP	0.5000	53	43.64	33.1	0.328	0.349	0.262	1708	1626	1225	1334	838	1.21	0.87
	0.2500	53	26.32	23.95	0.250	0.250	0.250			646	416	579		
P14U-COS-SP	0.5000	53	43.64	33.1	0.328	0.349	0.262	1680	1599	612	1334	838	0.56	0.88
	0.5000	53	43.64	33.1	0.500	0.500	0.500			878	2033	1600		
	0.2500	53	26.32	23.95	0.250	0.250	0.250			323	416	579		

C1=corrosion pattern 1 in both plates; C2=corrosion pattern 2 in both plates; COS=corrosion pattern 1 in only one plate; C1-SP=corrosion pattern 1 in both plates with a shingle plate on both sides; COS-SP=corrosion pattern 1 in only one plate with shingle plate only over the corroded plate

[a] – The average thickness of the Whitmore section by projecting all section loss between the Whitmore section and the adjoining member fastener lines onto the Whitmore section.
[b] – The average thickness of the full width shear plane considering the minimum shear section along that plane.
[c] – The average thickness of the partial shear plane considering the minimum section along that plane.
[d] – Cells shaded grey represent the failure mode of the connection.
[e] – Cells shaded green mean the calculated resistance is controlled by full plane shear yielding; yellow shading represents cases controlled by calculated compression resistance.

Rivet Shear Strength

Though this research did not address the strength of rivets extensively, the opportunity was taken to analyze the historical data available in the available literature to assess the current MBE technique (up to the 2011 2nd Edition) for evaluating rivet shear strength, which the FHWA Guide mostly copied.

Historically, fastener shear resistance equations took the form shown in Equation 11 and will be discussed in terms of rivets.

$$\phi R_n = \phi R_1 R_2 R_3 F_u A \quad \text{(Eq. 11)}$$

where:

ϕ is the resistance factor
R_1 is a shear-to-tensile ratio of the driven rivet stock
R_2 is a connection length factor
R_3 is a fill plate factor
F_u is the tensile strength of the driven rivet stock
A is the cross-sectional area of all the shear planes

In previous versions of the MBE and BDS, much of this equation was built-in to the resistance tables for individual fastener strength. The shear-to-tensile ratio, R_1, is commonly believed to be 0.58 based on the Von Mises shear failure; however, for fasteners it has been reported to be as high as 0.85.[10] The connection length reduction, R_2, accounts for the shear lag that develops through the length of connection in the direction of force and will be discussed further in another section. The fill plate factor accounts for a reduction in overall connection strength when filler plates are used in thickness transitions. The fill plate factor is not considered in this research. The ultimate tensile strength of the fastener is represented by F_u and the cross-section area, A, is the sum of all shear planes considering the *undriven rivet cross-section*.

Strength Data

The 2011 2nd Edition of the MBE published four factored strengths for rivets as shown in Table 28. The 18 ksi value for rivets constructed prior to 1936 or of unknown origin assumed that the tensile strength of the rivet stock was conservatively taken as 46 ksi with a 0.58 shear-to-tensile ratio and a ϕ-factor of 0.67.[27] Up until 1931, rivets fell under the ASTM A7 specification and it was published by Ferris that rivets from this era have tensile strengths that range from 46-56 ksi.[28] The ASTM A141 rivet specification was tentatively passed in 1932 and officially in 1933 and it cannot be determined why the code writers chose 1936 as the transition date over 1933. Likewise, once the A141 specification was passed, it listed rivet tensile strengths of 52-62 ksi which gives rise to the 21 ksi factored shear strength for rivets constructed after 1936. For A502 rivets, the MBE adopted the values published in the 2002 17th Edition of the Standard Specifications for Highway Bridges. However, the FHWA Guide increased the strengths of A502 rivets by 2 ksi over these values to "adjust for an error in calibration which took place in

the translation from older manuals."[29] All these strengths had to be reduced by an extra 20% when the connection length exceeded 50 inches, which is further explained in the next section.

A variety of ultimate rivet shear strength data was collected from available literature sources as well as tests performed as part of this research project reported in Appendix C.[30-52] Sources were published between the years of 1882 and 1970, and encompassed rivet grades of unknown origin, ASTM A141, ASTM A195, and ASTM A502 Grade 1. No test data for ASTM A502 Grade 2 could explicitly be found. Shown in Figure 63 is a histogram of all ultimate rivet shear strengths. It is most important to note that the *ultimate shear stresses are presented in terms of the undriven rivet area*. Therefore the shear stresses would be expected to be artificially high since they are based on the undriven rivet area, whereas in reality the rivet probably has an area equal to the standard oversize hole it has filled. However, built-in to the distribution would be cases of mis-installation where the rivet only partially filled the hole.

The data plotted as iron rivets are from six different reports from the Watertown Arsenal conducted between the years 1882 and 1896 from a total of 95 rivet or rivet group tests. Chemistries were never reported for the rivets and they were only reported as "iron" as opposed to "steel" rivets that were also tested. The iron rivets from the late 1800's are considered to be the worst possible rivet that could be found on a truss bridge with gusset-plated connections, and thought to be a good representative for rivets of an unknown origin. The data plotted as steel rivets encompass data reported as "steel" or "carbon" rivets produced between the years of 1882 and 1970 from 369 tests on rivets or rivet groups. Some of the steel rivets were reportedly alloyed with chrome and nickel. The data plotted as "Manganese" rivets appeared from one study conducted in 1940 that demonstrated much higher strength than those that were reported as "Carbon" rivets. In total there were 29 connection tests performed with Manganese rivets. Though they were reported as "Manganese" the chemical composition of these rivets met the ASTM A195 at the time.

The rivet shear statistics needed in the calibration are shown in Table 29. For the purposes of this evaluation, rivets will be divided into three categories: unknown origin, A141/A502 Gr.1, and A195/A502 Gr.2, which will be assigned ultimate tensile strengths, F_u, or 50, 60, and 80 ksi, respectively. These F_u values were thought to be representative values. However, a new shear-to-tensile ratio of 0.85 is being proposed, as it best fits the data using the assumed tensile strengths. Therefore the nominal shear strength will be $0.85F_u$ of the rivet stock. It is important to note that the assumed shear-to-tensile ratio is somewhat fictitious and really represents a curve-fit to shear test data. *That is, multiplying the ultimate tensile test result from a rivet removed from service by 0.85 will not produce an accurate ultimate shear stress for rating purposes*. The 0.85 factor is accounting for differences in the shear area based on normalizing the data back to an undriven rivet diameter, so in reality the ratio is more like 0.74 (considering oversized holes add about 15% additional shear area over the undriven rivet diameter). The average shear strength, respective bias factors to the nominal strength, and coefficients of variation are also shown in the table for each grade of rivet.

Table 28 Reproduction of Table 6A.6.12.5.1-1 from 2nd Edition MBE

Rivet Type and Year of Construction	ϕF (ksi)
Constructed prior to 1936 or of unknown origin	18
Constructed after 1936 but of unknown origin	21
ASTM A502 Grade I	25
ASTM A502 Grade II	30

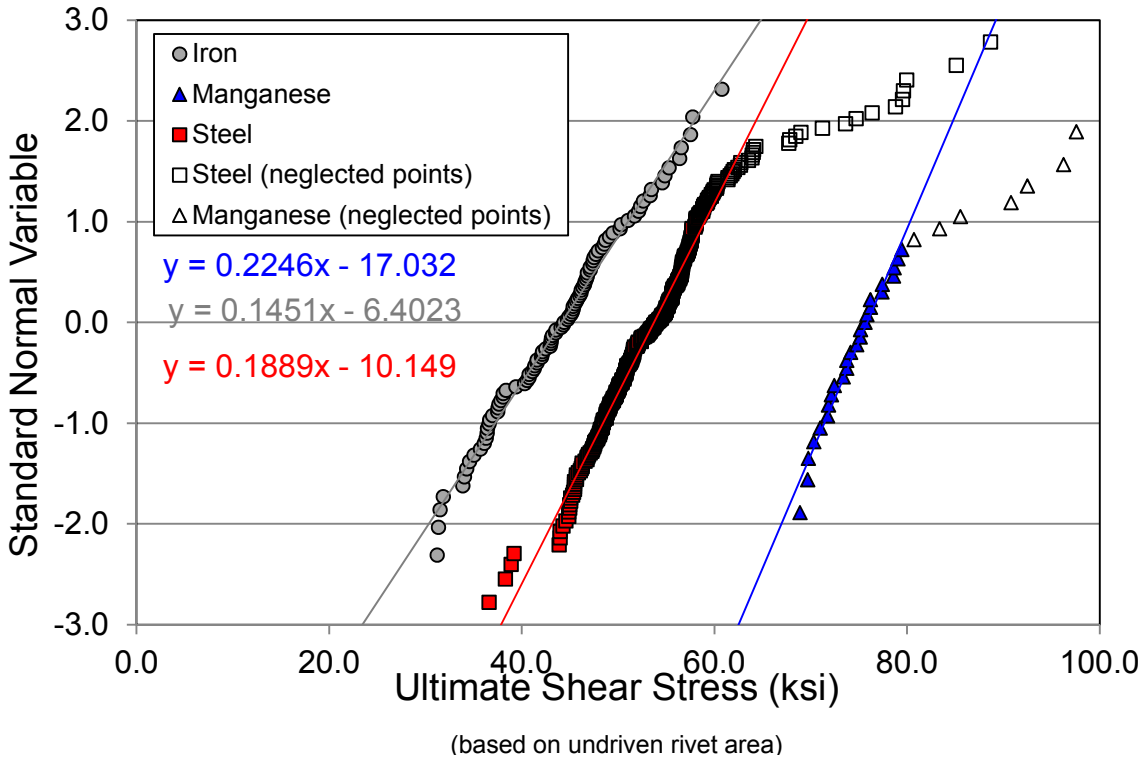

Figure 63. Ultimate rivet shear strength data (1882-1970) plotted on normal probability paper.

Table 29 Rivet Shear Strength Statistics

Rivet Type	Assumed Tensile Strength, F_u (ksi)	Assumed Shear Strength, $0.85F_u$ (ksi)	Experimental Average Shear Strength (ksi)	Bias Factor (λ)	Coefficient of Variation
Iron (unknown)	50	42.5	44.1	1.038	0.156
Steel (A141, A502 Gr. 1)	60	51.0	53.7	1.053	0.099
Manganese Steel (A195 and A502 Gr.2)	80	68.0	75.8	1.115	0.059

Connection Length Reduction

Connection tests have shown that, for very long connections, the shear strength of a fastener group does not equal the strength of a single fastener multiplied by the total number of fasteners in the connection. In prior design specifications, the connection reduction factor was taken as 0.8 for connections up to 50 inches in length and 0.64 for connections in excess of 50 inches. This was somewhat hidden as the initial factor was always built-in to the resistance and the code reader would only see an additional 0.80 reduction for connections in excess of 50 inches. This step function led to an enigma, because at 50 inches in length there was a sudden 20% reduction in strength when in reality it is probably a continuous function.

The data used to determine the connection length effect was that reported by Tide [53] (neglecting the two outlier points he outlined). In addition, the rivet connection data published by Davis and Woodruff [40] was added to this data set. The data is disseminated in terms of the connection length professional factor being the real strength divided by the predicted value. The predicted value of the connection strength is based on the strength of an individual fastener multiplied by the number of fasteners in the connection. The professional factor is plotted against the overall length of the connection and is shown in Figure 64, with the rivet and bolt data points segregated. As seen in the figure, the data is quite scattered especially for connections in excess of 40 inches in length (note that some of the data points are hidden by others).

Tide further showed that the scatter in the data can be better explained after considering the geometric proportioning of the joint. He outlined a two-folded check where the designer must check ratios between gross plate area to fastener shear area and compare to the respective yield and tensile properties of the plate.

$$A_{gross} > (0.85\ A_{s\_fastener}\ F_{v\_fastener})/F_{y\ plate} \quad \text{(Eq. 12)}$$

$$A_{net} > (0.85\ A_{s\_fastener}\ F_{v\_fastener})/F_{u\_\ plate} \quad \text{(Eq. 13)}$$

Once these two inequalities were checked, it was found that if the connection geometry was proportioned such that both or one of the inequalities passed, the data were banded about a reduction ratio of 0.90 for all connection lengths. Connections failing both inequalities demonstrated much lower connection reduction factors that are more tightly banded around a reduction of 0.70. To demonstrate this better, the data shown in Figure 64 is reproduced in Figure 65 where the data shown as circles pass both inequalities, squares represent connections that passed only one inequality, and data shown as triangles fail both inequalities. The data passing one or both inequalities shown in Figure 65 tend to band around a connection length reduction of 0.90, and those that fail both inequalities tend to band around a reduction of 0.7. Finally, the connection length professional factors are plotted on normal probability paper in Figure 66. The data was broken down into two sets, those that failed both Tide criteria, and those that met one or both Tide criteria. Both sets are fairly linear indicating the assumed normal probability distribution is accurate.

Table 30 shows the statistical parameters of the data shown in Figure 66 attained from the best-fit line through the data. The statistics are presented assuming that the resistance limit-state check will assume the designer or load rater will have to check the two Tide inequalities. Therefore, a 0.90 connection length reduction will be applied to all connections despite length. In this case, the data show an average reduction of 0.932 for a bias of 1.035 and COV of 0.077. The data for connections failing both Tide inequalities are assumed to have a reduction of 0.70 and show an average of 0.702 (bias of 1.002) and COV of 0.103. Since the statistical parameters are worst for connections that fail both Tide inequalities, only they will be used in rivet strength calibrations. From the perspective of the designer or load rater, resistance values will have to be multiplied by 0.78 (ratio of 0.7/0.9) to account for situations where connections fail both the Tide inequalities.

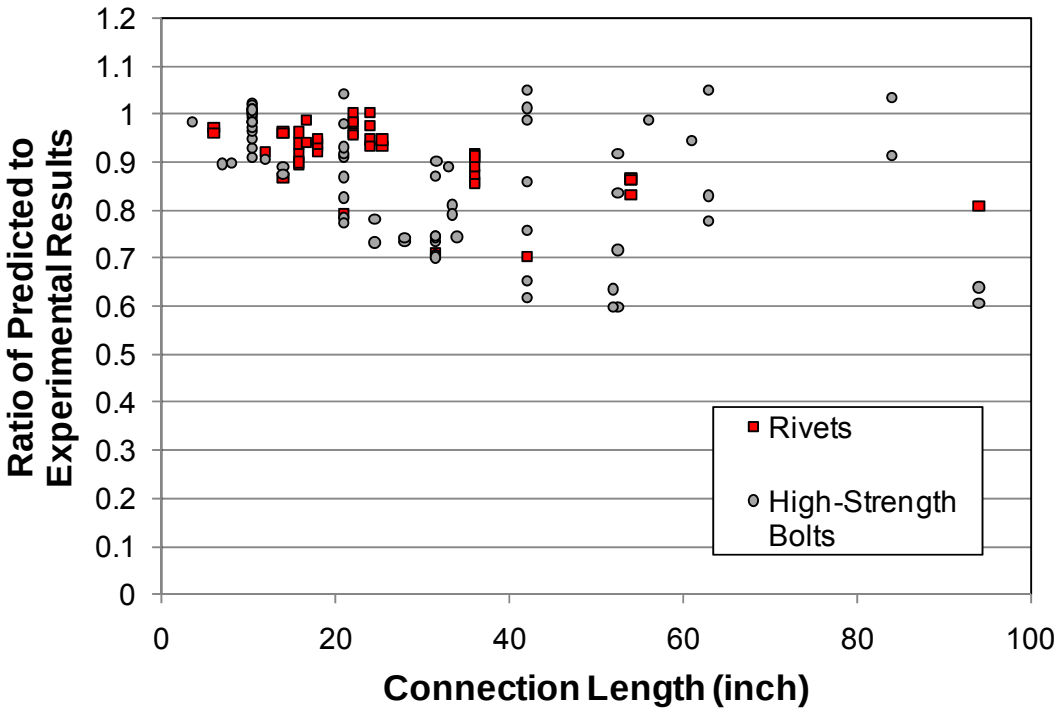

Figure 64. Bolt and rivet connection data showing connection length effect.

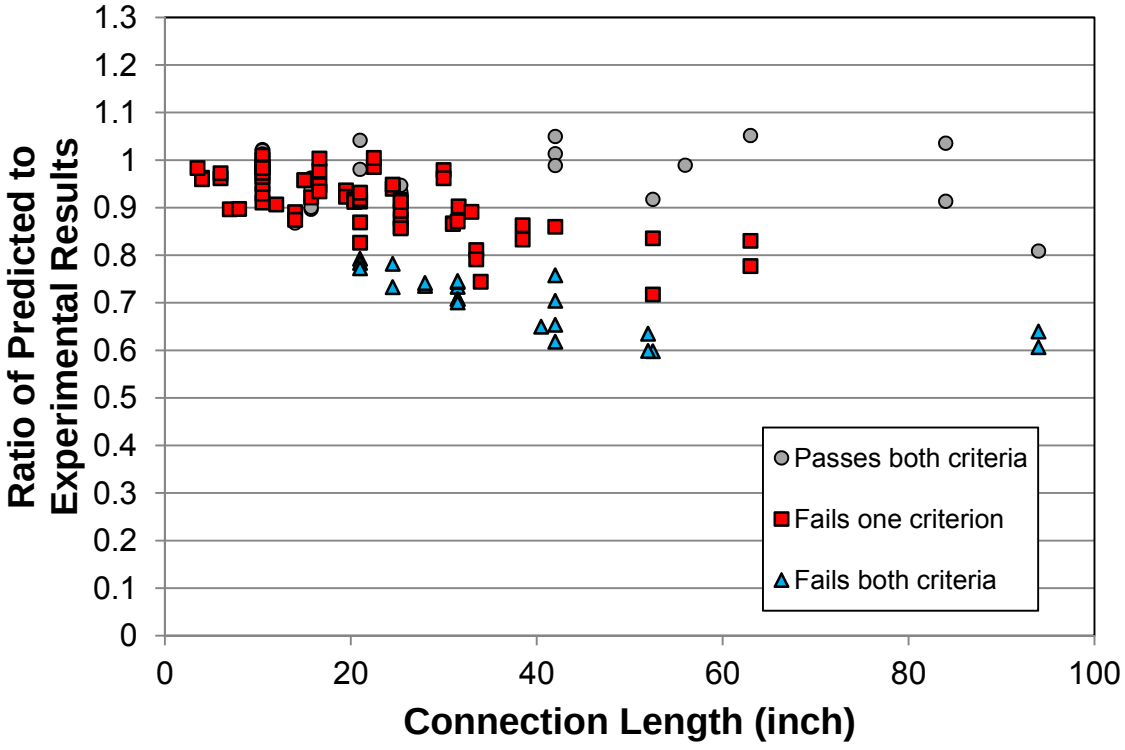

Figure 65. Bolt and rivet data segregated by Tide stiffness and strength criteria.

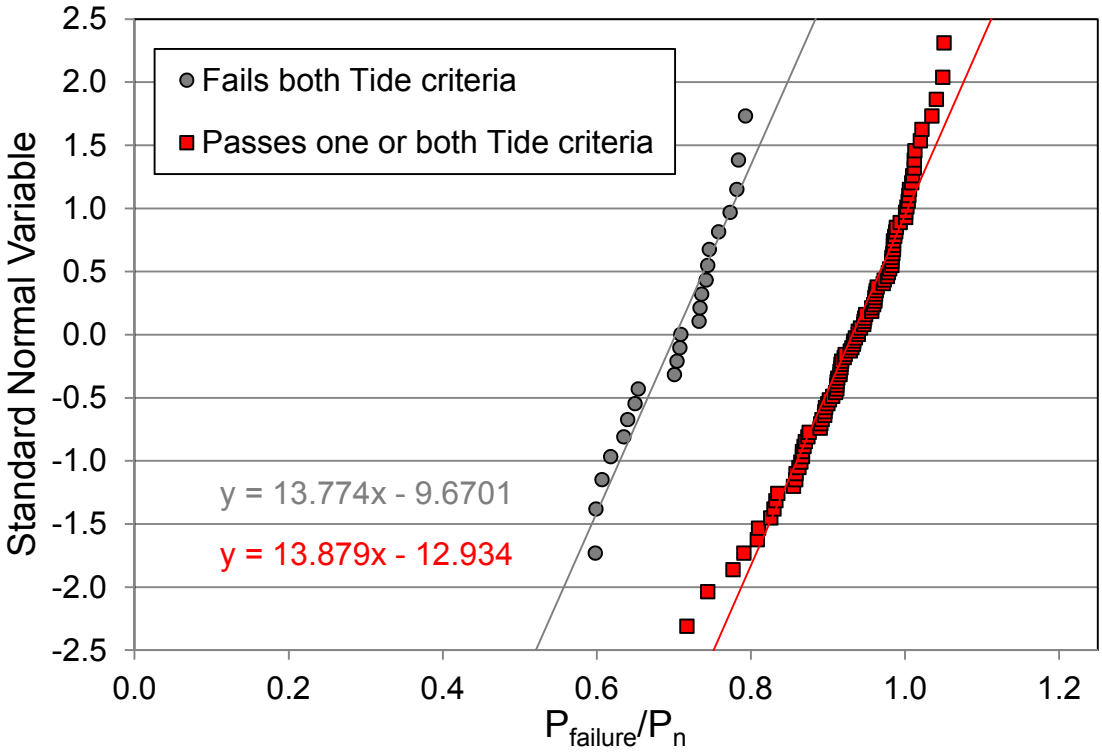

Figure 66. Connection length professional factors plotted on normal probability paper.

Table 30 Statistics of Connection Length Reduction

	Nominal Length Reduction, R_2	Average (μ_{R2})	Bias Factor (λ_{R2})	COV
One or both inequalities satisfied	0.90	0.932	1.035	0.077
Neither inequality satisfied	0.70	0.702	1.002	0.103

SUMMARY OF PROFESSIONAL FACTOR STATISTICS

Table 31outlines all the professional factor statistics for the various limit-states discussed in this chapter. Only the bias (λ) and the COV are shown. Limit-states involving net section failures do not have any professional factor data because none were observed in the experiments nor could the analytical models identify them. Therefore, only the limit-states shown in Table 31 will be calibrated in the next chapter.

Table 31 Summary of Professional Factor Statistics

Limit State		λ	COV
Full Plane Shear Yielding (ϕΩ) (all data considered)		1.017	0.069
Full Plane Shear Yielding (ϕΩ) (neglecting plates thinner than 0.375 inch)		1.017	0.069
Buckling	Whitmore Buckling (all data considered)	1.268	0.135
	Whitmore Buckling (neglecting plates thinner than 0.375 inch)	1.226	0.103
	Partial Plane Shear (all data considered)	1.139	0.144
	Partial Plane Shear (neglecting plates thinner than 0.375 inch)	1.183	0.116
Block Shear		1.180	0.060
Chord Splice (all data considered)		1.224	0.164
Chord Splice (neglecting plates thinner than 0.375 inch)		1.284	0.163
Rivet Shear	Unknown Origin (assumed 42.5 ksi shear strength)	1.038	0.156
	A141/A502 Gr. 1 (assumed 51.0 ksi shear strength)	1.053	0.099
	A195/A502 Gr. 2 (assumed 68.0 ksi shear strength)	1.115	0.059
	Connection Length Effect (failing both Tide criteria, 0.70)	1.002	0.103
	Connection Length Effect (passes one or both Tide criteria, 0.70)	1.035	0.077
Analysis Factor		1.000	0.000

CHAPTER 4. RESISTANCE FACTOR CALIBRATION

For the suggested limit-state equations to be properly integrated into the BDS and MBE, they must be calibrated. Since the goal is not to define new load factors, this only requires calibrating new resistance factors. This section will demonstrate how the calibration task was completed, and the results obtained by it.

CALIBRATION METHOD

For this research a partial reliability analysis was performed, meaning only resistance factors were determined through the reliability analysis. This was done so as not to add more load combinations to the existing suite within the AASHTO design specifications, and use the existing load combinations to only derive new resistance factors. Resistance factors were derived via Monte Carlo analysis for each limit-state according to the philosophy outlined in NCHRP 20-07(186).[54] In this analysis method, statistical parameters of bias and coefficient of variation (COV) are determined for the dead and live loads, as well as the limit-state resistance variables. A spreadsheet is used to create a list of randomly generated numbers that seed a statistical generation of loads and resistance values. Each line of the spreadsheet then contains a randomly generated set of dead and live loads, and associated resistance. A limit-state check is performed for each line of the spreadsheet where it is determined if the combination of loads exceeds the available resistance and if so, it is considered a failure.

The goal of the calibrations is to derive ϕ-factors that can attain a desired reliability index, β. The meaning of the reliability index is best illustrated with the assistance of Figure 67. The left-handed plot demonstrates the variability in applied load (Q) and available resistance (R) for a generic structural element. The right-handed plot of Figure 67 shows the probability density function for the function, *R*-*Q*. Any time the function *R*-*Q* is negative represents when the applied load is greater than the resistance and failure occurs. The overall distribution has a mean that is located away from the failure axis. The reliability index, β, describes how many standard deviations the mean of the *R*-*Q* distribution is away from the failure axis. When reading in reliability textbooks and when calculating reliability with spreadsheet functions, it is important to note that the reliability index is reported as a negative number because the probability is related to a standard normal distribution with a mean of 0.0 and standard deviation of 1.0, and the area of interest is the left-hand tail probability which is on the negative side of the standard normal distribution. In LRFD and LRFR discussions, reliability is presented as a positive number as a matter of convenience. The notional probability of failure associated with reliability indices of 3.5 and 4.5 are 0.02326% and 0.00034%, respectively.

All calibrations were performed at two reliability indices of 3.5 and 4.5. The reliability index of 3.5 is the current target level AASHTO uses for member-level reliability. [7, 54, 55] The reliability index of 4.5 is an alternative target for connection limit-states using the philosophy of the American Institute of Steel Construction (AISC), which will be described in a later section.

The Monte Carlo simulations were performed in a spreadsheet that conducted 600,000 random limit-state checks. The random analysis was conducted five times for a total of 3,000,000 simulations. The number of simulations came from the recommendation of the NCHRP 20-07(186) report that at least 10 failures should be observed at the target reliability index. To produce 10 failures with a probability of failure 0.00034% at a reliability index of 4.5 requires 2,943,191 simulations.

In addition, all simulations were performed using assumed dead-to-live load ratios with the AASHTO Strength I and IV load combinations. Prior AASHTO calibrations have used only the Strength I load combination, but the results of the Strength IV combination are presented because it may be a controlling combination for many long-span trusses. As will be described in subsequent sections, the ϕ-factors derived from the Strength I and IV load combinations converge around a dead-to-live load ratio of 6.0 and perhaps this should be observed considering that trusses are typically dominated by dead load. Additionally, the reliability indices of the derived ϕ-factors were analyzed to see how far they deviate from the assumed 2.5 when used with the MBE Operating load combination.

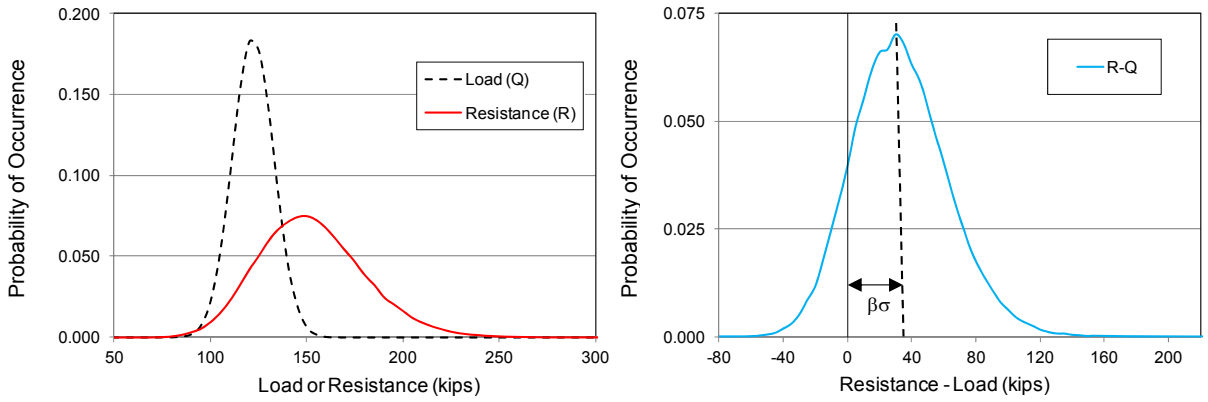

Figure 67. Illustrative explanation for the reliability index, β.

Assumed Calibration Statistics

The Monte Carlo analysis requires statistical data in the form of bias and coefficient of variation based on real data to provide an accurate estimation of the real variations expected in the limit-state variables. The bias is the ratio between the mean and the specified value, and the COV is the ratio of the standard deviation divided by the mean. In the previous chapter, much of the statistical data was reported as the professional factor, which is the same as the bias because the nominal mean value is 1.00.

Statistical analysis of live and dead loads on a suite of trusses was not performed as part of this calibration process. Rather these load statistics were assumed based on judgment and from the data presented in the NCHRP 20-07(186) report.[54] The dead load was assumed to have a bias of 1.05 and a COV of 0.10 which comes from the data reported for cast-in-place elements because

much of the weight in the truss is from a cast-in-place deck. The live load bias was assumed to be 1.15 with a COV of 0.12. The chosen bias was a gross average of all the reported live load biases in NCHRP 20-07(186). The COV of 0.12 is reported not to include the effects of impact, therefore the impact factor is not included in the Monte Carlo analysis, also as reported in NCHRP 20-07(186).

For the resistance side of the limit-state, the overall resistance is the nominal resistance multiplied by professional (P), material (M), and fabrication (F) factors as shown in Equation 14.

$$R = R_n * P * M * F \quad \text{(Eq. 14)}$$

The professional factor accounts for variations in real resistance versus calculated resistance from an equation. The material factor accounts for the variation in material properties such as yield and tensile strength. The fabrication factor takes into account the variations in the accuracy of elements from which a structure is created; this would include such things as variation in plate thickness and fabrication tolerances.

The statistical data for professional factors was presented in Chapter 3 for all the various limit-states. As for the M-factor, the only variable considered in the many gusset plate limit-states is either yield or ultimate stress. The authors of the NCHRP 20-07(186) report referenced back to the NBS 577 [21] document for the values used in that calibration. NBS 577 reported various values of bias and COV values of hot-rolled steel products, but did mention that material from webs of hot-rolled product and structural plates had bias of 1.10 and COV of 0.11 for both yield and tensile strength. These values have been revised in more recent studies to account for changes in modern plate processing, but it was felt that since the majority of trusses being rated predate the publishing of the NBS 577 report, those values would be most appropriate. In addition, NBS 577 also recommended a bias of 1.11 and COV of 0.10 for shear yielding; however, this represents little difference over tensile yield properties and since the shear limit-state equations use tensile yield properties, tensile yield statistics were used. Finally, as also reported in NBS 577, the F-factor was assumed to have values of 1.00 for bias and 0.05 for COV. No additional work was performed as part of this research to quantify the dimensional variations of gusset plates and there is no better published data to query to refine the F-factor statistics.

Table 32 outlines all the assumed bias and COVs for various parameters used in this research's resistance factor calibration.

Table 32 Assumed Calibration Statistics

	Bias Factor (λ)	COV
Dead Load	1.05	0.10
Live + Impact	1.15	0.12
Yield or Tensile Strength (F_y or F_u)	1.10	0.11
Fabrication Factor (F)	1.00	0.05

System Factors

The Monte Carlo simulations did not account for any additional reductions due to system or condition factors that are currently considered optional in the Manual of Bridge Evaluation. Therefore, it is assumed that both of these factors have values of 1.00.

Dead-to-Live Load Ratios for Trusses

To make the calibration process easier without conducting a series of live load analyses through a suite of various trusses, it is often easier to assume a dead-to-live load ratio. The question then becomes what is the spectrum of dead-to-live load ratios for truss bridges.

As described in Chapter 1, the research team received construction plan sets (and sometimes shop drawings) for 20 different trusses, from eight different states. The trusses utilized various configurations and were all built between the years of 1929 and 1990, the majority being built in the 1950's, 60's, and 70's. More information on these trusses can be found in Appendix A. The dead and live loads reported within the construction plans were assumed to be correct and recorded in a spreadsheet for further statistical analysis. It is important to note that many different live load models were assumed in the design of this suite of trusses including H15, H20, and HS-20. This is important to note because the calibration task is being conducted using the load factors derived around the HL-93 live load model, which is more stringent than the three mentioned legacy live load models.

Shown in Figure 68 is a histogram of all the dead-to-live load ratios (DL/LL) for all the data broken out into the three member types of chords, diagonals, and verticals. Chord members are fairly uniformly distributed between ratios of 0.5 to 6.0. Diagonals demonstrated a wide-banded Gaussian distribution between ratios of 0.5 and 6.0 peaking with an average around 3.0. Vertical members show a narrow-banded Gaussian distribution between ratios of 0.5 and 3.0 with a peak at 2.0. The high frequencies of members with a ratio of 10.0 are an aberration; these are meant to represent members that did not have any reported live load (i.e., the divide-by-zero anomaly was

represented by the dead-to-live ratio of 10.0). The majority (94%) of members with no live load were vertical members. Figure 69 shows a histogram of all the data that is independent of the member type which shows a skewed, wide-banded Gaussian distribution with an average of 2.3, and a standard deviation of 1.4 (neglecting the members with no live load).

The histograms of dead-to-live load ratios are based on the older live load models (H15, H20, and HS-20); therefore, the spectrum of ratios would be expected to shift to the left given an HL-93 live load model. Given this data, it was decided to investigate the calibration using dead-to-live load ratios of 0.5, 1.0, 2.0, 3.0, 4.0, 6.0, and 8.0. The original LRFD calibration of AASHTO used actual bridge designs; however, NCHRP 20-07(186) reported the DL/LL ratios of the girders varied from 0.3 to 4.5. Therefore, the DL/LL of trusses is slightly higher than girders, as expected.

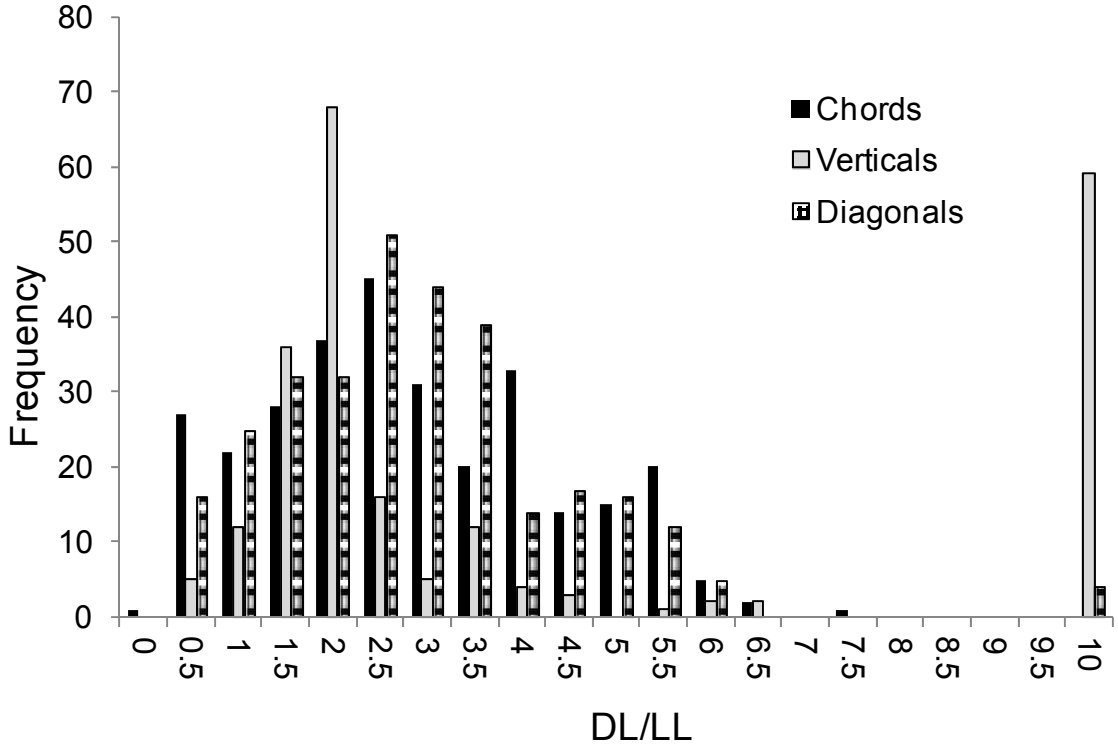

Figure 68. Dead-to-live load ratios for three member types.

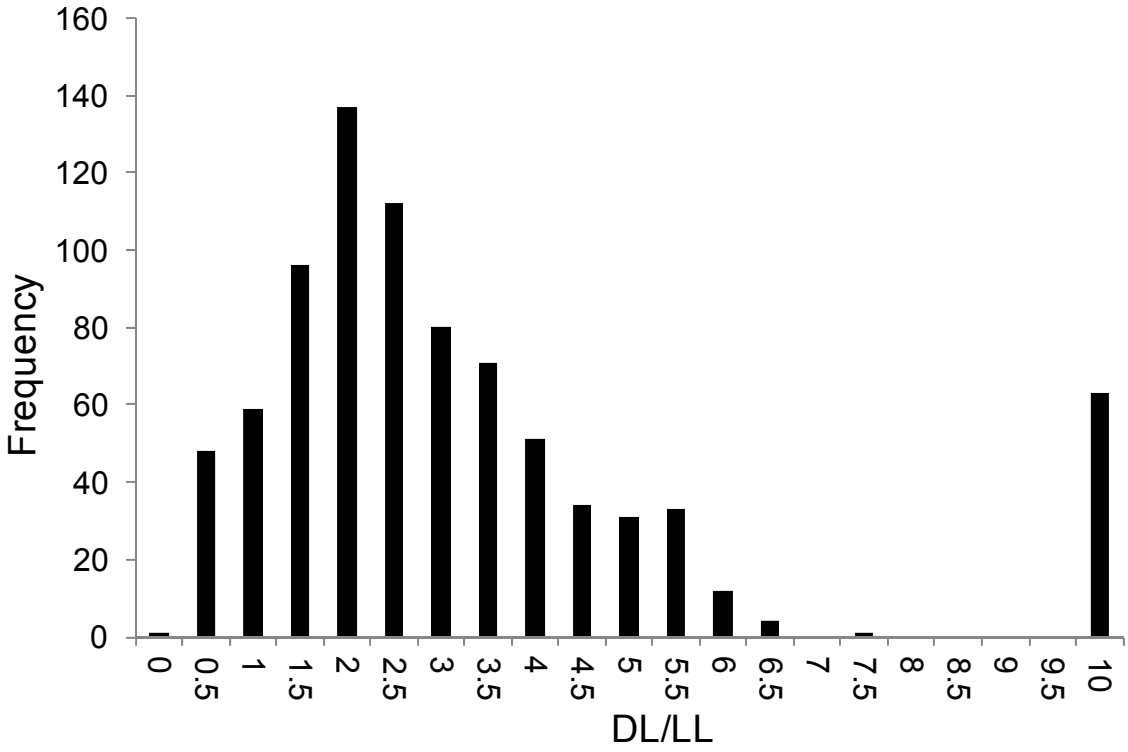

Figure 69. Dead-to-live load ratios for all members.

EXISTING FHWA GUIDE LEVEL OF RELIABILITY

The experimental and analytical failures described in Chapter 3 were analyzed using the FHWA Guide document to determine the existing level of reliability of gusseted connections. This exercise helps put prospective on the target level of reliability for the proposed new approach and its associated calibration of ϕ-factors. The existing levels of reliability were only evaluated for the limit-states of buckling, full plane shear yielding, and block shear. Since only three analytical connections failed in a tension member mode, there were not enough data to determine reliability statistics for tensile failure modes. The following section will describe the results for each failure mode.

Buckling Failure

There were 124 total observed pure buckling failures, neglecting the buckling failures of models with simulated corrosion, multi-layered plates, and edge stiffeners. To assess the reliability associated with the FHWA Guide, the models that failed must be compared to the predictions using the resistance equations from the FHWA Guide to define the professional factors for use in the Monte Carlo simulations. Examples of the professional factor variation using the FHWA Guide were shown in Figure 49, where K-factors of 1.2 and 0.50 are used, respectively.

The data sets had to be parsed into smaller subsets of λ_{avg} values to properly account for the linear trend in the data (more so when K=1.2). In each case, a running average was used to define the professional factor bias and COV at discrete values of λ_{avg}. Then for each set of statistics attained at each value of λ_{avg} a Monte Carlo simulation was run using the FHWA Guide limit-state equation and the existing ϕ=0.90. The result of all these simulations is shown in Figure 70 for the two K-factors (1.2 and 0.50) used in the evaluation.

What the plots in Figure 70 show is that the existing FHWA Guide limit-state equation produces a wide array of reliability indices varying from 0.75 to 5.0 depending on the value of λ_{avg}. The extreme linear variation shown in the reliability index is directly attributed to the widely ranging professional factors that were shown in Figure 49. With low values of λ_{avg} the professional factors are typically less than 1.0 leading to a low reliability index. However, when λ_{avg} >1.0 the professional factors are much greater than 1.0 leading to favorable and conservative reliability indices.

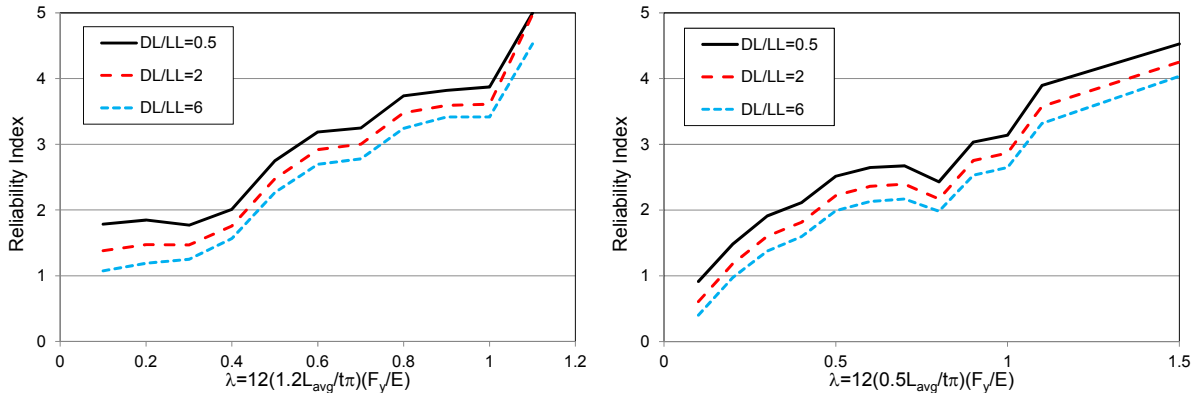

Figure 70. Existing level of reliability variation using ϕ_c=0.90 with respect to λ_{avg} and DL/LL ratio. (Left) K=1.2. (Right) K=0.50.

Shear Failure

The data presented in Chapter 3 showed that full plane shear yielding failures had average professional factors of 1.017 and a COV of 0.069 when Ω=1.00. When Ω=0.74, the average increases to 1.374 with no change in the COV. These two professional factor statistics were used in the Monte Carlo simulations to determine the reliability associated with the existing FHWA Guide resistance equation for shear yielding (using ϕ=0.95). The results from those simulations are shown in Table 33. When Ω=0.74, the reliability varies from 4.22 to 5 depending on the DL/LL ratio. Likewise, when Ω=1.00, the reliability index varies from 2.27 to 3.19.

Table 33 Shear Yielding Reliability Using Existing FHWA Guide

	Reliability Index, β						
DL/LL	0.5	1	2	3	4	6	8
Ω=0.74 ϕ=0.95 (μ=1.375, COV=0.064)	>5.00	4.97	4.55	4.75	4.43	4.27	4.22
Ω=1.00 ϕ=0.95 (μ=1.017, COV=0.064)	3.19	3.01	2.75	2.58	2.47	2.34	2.27

Block Shear

The FHWA Guide adopted the block shear equations out of the BDS 4th Edition.(57) However, the BDS 5th Edition (7) changed the block shear equations to be unified with the 13th Edition of the AISC Steel Construction Manual.(56) Therefore, the existing reliability will be calculated for the new block shear equations from the 5th Edition as this reflects the state-of-the-art. As described in Chapter 3, the professional factor average and coefficients of variation for these block shear equations are 1.180 and 0.060, respectively. These statistical values were used in the Monte Carlo simulations to show the existing level of reliability with ϕ=0.80. The variation of reliability index versus the DL/LL ratio is shown in Table 34. The existing level of reliability is between 4.37 and 5 depending on the DL/LL ratio.

Table 34 Block Shear Reliability Using Existing FHWA Guide

	Reliability Index, β						
DL/LL	0.5	1	2	3	4	6	8
ϕ=0.80 (μ=1.180, COV=0.060)	>5.00	4.97	5	4.97	4.48	4.50	4.37

Recommended Target Reliability Index

The existing level of reliability of the FHWA Guide for shear, buckling, and block shear is variable between 1.0 and 5.0 depending on the limit-state and the DL/LL ratio. Because of the wide range in the level of reliability, the FHWA Guide is not a precise indicator of the target reliability. Specifying reliability indices higher than 4.5 would be unnecessarily conservative.

It was beyond the scope of this research to perform a rigorous analysis of the existing level of reliability for truss structures for all applicable limit-states. Additional research may be desired to better grasp the reliability of truss systems and how it would interact with target reliability indices for use in ϕ-factor calibrations.

The BDS has been calibrated around a member-level reliability index of 3.5 using the Strength I load combination. This is also the same as the MBE Inventory Level, but the Operating Level has an implied reliability of 2.5. It would be wise to consider using a higher reliability index for connection-level limit-states as is done in AISC since AASHTO already provides a higher level of reliability for block shear and fastener limit-states (as they are adopted from AISC). AISC uses a member-level reliability of 2.8 for members and 4.0 for connection elements. Therefore, since AASHTO uses a member reliability of 3.5, bridge connection limit-states could have a reliability of 4.5. However, the higher level of reliability was mainly imposed on the connectors (bolts and welds), not for the other connection-specific failure modes (except for block shear).

Until further research can justify a different target reliability index, it is recommended for design that a target reliability index of 4.5 be selected. This decision is fairly inconsequential for design because it is easy to add plate thickness before a bridge is fabricated. However, in load rating, the plate thickness is predetermined and expensive retrofitting or load posting must be performed if the rating factors are less than favorable. The NCHRP panel conducted some spot checks using the design criteria for rating and determined that much of the existing inventory would not rate. While it may appear that a higher reliability index for rating is justified, the economics of posting every truss are not. Economics was not the only consideration in the decision; accepting a lower reliability index also meant acknowledging the long performance history of gusset plates with no problems (except I-35W) and the nebulous nature of various design specifications that have higher levels of reliability for "connections," though only enforced through fastener and weld limit-states. Therefore, a lower level of reliability for rating was justified. It is recommended that gusset plate limit-states in the MBE be calibrated at a reliability index of 3.5. This is also predicated on the notion that AASHTO mandate the use of the system factors for at least gusset plates, as currently system factors are considered optional.

SAMPLE ϕ-FACTOR EXPLANATION

Throughout the remainder of this chapter, plots such as those shown in Figure 71 will show the variation of the "calibrated" ϕ-factor versus the DL/LL ratio. The calibrations are performed using the AASHTO Strength I and IV load combinations. For the Strength IV load combination, there is a general increase in the required ϕ-factor as the DL/LL increases. It is difficult to describe exactly why this trend occurs because it is interrelated with the load factors and various bias and COV values. However, it must be recognized that in the Monte Carlo simulation the trial "design" (whether it is cross-sectional area, moment of inertia, etc.) is calculated based on the factored load combination using nominal values; however, the nominal loads are randomized based on their statistical properties to obtain real values. In particular for the Strength IV load combination, it may seem that there should be no variation in the ϕ-factor with the DL/LL ratio as that load combination only used dead load. But the factored load combination is only used to define a trial "design" value, yet the dead and live loads are still randomized in the simulation, hence why there is a variation in ϕ with DL/LL. Likewise, using the Strength I load combination, the calibrated ϕ-factor must decrease as the DL/LL ratio increases. This is a well-recognized trend that was noted in the first LRFD calibration of AASHTO. It has to do with the dead load

factor being smaller than the live load factor, forcing the trial design to become "lighter" as the live load diminishes and the simulation is affected more by the statistical distribution of the dead load rather than the resistance.

It is essential that users of this report are careful not to misinterpret why the ϕ-factors are being reported for both the Strength I and IV load combinations. *The plots to be shown throughout this chapter are not meant to represent a different set of ϕ-factors to use with each load combination (i.e., very small ϕ-factors should not be used with the Strength IV load combination, especially at small DL/LL ratios)*. The reason both curves are shown is that for all the limit-states the two curves tend to intersect at DL/LL ratio between 6.0 and 8.0. This notion can be used to justify reporting ϕ-factors at a DL/LL ratio of 6.0 because it represents the minimized ϕ-factor that works for both load combinations. The controlling ϕ-factor is illustrated as the black line in Figure 72 which in this instance is controlled by Strength I up to DL/LL=6 and controlled by Strength IV at higher DL/LL ratios.

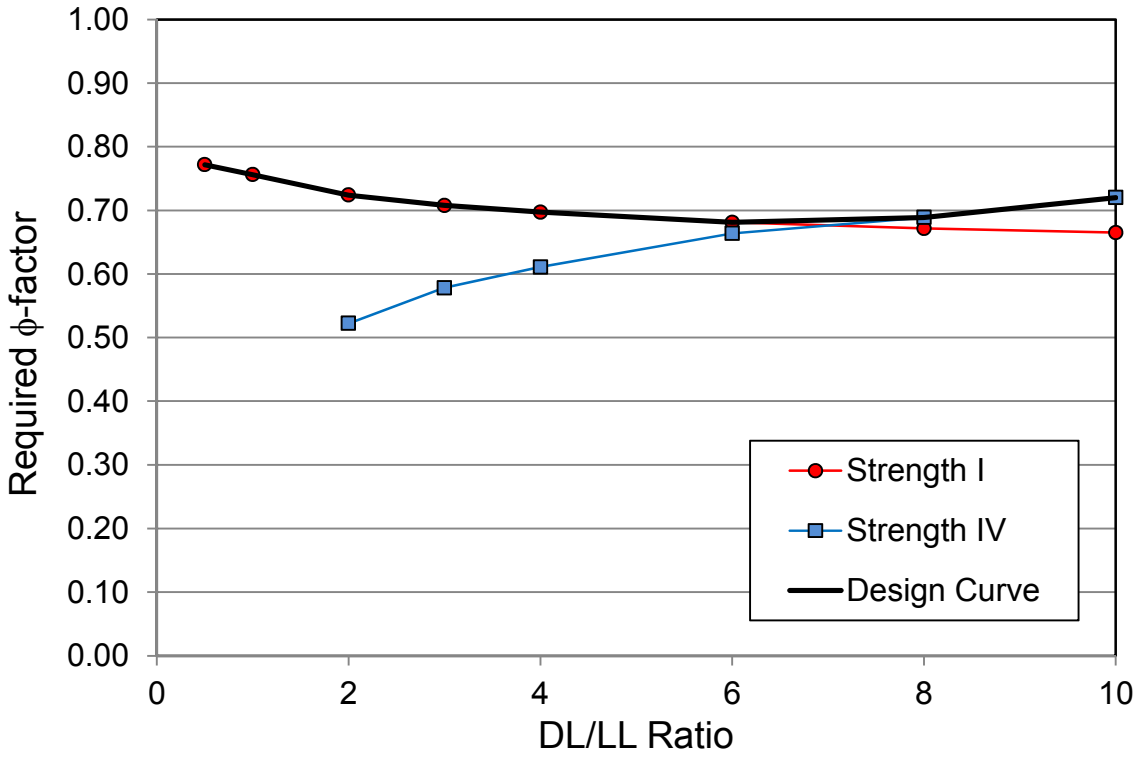

Figure 71. Sample ϕ-factor variation with DL/LL ratio.

SHEAR CALIBRATION

The professional factor for all the specimens and models that failed in shear had an average of 1.017 with a COV of 0.0649 just considering $0.58F_yA_g$ as the resistance equation. The statistics for plates thinner than 3/8 of an inch were the same. The result of the Monte Carlo calibration is

shown in Figure 72 that is presented in terms of the required ϕΩ-factor for DL/LL ratios varying from 0.5 to 6.0. Based only on the Strength I load combination, the combined ϕΩ-factor would have to range from 0.70 to 0.90 for both design and rating depending on the reliability index and DL/LL ratio.

Shear Rupture

No shear rupture was observed in the experimental testing and the analytical models did not have the fidelity to capture such a limit-state. Therefore, no changes to the shear rupture resistance equation used in the FHWA Guide can be derived from this research.

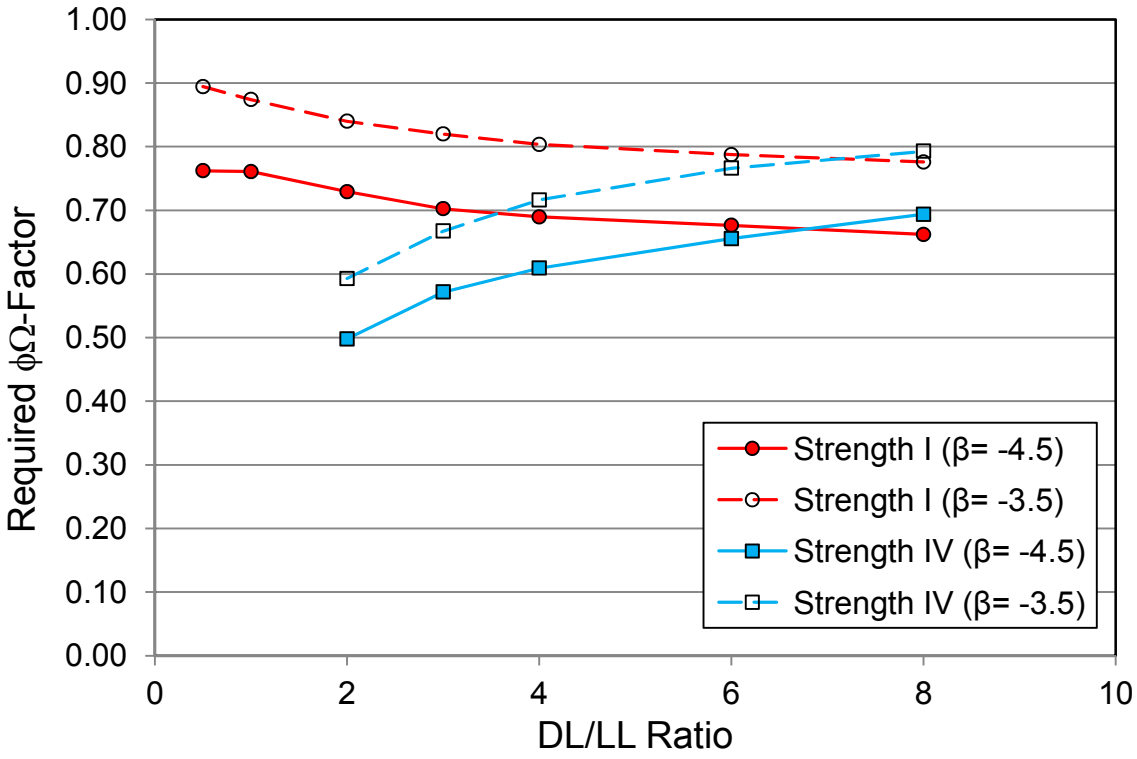

Figure 72. Plot of required ϕΩ-factor to attain target reliability at various DL/LL ratios.

BUCKLING CALIBRATION

In Chapter 3, data were presented for all 124 specimens and models that failed by buckling; this is summarized in Tables 14 through 18. This calibration is for the new method of evaluation that uses a fixed K-value of 0.5 and L_{mid}. Of these 124 failures, only 62 were controlled by the Whitmore buckling criterion; the remaining were controlled by partial plane shear yielding. In looking at the plot of professional factors in Figure 53, there is a general increase in the professional factor as the λ_{mid} value also increases. The column curve is controlled by two functions demarcated at λ_{mid}=2.25. The critical case is for λ_{mid}<2.25 because those are the professional factors nearest to 1.0. The professional factors of buckling failures predicted by

Whitmore and λ_{mid}<2.25 had an average of 1.24 and COV of 0.127. The derived ϕ-factor would be conservative for cases where λ_{mid}>2.25 as the professional factors are much higher than 1.0. A plot of the required ϕ-factors for rating and design versus the DL/LL ratio is shown in Figure 73 and 74 for both load combinations and reliability indices. The required ϕ-factor was found to vary from 0.96 to 1.00 depending on the target reliability index and DL/LL ratio.

Since the buckling resistance relies on both the Whitmore buckling and partial plane shear yielding criteria, the partial plane shear yield also has to be calibrated. A plot of the required ϕ-factors for rating and design versus the DL/LL ratio is shown in Figures 75 and 76 for both load combinations and reliability indices. The required ϕ-factor was found to vary between 0.60 and 0.95 depending on the target reliability index and DL/LL ratio. Since the partial plane shear requirement is a shear-initiated limit-state, this ϕ-factor should be unified with the full plane shear yielding $\phi\Omega$ term calibrated from the full plane shear yielding presented in the prior section. The two calibrations are similar; perhaps a $\phi\Omega$ should be carefully selected to satisfy both full and partial plane check such that special provisions do not have to be written for partial shear plane checks.

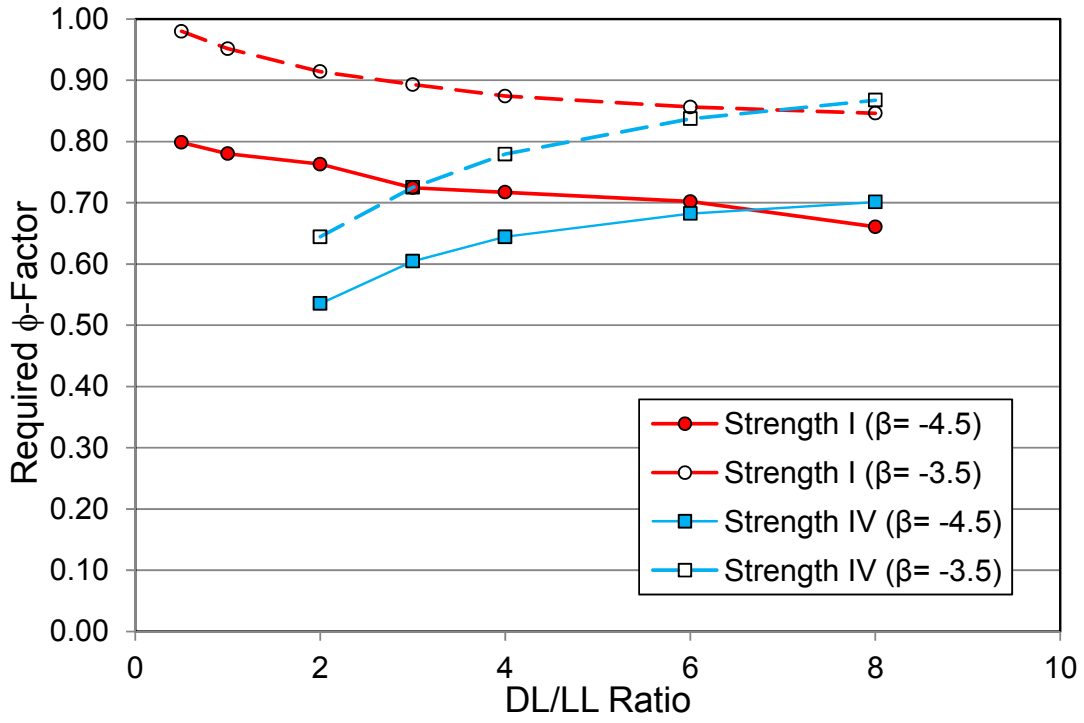

Figure 73. Required ϕ-factor for Whitmore compression resistance considering all data, to be used in rating.

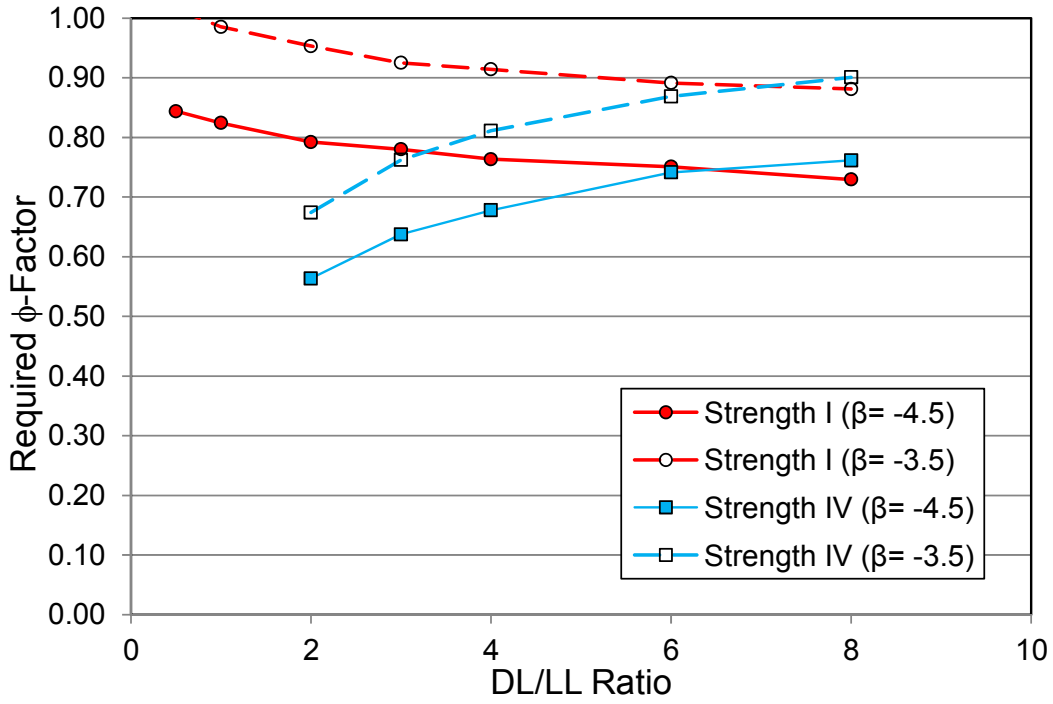

Figure 74. Required ϕ-factor for Whitmore compression resistance neglecting plates thinner than 0.375 inches for use in design.

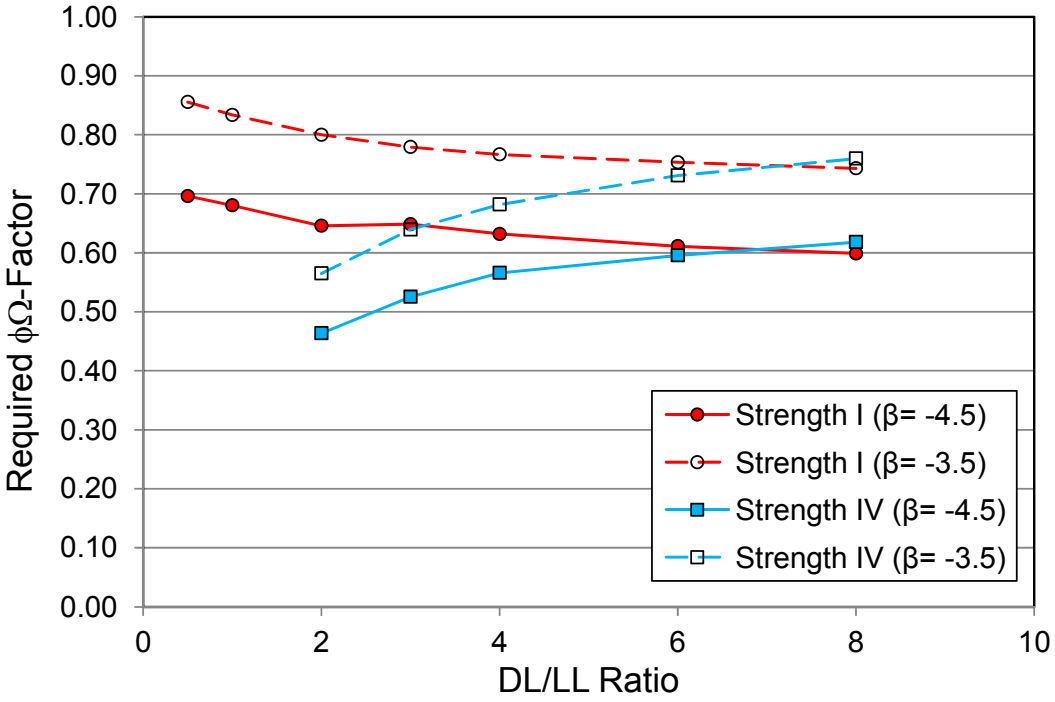

Figure 75. Required ϕ-factor for partial shear plane yielding considering all data, to be used in rating.

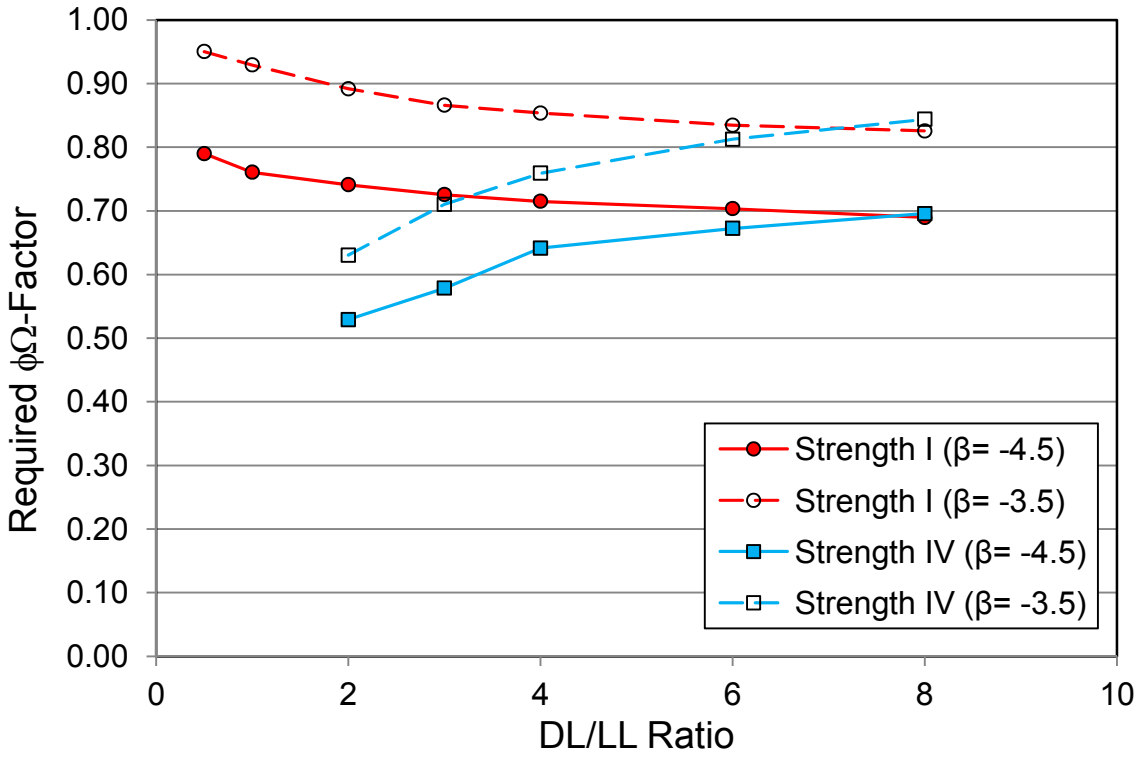

Figure 76. Required ϕ-factor for partial shear plane yielding neglecting plates thinner than 0.375 inches for use in design.

TENSION CALIBRATION

Unfortunately, throughout the NCHRP 12-84 project, no tension failures were observed in the experimental program. In addition, there were only three models in the parametric study that failed around a tension member. With so little data, no firm conclusions could be drawn to refine or refute the existing FHWA Guide and no changes are recommended for the Whitmore gross and net section resistance equations around tension members.

However, the available literature does contain relevant data for a calibration of block shear and the professional factor data had an average of 1.18 and COV of 0.060. Figure 77 shows the required ϕ-factor versus the DL/LL ratio. The required resistance factor was found to vary from 0.80 to 1.00 depending on the target reliability index and the DL/LL ratio.

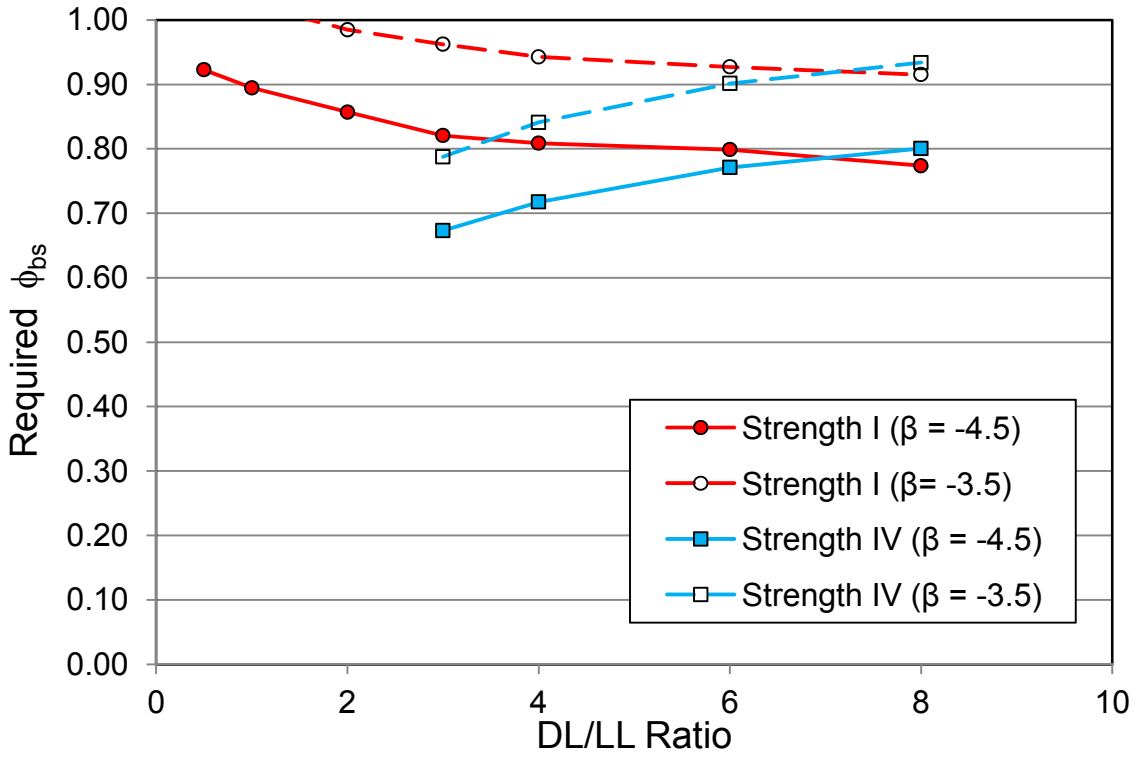

Figure 77. Plot of required ϕ-factor for block shear.

CHORD SPLICES

The procedure for evaluating chord splices presented in Chapter 3 produced two sets of professional factor statistics considering all the data (rating), and neglecting data from plates thinner than 3/8 inch thick (design). These statistics were derived from 33 failures of both tension and compression chord splice failures noted in the analytical studies. Figures 78 and 79 present the results of the Monte Carlo simulations in terms of the required φ-factor for various DL/LL ratios, for both the rating and design specifications respectively. The required φ-factor ranges from 0.60 to 0.92 depending on the reliability index and DL/LL ratio.

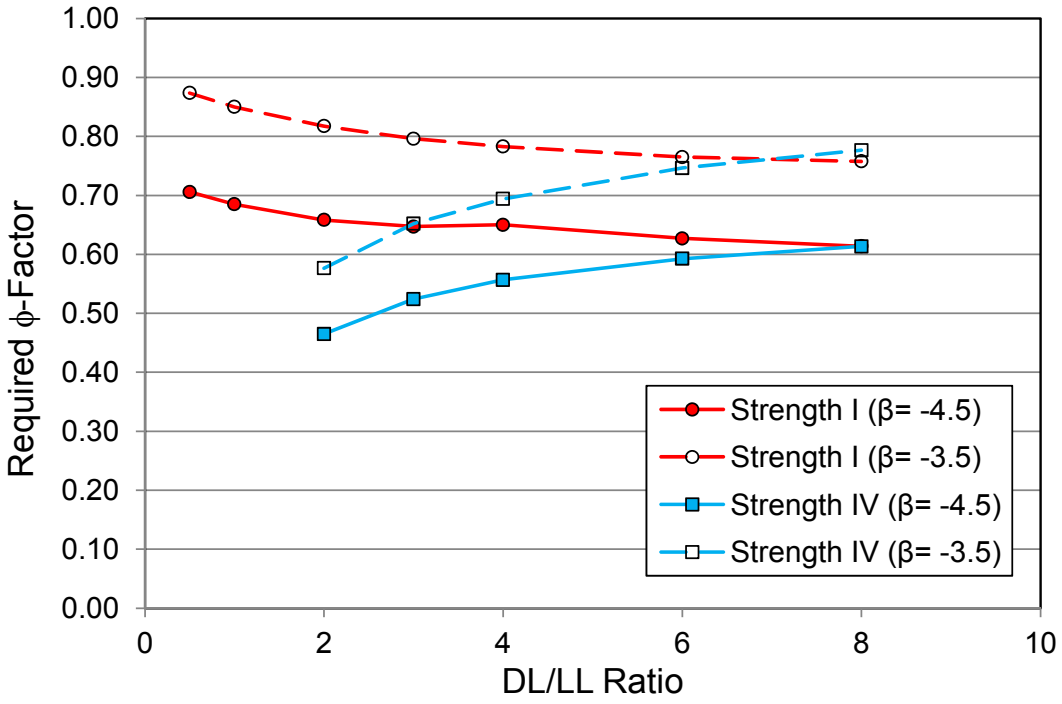

Figure 78. Required ϕ-factor for chord splices considering all data, for use in rating.

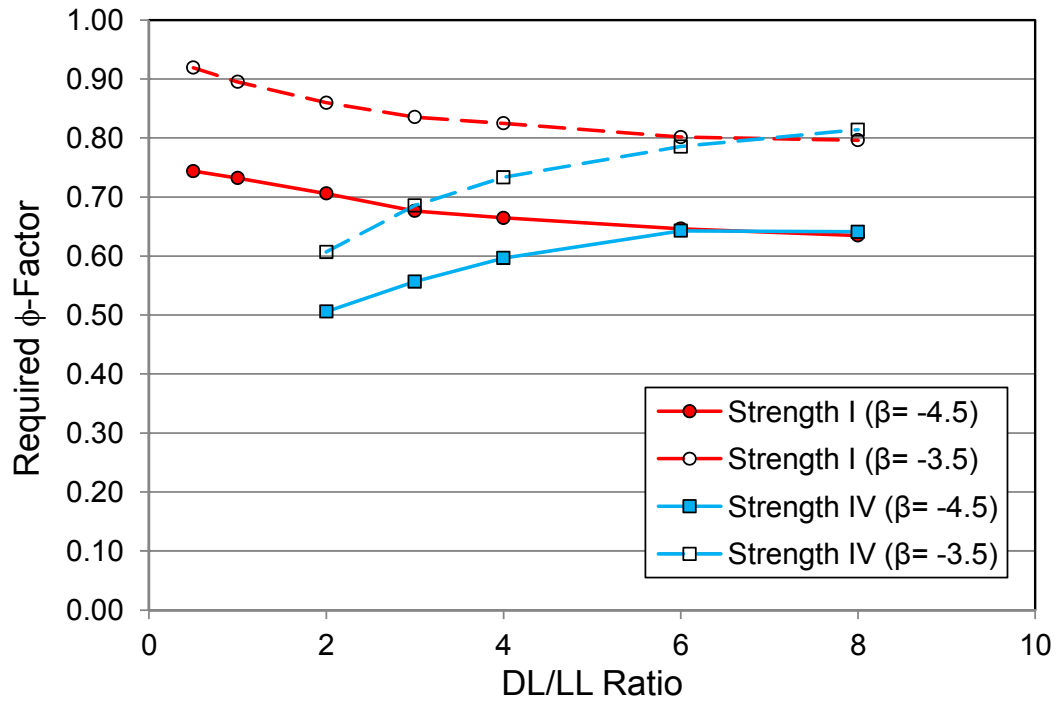

Figure 79. Required ϕ-factor for chord splices neglecting plates thinner than 0.375 inches, for use in design.

RIVET SHEAR CALIBRATION

In Chapter 3, Equation 11 defines a generalized fastener resistance equation. The assumed values of the shear-to-tensile ratio and rivet stock tensile strength were presented along with the average, bias, and COV from test data found in the available literature. The rivets were segregated into three different strength levels and a ϕ-factor calibration needed to be performed for each of them. It was also shown that the connection length reduction factor also has a role and it is assumed that the nominal reduction will be 0.90. Provided both of the Tide inequalities are satisfied, then the bias and COV of the connection length reduction factor is 1.035 and 0.077, respectively. However, the statistics for the connection length effect are different if both Tide criteria fail where the bias and COV are 1.002 and 0.103, respectively. The statistics assuming both Tide criteria fail were used in the rivet calibration because those are less favorable from a calibration standpoint and represent the lower bound. Therefore, resistance factors will be conservative for connections that meet one or both of the Tide criteria.

Figures 80 through 82 outline the required ϕ-factor for the three rivet strength levels. As expected, there is not one all-encompassing ϕ-factor to describe all rivets without unnecessarily penalizing one of the strength levels. The required ϕ-factor ranged from 0.50 to 0.80 depending on grade, target reliability index, and DL/LL ratio.

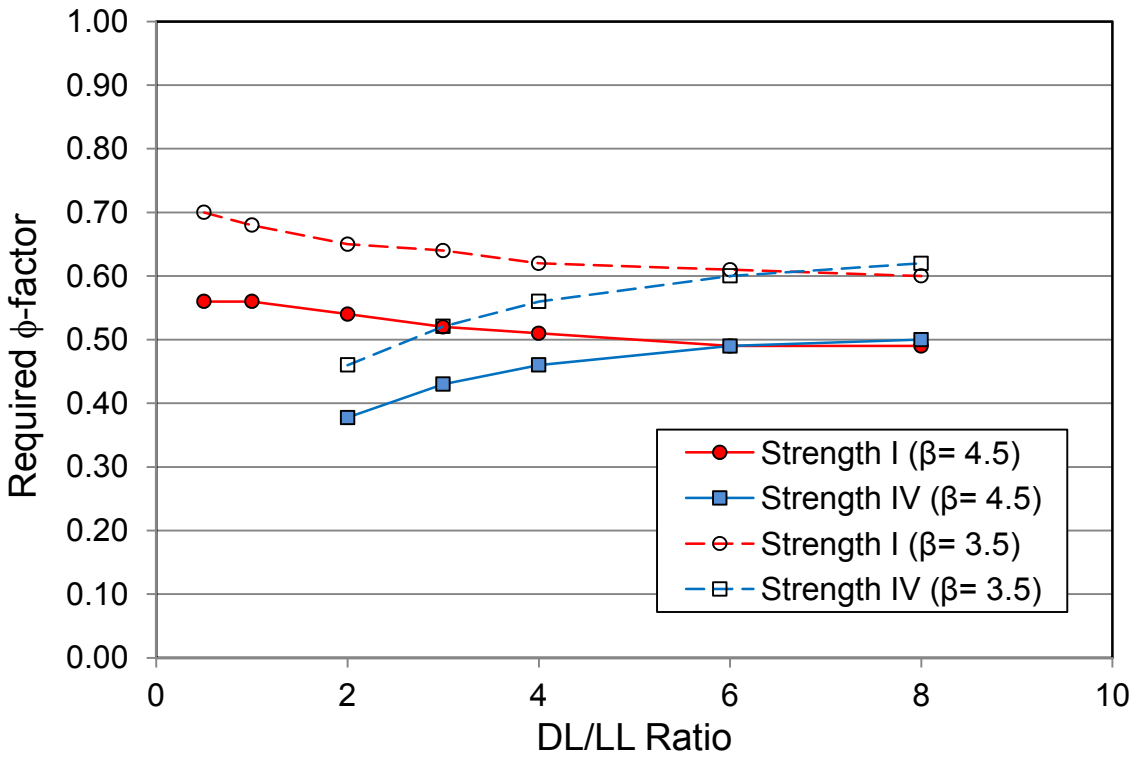

Figure 80. Required ϕ-factor for rivets of unknown origin.

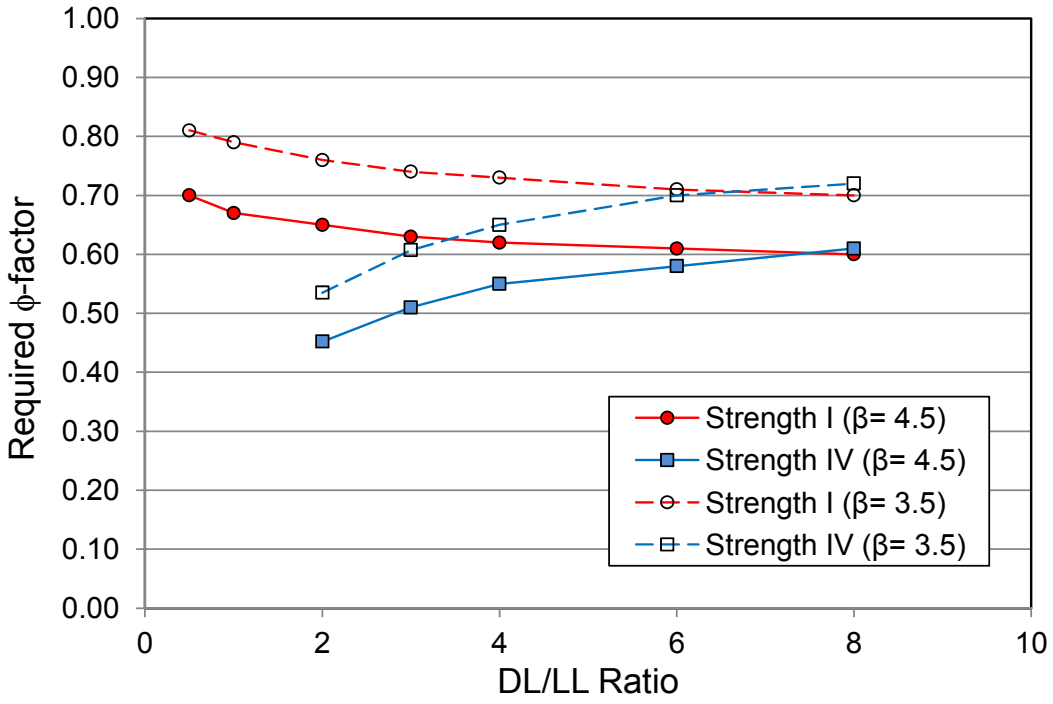

Figure 81. Required ϕ-factor for A141 or A502 Grade 1 rivets.

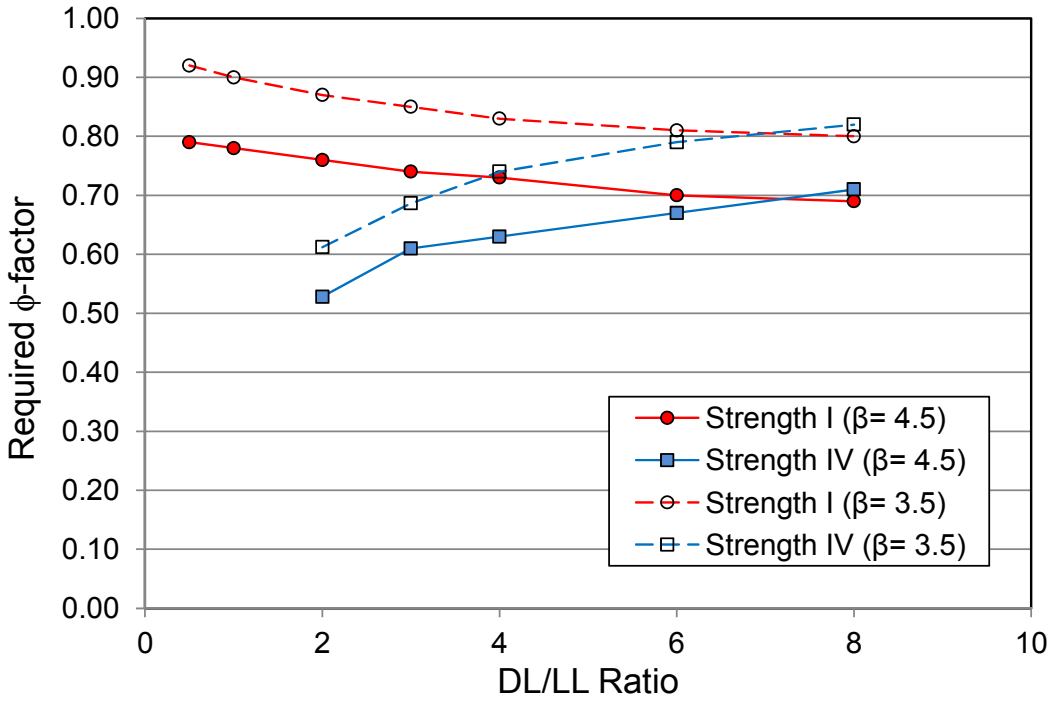

Figure 82. Required ϕ-factor for A195 or A502 Grade 2 rivets.

ANALYSIS FACTOR CALIBRATION

The various resistance equations have been calibrated based on experimental and analytical failure results from a variety of connection geometries. As such, "one size fits all" resistance equations were defined and calibrated and they may produce conservative results for some connection geometries. Therefore, AASHTO may wish to consider allowing for higher level analysis to determine the resistance of some connections in lieu of using the simplified resistance equations. This would require detailed finite element modeling of connections using the modeling philosophy in Chapter 2, and could be helpful in determining more accurate shear or buckling resistance of some connections which have unfavorable ratings using the simplified resistance equations.

When performing an LRFD analysis of a refined connection model, the variability of the loads, material factors, and fabrication factors are not taken into account. Therefore, the failure loads attained from the model must be factored to account for these unknowns that cannot be explicitly accounted for in the model. A special resistance factor for use with simulation analysis must be derived and to do this a Monte Carlo analysis is run considering a professional factor average of 1.00 and COV of 0.00. This assumes the model failure prediction is perfect and the analysis factor only accounts for the uncertainty in the load, material, and fabrication models. The results of the Monte Carlo simulations are shown in Figure 83 for various DL/LL factors. The required analysis factor was found to vary from 0.70 to 0.95 depending on the target reliability and DL/LL ratio.

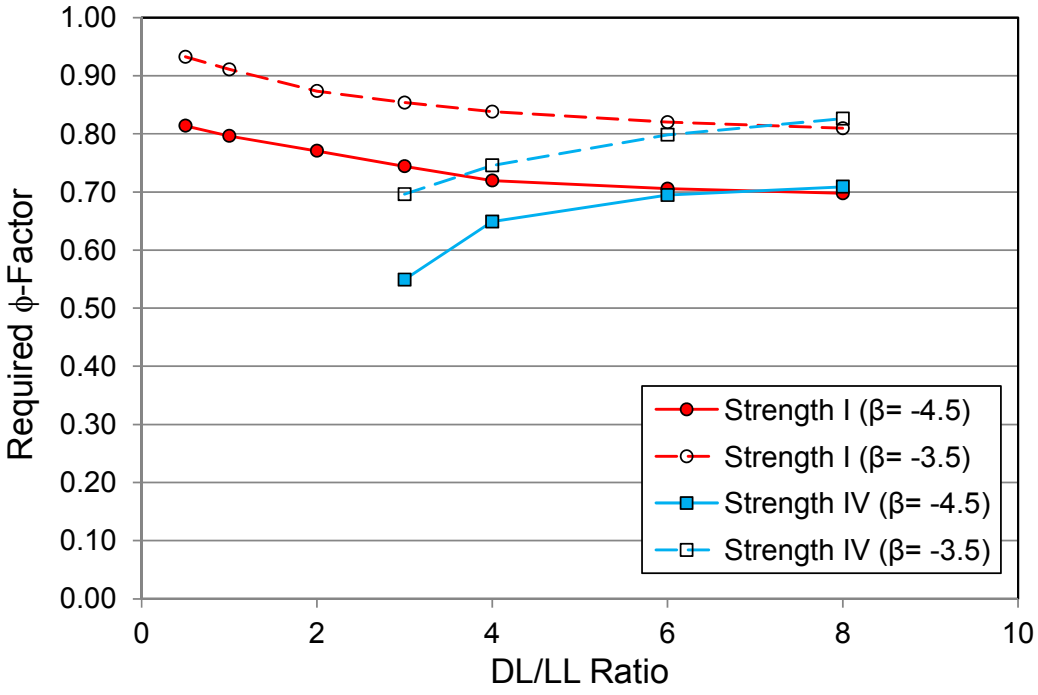

Figure 83. Plot of required analysis factor.

SUMMARY OF RESISTANCE FACTORS

This project was able to provide six resistance equations calibrated to a LRFD/LRFR philosophy. An additional calibrated analysis factor is also provided to demonstrate how the variability associated with refined analysis may be integrated into a LRFD/LRFR philosophy. It was beyond the scope of this project to determine the target reliability index associated with gusset plates, primarily for lack of data. As such, the calibrations were performed at two levels of reliability of 3.5 and 4.5, where it is optimal that design use a reliability index of 4.5 and rating use a reliability of 3.5.

Table 35 outlines the associated ϕ-factors for each resistance equation, at both reliability indices and four different DL/LL ratios. The ϕ-factors presented in the table are exact to attain the desired reliability index, though for implementation in design and rating specifications they should be rounded to the nearest 0.05 as shown in Table 36.

Since the ϕ-factor has a dependency on the DL/LL ratio, a decision had to be made about where to select the ϕ-factor. For the purposes of design, the ϕ-factors were selected at a DL/LL ratio of 6.0. This would provide ϕ-factors that are always conservative in all situations despite the span length of the truss, because in design it may be difficult to estimate the DL/LL ratio. However, for load rating the loads are known and a variable ϕ-factor may be used to account for the variation with the DL/LL ratio. For rating, the ϕ-factors were selected at DL/LL ratio of 1.0. The following section will describe the reasons behind this.

Reliability at Manual for Bridge Evaluation (MBE) Operating Level

The National Bridge Inspection Standards require bridge ratings be reported at the Strength I Inventory and Operating Levels. In LRFR the only differences between the two are the live load factors which should provide a reliability index of 3.5 at the Inventory level, and 2.5 at the Operating level. Since the ϕ-factor calibrations were performed using the BDS Strength I (and hence to MBE Inventory Level too), those ϕ-factors should be checked to ensure they provide a 1.0 decrease in the reliability index with the 1.35 MBE Operating level live load factor.

The results of the simulations that performed this are reported in Table 37. These simulations used the exact ϕ-factors derived at a reliability index of 3.5 but assessed the reliability using the MBE Operating load combination. It would be expected that the reliability index would be approximately 2.5 to reflect the 1.0 decrease in reliability using the lower live load factor. In fact, this assumption of the MBE is extremely sensitive to the DL/LL ratio. It can be seen that there is little change in reliability between the Inventory and Operating levels at the high DL/LL ratio of 6.0. However, for many of the limit-states, a DL/LL ratio of 0.5 produces reliabilities less than expected. It would appear that to maintain consistency of the MBE assumption of Inventory and Operating level reliability, ϕ-factors should be selected at a DL/LL of approximately 1.0. However, to ensure long-span trusses are also properly rated, an additional reduction factor should be prescribed to account for the decrease in the ϕ-factor for trusses with DL/LL ratios

greater than 1.0. By inspection of ϕ-factors in Table 35 it can be seen that for all the limit-states, there is approximately a 0.90 reduction of the resistance factor at DL/LL=1.0 to the resistance factor at DL/LL=6.0. Inspection of all the graphs shown in Figures 72 through 83 show that a linear approximation would be prudent in this region and it is recommended that for rating a variable ϕ-factor reduction be applied when the DL/LL is between 1.0 and 6.0.

Again, it is difficult to explain why there is sensitivity to the DL/LL ratio, but the reason is the same as the explanation of why ϕ-factors vary with the DL/LL ratio. As the DL/LL ratio increases, the trial design becomes lighter due to the diminishing influence of the live load factor. Therefore, the variability in the loading decreases since the live load has a higher bias and COV, hence a lower change in the reliability index.

Ω-Factor for Shear Yielding Limit-State

In an earlier discussion on shear yielding, the resistance factor was coupled with the Ω-factor. One option was to use the use the existing ϕ_y=1.00 that AASHTO uses for shear and use the Ω-factor to provide the required reliability. However, this leads to the conundrum in the MBE that there would then be a variable definition of the Ω-factor to account for the DL/LL variation, which could distort the meaning of Ω. Therefore, a fixed value of the Ω-factor should be selected and new gusset plate shear yielding ϕ-factors should be defined for both design and rating. On average Ω was 1.02 and it would be logical to select Ω=1.00 as the factor, though specifying a factor to be 1.00 serves no purpose, whereas the point of specifying an Ω-factor is to make a distinction that shear yielding in gusset plates is different than in beams. As such, Ω was selected to be 0.88 because this would lead to gusset shear yielding resistance factors in design and rating that would be nearly rounded to the nearest 0.05. For instance, in Table 36 the combined design and rating shear yielding resistance factors (ϕΩ) were 0.70 and 0.85 respectively. Considering the fixed value of Ω=0.88 leads to the shear yielding resistance factors of 0.80 and 1.00 respectively for design and rating.

Rivets

Since the current 2011 MBE Interim specifying rivet strength lists the factored shear strengths, a similar approach is recommended so each rivet type can be assigned its own ϕ-factor. Table 38 lists the factored shear resistance (ϕV_n) for each of the rivet strengths at a reliability level of 4.5 and a DL/LL ratio of 1.0. It was described earlier in this chapter that other design codes specify higher reliability for connection limit-states, though they do this by imposing higher reliability on the connectors, such as the rivets. For this reason, the recommended factored shear strength of rivets is reported at the higher reliability of 4.5 and this aligns with the current calibration of high-strength bolts.[58] Two factored shear strength values are presented considering the two different connection length factors discussed in Chapter 3.

Also shown in Table 38 are the factored rivet shear values from the FHWA Guide, and those from the 2011 MBE Interims. Both use a different approach to account for the connection length

effect than is done with the Tide approach presented in the previous chapter. Therefore, the comparison of all the factored shear strengths in this table must be made carefully. For instance, the new values passing the Tide criteria are best compared to those in the 2011 MBE Interims with no length reduction. Likewise, the new value failing both Tide criteria is best compared with the 2011 MBE Interims with a full length reduction.

What the results in the table show are that the current approach used in the 2011 MBE Interims is adequate. The new calibrated values are lower for unknown rivets, about the same for the A141/A502 Gr. 1 rivets, and much stronger for the A195/A502 Gr.2 rivets. However, this statement must be qualified. The data used to define the strength statistics for unknown rivets may be biased as that came from research reports from the same institution over a short period of time and it was unclear how many lots of rivets they encompassed. Likewise, most of the data for A195/A502 Gr. 2 rivets were from one source and do not give an indication of the true variation possible. The strength data for the A141/A502 Gr. 1 rivets were taken from a broad variety of sources and encompassed a large period of time; therefore, that is probably the most reliable data to compare to.

Since the new approach and that published in the 2011 MBE Interims is nearly the same for the A141/A502 Gr.1 rivets, and the change to the Tide criteria would be unprecedented, no change of rivets shear strengths could be recommended. If further strength data could be uncovered for unknown and A195/A502 Gr. 2 rivets to buttress the statistical variations, then this topic could be revisited.

Table 35 Summary of Exact Resistance Factors

Reliability Index		β= 4.5				β= 3.5			
DL/LL ratio		0.5	1.0	2.0	6.0	0.5	1.0	2.0	6.0
Full Plane Shear Yielding ($\phi\Omega$)		0.76	0.76	0.73	0.68	0.89	0.87	0.84	0.79
Buckling	Whitmore Buckling (all data considered)	0.80	0.78	0.76	0.70	0.98	0.95	0.91	0.86
	Whitmore Buckling (neglecting plates thinner than 0.375 inch)	0.84	0.82	0.79	0.75	1.02	0.99	0.95	0.89
	Partial Plane Shear (all data considered)	0.70	0.68	0.65	0.61	0.86	0.83	0.80	0.75
	Partial Plane Shear (neglecting plates thinner than 0.375 inch)	0.79	0.76	0.74	0.70	0.95	0.93	0.89	0.83
Block Shear		0.92	0.89	0.86	0.80		1.02	0.98	0.93
Chord Splice (all data considered)		0.71	0.68	0.66	0.63	0.87	0.85	0.82	0.77
Chord Splice (neglecting plates thinner than 0.375 inch)		0.74	0.73	0.71	0.65	0.92	0.90	0.86	0.80
Rivet Shear	Unknown Origin	0.56	0.56	0.54	0.49	0.70	0.68	0.65	0.61
	A141/A502 Gr. 1	0.70	0.67	0.65	0.61	0.81	0.79	0.76	0.71
	A195/A502 Gr. 2	0.79	0.78	0.76	0.70	0.92	0.90	0.87	0.81
Simulation Analysis		0.81	0.80	0.77	0.71	0.93	0.91	0.87	0.82

Table 36 Summary of Resistance Factors Rounded to Nearest 0.05.

Reliability Index		β= 4.5				β= 3.5			
DL/LL ratio		0.5	1.0	2.0	6.0	0.5	1.0	2.0	6.0
Full Plane Shear Yielding (ϕΩ)		0.75	0.75	0.75	0.70	0.90	0.85	0.85	0.80
Buckling	Whitmore Buckling (all data considered)					1.00	0.95	0.90	0.85
	Whitmore Buckling (neglecting plates thinner than 0.375 inch)	0.85	0.80	0.80	0.75				
	Partial Plane Shear (all data considered)					0.85	0.85	0.80	0.75
	Partial Plane Shear (neglecting plates thinner than 0.375 inch)	0.80	0.75	0.75	0.70				
Block Shear		0.90	0.90	0.85	0.80		1.00	1.00	0.95
Chord Splice (all data considered)						0.85	0.85	0.80	0.75
Chord Splice (neglecting plates thinner than 0.375 inch)		0.75	0.75	0.70	0.65				
Rivet Shear	Unknown Origin	0.55	0.55	0.55	0.50	0.70	0.70	0.65	0.60
	A141/A502 Gr. 1	0.70	0.65	0.65	0.60	0.80	0.80	0.75	0.70
	A195/A502 Gr. 2	0.80	0.80	0.75	0.70	0.90	0.90	0.85	0.80
Simulation Analysis		0.80	0.80	0.75	0.70	0.95	0.90	0.85	0.80

Table 37 Associated Reliability Indices for MBE Operating Level Rating with ϕ-Factors Derived at a Reliability Index of 3.5

DL/LL ratio	0.5	2.0	6.0
Full Plane Shear Yielding	2.39	2.86	3.19
Whitmore Buckling	3.19	3.65	3.90
Partial Plane Shear Yielding	2.58	3.01	3.28
Block Shear		2.83	3.18
Chord Splice	2.67	3.01	3.27
Unknown Rivet Shear	2.60	3.03	3.30
A141/A502 Gr. 1 Rivet Shear	2.44	2.91	3.27
A195/A502 Gr. 2 Rivet Shear	2.31	2.79	3.21
Analysis Factor	2.14	2.67	3.00
Expected Value	***2.5***		

Table 38 Recommended LRFR Rivet Shear Strengths

Reliability Index	Rivet Type	Unknown Origin (F_u=50 ksi)	A141 or A502 Gr. 1 (F_u=60 ksi)	A195 or A502 Gr. 2 (F_u=80 ksi)
β= 4.5 (DL/LL=1.0)	ϕ-factor [a]	0.56	0.67	0.78
	(fails both criteria) ϕV_n (ksi) [b]	16	23	37
	(otherwise) ϕV_n (ksi) [c]	21	30	47
	FHWA Guide (ksi)	18	27	32
	2011 MBE Interims (ksi) (*with full length reduction*)	20	24	32
	2011 MBE Interims (ksi) (*no length reduction*)	27	32	43

[a] – Should be reduced for DL/LL ratios greater than 1.0. The additional reduction decreases linearly from 1.00 to 0.90 as the DL/LL ratio changes from 1.0 to 6.0. The additional reduction shall not be less than 0.90.

[b] – This aggregate term assumes $0.85F_u$ multiplied by an implied 0.70 connection length reduction factor considering both Tide criteria fail. It also does not consider additional reduction from the presence of filler plates.

[c] -This aggregate term assumes $0.85F_u$ multiplied by an implied 0.90 connection length reduction factor considering one or both Tide criteria are met. It also does not consider additional reduction from the presence of filler plates.

CHAPTER 5. CONCLUSIONS AND RECOMMENDATIONS

This research project primarily consisted of the experimental testing of 12 full-scale gusset plate connections. These 12 connections were used to investigate shear and buckling limit-states, as well as to consider the effects of simulated section loss, multi-layered gusset plates, and edge stiffening. The experimental matrix was limited to a single geometry: a five member connection with collinear chords, two diagonals entering into the connection at 45 degrees to the chords, and one vertical entering the connection perpendicular to the chords. However, to account for the variety of connection geometries and load combinations found in the bridge inventory, a finite element parametric study was used to appropriately extend the experimental results. A robust finite element modeling methodology was established by comparing the finite element simulations to the experimental results. These comparisons established high confidence in both the modeling method used and the interpretation of the simulations, ensuring that the 201 connections modeled as part of the analytical parametric study produced trustworthy results.

To draw conclusions, the results of both the experimental and analytical studies were grouped by failure mode to establish professional factors that could be used in an LRFD/LRFR calibration of predictive resistance equations. Also, because bridge owners have relied on the FHWA Guide to load rate gusset plates in response to the recommendations made in Technical Advisory T 5140.29, *Load-carrying Capacity Considerations of Gusset Plates in Non-load-path-redundant Steel Truss Bridges*, an attempt was made to maintain the existing predictive resistance equations of the FHWA Guide during this research. The following list of observations and recommendations highlights the major findings of this project.

1. It was recognized that the influence of the developed resistance equations on the design of new gusset plates would be minimal, at most requiring thicker gusset plates. The largest implications of the developed resistance equations would be in the rating of the existing inventory where repair and retrofitting is difficult. In keeping within the scope of the project, this research only focused on an LRFD/LRFR philosophy.

2. The limit-states for design were calibrated to a target reliability index of 4.5, and ϕ-factors were selected at a DL/LL of 6.0. For rating, a lower target reliability index of 3.5 was deemed tolerable, and ϕ-factors were selected at a DL/LL ratio of 1.0. The justification of using a lower reliability index for rating is predicated on AASHTO mandating the use of system factors in rating gusset plates, where currently they are considered optional. In addition, the resistance factors must be further reduced for only rating provided the DL/LL ratio is greater than 1.0. The additional reduction decreases linearly from 1.00 to a minimum of 0.90 as the DL/LL ratio changes from 1.0 to 6.0.

3. A minimum plate thickness for use in the design of new gusset plates is recommended. This research found that plates thinner than 0.375 inches contributed greatly to the scatter of some limit-states, particularly gusset plate buckling. The selected ϕ-factors for design

assume this limit is adopted. If not adopted by AASHTO, some ϕ-factors may have to be reduced for design. A minimum plate thickness limit is not needed for rating, though the recommended ϕ-factors for rating account for the greater scatter associated with plates thinner than 0.375 inches thick. For this reason, owners who are trying to prioritize rating their gusset plate inventory should consider focusing on those gusset plates 0.375 inches thick or thinner.

4. The general formulation of shear yielding, $0.58F_yA_g$, used in LRFD and the FHWA Guide was proven to be appropriate. On average the Ω-factor was found to be 1.02, though a fixed value of 0.88 is assumed for both design and rating. A new ϕ-factor for gusset plate shear yielding is recommended for both the BDS and MBE. This ϕ-factor would be 0.80 for design and 1.00 for rating.

5. The current definition of Ω needs to change, though this only applies to the existing FHWA Guide where it is used. It was found that gusset plates would plastify through the shear plane at the shear yielding limit-state. As a result, the present correlation of Ω to a bending shear distribution was found to be weak as it has a much stronger association with a uniform shear distribution.

6. No data were specifically collected that either supported or questioned the formulation of the shear fracture resistance equation. However, in the seven experimental tests that resulted in shear failures, there were no shear fractures and two of the seven exceeded the predicted shear fracture strength before yielding in shear. Therefore, there is no recommendation to change this limit-state from what is published in the FHWA Guide.

7. Evaluating the capacity of gusset plate shear planes that pass over connected members was found to be inappropriate. Close inspection of the stress contours evaluated for each simulation revealed that yielding along gusset plate shear planes that also passed over a chord was dominated by shear away from the chord and by normal stress due to splice action near the chord. Therefore, shear yielding and fracture resistance equations need only be evaluated on shear planes that can mobilize without interacting with a connected member. While it was recognized that a plane cannot mobilize when it passes over a member, it is speculated that a shear plane could mobilize through the chord splice provided it is only lightly reinforced with alternate splice plates, although no evidence of this possibility developed during the research.

8. The existing Whitmore buckling resistance used in the FHWA Guide produces highly variable resistance predictions, especially based on the assumed effective column length factor (i.e., K-factor). A better prediction of buckling was found with a fixed value of K=0.5 used in combination with L_{mid} rather than L_{avg} used in the FHWA Guide. The calibrated ϕ-factor for the Whitmore buckling check was found to be 0.75 for design and 0.85 for rating. For compact connections where the members are clustered close together, Whitmore buckling was found to be a poor predictor of buckling resistance. Instead, the

research showed that the load determined to cause a partial shear plane to yield was also a much better predictor of buckling.

9. Although it may seem odd to use a shear formulation to predict buckling, the research showed that once a partial shear plane in the gusset plate along a compression member yields, its elastic modulus decreases and thus reduces the out-of-plane rotational restraint the plate can provide to the idealized column. The factored resistance formulation described in Recommendation #4 applied to the partial shear plane was sufficient to predict this effect; different ϕ-factors are not needed for the partial plane shear yielding criteria.

10. The proposed two-folded approach to buckling may find gusset plates will have a reduction in rating values for compression resistance despite the FHWA Guide producing favorable ratings. In particular, the Whitmore buckling criteria overestimates buckling strength of compact joints and the partial shear yielding check will control and produce lower resistances. The connections most susceptible are those with prior λ_{avg} values less than 1.0 using the FHWA Guide. On the contrary, the Whitmore buckling criteria in the FHWA Guide, especially assuming K=1.2, produced overly conservative resistance predictions when λ_{avg} was greater than 1.5. The new approach with a fixed K=0.5 and using L_{mid} will predict higher resistance for these joints. In the transition region between $1.0< \lambda_{avg} <1.5$ it could go either way.

11. Only three analytical simulations produced tension failures and none of the experimental specimens experienced tensile failures. Therefore, there was insufficient data to either support or question the Whitmore gross and net section checks for tension members used in the FHWA Guide. As a result, it is recommended to keep these existing resistance equations and associated ϕ-factors.

12. A calibrated ϕ-factor is presented for block shear based on the current block shear equations included in the BDS. The required ϕ-factor for design was found to be 0.80 and for rating it was 1.00.

13. The research found that the Whitmore criteria should no longer be used to check the chord splice because it does not characterize the true stress distribution well. Rather, a new chord splice procedure was developed that equates the gusset plate stress in the chord splice with the stress distribution produced assuming a linear bending gradient resulting from the eccentric loading. The ϕ-factor for design was found to be 0.65 and for rating it was found to be 0.85.

14. For gusset plate connections built-up from multiple layers of individual plates, the research found that treating the individual plates as uncoupled and summing their individual resistances produced results within the scatter band of the associated resistance calibration.

15. The consideration of section loss in gusset plates in determining resistance was evaluated as part of this research. A "smeared" section loss model was considered and found to be conservative. This approach determines an equivalent plate thickness on the relevant failure plane depending on whether a shear or buckling failure mode is being evaluated. It was found in shear failure scenarios with section loss that failure occurred after plastification of the entire failure plane. It did not matter if the section loss was non-uniform in the plate itself or unbalanced between two gusset plates in the same connection.

16. An attempt was made to collect all historical rivet shear strength data from the existing literature. Multiple sources were found dating back to 1882. All of the rivet shear strength data identified was evaluated statistically and an alternate approach of considering the connection length effect originally proposed by Tide was assessed. Using the Tide inequalities to characterize the proportioning of the connection, it was found that the connection length factor can be defined by two fixed values. It was also found that the population of rivets could be broken down into three strength categories: A141/A502 Grade 1 rivets, A195/A502 Grade 2 rivets, and all other unknown rivets (rivets not from one of those four grades). The statistics for the unknown and A195/A502 Grade 2 rivets were biased from lack of data and the factored shear strengths for them were considered unreliable. The factored resistances for the A141/A502 Grade 1 rivets were developed from a large pool of data and were very similar to those values currently published in the 2011 MBE Interims. Therefore, no changes in the values were considered necessary at this time, without a better pool of strength data for unknown or A195/A502 Grade 2 rivets.

17. The research found no correlation to the slenderness of a gusset plate free edge and the associated compression buckling resistance. Therefore, it is recommended that AASHTO revise their specification language to clarify the intent of the slenderness limit in the BDS to say it represents good detailing practice and reduces initial imperfections, but is not meant to enhance buckling resistance. It is also recommend that the MBE not require rating based on the slenderness of the gusset plate free edge. However, if properly implemented, edge stiffening can be used to enhance buckling resistance if it adds out-of-plane stiffness to the compression member relative to the adjoining members.

18. It was recognized given the number of different connection geometries used to define the resistance equations that the equations will be overly conservative in some situations to ensure that all connections would be conservative. Therefore, if bridge owners do have gusset plates with unfavorable load ratings based on the resistance equations developed from this research, they also have the option to conduct a refined analysis. However, a refined analysis would not address the inherent variability of material properties and the fabrication process that a ϕ-factor is meant to account for. Therefore, an analysis factor was developed to account for these variabilities when applied to the results of a refined analysis. The analysis factor was found to be 0.70 for design, and 0.90 for rating.

19. According to national policy, Load Factor Ratings (LFR) are still admissible for reporting to the National Bridge Inventory. According to this project's scope, LFR was not studied. However, in Appendix J recommended language was proposed to Section 6B of the MBE to provide LFR rating procedures for gusset plates since AASHTO is no longer maintaining the Standard Specifications. A reverse calibration from LRFR to LFR cannot be performed as the project did not attempt to look at the live load variability associated with short- and long-span trusses. Therefore, one cannot use the LRFR resistance factors in LFR because of the differences between the HS-20 and HL-93 live load models. Limit-states that changed from what was published in the FHWA Guide (like buckling and shear) were assigned an LFR resistance factor of 1.00. If nothing changed from that published in the FHWA Guide, the factor from the FHWA Guide was copied.

For clarity, the major recommended changes to the BDS and MBE are represented in Table 39. This table compares the recommendations to those in the FHWA Guide.

Table 39 Summary of Recommended Changes Compared to FHWA Guide

Limit State	Factor	FHWA Guide	Proposed LRFD (β=4.5 @ DL/LL=6)	Proposed LRFR (β=3.5 @ DL/LL=1) [a]
Buckling	ϕ	0.90	0.75	0.95
	K	0.65 to 2.0	0.5	0.5
	Whitmore Section	30°, L_{avg}	30°, L_{mid}	30°, L_{mid}
Shear Yielding	ϕ	0.95	0.80 [b]	1.00 [b]
	Ω	0.74 or 1.00	0.88 [b]	0.88 [b]
Shear Fracture	No changes from existing FHWA Guide			
Block Shear	ϕ	0.80	0.80	1.00
Chord Splices	ϕ	0.90 or 0.95 using Whitmore section for compression and tension respectively	0.65	0.85
Tension Members	No changes from existing FHWA Guide			
Rivet Shear Strength	No changes from existing 2011 MBE Interims			
Simulation Analysis	ϕ	Not applicable	0.70	0.90

[a] – An additional reduction shall apply for DL/LL ratios greater than 1.0. The additional reduction decreases linearly from 1.00 to 0.90 as the DL/LL ratio changes from 1.0 to 6.0. The additional reduction shall not be less than 0.90.
[b] – Will now apply to partial planes around compression members.

SUGGESTED RESEARCH

1. Additional research is needed to establish the ideal target reliability index for trusses and gusset plates. It was beyond the scope of this project to investigate this rigorously and an assumed value of 4.5 for design and 3.5 for rating was used in this work. Generally, reasonable but conservative choices of various parameters have been chosen when extracting proposed design and rating specification provisions from this research. In particular, the choices of statistical parameters such as the mean and coefficient of variation (COV) of loads as well as the assumption that the physical properties of two or more gusset plates making up a joint, and the loads applied to them, are totally uncorrelated are assumptions that could be reviewed and refined at a later date. The possibility that the COV of the lower tail of the distribution of steel yield strengths, both modern and legacy, is lower than the COV calculated for the full population of test data may be fertile ground for the study leading to improvement in the published calibration results of this report.

2. In two of the analytical simulations that failed around tension members, the three tension limit-state checks used by the FHWA Guide unconservatively predicted the failure load. In these three connections it appears that coupled mechanisms were formed that are not addressed by either the block shear or regular shear checks. The coupled mechanisms involved either multiple members pulling out from the gusset plate simultaneously, or having an entire corner of gusset plate pull out with the member. As a result, this is an area of needed additional research.

3. It is critical that further work be performed to determine whether or not the connection length effects exist and the Tide criteria are valid. In addition, it is necessary that further work be performed to gather rivet strength data for rivets of unknown origin or those made to the A195/A502 Grade 2 specification. The data from both exercises could be used to further refine the factored rivet shear strengths.

REFERENCES

1 National Transportation Safety Board, "Collapse of I-35W Highway Bridge, Minneapolis, Minnesota, August 1, 2007," Highway Accident Report NTSB/HAR-08/03. Washington, D.C., 2008.

2 Holt, R. and Hartmann, J., "Adequacy of the U10 Gusset Plate Design for the Minnesota Bridge No. 9340 (I-35W Over the Mississippi River)," Turner-Fairbank Highway Research Center Report, Oct. 2008.

3 Technical Advisory, "Load-Carrying Capacity Considerations of Gusset Plates in Non-Load-Path redundant Steel Truss Bridges," TA No. T 5140.29, Federal Highway Administration, Jan. 15, 2008.

4 Ibrahim, F.I.S., "Load Rating Guidance and Examples for Bolted and Riveted Gusset Plates in Truss Bridges," Federal Highway Administration Publication No. FHWA-IF-09-014, Washington, D.C., February 2009.

5 Yamamoto, K., Akiyama, N., and Okumura, T., "Elastic Analysis of Gusseted Truss Joints," *Journal of Structural Engineering*, Vol. 111, No. 12, pp. 2545-2564, December 1985.

6 Yamamoto, K., Akiyama, N. and Okumura, T. "Buckling Strength of Gusseted Truss Joints." *Journal of Structural Engineering* 114(3), pp. 575-590, 1988.

7 American Association of State Highway and Transportation Officials, AASHTO LRFD Bridge Design Specifications, Fifth Edition, Washington, D.C., 2010.

8 American Association of State Highway and Transportation Officials, The Manual for Bridge Evaluation, Second Edition, Washington, D.C., 2011.

9 Whitmore, R.E., "Experimental Investigation of Stresses in Gusset Plates," Bulletin No. 16, Engineering Experiment Station, University of Tennessee, May 1952.

10 Kulak, G.L., Fisher, J.W., and Struik, J.H.A., "Guide to Design Criteria for Bolted and Riveted Joints – 2nd Ed.," American Institute of Steel Construction, Chicago, IL, 2001.

11 Richard, R. M., Rabern, D. A., Hormby, D. E., and Williams, G. C., "Analytical Models for Steel Connections," *Behavior of Metal Structures, Proceedings of the W.H. Munse Symposium,* Edited by W. J. Hall and M. P. Gaus, American Society of Civil Engineers, May 17, 1983.

12 Cai, Q. and Driver, R.G. "Performance of the Unified Block Shear Equation for Atypical Failure Paths," Proceedings, *Connections VI*, 2008.

13 Brown, V.L.S., "Stability of Gusseted Connections in Steel Structures," Ph.D. dissertation, University of Delaware, 1988. (Eugene Chesson, Advisor).

14 Huckelbridge, A.A., Jr., Palmer, D.A., and Snyder, R.E., "Grand Gusset Failure," *Civil Engineering*, Sept. 1997, pg. 50.

15 Prucz, Z. and Kulicki, J.M., "Accounting for Effects of Corrosion Section Loss in Steel Bridges," *Transportation Research Record 1624*, TRB, National Research Council, Washington, D.C., 1998, pp. 101-109.

16 Mentes, Y.; "Analytical and Experimental Assessment of Steel Truss Bridge Gusset Plate Connections," PhD Dissertation, School of Civil and Environmental Engineering, Georgia Institute of Technology, December 2011.

17 Ocel, J. M., and Wright, W. J., "Finite Element Modeling of I-35W Bridge Collapse – Final Report," Federal Highway Administration Turner-Fairbank Highway Research Center Report, McLean, VA, 2008.

18 Simulia, "Abaqus Analysis User Manual, Version 6.8." Providence, RI, 2008.

19 American Welding Society, AASHTO/AWS D1.5:2010 Bridge Welding Code, Miami, FL, 2010.

20 Roeder, C.W., Leon, R.Y., and Preece, F.R., "Strength, Stiffness, and Ductility of Older Steel Structures under Seismic Loading," Report SGEM 94-4, Department of Civil Engineering, University of Washington, Seattle, WA, 1994.

21 Ellingwood, B., Galambos, T. V., MacGregor, J. G., and Cornell, C. A., "Development of a Probability Based Load Criterion for American National Standard A58," National Bureau of Standards Special Publication 577, June 1980.

22 Nowak, A. S. and Collins, K. R., *Reliability of Structures, Second Edition*, CRC Press, 2012.

23 Higgins, C., Hafner, A., Turan, T., and Schumacher, T., "Experimental Tests of Gusset Plate Connections with Sway-Buckling Response," submitted to the ASCE Journal of Bridge Engineering, in review.

24 Kulicki, J. M. and Reiner, B. M., "Chapter 13 – Truss Bridges, *Structural Steel Designer's Handbook, 5th Edition* edited by Roger Brockenbrough and Frederick Merritt, McGraw-Hill Professional, 2011.

25 Huns, B. S., Grondin, G. Y., and Driver, R. G., "Tension and Shear Block Failure of Bolted Gusset Plates," Canadian Journal of Civil Engineering, Vol. 33, pp. 395-408, 2006.

26 Astaneh-Asl, A., "Gusset Plates in Steel Bridges – Design and Evaluation," Steel Tips #107, Structural Steel Education Council (www.steeltips.org), April 2010.

27 Personal communication with Bala Sivakumar, 27 September 2010.

28 American Institute of Steel Construction, Edited by Herbert W. Ferris, "Historical Record – Dimensions and Properties – Rolled Shapes, as rolled in USA, Period 1873 to 1952, 1953.

29 Personal communication with Firas Ibrahim, 16 September 2010.

30 DeJonge, A.E.R., "Riveted Joints: A Critical Review of the Literature Covering their Development," American Association of Mechanical Engineers, New York, 1945.

31 Fisher, J.W. , and Beedle, L.S., "Bibliography on Bolted and Riveted Structural Joints," Report No. 302.1, Fritz Engineering Laboratory, Lehigh University, Bethlehem, PA., 1964.

32 Fisher, J.W., Kormanik, R., and Allan, R.N., "Supplement to the Bibliography on Bolted and Riveted Joints," Report No. 302.1, Fritz Engineering Laboratory, Lehigh University, Bethlehem, PA., 1966.

33 Government Board of Engineers, *The Quebec Bridge*, Vol. 1, Department of Railways and Canals, Ottawa, 1919.

34 Hechtman, R. A., A Study of the Effects of Heating and Driving Conditions on Hot-Driven Structural Steel Rivets, Ph. D. thesis, Department of Civil Engineering, University of Illinois, Urbana, IL, 1948.

35 Munse, W.H., "Fifty Years of Riveted, Bolted, and Welded Steel Construction," J. of Construction Division, American Society of Civil Engineers, September, 1976, Vol. 102, CO3, pp. 437-447, 1976.

36 Munse, W. H., and Cox, H. L., "The Static Strength of Rivets Subjected to Combined Tension and Shear," *Engineering Experiment Station Bulletin No. 437*, University of Illinois, Urbana, IL., 1956.

37 Wilson, W. M., and Oliver, W. A., "Tension Tests of Rivets," University of Illinois Engineering Experiment Station, Bulletin No. 210, Urbana, IL., 1930.

38 American Railway Engineering and Maintenance-of-Way Association, "Tests of Riveted Joints," Proceedings of the Sixth Annual Convention of the American Railway Engineering and Maintenance-of-Way Association, Chicago, IL, pp. 272-420, March 21-23, 1905.

39 Bendigo, R. A. and Rumpf, J. L., "Static Tension Tests of Long Bolted Joints," Fritz Laboratory Report No. 271.8, Lehigh University, Bethlehem, PA, 1960.

40 Davis, R. E. and Woodruff, G. B., "Tension Tests of Large Riveted Joints," Transaction of the American Society of Civil Engineers, Vol. 105, pp.1193-1299, 1940.

41 Dlugosz, St. W., "Static Tension Tests of Long Riveted Joints," Master's Thesis of Lehigh University, June 1962.

42 Fuller, J. R., Leahey, T. F., and Munse, W. H., "Static Tensile Tests of Large I-Section Connections," University of Illinois Engineering Experiment Station, College of Engineering, University of Illinois at Urbana-Champaign, 1954.

43 Rivera, U. and Fisher, J. W., "Load Partition and Ultimate Strength of Shingle Joints," Fritz Engineering Laboratory Report No. 340.6, Lehigh University, Bethlehem, PA 1970.

44 Talbot, A. N. and Moore, H. F., "Tests of Nickel-Steel Riveted Joints," Bulletin No. 49, University of Illinois Engineering Experiment Station, College of Engineering, University of Illinois at Urbana-Champaign, 1911.

45 Watertown Arsenal, "Remarks on Riveted Joints," Report of the Tests of Metal and Other Materials for Industrial Purposes, pp. 9-141, Fiscal Year ending June 30, 1882.

46 Watertown Arsenal, "Tensile Tests of Riveted Joints," Report of the Tests of Metal and Other Materials for Industrial Purposes, pp. 710-943, Fiscal Year ending June 30, 1885.

47 Watertown Arsenal, "Single Riveted Butt-Joints, Steel Plate," Report of the Tests of Metal and Other Materials for Industrial Purposes, Part II, pp. 1263-1828, Fiscal Year ending June 30, 1886.

48 Watertown Arsenal, "Riveted Joints," Report of the Tests of Metal and Other Materials for Industrial Purposes, Part II, pp. 882-923, Fiscal Year ending June 30, 1887.

49 Watertown Arsenal, "Riveted Joints," Report of the Tests of Metal and Other Materials for Industrial Purposes, pp. 445-589, Fiscal Year ending June 30, 1891.

50 Watertown Arsenal, "Riveted Joints," Report of the Tests of Metal and Other Materials for Industrial Purposes, pp. 247-339, Fiscal Year ending June 30, 1896.

51 Wilson, W. M. and Thomas, F. P., "Fatigue Tests of Riveted Joints," University of Illinois Engineering Experiment Station Bulletin No. 302, Urbana, IL, 1938.

52 Yoshida, N. and Fisher, J. W., "Large Shingle Splices that Simulate Bridge Joints," Fritz Engineering Laboratory Report No. 340.2, Lehigh University, Bethlehem, PA, 1968.

53 Tide, R.H.R., "Bolt Shear Design Considerations," *Engineering Journal*, Vol. 47, No. 1, (1st Qtr.), American Institute of Steel Construction, Chicago, IL, 2010.

54 Kulicki, J. M, Prucz, Z., Clancy, C. M., Mertz, D. R., and Nowak, A. S.; "Updating the Calibration Report for AASHTO LRFD Code," Final Report for NCHRP Project 20-07/186, Transportation Research Board, Washington, D.C., January 2007.

55 Nowak, A.S., *NCHRP Report 368: Calibration of LRFD Bridge Design Code*, TRB, National Research Council, Washington, D.C., 1999.

56 American Institute of Steel Construction; "Steel Construction Manual, Thirteenth Edition," American Institute of Steel Construction, Chicago, IL, 2008.

57 American Association of State Highway and Transportation Officials, AASHTO LRFD Bridge Design Specifications, 4th Edition, Washington, D.C., 2007.

58 Moore, A. M., Rassati, G. A., and Swanson, J, A., "Evaluation of the Current Resistance Factors for High-Strength Bolts," Report to Research Council on Structural Connections, January 2008.

APPENDICES

NOTE: The following appendices are not published herein, but are available as individual documents on the TRB website at http://www.trb.org/Main/Blurbs/168923.aspx.

APPENDIX A – REVIEW OF BRIDGE PLANS

APPENDIX B – LOAD FRAME

APPENDIX C - FASTENER CHARACTERIZATION

APPENDIX D – MATERIAL TEST RESULTS

APPENDIX E – PHOTOSTRESS DATA

APPENDIX F – DIC DATA

APPENDIX G – STRAIN GAUGE DATA

APPENDIX H – FARO DATA

APPENDIX I – GEORGIA TECH PARAMETRIC STUDY FINAL REPORT

APPENDIX J – PROPOSED CHANGES TO AASHTO SPECIFICATIONS

APPENDIX K – DESIGN EXAMPLES BASED ON DRAFT SPECIFICATION